DEVELOPMENT OF A TEST FACILITY AND PRELIMINARY TESTING OF FLOW BOILING HEAT TRANSFER OF R410A REFRIGERANT WITH AL_2O_3 NANOLUBRICANTS

By

THIAM WONG

Bachelor of Science in Mechanical Engineering

Oklahoma State University

Stillwater, Oklahoma

2013

Submitted to the Faculty of the
Graduate College of the
Oklahoma State University
in partial fulfillment of
the requirements for
the Degree of
MASTER OF SCIENCE
December, 2015

DEVELOPMENT OF A TEST FACILITY AND

PRELIMINARY TESTING OF FLOW BOILING HEAT

TRANSFER OF R410A REFRIGERANT WITH AL_2O_3

NANOLUBRICANTS

Thesis Approved:

Dr. Lorenzo Cremaschi

Thesis Adviser

Dr. Christian Bach

Dr. Arvind Santhanakrishnan

ACKNOWLEDGEMENTS

I would like to express my gratitude toward my advisor Dr. Lorenzo Cremaschi for his guidance that led to the completion of the work required for my degree. I'd like to thank the members of my committee Dr. Christian Bach and Dr. Arvind Santhanakrishnan for taking the time to review my thesis work.

I sincerely thank Pratik Deokar for his continual help and support in my thesis work, who was always present when I needed assistance. I acknowledge and appreciate the contribution of Andrea M. Bigi, Amy Wong and Gennaro Criscuolo who have helped me with my thesis work. I would like to thank other members of the research group for maintaining a very pleasant work environment.

I would like to express my most heartfelt appreciation to my family, this milestone in my life would not have been possible without their unconditional love and support.

Name: THIAM WONG

Date of Degree: DECEMBER, 2015

Title of Study: DEVELOPMENT OF A TEST FACILITY AND PRELIMINARY TESTING OF FLOWBOILING HEAT TRANSFER OF R410A REFRIGERANT WITH AL_2O_3 NANOLUBRICANTS

Major Field: MECHANICAL AND AEROSPACE ENGINEERING

Abstract:

In vapor compression cycles, a small portion of the oil circulates with the refrigerant throughout the system components, while most of the oil stays in the compressors. In heat exchangers, the lubricant in excess penalizes the heat transfer and increases the pressure losses: both effects are highly undesired but yet unavoidable. Nanoparticles dispersed in the excess lubricant are expected to provide enhancements in heat transfer. While solubility and miscibility of refrigerants in polyolesters (POE) lubricant are well established knowledge, there is a lack of information regarding if and how nanoparticles dispersed in the lubricant affect these properties. This thesis presents experimental data of solubility of two types of Al2O3 nanolubricants with refrigerant R-410A. The nanoparticles were dispersed in POE lubricant by using different surfactants and dispersion methods. The nanolubricants appeared to have slightly lower solubility than that of R-410A but actually the solid nanoparticles did not really interfere with the POE oil solubility characteristics. A test facility and experimental methodology was developed for the investigation of heat transfer coefficient and pressure drop. The pressure drop of the refrigerant lubricant mixtures during flow boiling depended on the mass flux of the refrigerant. Greater augmentation was seen in the pressure drop results with decreasing mass flow rate. Pure refrigerant R410A showed the lowest pressure drop, addition of nanolubricants to the refrigerant showed a slightly higher pressure drop and POE-refrigerant mixture showed the highest pressure drop in the tests conducted. Enhancement or degradation in heat transfer coefficient during flow boiling depended on the nanoparticle concentration in the lubricant as well as the lubricant concentration in refrigerant. R410A showed the highest heat transfer coefficient for all conditions tested. For a concentration of 1% nanolubricant in refrigerant, the heat transfer coefficient showed more enhancement with increase in nanoparticle concentration compared to POE refrigerant mixtures. For a concentration of 3% nanolubricant in refrigerant mixtures there was little to no enhancement for tests conducted.

TABLE OF CONTENTS

LIST OF TABLES

LIST OF FIGURES

CHAPTER 1

INTRODUCTION

1.1 Background

Energy consumption in buildings for heating ventilation and air conditioning (HVAC) systems is a large contributor to the total global energy consumption (EIA, 2009) and nanolubricants -- a lubricant with dispersed nano-size particles have the potential to be a cost-effective technology for reducing the energy consumption of chillers that cools large buildings and of air conditioners used in residential homes. In space conditioning, vapor compression cycles provide heating and cooling. The working fluid is a refrigerant and oil mixture. A small amount of oil is needed to lubricate and to seal the sliding parts inside the compressors. In heat exchangers the lubricant in excess penalizes the heat transfer exchange and increases the flow losses: both effects are highly undesired but yet unavoidable. Nanolubricants are of great interest because their unprecedented thermal transport phenomena surpass the fundamental limits of conventional macroscopic theories of multiphase flow and of in-tube heat transfer (Choi, 2009). Several researchers postulated that the magnitude of the heat transfer enhancement is much higher than the gain in the liquid thermal conductivity and that the nano-scale interactions between the nanoparticles and the refrigerant/oil liquid layers are responsible for the heat transfer intensification. Enhancements were observed in pool boiling (Kedzierski, 2009a; 2009b; Peng *et al.*, 2010; Wen & Ding, 2004; 2005b) and in one experimental work for flow boiling in a horizontal tube (Bartelt *et al.*, 2008). Work on nanolubriant is still in its infancy and this thesis aims to provide new experimental data of solubility, heat transfer coefficient and pressure drop characteristics for refrigerant R-410A and nanolubricant mixtures. In addition, the solubility refrigerant R-410A with two types of nanolubricants that had the same Al_2O_3 nanoparticles but different surfactants, were investigated. A test facility and experimental methodology was developed for the heat transfer coefficient and pressure drop experiments. Preliminary tests for heat transfer coefficient and pressure drop were conducted to establish baseline results for pure R410A and R410A-POE mixtures. Tests were then conducted with R410A-nanolubricant mixtures, and compared with R410A and R410A-POE mixtures.

1.2 Objectives

The main objective of this thesis was to develop an experimental test facility to measure the heat transfer coefficient and pressure drop of refrigerant R410A, R410A-POE and R410A-nanolubricant mixtures during in-tube flow boiling. Several different designs of the test facility were developed and realized in order to achieve this objective. The specific goals of my thesis were as follows:

1. To conduct a review on the latest techniques and experimental methodologies used to measure the heat transfer coefficient and pressure drop of refrigerant, refrigerant-oil and refrigerant-nanolubricant mixtures. This included details of the test setup used in similar experiments, the data reduction procedures, and the results from experiments in the state-of-the-art literature.
2. To design an experimental facility that measure the in-tube flow boiling heat transfer coefficient and two-phase flow pressure drop of refrigerant R410A, of R410A-POE, and R410A-nanolubricant mixture. The test apparatus included a system to inject the lubricant into the flow, and a system to extract the lubricant from the system at the end of a test. Plus, the layout of the experimental facility minimizing, if not eliminating any oil traps.
3. To implement the design and construct the experimental test setup.
4. To calibrate and validate the various sensors and instrumentation used in the test setup.

5. To develop an experimental methodology for controlling the test conditions. This included experimental procedures for uniformly metering the oil in the main refrigerant flow circulating in the test section, testing protocols, cleaning procedures and verification tests to verify that the tube's initial internal surface conditions were reestablished after the cleaning of the tube.
6. To take some preliminary measurements of the two phase flow boiling heat transfer coefficient and pressure drop for refrigerant R410A, R410A-POE and R410A-nanolubricant mixtures in order to document the experimental uncertainty and limitations of the test apparatus.

An important aspect of the work was to measure the solubility of the R410A-nanolubricant mixtures. While information on the solubility of R410A-POE mixtures is known in literature, there is not information on the solubility of refrigerant R410A in Al_2O_3 nanolubricants. Solubility tests were conducted in this thesis to test for the compatibility of the R410A-Al_2O_3 nanolubricant mixtures. The specific tasks of this part of the work were as follows:

1. To conduct a literature review on similar experiments previously performed on refrigerant-lubricant solubility experiments.
2. To design a test setup to effectively measure the solubility of refrigerant-lubricant mixtures following ASHRAE standard 41.4.
3. To implement the design and construct the test setup for the experiment.
4. To calibrate and validate the instrumentation and sensors required for testing.
5. To conduct the validation the test setup by comparing solubility of R410A in POE found in the ASHRAE *Refrigeration* (2010) handbook.
6. To perform data analysis in order to obtain results from experimental measurements.
7. To discuss the results obtained for the solubility of R410A-Al_2O_3 nanolubricant mixtures

1.3 Organization of the thesis

The objectives of this thesis was to determine the solubility, flow boiling heat transfer coefficient and pressure drop of Al_2O_3 nanolubricants in refrigerant R410A. Chapter 1 provides the introduction, background and objectives of the work investigated in this thesis. Chapter 2 is a review of the literature available, and presents work on similar experiments performed in this thesis. Chapter 3 describes the instrumentation and experimental facility that was used to conduct the experiments. One of the main works of this thesis which is the development of the test facility to measure the heat transfer coefficient and pressure drop of refrigerant-nanolubricant mixtures is described in this chapter. Chapter 4 describes the experimental methodology developed to conduct the experiments to obtain repeatable results. The testing, cleaning and verification procedures for the heat transfer coefficient and pressure drop experiments that were refined by performing the experiments are described in this chapter. Chapter 5 presents the results and includes a discussion of the results for the experiments conducted. The figures obtained from the tests conducted are shown and the comparisons are made in this chapter. Further discussions are made about the results and the findings from the different test setups used during the experiments in this chapter. Chapter 6 describes the conclusions drawn from the thesis work, and the recommendations for future potential research in this field.

CHAPTER 2

Literature Review

Abundant literature exist on refrigerant and lubricant mixture properties and on low viscosity mixtures called nanofluids. Emphasis was on studies in the literature that focused on nanoparticles dispersed in high viscosity media such as oil, these mixtures are called nanolubricants. To the authors' best knowledge, there is very limited information on the thermodynamic, thermal, and transport properties of nanoparticles in POE lubricants and studies on solubility and miscibility are yet to be found on open domain literature. The main properties investigated in this thesis and a summary of the associated studies in literature are briefly discussed next.

2.1 Solubility and miscibility of refrigerant R410A with nanolubricants

Solubility and miscibility of oil-refrigerant mixtures affects the density, viscosity, specific heat, and thermal conductivity of the liquid phase of the mixture in the two phase region. Nanoparticles dispersed in POE oil with surfactants might alter the degree of solubility of the refrigerant. In addition, quote, "*taking into account the presence of oil in the enthalpy calculation, which often is neglected, can have drastic consequences on the enthalpy change through the evaporator under particular conditions*" (Youbi, 2003). Studies conducted by Cremaschi *et al.* (2005) suggested that poor solubility and miscibility between oil and refrigerant, can cause a higher amount of oil retention in evaporators and condensers and it was observed that the COP of the system might be penalized by as much as 9% due to a drop in cooling capacity.

Solubility of refrigerant in oil depends on the temperature and pressure of the mixture. In previous experiments, solubility of refrigerant in oil was determined by analyzing the weight fraction of refrigerant present in oil equilibrated at particular temperature and pressure conditions (Bobbo *et al.*, 2010). For oil-refrigerant mixtures, solubility and miscibility are well established knowledge for various oil and refrigerant mixtures. In particular, data for R-410A and ISO 32 POE mixed acid polyolester oil can be found in the ASHRAE Refrigeration handbook (*Refrigeration*, 2010). However, there is lack of information about the changes in solubility as a result of addition of nanoparticles (Bobbo *et al.*, 2010) or of surfactants. While abundant literature is available on nanofluids and their properties, the dispersion of nanoparticles in high viscosity suspensions requires further investigation. Alumina nanoparticles dispersed in Polyolester (POE) oil was studied, and this thesis provides new experimental data of solubility properties.

2.2 Heat Transfer Coefficient and Pressure drop

Several studies have been performed to investigate the heat transfer coefficient and the pressure drop of refrigerant, refrigerant-oil mixtures and refrigerant-nanofluid mixtures. Shen and Groll (2003) provide an extensive review on the effect of oil on the heat transfer coefficient and pressure drop during flow boiling of refrigerants and they highlighted various factors that could influence the flow boiling characteristics with the addition of oil such as effects of flow pattern, mixture viscosity, vapor quality and effect of mass flux. Hu *et al.* (2008a) concluded that presence of oil enhanced heat transfer at a refrigerant quality lower than 0.4, but deteriorated heat transfer for refrigerant qualities higher than 0.65. A study on pressure drop as a function of quality of R410A-POE mixture was performed by Hu *et al.* (2008b). They used a 7 mm micro-fin tube, a mass flux range of 200 to 400 kg/(m^{2}s), a heat flux range of 7.56 to 15.12 kW/m^2. Oil concentration was varied from 0% to 5%. From their study, it was concluded that the frictional pressure drop of R410A-POE mixture increased with mass flux. The presence of oil increased the two-phase frictional pressure drop and the pressure drop increased with increase in oil concentration. Bartelt *et al.* (2008) investigated the pressure drop of R134A-POE-CuO nanolubricant mixture and they concluded that nanoparticle dispersed in the liquid phase during two-phase flow boiling did not have significant effect on pressure drop. This finding is confirmed in the present work as well, as it will be discussed later in this thesis. Another experiment was performed by Mahbubul *et al.* (2011) using R123 and TiO_2 nanofluid mixture. The authors compared their findings with another study using R113-CuO nanofluid mixture conducted by Peng *et al.* (2009). From their findings, it was observed that augmentation in pressure drop was higher when mass flux was low, although the pressure drop increased with increase in mass flux. This finding is later confirmed in this study.

Bartelt *et al.* (2008) also investigated the flow boiling of R-134a with CuO-POE nanolubricants. In their study, for a nanoparticle concentration of 4% by volume in POE, and a 0.5% nanolubricant concentration in R-134a, no effect was seen on the flow boiling heat transfer coefficient compared to R-134a-POE mixtures. When the nanolubricant mass fraction was increased to 1%, enhancement was seen up to 82%. Further increase in the lubricant concentration to 2% increased the heat transfer coefficient between 50 to 101% in their study.

According to (Kedzierski, 2009b), nanoparticle concentration is an important factor in determining the heat transfer enhancement. Their study was performed on pool boiling of R134A-polyolester mixtures with addition of copper(II) oxide (CuO) nanoparticles. From their study, it was seen that when 4 percent volume fraction of nanoparticle-lubricant (nanolubricant) mixture is mixed with 0.5 percent nanolubricant-R134A (oil concentration ratio), heat transfer enhancement compared pure R134a/polyolester was seen between 50 to 275 percent. Increasing the oil concentration ratio in the nanolubricant to 1 percent volume fraction decreased the heat transfer enhancements to an average of 19%. Their study also showed that reducing the nanoparticle concentration by half (2% by volume) showed no enhancement or degradation when compared to the R410a/Polyolester mixtures. From their experiment they conclude that significant enhancements can be achieved with nanoparticles depending on nanoparticle concentration. In another study, Kedzierski (2009a) performed with Al_2O_3 nanoparticles added to R134A-polyolester mixtures it was seen that for 0.5% nanolubricant mass fraction in refrigerant, enhancement as large as 400% was seen relative to R134a-polyolester mixtures. In this study it was found that enhancement in heat transfer coefficient increased with decreasing heat flux, and that small nanoparticle size and large nanoparticle volume enhanced heat transfer.

2.2.1 Experimental setups and instrumentation used in previous heat transfer coefficient and pressure drop experiments

Two types of experimental setups were primarily used for heat transfer coefficient and pressure drop tests. Some researchers use a thermal amplification technique to provide heat flux into the refrigerant, while others use electrical heaters to provide heat flux into the refrigerant.

The test section used at the National Institute of Science and Technology (NIST) is based on the thermal amplification technique (Sawant *et al.*, 2007). The test section is 6.68m (21.92') long, and is fundamentally a tube-in-tube annular heat exchanger with the refrigerant tube inside another tube which water passes through. The annulus is made of 14 flanges and these flanges are gasketed at 10 locations to allow the thermocouple wires which are soldered on to the refrigerant tube surface to pass out of the test section. Surface temperatures were measured at the bottom, top and side of the refrigerant tube. A chain of thermopiles were built into the water tube each consisting of 10 thermocouples and evenly spaced around the circumference of the annulus. In this type of test section the water flowing in the annular jacket provides the heat flux into the refrigerant. The water in the annular jacket is circulated at a very high mass flow rate, such that there is minimal temperature difference between the inlet and the exit of the test section. This is done to provide a constant heat flux into the test section with an approximate constant temperature of the flowing water.

Another kind of test section used by other researchers (Hu *et al.*, 2008a) use electrical heaters wrapped on to the refrigerant tube, the thermocouples are soldered to the refrigerant tube and heat flux is provided to the refrigerant from the electrical heater.

CHAPTER 3

EQUIPMENT AND INSTRUMENTATION

The nanolubricant samples were prepared with the equipment described in this section. The solubility, heat transfer coefficient, and pressure drop characteristics were measured with the instrumentation as follows.

3.1 Equipment for mixing the nanoparticles in the POE lubricant

A Sonics VC 750 ultrasonic mixer was used for developing uniform dispersions of the metal Al_2O_3 nanoparticles in the POE oil. The ultrasonic mixer is shown in Figure 1.

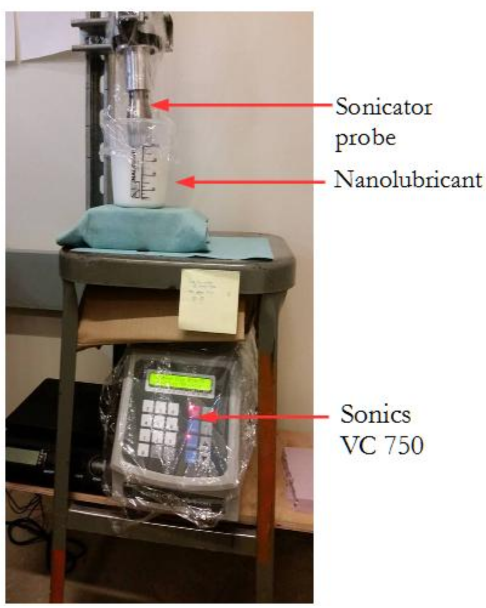

Figure 1: Ultrasonic mixer used for stable dispersion of nanoparticles in POE

The net power output of the ultrasonic mixer was 750 Watts, at a frequency of 20 kHz. Different probes were used with this device based on the amount of nanolubricant that had to be prepared. For the processing of smaller samples, a ½" (13mm) diameter probe was used with a griffin beaker while for the processing of larger volumes a graduated cylinder was used with the 1" (25 mm) diameter probe. The time of sonication varied from 8 hours to 24 hours, depending on the volume of the nanolubricant sample that was processed. The sonication was pulsed in cycle of 30 seconds on/off. The concentration of the metal Al_2O_3 nanoparticles in the POE oil, $w_{\%NL}$, was defined as weight percent of the nanoparticles in the total solid-liquid mixture, as shown in eq (4).

$$w_{\%NL} = \frac{w_{Al_2O_3}}{w_{Al_2O_3} + w_{POE}} \tag{4}$$

,*where* $w_{\%NL}$ *is the weight percent of the nanolubricant*
$w_{Al_2O_3}$ *is the weight of the nanoparticles*
w_{POE} *is the weight percent of the POE*

3.2 Equipment for measuring the solubility of refrigerant R-410A in nanolubricants

The experimental setup for measuring the solubility of refrigerant in nanolubricant was custom built in the present work. Figure 2 shows the schematic of the instrumentation used for measuring the solubility of the nanolubricant samples.

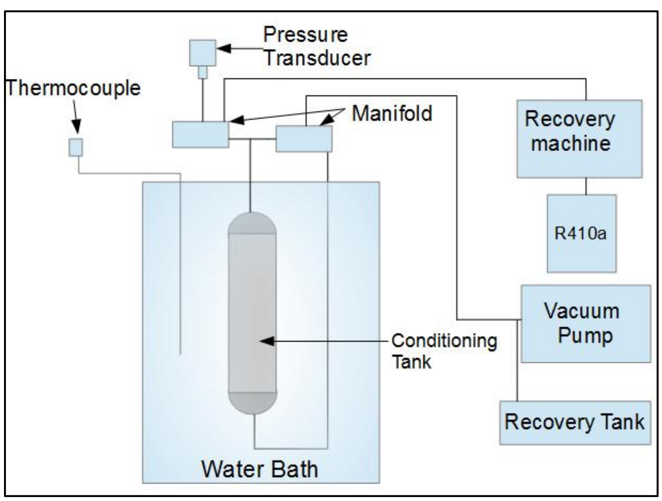

Figure 2: Experimental setups for measuring and Solubility of nanolubricants

It consisted of mainly four components: a temperature bath, a large reservoir, a smaller sample cylinder (recovery tank in Figure 2), and a pressure transducer. A vacuum pump was used for depressurization of the large conditioning tank. For weight measurements, a precision scale with an accuracy of ±0.2g was used. The large reservoir was a stainless steel tank with a working pressure of 1800 psig (12410 kPa) and with a 1 gallon (0.0037 m^3) volumetric capacity. The smaller sample cylinder was a custom made 500mL leak proof tank made out of copper.

3.3 <u>Test Facility and instrumentation to measure Heat Transfer Coefficient and Pressure Drop</u>

A schematic of the test setup used to measure the heat transfer coefficient and pressure drop is shown in Figure 3.

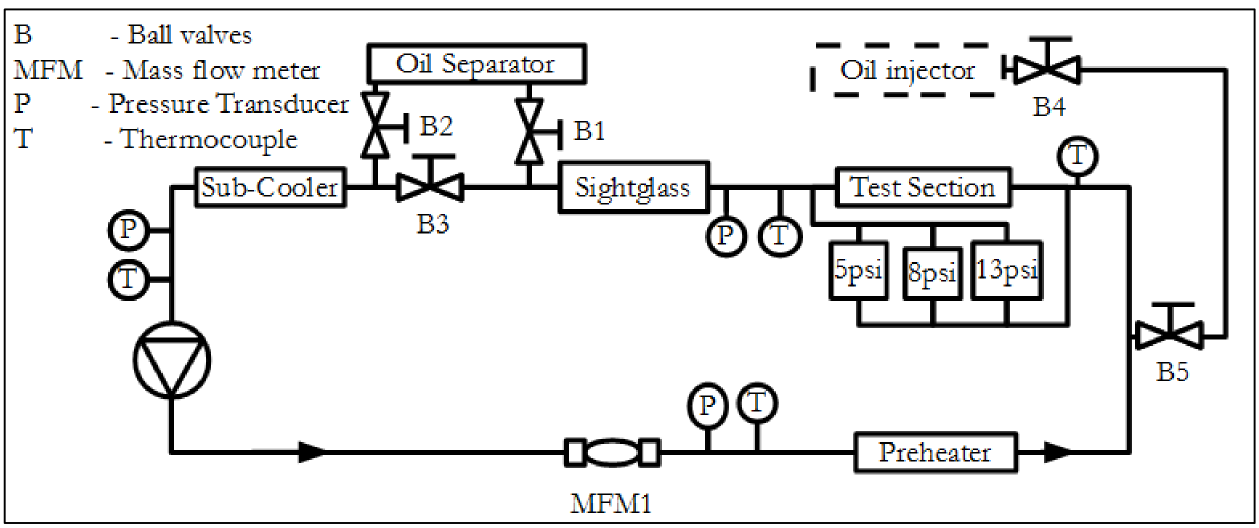

Figure 3: Test setup for measuring HTC and Pressure Drop

The purpose of the setup is for the refrigerant to enter the test section at a known quality, provide a specific amount of heat flux in the test section, and determine the heat transfer coefficient and pressure drop with varying quality in the test section. The following is a brief description of the processes and the components involved in the test setup.

The mass flow rate of a known charge of refrigerant circulated through the system with a variable speed refrigerant pump is measured using coriolis a mass flow meter. The pressure and temperature sensors placed before the preheater determines the degree of sub-cool entering the preheater. Knowing the inlet enthalpy of the refrigerant (because it is subcooled) at the preheater inlet, the exit quality of the preheater can be determined from the heat input of the preheater. A known amount heat flux is then applied to the test section, when required conditions are achieved, measurements are then taken to determine the heat transfer coefficient and pressure drop.

To achieve the required saturation conditions of the refrigerant, several components are used in the experimental setup; a brief description of the components are as follows:

3.3.1 Subcooler

The subcooler is a brazed plate heat exchanger which lowers the temperature of the refrigerant in the test setup. The subcooler ensures that there is enough subcool for the refrigerant pump to circulate the refrigerant through the system avoiding cavitation. Heat is exchanged between the refrigerant and an auxiliary 2 ton chiller which circulates HC50 through the subcooler. The low temperature HC50 exchanges heat with the higher temperature refrigerant cooling the refrigerant circulating in the system. The subcooled refrigerant is then sent to the refrigerant gear pump and circulated in the test setup.

3.3.2 Preheater

The preheater is a counter flow tube in tube heat exchanger which provides heat gain to the refrigerant to achieve the desired quality during tests by increasing or decreasing the quality entering the test section. The mass flow rate of hot water circulated in the outer tube of the preheater is measured with a coriolis mass flow meter, and the temperature entering and exiting the preheater is measured using thermocouples, these readings give us the heat input of the water side of the preheater. The enthalpy of the refrigerant at the inlet of the preheater is determined from temperature and pressure readings as the refrigerant at this section of the setup is subcooled.

3.3.3 Oil injection system

The system to smoothly and uniformly metered the oil in the main refrigerant flow circulating in the test section is referred as to oil injection system and it consisted of a custom built tank shown in Figure 4. The oil injection system is built with a sight glass to observe the oil injection rate of the lubricant into the system. Since the sight glass could not hold all the lubricant required during injection, a reservoir tank is built to hold lubricant in parallel with the sight glass. With such a design, the oil level in the sight glass as well as the reservoir tank has the same level of oil as seen by the sight glass.

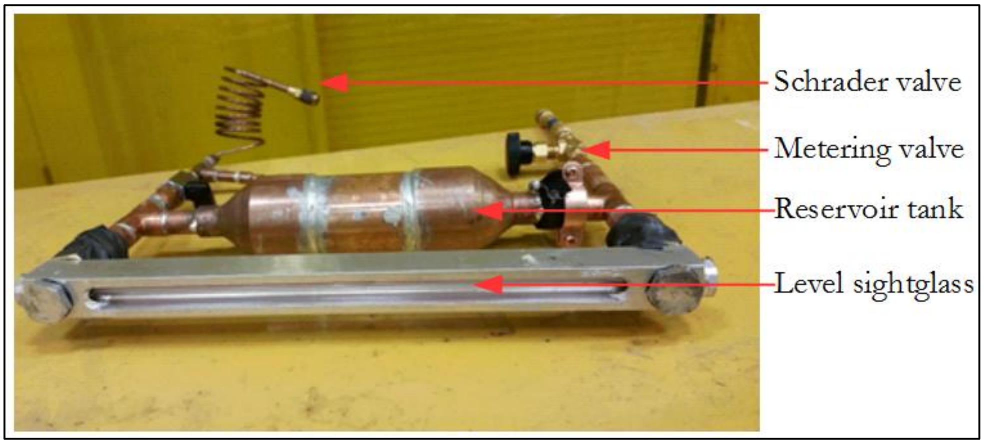

Figure 4: Oil injection system

3.3.4 Oil Separator

An oil separator is installed after the test section to separate oil after experimentation. This system is closed and bypassed with the use of ball valves and a bypass line during testing, and is only used as a system to remove the oil from the system once tests have been conducted. The oil separator is shown in Figure 5.

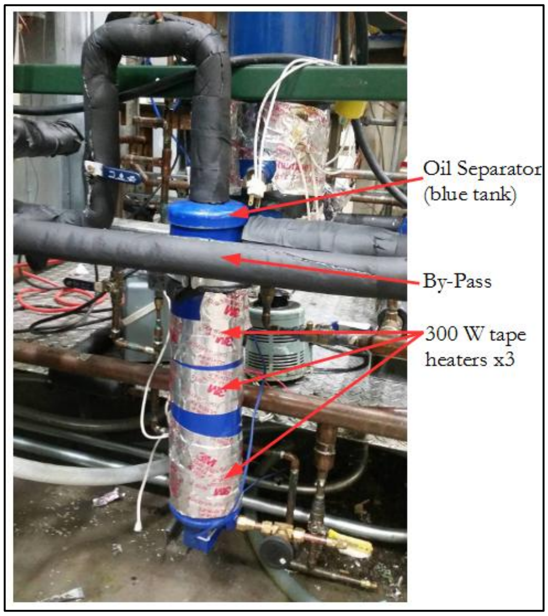

Figure 5: Oil separator at the end of the test section

3.3.5 Temperature sensors

Accurate temperature measurements were critical in determining the heat transfer coefficient of the refrigerant in the test section. Temperature measurements were made using three different kinds of sensors. Resistance temperature detectors (RTDs) were used where accuracy of the measurement were most critical for the experiment. These were used for measuring temperatures at the water side inlet and exit of the test section where temperature difference between the inlet and the outlet of the water loop was less than 1°F. The RTDs used had an accuracy of 0.05°F with a 6 inch long probe, 1/8 inch in diameter.

Inline thermocouples were used to measure the temperature of the liquid phase of the refrigerant in the system, these were located at the preheater inlet, preheater exit and the test section exit in the system. These were T-type thermocouples with an accuracy of 0.1°F. The probes were 6 inches long, and 1/8 inch in diameter. The third type of temperature sensor used in the system were custom made T-type bead thermocouples. These thermocouples were made with commercially available 30 gage thermocouple wires for the test sections made using the thermal amplification technique, and 36 gage thermocouple wires for the second test section. These thermocouples were soldered on to the surface of the enhanced ¼ inch refrigerant tube for surface temperature measurements. The accuracy of the bead thermocouples was 0.1°F. Table 1 provides details of the temperature sensors used in the system these were calibrated in situ before construction of the test section.

Table 1: Details of temperature sensors used in the system

Label	Measurement Location	Sensor Type	Model #	Accuracy
$T_{r_{preheater}}$	Refrigerant Preheater Inlet	Thermocouple	OMEGA TQSS-125G	±0.1°F
$T_{w_{inlet}}$	Preheater Water Inlet	Thermocouple	OMEGA,TQSS-125G	±0.1°F
$T_{w_{outlet}}$	Preheater Water Outlet	Thermocouple	OMEGA, TQSS-125G	±0.1°F
$T_{r_{inlet}}$	Test Section Refrigerant Inlet	Thermocouple	OMEGA, TQSS-125G	±0.1°F
$T_{r_{outlet}}$	Test Section Refrigerant Outlet	Thermocouple	OMEGA, TQSS-125G	±0.1°F
T_1	Hot Water Inlet	RTD	OMEGA P-M-1/3-1/8-6-0-T-3	±0.05°F
T_2	Hot Water Outlet	RTD	OMEGAP-M-1/3-1/8-6-0-T-3	±0.05°F
T_3	Intermediate Loop Inlet	RTD	OMEGAP-M-1/3-1/8-6-0-T-3	±0.05°F
T_4	Intermediate Loop Outlet	RTD	OMEGA P-M-1/3-1/8-6-0-T-3	±0.05°F
T_5	Test Section Water Inlet	RTD	OMEGA P-M-1/3-1/8-6-0-T-3	±0.05°F
T_6	Test Section Water Outlet	RTD	OMEGA P-M-1/3-1/8-6-0-T-3	±0.05°F
$T_{surface}$	12 thermocouples Soldered to Test Section	Bead Thermocouple	OMEGA TT-T-36-100	±0.1°F

3.3.6 Flow rate sensors

Four mass flow meters were used to determine mass flow rates of water and refrigerant in the system. The mass flow meters used to measure the refrigerant flow rate and the plate flow rate of the test section water (loop1 in Figure 19) were accurate up to 0.1% of the reading. And the mass flow meter used for the preheater was accurate up to 0.6% of the reading. A mass flow meter was placed at the water side of the preheater loop to determine the mass flow rate of the water in the preheater, which was a critical measurement in the heat transfer coefficient and pressure drop experiment to determine the heat input into the refrigerant at the preheater section of the test setup. The mass flow meter used for the preheater loop was a Micromotion CMF050. A Micromotion CMF025 was used for the measurement of the flow rate of the water in the plate heat exchanger which provides heat flux into the refrigerant in the test section this measurement was critical to determine the heatflux into the refrigerant in the test section. Compared to the ranges of mass flow rates in the plate heat exchanger (0.36lb/min to 1lb/min) and the preheater (0.8lb/min to 10 lb/min) during experimentation in different conditions, the mass flow rate of the water loop in the test section was significantly higher (160lb/min) so a CMF100 was used to measure the water mass flow rate of the water in the test section, this mass flow meter served as an additional verification of heat input into the system from the water side of the test section. To verify the reading of the water mass flow meters, water was passed through the mass flow meter in an open loop and collected in a large drum for 2 minutes. The flow rate of the water could then be calculated from the mass of the water collected in the known amount of time. A Micromotion CMF025 was used for measurement of the refrigerant mass flow rate and is located at the exit of the refrigerant gear pump where the refrigerant is in subcooled condition. The mass flow meter for the refrigerant was already installed in the test section which could not be contaminated with water, so verification of the mass flow meter was performed with refrigerant in the system and confirmed in conjunction with the verification of the preheater as described in section 4.2.2. Figure 6 shows one of the mass flow meters, Micromotion CMF100 and the corresponding user interface for the meter.

(a) (b)

Figure 6:(a) Mass flow meter CMF100 (b)Flow meter interface

3.3.7 Pressure sensors

Two types of pressure transducers were used for pressure measurements in the test setup, absolute pressure transducers to measure the local pressure at different parts of the setup, and differential pressure transducers to measure the pressure drop across the test section. An Omega DPGM409-10BA high precision pressure transducer was used at the exit of the test section. The saturation pressure of the test was determined using this pressure transducer and its calibration was NIST traceable certified with an accuracy of 0.12psi. Figure 7 shows the transducer used at the exit of the test section, and Table 2 summarizes the specifications of the pressure transducers.

Table 2: Pressure measurement details

Location	Model#	Accuracy	Verification Technique
Parallel to test section	Validyne P55D1N4XXS-4-A	±0.25%	High Precision Manometer
Test Section Refrigerant Outlet	OMEGA DPGM409-10BA	±0.12 psi	Isobaric Comparison
Refrigerant Preheater Inlet	Setra 206, (500psig max)	±0.7 psi	Isobaric Comparison

Figure 7: OMEGA DPGM409-10BA pressure transducer

A Setra 206 (500psig max) pressure transducer was installed at the inlet of the preheater to determine the inlet conditions of the preheater in conjunction with the inline thermocouple installed at this location. The accuracy of this pressure transducer was 0.7psi. Figure 8 shows the pressure transducer used at the inlet of the preheater.

Figure 8: Setra 206 Pressure transducer

The inlet and the outlet of the test section is connected to the differential pressure transducers. There are 3 differential pressure transducers to measure the pressure drop across the test section. Lower range differential pressure transducers were used to measure the pressure drop which was lower with higher accuracy. During experimentation only one of the pressure transducers are active depending on the range of the pressure drop. For experiments where the pressure drop was lower than 5psi, the 5psi differential pressure transducer was used, similarly the 8 and the 13 psi transducers were used for higher ranges of pressure drop. The differential pressure transducers were calibrated at the start of each experiment with the help of a digital manometer.

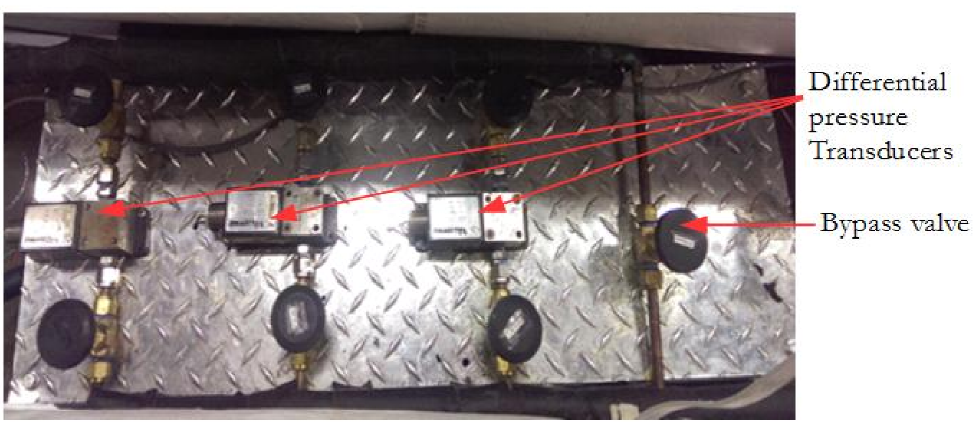

Figure 9: Differential pressure transducers

Figure 9 above shows three differential pressure transducers used for the experiment, and Table 3 summarizes the details of the sensors.

Table 3: Differential pressure transducer details

Transducer Brand (Model number)	Accuracy	Full scale
Validyne (P55D-1-N-4-36-S-4-A)	±0.25% FS	5 psi
Validyne (P55D-1-N-4-38-S-4-A)	±0.25% FS	8 psi
Validyne (P55D-1-N-4-42-S-4-A)	±0.25% FS	15 psi

3.4 Summary of the test sections developed and used in the present thesis for measuring in-tube two-phase flow boiling heat transfer coefficient and pressure drop

The realization of the test apparatus to measure the heat transfer coefficient (HTC) and pressure drop of refrigerant and lubricant (or nanolubricant) mixtures during in-tube flow boiling processes was an iterative process during this thesis period. From the first test section, referred as to TS-1, to the most recent test section, TS-5, the fifth prototype developed, instrumentation was upgraded, components were modified, and the configurations were changed in order to improve the accuracy and repeatability of the measurements. In some cases, the reconstruction of the tube test section was necessary because clean conditions of the internal walls of the tube were not restored. This challenge might have been due to nanoparticles trapped in the system, chemical attack of the internal surfaces from solvents used during the cleaning of the tube, or oil traps present in the refrigerant loop. While the TS-4 and TS-5 were the final and successful test sections used for the majority of the data presented in this thesis, TS-1 also provided good data for the two phase pressure drop measurements. A brief chronological summary of each test section is given next in order to highlight the advantages and strengths of the most recent test section design, that is, of TS-5.

3.4.1 Test section 1(TS-1)

The first test section built for the HTC and pressure drop experiment implemented the thermal amplification technique to provide heat flux into the refrigerant in the test section, this test section was named TS-1. Details for this test section can be found in a previous thesis work (Smith, 2015)but is described briefly to highlight the development of the test sections for the HTC and pressure drop experiments for this thesis work. Figure 10 shows the frontal view of the test section.

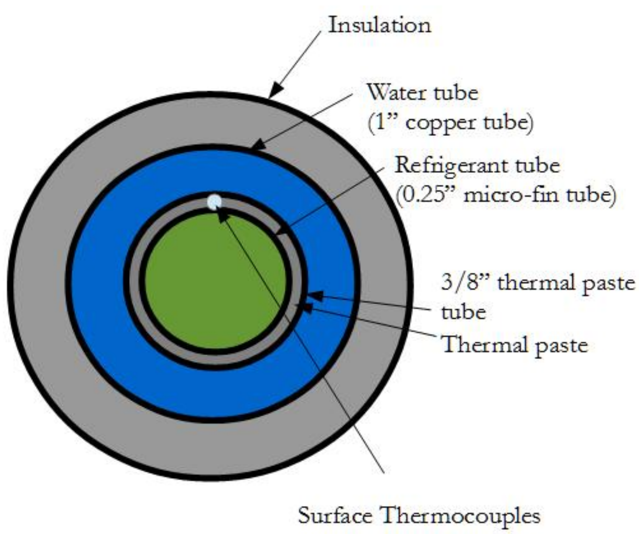

Figure 10: TS-1 developed for HTC and pressure drop experiment (frontal view)

The inner most tube was a 1/4” microfin tube which circulated the refrigerant. 8 adhesive patch thermocouples shown in Figure 11 were pasted on to the top surface of the refrigerant tube. A 3/8” smooth copper tube was then slid concentric to the refrigerant tube, and the gap was filled with thermal paste. Concentric to the 3/8” tube was a 1” copper tube which circulated water, the circulating water provided the heatflux into the refrigerant through the tube with thermal paste. The water tube was then insulated with two layers of insulation, which together was about 3 inches thick.

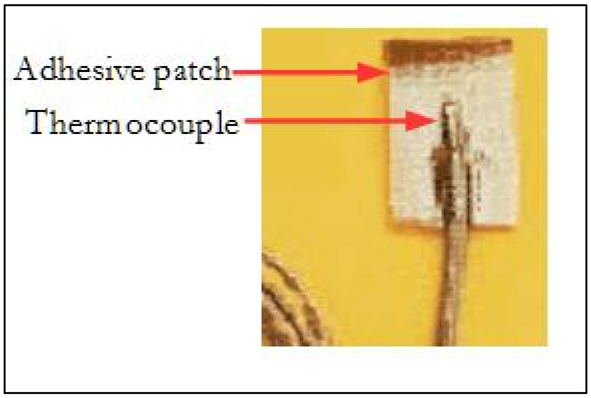

Figure 11: Adhesive Patch thermocouple used on TS-1

For the comparison of refrigerant lubricant mixtures, a test section with high precision surface temperature measurements was required. The use of the thermal paste between the refrigerant tube and the hot water introduced a slightly higher degree of uncertainty into the surface temperature measurements, which were critical to determine and compare the heat transfer coefficient of refrigerant-lubricant mixtures. Details of the accuracy of TS-1 is described in Section 5.4 To effectively capture the influence of lubricant on HTC of the test section, a more accurate test section had to be built.

3.4.2 Test section 2(TS-2)

An attempt was made to measure the HTC and pressure drop implementing a test section design where electrical heaters were wrapped directly on to the refrigerant tube. The heat flux into the refrigerant was provided from the electrical heater. Figure 12 shows a schematic of TS-2.

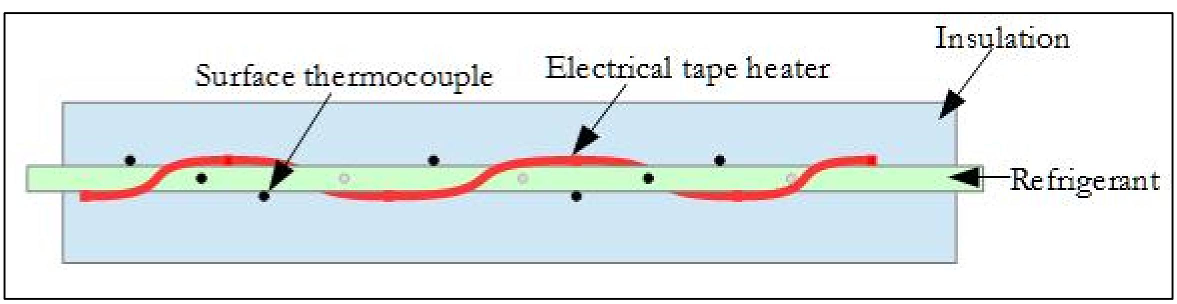

Figure 12: Test section with electrical tape heater (TS-2)

10 bead thermocouples were taped on to the test section using aluminum duct tape as shown in Figure 13.

Figure 13: Thermocouple taped on TS-2

When tests were performed at a heat flux of 7 $\frac{kW}{m^2K}$ with this design, considerably high temperatures were seen for the test section tube surface. Much higher temperatures were shown by the surface thermocouples compared to TS-1 which used the thermal amplification technique. For example, at a saturation temperature of 39.2°F, heat flux of 12$\frac{kW}{m^2K}$ and a mass flux of 350 $\frac{kg}{m^2s}$, the surface temperature of the refrigerant tube as measured by the surface thermocouples in TS-1 was about 10°F higher than the temperature of the refrigerant inside the refrigerant tube. The surface temperature for TS-2 was about 40°F higher than the temperature of the refrigerant inside the tube at the same conditions. It was hypothesized that the wire heaters influenced the surface temperature readings of the thermocouples, causing the thermocouples to show higher temperatures. After some burning odor of insulation of the test section was noticed at the higher heat flux tests of 12$\frac{kW}{m^2K}$, it was decided to open the insulation and check the test section for damage. Upon inspection of the thermocouples, it was seen that the thermocouples were burnt to a charcoal-like texture, the glue on the aluminum tape had vaporized, and the thermocouples were no longer tightly held to the tube surface. The thermocouples were still operational even though damaged by the heat from the tape heater.

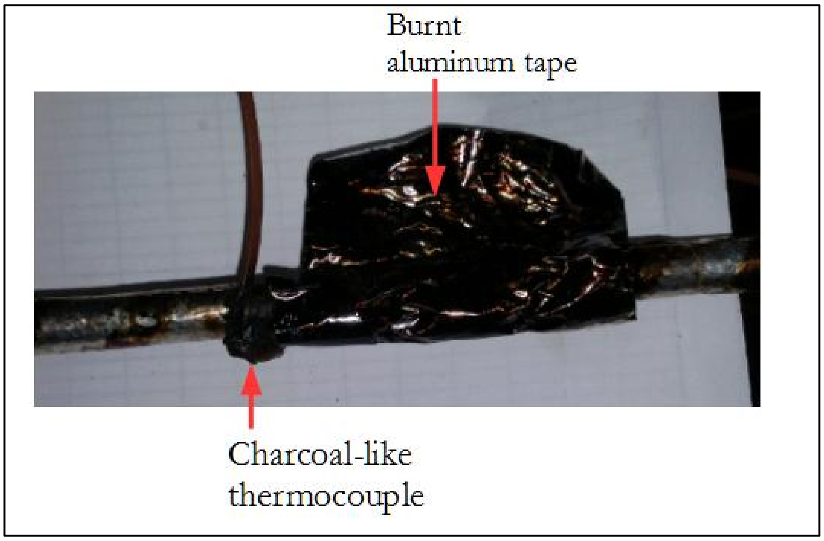

Figure 14: Thermocouple after attempted test on TS-2

To determine the HTC, it was required to have accurate measurements from the surface thermocouples. From the observed higher temperatures and the burnt thermocouples, it was decided that this design would not be used for testing nanolubricant-R410A mixtures.

3.4.3 Test section 3(TS-3)

Another attempt was made to measure the heat transfer coefficient using electrical heaters on a test section which would use a thermal conduction technique to provide heat flux into the refrigerant. The following is a description of the test section.

Figure 15 and Figure 16 shows the test section using the thermal conduction technique to provide heat flux into the refrigerant.

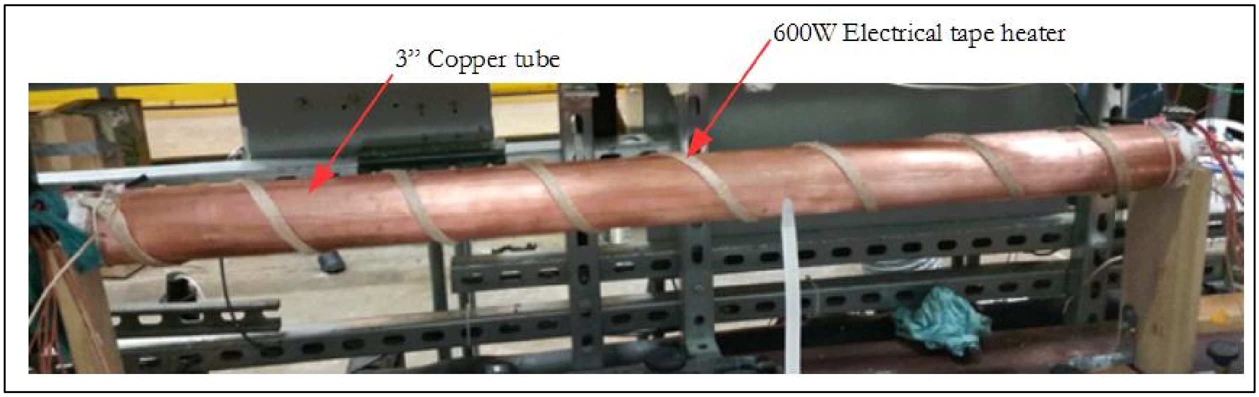

Figure 15: Thermal conduction test section with tape heater

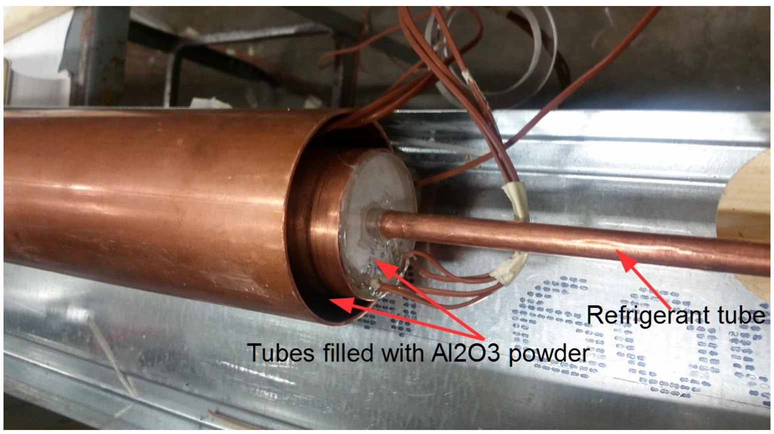

Figure 16: Thermal conduction test section

The test section is made of 3 concentric tubes. Refrigerant passes through the inner most tube and a 2 inch tube, filled with alumina powder is built concentric to the refrigerant tube. Thermocouples are taped on the surface of both the 1/4th inch refrigerant tube and the 2inch tube copper using aluminum tape. The outer most tube is a 3 inch tube on which a wire heater is wrapped, which provides the heat input into the system.

A schematic of this test section is shown in Figure 17.

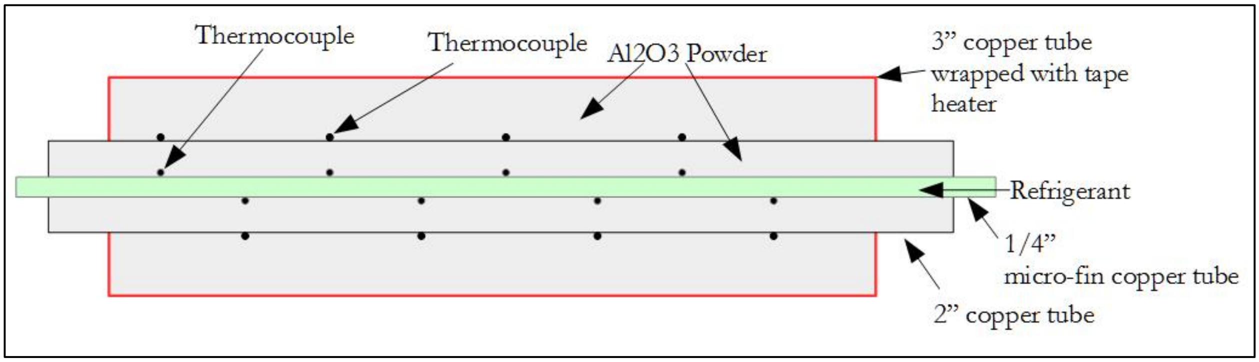

Figure 17: Conduction test section design

After the test section was built it was seen that the alumina powder did not have a high enough thermal conductivity, and applying heat flux on the outer 3 inch tube only heated the outer surface of the 3 inch tube and the alumina powder did not conduct enough heat into the test section to provide the heat flux need for the experiments. After several attempts were made to achieve the desired heatflux without success, this test section design was abandoned.

3.4.4 Test section 4 (TS-4)

After attempts on test sections using electrical heaters, another test section was made using the thermal amplification technique. This test section worked on the same principle as TS-1. However there were several improvements in the design from the lessons that were manifested from the 255 data points conducted on TS-1. Figure 18 shows a frontal view of the test section.

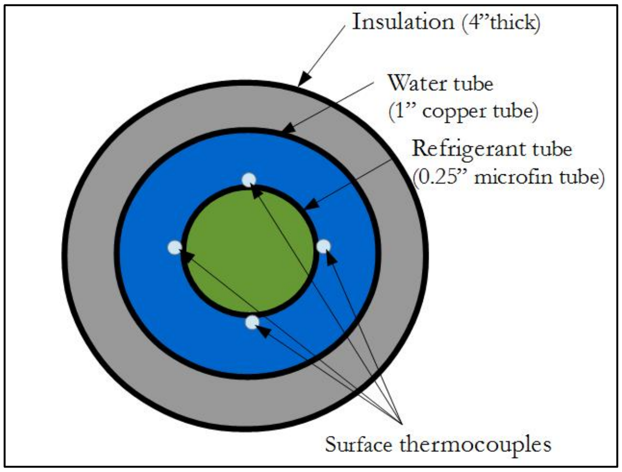

Figure 18: Frontal view of TS-4

Comparing TS-4 to TS-1, the tube containing the thermal paste in the design of TS-1 was removed, and the refrigerant tube was exposed to the water in the outer tube providing the required heat flux for the experiments, the refrigerant flows in the inner tube exchanging heat with the water. Exposing the refrigerant tube also meant exposing the surface thermocouples to high velocity water, which was 160lb/min through the 1" tube during tests. To ensure that the thermocouples were secure from detachment due to the high velocity water, they were soldered on to the surface of the refrigerant tube. The water tube was then insulated with 3 layers of insulation, the first layer in contact with the 1 inch water tube was 1" thick rubber insulation, the second layer of insulation used was a 2 inch thick fiber glass insulation, another 1" thick rubber insulation was wrapped around the fiber glass insulation. Figure 19 shows a schematic of the test section which is fundamentally a 6ft long tube in tube heat exchanger.

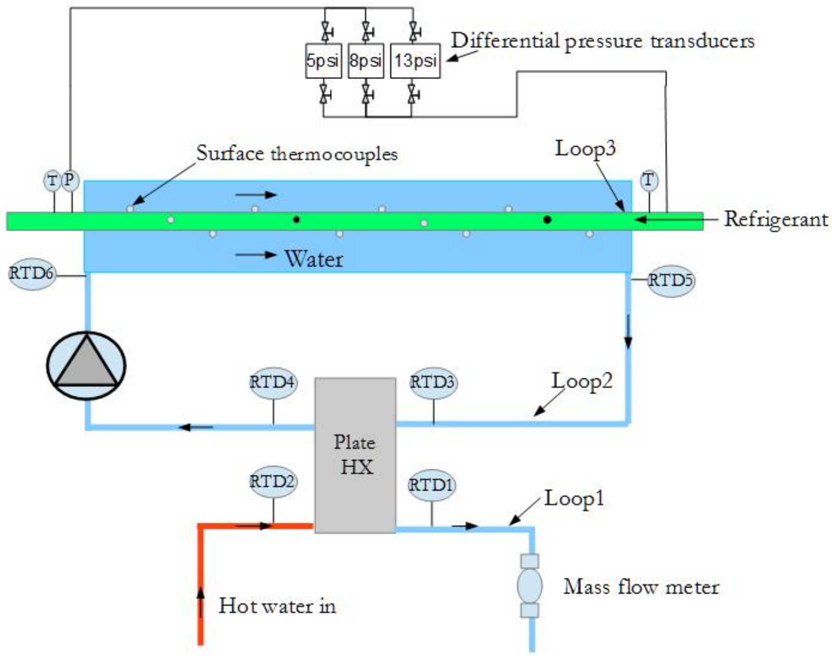

Figure 19: Schematic of the test section

Heat is gained by the refrigerant from the centrifugal pump which circulates the water in loop2. The hot water in loop 1 transfers heat into the water circulating in loop2 which in-turn transfers heat into the refrigerant. The outlet of the test section has an inline thermocouple and an absolute pressure transducer, and the inlet of the test section has an inline thermocouple as well. A differential pressure transducer is used to measure the pressure drop across the test section. Twelve 30gage wire thermocouples were soldered on to the surface of the refrigerant tube to measure the surface temperature. Figure 20 shows a thermocouple that was soldered to the test section.

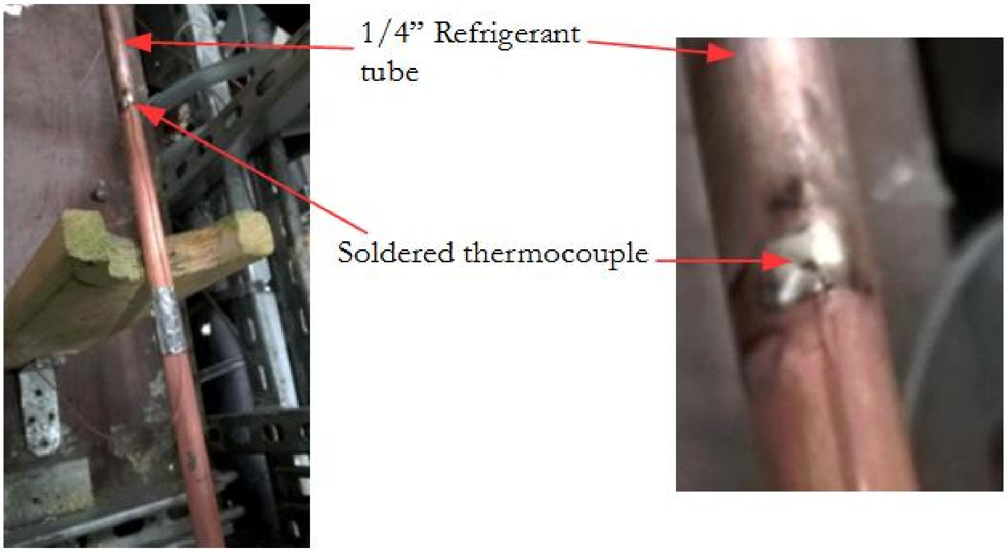

Figure 20: Test section thermocouples

The refrigerant tube (microfin tube) was donated by Wolverine Tube and is the model Turbo A pipe, the geometry of this tube is described in Table 4. The parameters for equivalent diameter, cross-sectional area, and inner surface area were calculated using the method described in Choi *et al.* (1999) (see equations (1) to (6)). The length "L" of the test section is the active heat transfer length in the axial direction, determined by the inlet and outlet location of the water providing the heat flux into the refrigerant tube. Other parameters were obtained from the Wolvirine Tubes product datasheet for the Turbo A tube. A schematic of the cross sectional geometric details is shown in Figure 21. All test sections were built using this type of microfin tube, a new length of tube was used for the construction of each design during development of the test section.

Table 4: Geometry of the Turbo A microfin tube

Parameter	Dimension	Use
Outer diameter, d_o =	9.53 mm (0.375 in)	Multiple Geometry Calculations
Number of internal Fins, N =	60	Multiple Geometry Calculations
Fin Length, L_f =	0.203 mm (0.008 in)	Multiple Geometry Calculations
Apex angle, γ =	30°	Multiple Geometry Calculations
Equivalent diameter, d_e =	8.8 mm (0.35 in)	Comparison Purposes
Wall thickness, t_w =	0.3 mm (0.012 in)	Determination Of Inner Diameter
Length, L =	2.4 m (7.83 ft.)	Determination Of Surface Area
Cross Sectional Area, A_c =	60.8 mm^2 (0.094 in^2)	Calculation of Mass Flux
Helical Angle, β =	18°	Determination of Hydraulic Diameter
Wetted Perimeter, P_w	46.7 mm (1.84 in)	Calculation Of Surface Area
Inner Heat Transfer Surface Area, $A_{Surface}$	107,040 mm^2 (165.9 in^2)	Calculation of Heat Flux

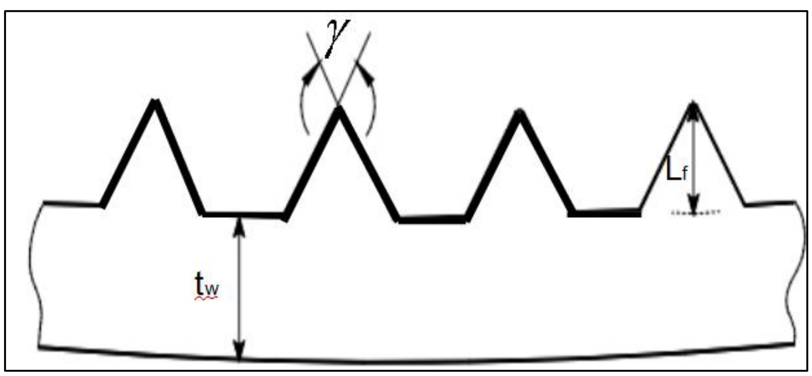

Figure 21: Micro-fin tube geometry

$$d_i = d_o - 2 \cdot t_w \tag{1}$$

$$A_f = \frac{L_f^2}{2 \cdot \tan(\frac{\gamma}{2})} \tag{2}$$

$$A_c = \frac{\pi \cdot d_o^2}{4} - N \cdot A_f \tag{3}$$

$$d_e = \sqrt{\frac{4 \cdot A_c}{\pi}} \tag{4}$$

$$P_w = d_i \cdot \pi + \left(\left(-2 \cdot L_f \cdot \tan\left(\frac{\gamma}{2}\right)\right) + \left(2 \cdot \frac{L_f}{\cos\left(\frac{\gamma}{2}\right)}\right)\right) \cdot N \tag{5}$$

$$A_{Surface} = P_w \cdot L \tag{6}$$

3.4.5 Test section 5(TS-5)

Due to reasons discussed in section 5.5, another test section similar to TS-4 was built. The only difference between the two test sections were that for TS-4, 30 gage thermocouple wires were used for the surface thermocouples soldered on to the test section, whereas for TS-5, finer-36gage wires were used as surface thermocouples. However, TS-4 and TS-5 showed the same results which is later discussed in section 5.5.

3.5 Uncertainty analysis

The methods of error analysis and uncertainty propagation outlined in (Taylor, 1997) was used for calculating the uncertainties of experiments, and the values of the uncertainties is shown in the table below.

Table 5. Experimental uncertainties of experiments

Measurement objective	Parameter	Uncertainty
Solubility	$\frac{\delta w_{\%r}}{w_{\%r}}$	±1.04 ($0 \leq w_{\%r} < 5$) ±0.55 ($5 \leq w_{\%r} < 10$) ±0.09 ($10 \leq w_{\%r} < 40$)
Heat transfer Coefficient ratio	$\frac{\alpha}{\alpha_0}$	±10.7
Pressure drop ratio	$\frac{\delta(\Delta P/\Delta Po)}{\Delta P/\Delta Po}$	±0.02

Uncertainties are expressed with confidence level of 95.5%

CHAPTER 4

EXPERIMENTAL METHODOLOGY

4.1 Procedure to measure the solubility of refrigerant R-410A in the nanolubricants

Tests were conducted which could be compared to literature for the solubility tests to verify the solubility test setup. The solubility results of R410A and POE were within 5% agreement with Cavestiri's results found in the ASHRAE Refrigeration Handbook (2010). The results of the validation of the test setup is shown discussed in the results section of this experiment.

The solubility tests were conducted by measuring the weight of refrigerant that was solubilized in the nanolubricant. This was done by submerging the conditioning tank into the water bath which was maintained at constant temperature. The conditioning tank was then depressurized to approximately 1.5 psia (10.34 kPa) using the vacuum pump. 200mL of nanolubricant was introduced into the conditioning tank through the Schrader valve at the bottom of the conditioning tank, taking advantage of the pressure difference between the atmosphere and the conditioning tank. Refrigerant R-410A was introduced into the tank through the bottom of the tank until the required pressure was achieved. The mixture was allowed to reach thermal equilibrium under the specific temperature and pressure. The temperature of the bath was monitored using a thermocouple, and the pressure was monitored using an absolute pressure transducer. To make sure that equilibrium was achieved, the vapor pressure of the conditioning tank was monitored until the pressure stabilized at the desired pressure of measurement. The recovery tank was then depressurized to a pressure of about 1 psia (6.8 kPa), using the vacuum pump. The tare weight of the recovery tank was measured and recorded as w_o. The refrigerant-nanolubricant mixture was then extracted into the recovery tank and the weight of the mixture and the recovery tank was recorded as w_{NL+Ref}. The recovery tank was then placed into a hot water bath at a temperature of about 60°C, the vacuum pump was used to depressurize the tank to approximately 1 psia (6.8 kPa). The remaining oil in the recovery tank was then measured and recorded as w_{NL}. The weight of the refrigerant vacuumed out of the recovery tank divided by the weight of the refrigerant and oil after extraction was the weight percent of refrigerant in the nanolubricant shown in Eq.5.

$$w_{\%ref} = \frac{w_{ref}}{w_{NL} + w_{ref}} \quad \textbf{(7)}$$

4.2 Procedure to measure heat transfer coefficient and pressure drop

A known quantity of R410A is first charged into the system until there is enough subcool for the variable speed gear pump to circulate the refrigerant. The mass flow rate of the refrigerant is regulated by adjusting the speed of the variable speed gear pump. The mass flow rate of the hot water in the preheater is adjusted to provide the amount of heat input needed to achieve the required test section inlet quality. The flow rate of the water in the test section is then adjusted to provide the right amount of heat flux for the test. Once the system is in equilibrium with the required conditions of temperature, pressure, heatflux, and massflow rate a recording is taken in LabView.

During the heat transfer experiments, the inlet of the test section was in the two phase region and Equation (8) was used to solve for the test section inlet enthalpy of the refrigerant, h_{TS_in}. Equation (8) is an energy balance on the preheater of the test setup where the LHS of is known from water properties and the measured mass flow rate, $\dot{m}_{PHwater}$, and inlet and outlet temperatures of the water. The refrigerant at the preheater inlet was always at subcooled condition. With measured pressure and temperature values, the enthalpy of the refrigerant at the inlet of the preheater could be determined.

$$\dot{m}_{PHwater} \cdot C_{p_{water}} \cdot \left(T_{w_i} - T_{w_o}\right) = \dot{m}_{ref} \cdot (h_{r_{pre_{out}}} - h_{r_{pre_{in}}}) \quad \textbf{(8)}$$

where

$$h_{pre\_out} = h_{TS\_in}$$

The heat transfer into the test section was calculated by adding the individual components contributing to the heat input into the refrigerant in the test section. Details of how these values are determined are discussed in detail in section 4.2.3.

$$Q_{TSr} = Q_{plate} + Q_{pump} \quad \textbf{(9)}$$

The heat flux into the test section, $q"$, was then calculated by simply dividing the heat transfer rate into the refrigerant, Q_{TSr}, by the surface area of the test section, $A_{surface}$. This is the heat flux reported in the results of the experiments.

$$q" = Q_{TSr}/A_{surface} \quad \textbf{(10)}$$

The enthalpy of the refrigerant at the test section outlet, h_{TS_out}, is then calculated using the heat transfer rate into the test section Q_{TSr} in the following equation:

$$h_{TS\_out} = \frac{Q_{TSr}}{\dot{m}_{ref}} + h_{TS\_in} \quad \textbf{(11)}$$

The quality at the exit of the test section is then determined as a function of temperature and enthalpy:

$$x_{TS\_out} = f(T_{TS\_out}, h_{TS\_out}) \quad \textbf{(12)}$$

Once the outlet quality of the refrigerant exiting the test section was obtained, the average quality of each test during the experiment could be calculated using equation (13). This is the average quality with respect to which the heat transfer coefficient and pressure drop results are reported in the results.

$$x_{TS\_av} = \frac{x_{TS\_in} + x_{TS\_out}}{2} \qquad \textbf{(13)}$$

The internal wall temperature of the refrigerant tube could be calculated from the measured outer wall surface temperatures using the radial heat conduction equation for a tube shown in equation (14), where d_o is the outer diameter of the refrigerant tube and d_i is the inner diameter of the refrigerant tube.

$$T_{wall\_in} = T_{surface\_out} - \frac{q" \cdot \ln(d_o/d_i)}{2\pi k} \qquad \textbf{(14)}$$

The heat transfer coefficient α is then calculated using the convection heat transfer equation shown in equation (15).

$$\alpha = \frac{q"}{T_{r,sat} - T_{wall,in}} \qquad \textbf{(15)}$$

Pressure drop in the test section was a direct measurement using one of three differential pressure transducers installed across the test section shown in Figure 3. The differential pressure transducers covered 3 ranges of pressure drop, one for the low range from 0 to 34 kPa (0 to 5 psi), of 0-55 kPa (0-8 psi) for medium range, and one for the high range from 0 to 89.63 kPa (0 to 13 psi). The accuracy of each pressure transducer was ±0.1% of the full scale reading.

The measured pressure drop was divided by the length between the two pressure taps in the test section in order to obtain an average pressure gradient along the test section for each saturation temperature and quality.

4.2.1 Calibration and validation of the thermocouples in the HTC and pressure drop test setup

All thermocouples were calibrated in a temperature bath to an accuracy of 0.1°C (0.2°F) using a calibration bath. Since the surface thermocouples were soldered on to the outer surface of the test section which was a 6ft long tube, validation of these thermocouples could not be performed in the temperature bath. Instead, validation of temperature readings of the surface thermocouples were done using refrigerant while the test setup was operational. The following is a description of the tests performed to validate the surface thermocouples and the inline thermocouples at the test section inlet and exit.

Figure 22 shows the surface temperature pattern of 11 thermocouples during flow boiling at a saturation temperature of approximately 4°C (39.2°F). During the first 40 minutes of the recording, the refrigerant is in the two phase region. After about 40 minutes into the experiment, the quality at the inlet of the test section was increased until the quality of the refrigerant is close to saturated vapor (dry out). When the refrigerant is in this region of quality, dry out of the refrigerant occurs and the surface temperature of the refrigerant tube fluctuates between the liquid refrigerant temperature and the vapor temperature. After the refrigerant achieves superheat, the surface thermocouples stabilize (with regard to fluctuation between liquid and vapor temperature during dry out) showing the temperature of the superheated refrigerant in the tube. It is to be noted that the temperature variation of the surface thermocouples with regard to each other in the superheat region is much narrower in than in the two phase region as seen in the figure below.

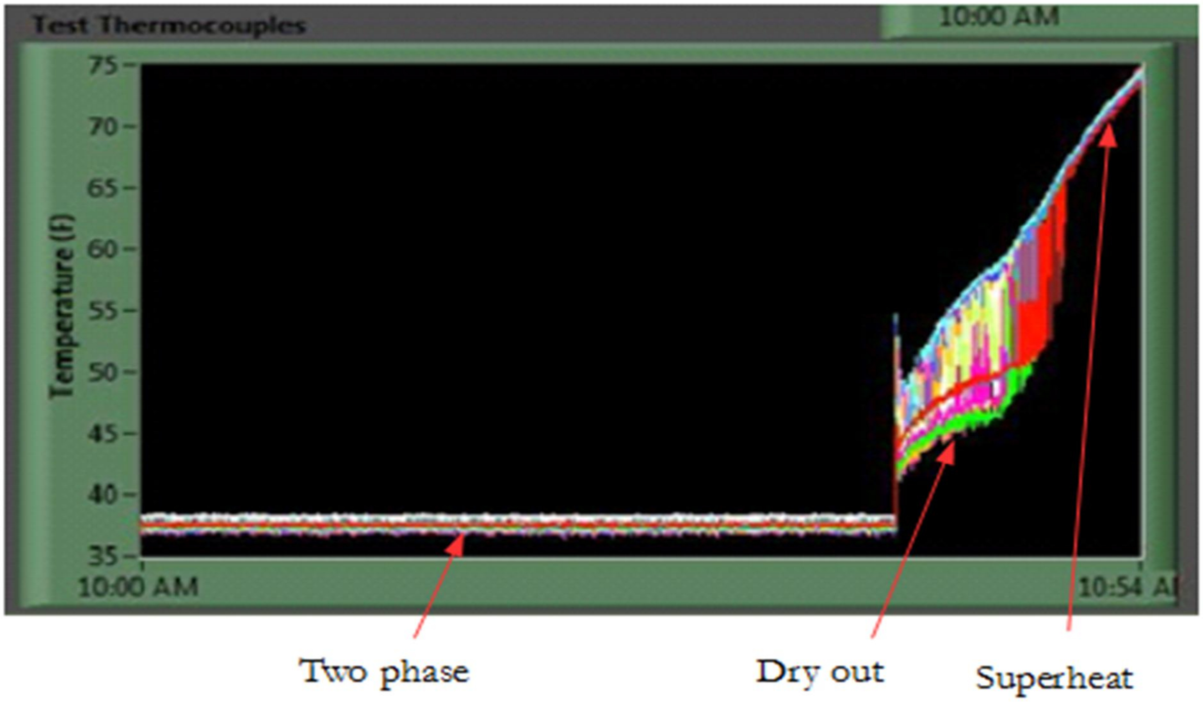

Figure 22: Surface temperature pattern of surface thermocouples during flow boiling

Once the temperatures of the inline and surface thermocouples stabilized at a certain temperature, the condition of the test section was regarded as isothermal with minimal variation between the inlet and outlet temperatures, as shown in the following figure. The isothermal tests were performed with no heat flux into the test section, allowing an approximate isothermal condition in the test section.

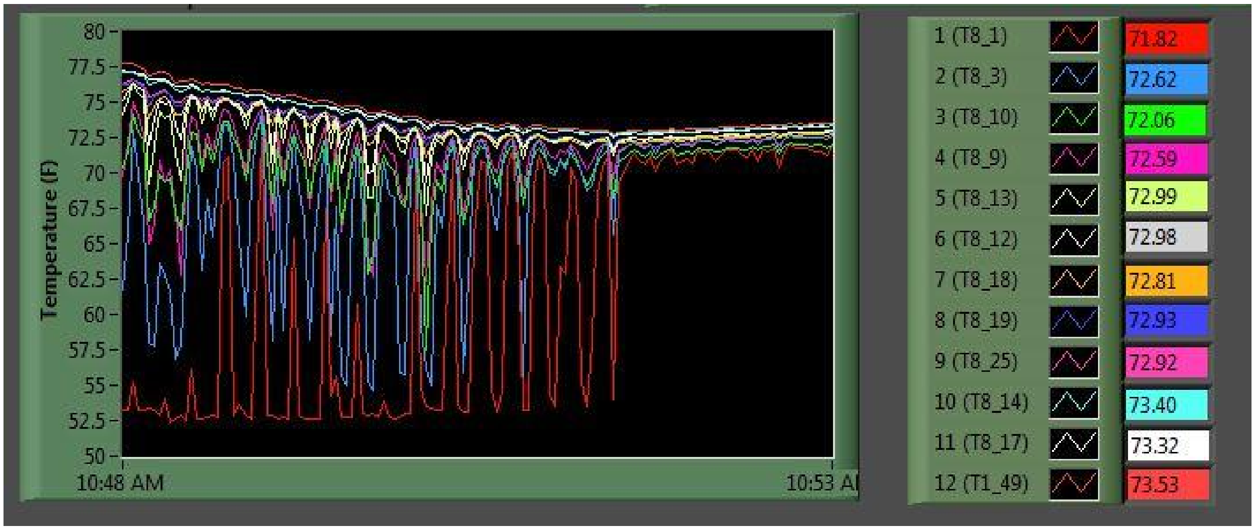

Figure 23: Achieving equilibrium in superheat condition

Figure 24 shows the thermocouple values obtained from the experiment. The inline thermocouples at the inlet and the exit of the test section varied by about 0.4°C (0.8°F). It is seen that the surface thermocouples also have a linearly decreasing trend in temperature readings and is bounded by the values of the inline thermocouples. The difference between the individual thermocouples and the line drawn between the two inline thermocouples were calculated and the values of the temperature readings were within the uncertainty of the thermocouples, 0.1°C (0.2°F). This was a confirmation that the surface thermocouples were within calibrated values after the construction of the test section. This was an important confirmation as the heat transfer coefficient results calculated was extremely sensitive to the surface temperature measurements. A deviation of 0.4°F on the average surface thermocouple readings could offset the heat transfer coefficient results by 40 percent!

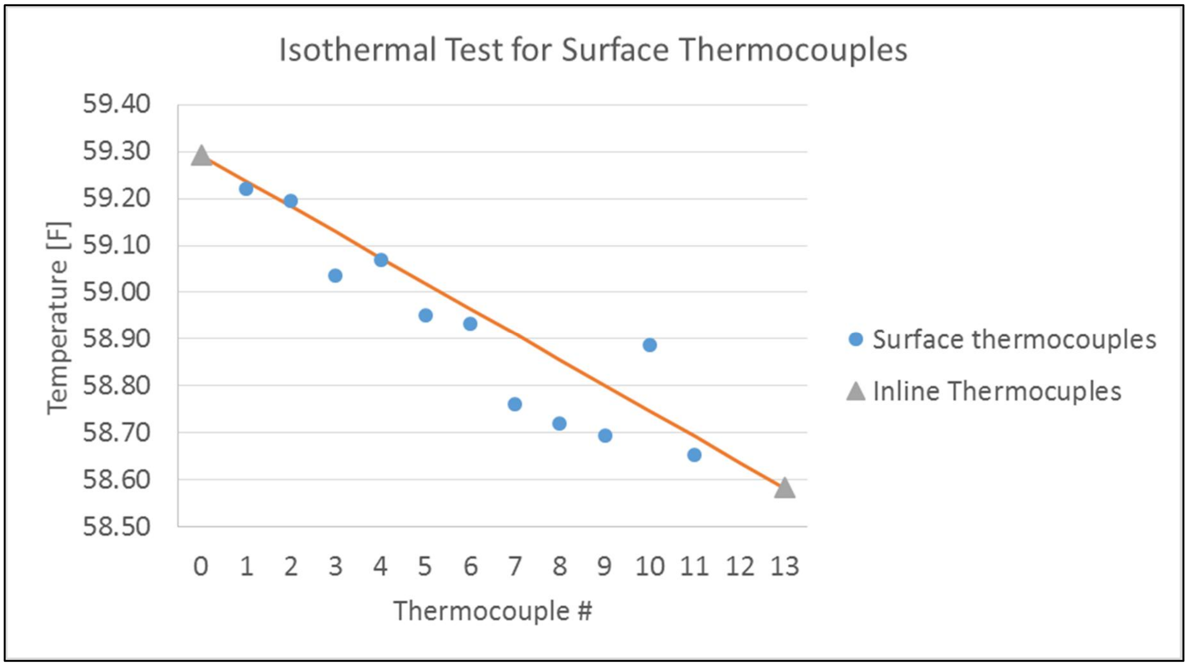

Figure 24: Surface thermocouple temperatures of 11 thermocouples during the isothermal experiment

4.2.2 Validation of heat transfer in the preheater

A heat balance was performed at the preheater to determine if heat was exchanged effectively in the preheater between the water and the refrigerant in the preheater section. To perform this validation, the refrigerant was made to enter the preheater in sub-cooled condition and exit the preheater in super heat condition, this was done so that the enthalpy change of the refrigerant can be found from the temperature and pressure readings at the entrance and the exit of the preheater, this could not be done if either the entrance or the exit of the preheater was in two phase as phase change occurs at the same temperature and pressure and the enthalpy of the refrigerant cannot be determined from pressure and temperature in the saturated region. The heat gained by the refrigerant in the preheater is then determined using:

$$\dot{Q}_{PH\_r} = \dot{m}(h_{PH\_out} - h_{PH\_in}) \qquad \textbf{16)}$$

And the heat loss from the water in the preheater is:

$$\dot{Q}_{PH\_w} = \dot{m}_{PH\_w} c_p (T_{PH\_w,out} - T_{PH_w,in}) \quad \textbf{(17)}$$

Table 6 shows the results obtained from the heat balance tests which compare the heat gained by the refrigerant and the heat lost by the water in the preheater tests 1 through 4 are performed with the refrigerant in the test section in superheat condition, and tests 5 through 7 are performed with the refrigerant in the test section in saturated vapor state. The heat balance of the preheater was within 2%.

Table 6: Heat balance of the preheater

Test #	Qref Preheater [BTU/min]	QwaterPre [Btu/min]	Heat Balance Preheater %
1	258.54	258.50	-0.74
2	260.32	259.87	-0.04
3	260.30	259.36	-0.09
4	264.92	264.43	-0.05
5	173.37	173.37	0.00
6	169.16	169.16	0.00
7	147.15	154.32	1.19

4.2.3 Validation of heat transfer in the test section

Tests were performed to determine the heat transfer in the test section. Figure 25 shows a schematic of the components which are involved in heat transfer in the system.

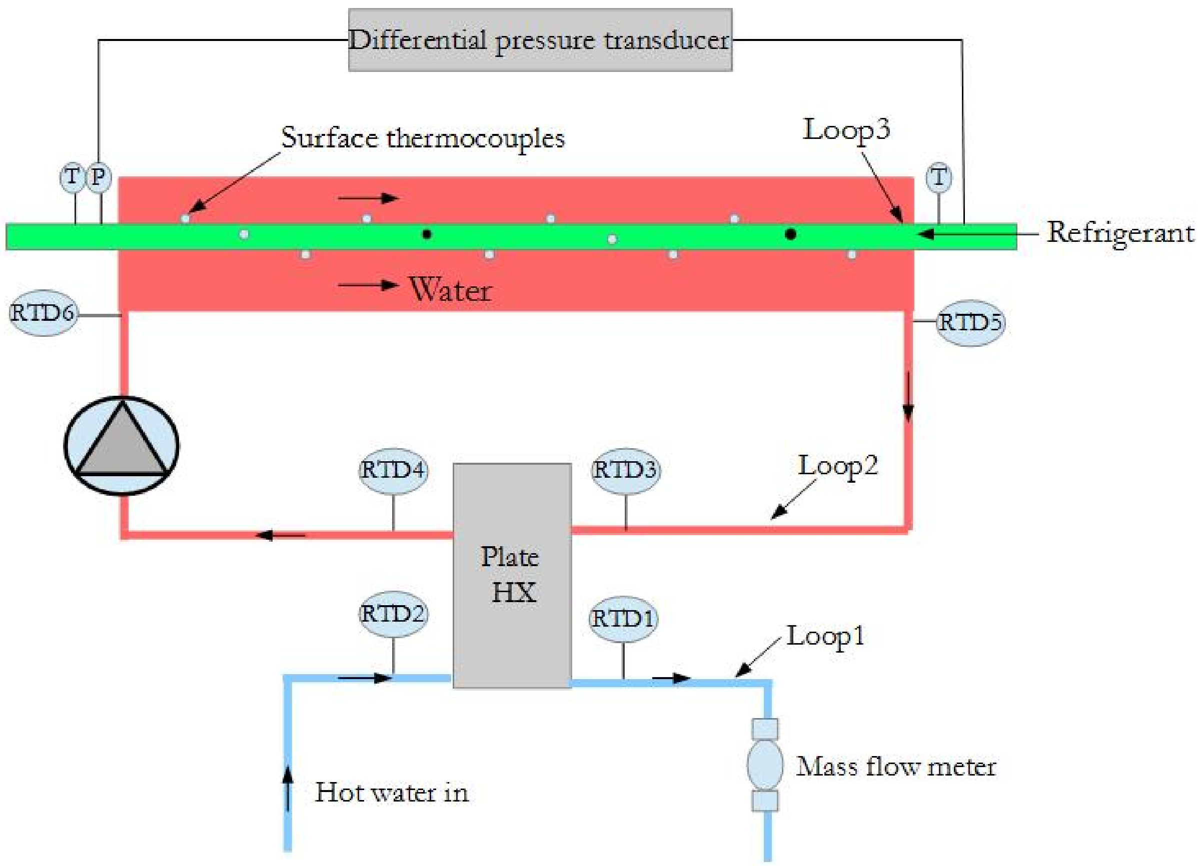

Figure 25: The TS-4 during heat balance in super heat condition

Loop1 transfers heat across the plate heat exchanger with the water in loop 2 which is circulated with a pump at a constant speed. The water pump in loop 2 adds a certain amount of heat in the system which was unknown and had to be determined accurately. To find this power added to the system by the pump, an experiment was performed where loop 2 had the highest temperature relative to loop 3 and loop 1. When the setup was operated in this condition the heat generated by the pump was transferred to the refrigerant in the test section and the plate. An energy balance of loop 2 would yield:

$$\dot{Q}_{pump} = \dot{Q}_{ref} + \dot{Q}_{plate} \tag{18}$$

Tests were conducted at different water temperatures in loop 2. The enthalpies of the subcooled refrigerant at the inlet and the superheated refrigerant at the exit of the test section could be calculated using the pressure and temperature measurements of the refrigerant. $\dot{Q}_{ref}$ was calculated using

$$\dot{Q}_{ref} = \dot{m}_{ref}(h_{out} - h_{in}) \tag{19}$$

The heat transfer of the water on the plate was calculated as

$$\dot{Q}_{plate} = \dot{m}_{water}(T_{out} - T_{in}) \tag{20}$$

The electrical power ($\dot{W}_{pump}$) consumed by the pump was measured using a watt meter. Tests were conducted to observe the power input of the pump into the system at different conditions of water temperature and mass flow rate of the water, and the results are shown in Table 7. Tests number 1 through 4 were performed with the refrigerant in the test section in super heat condition. From the experiment, it was determined that with varying conditions, the heat transfer into the plate and the refrigerant vary with different temperature in loop 2, but it was found that the sum of the heat going into the plate and the refrigerant was always 0.69 times the electrical power consumed by the pump for all four tests.

Table 7: Results of tests conducted to determine pump power with vapor refrigerant flow in the test section tube

Test #	Qref_TS [BTU/min]	Qpump [btu/min]	Coefficient	Qplate_hot [BTU/min]	Q_TS_water [BTU/min]	Pump power Wdot [Btu/min]
1	20.99	47.90	0.69	-26.91	25.56	69.85
2	18.54	47.79	0.68	-29.26	12.42	69.95
3	18.52	52.34	0.69	-33.81	13.24	76.24
4	14.29	56.35	0.69	-42.06	12.85	81.70

However, during actual tests of two phase flow boiling, both the heat gain from the pump as well as the plate go into the refrigerant. With the system in this condition, the energy balance of the system is:

$$\dot{Q}_{ref} = \dot{Q}_{pump} + \dot{Q}_{plate} \tag{21}$$

Tests 5 through 7 in Table 8 was conducted in conditions where the refrigerant is in two phase in the test section and exit the test section at superheat condition.

Table 8: Results of tests conducted to determine pump power with two phase flow refrigerant in the test section tube

Test #	Qref_TS [BTU/min]	Qpump [btu/min]	Coefficient	Qplate_hot [BTU/min]	Q_TS_water [BTU/min]	Pump power Wdot [Btu/min]
5	81.60	43.13	0.67	38.47	70.53	64.23
6	88.16	46.67	0.72	40.67	76.80	64.53
7	128.68	44.48	0.69	80.00	111.25	64.26

The heat gain into the refrigerant is calculated using equation (21), and the coefficient was found to be approximately 0.69 again. Therefore it was established that the water received energy from the pump in the form of work rate required to circulate the water and in the form of heat transfer rate from heat conduction from the (warm) electric motor of the pump to the pump shaft rotor, impeller, and casing. The overall coefficient that characterized the conversion efficiency from the electric work given to the pump to the combined effect of work and heat transfer rates given to the fluid was $\eta_{pump} = 0.69$. This factor η_{pump} can be thought as the combined pump mechanical and electrical efficiency and it also included the part of heat transfer rate that was rejected to the water circulating inside the pump and coming from heat conduction from the pump electric motor. Thus, the total energy, $\dot{Q}_{pump}$, provided to the water flow that circulated in the pump was:

$$\dot{Q}_{pump} = 0.69 \cdot \dot{W}_{pump} \tag{22}$$

4.2.4 Corollary1 for the validation of the heat transfer in the preheater and test section

It is to be noted that during the validation tests conducted with two phase entering the test section and superheat at the exit of the test section (i.e., tests 5 to 7 in Table 8). The fluid is entering the test section in two phase, and the exact quality of the refrigerant at this section of the setup cannot be determined by the temperature and pressure readings alone. To overcome this problem, the heat input from the water side of the preheater is used to locate the quality at the preheater exit/test section inlet, since the heat balance at the preheater was determined to be less than 2% from section 4.2.2. The properties of the subcooled refrigerant at the inlet of the preheater is known from temperature and pressure measurements. With known refrigerant enthalpy at the inlet of the preheater, and known heat gain from the water side, the enthalpy of the two phase refrigerant at the inlet of the test section could be determined using:

$$h_{PHout} = \frac{\dot{Q}_{PH\_w}}{\dot{m}_r} + h_{PH\_in} \tag{23}$$

And quality at the test section inlet is determined from the refrigerant thermodynamic table as a function of temperature and enthalpy,

$$x_{TS\_in} = f(T_{PHout}, h_{PHout}) \qquad \text{,where } T_{PHout} \text{ is measured} \tag{24}$$

The enthalpy of the superheated refrigerant at the outlet of test section is found using the temperature and pressure readings. Knowing the enthalpy difference of the refrigerant at the test section, the heat gain into the refrigerant is calculated with equation (19). This was then compared to the heat transfer from the pump and the plate represented by equation (21). As seen in tests 5 through 7 in Table 8, it was found that.

$$\dot{m}(h_{TSout} - h_{TSin}) = {\sim}0.69 \cdot \dot{W}_{pump} + \dot{Q}_{plate} \tag{25}$$

However using the preheater water side to determine the enthalpy at the inlet of the test section introduced an uncertainty which changed the coefficient value to range from 0.67 to 0.72. It is assumed that this uncertainty arises from heat loss in the preheater to the ambient at a rate of about 2% which changes the enthalpy at the inlet of the test section. It was decided to proceed with the experiment with a coefficient value of 0.69· W_{pump} for the contribution of the pump toward heat gain of the test section.

4.2.5 Determination of Saturation Temperature

The calculated heat transfer coefficient in equation (15) depends on the refrigerant saturation temperature, since R410A is a commercially prepared mixture of difluoromethane (CH_2F_2, called R-32) and pentafluoroethane (CHF_2CF_3, called R-125), there may be differences in composition of the refrigerant mixture when produced by the manufacturers. As a result of the deviation in composition, there may be differences in the properties of the refrigerant with regard to the saturation temperature and pressure relationship. To capture this difference in saturation temperature experiments were performed to determine the actual saturation conditions of the refrigerant.

Temperature and pressure readings at the test section were taken at the range of qualities tested, and the values were used to solve for the coefficients of the correlation used in a similar experiment (Sawant *et al.*, 2007), this co-relation was found in an earlier work where the saturation conditions of temperature and pressure for several refrigerants were tested and co-related (Thome, 1995).

$$\frac{1}{T_{sat}} = A_0 + A_1 \cdot \ln(P_{sat}) + A_2 x \tag{26}$$

The test setup was operated without any heat input in the test section. The temperature, pressure of three tests at different quality was used to formulate a system of three equations and three unknowns to determine the coefficients, $A_0,\ A_1, and\ A_2$. After solving for the coefficients, the pressure was then used to solve for the saturation temperature of the experiments during data reduction. The values of the constants for the pure refrigerant was found to be:

Table 9: Coefficients for saturation co-relation

A_o [K^{-1}]	A_1 [K^{-1}]	A_2 [K^{-1}]
5.96 x 10^{-3}	-3.44 x 10^{-4}	-4.548 x 10^{-7}

4.2.6 Determination of saturation conditions with oil and nanolubricants

Addition of oil adversely affects the local saturation temperatures. A comprehensive method was developed by (Thome, 1995) to capture the effect of refrigerant-oil mixtures on the saturation properties and the heat transfer characteristics of the refrigerant. From their study, a co-relation was developed to capture the effect of addition of oil on the saturation temperature and corresponding saturation pressure with the following equation:

$$\frac{1}{T_{sat,o}} = \frac{\ln\left(P_{sat,o}\right) - b + \frac{A_2}{A_1} x_o}{a} \tag{27}$$

Where a and b are fourth degree polynomials calculated with the local lubricant mass fraction:

$$a = -2292.34K + 182.5K \cdot w_1 - 724.2K \cdot {w_1}^2 + 3868.0K \cdot {w_1}^3 - 5268.8K \cdot {w_1}^4 \tag{28}$$

$$b = 15.146 - 0.722 \cdot w_1 + 2.391 \cdot {w_1}^2 - 13.779 \cdot {w_1}^3 - 17.066 \cdot {w_1}^4 \tag{29}$$

Where the local lubricant mass fraction w_1 was calculated from the quality and the lubricant mass fraction (w_b), using the equation found in (Thome, 1995).

$$w_1 = \frac{1}{\frac{1-x}{w_b} - 1} \tag{30}$$

The first term in equation (29) was adjusted such that equation (27) produced the same saturation temperature as in the case of pure refrigerants calculated with equation (26).

4.2.7 Lubricant injection procedure for POE and nanolubricant tests

The oil injection system was first vacuumed using a vacuum pump removing the air inside the system. With the low pressure in the oil injector, lubricant was then sucked into the oil injection system. The bottom metering value was then closed and the oil injector containing the oil was then vacuumed for 30 minutes. At first air bubbles were seen as the air inside the lubricant was released from the oil due to the low pressure, the vacuum process was stopped when no bubbles being released from the oil was observed, this process generally took twenty to thirty minutes. After the oil was vacuumed, R410A at room temperature was introduced into the oil injection system. Compared to the refrigerant in the system at 4°C (39.2 °F) the refrigerant used to inject the lubricant was at a much higher pressure. The bottom metering valve of the oil injector was then slightly opened (about three fourths of a turn) and the ball valve isolating the test setup from the oil injection system was opened. This enabled the lubricant to travel into the system. The sight glass attached to the oil injection system shown in Figure 4 was used to keep track of the injection rate of oil into the system. It was made sure that the oil was injected at a slow rate such that the lubricant was mixed in the refrigerant flowing in the system evenly. The amount of refrigerant entering the system was recorded by measuring the weight of the tank containing the R410A at room temperature at the beginning of lubricant injection. After injection was complete, the weight of the tank was measured again and the difference between the start weight and the weight of the tank after the injection was recorded. This was done to keep an accurate account of the refrigerant present in the system during tests. A marginal amount of refrigerant was introduced to the system while injecting oil, the amount was approximately 0.1 lbs (0.045 kg). Once injection was complete, the ball valve on the system was closed and the metering valve on the oil injector was closed. The weight of residue oil which stuck to the surface of the tube of the oil injector was measured to keep an account of the oil injected into the system.

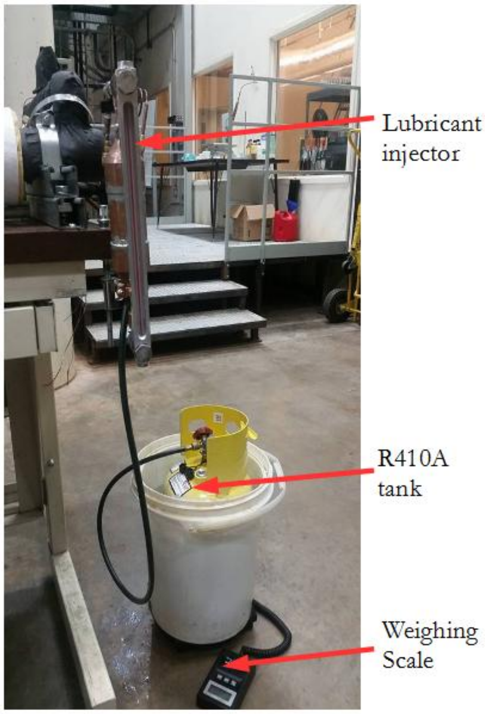

(a)

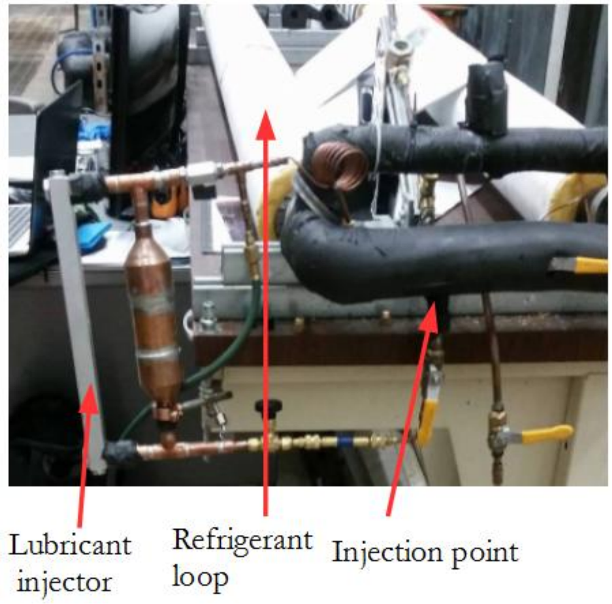

(b)

Figure 26: Oil injection procedure (a) front view (b) side view

4.2.8 Lubricant separation procedure after lubricant injection

Cleaning procedures were developed to ensure that oil and nanolubricant were separated from the refrigerant and after separation, removed from the system. The lubricant injected in the system was first separated from the refrigerant using the oil separator at the end of the test section. During separation, it was made sure that the refrigerant-lubricant mixture was in two phase while entering the oil separator as solubility of the oil in refrigerant effectively takes place in two phase condition compared to saturated vapor. This was made sure by means of a sight glass between the test section and the oil separator as shown in Figure 27 where two phase refrigerant is seen in the sightglass. Using this method it could be confirmed that the refrigerant oil mixture entered the oil separator in two phase and the oil solubilized in the refrigerant was carried from the system to the oil separator. Three 300W tape heaters were installed on the outer surface of the oil separator to ensure that the refrigerant exited the oil separator in super heat condition. Another sight glass is installed at the end of the oil separator to visually determine the phase of the refrigerant.

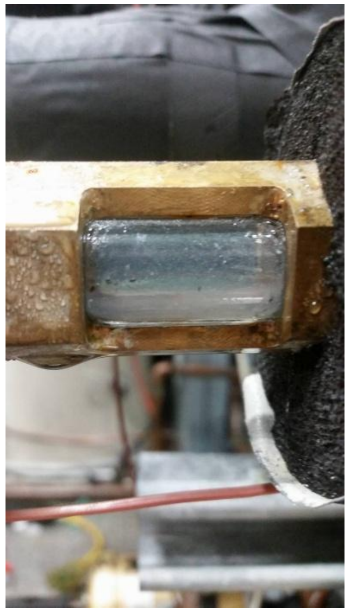

Figure 27: Sight glass at the end of the test section

After separating the lubricant from the refrigerant, the mass of the refrigerant recovered from the oil separator were measured to determine the difference in mass of lubricant injected into the system, and the mass of lubricant recovered from the system. A sample of POE recovered during 3% POE in 15lbs of R410a is shown in Figure 28, there was only change in coloration of the POE and no particles were present in it.

Figure 28: POE recovered from 3% POE tests

For 1% lubricant concentration in R410a tests the mass of lubricant recovered from the system was approximately 80% of the mass of lubricant injected, and for the 3% lubricant concentration in R410a tests, approximately 90% of lubricant was recovered. Figure 29 (a) and (b) show the nanolubricant T1S10 injected into and recovered from the system respectively, it is seen that the color of the nanolubricant changes after tests were conducted. However, the nanoparticle dispersion was still stable in the POE after recovery of the nanolubricant.

(a) (b)

Figure 29: (a) Nanolubricant before injection (b) Nanolubricant recovered after tests

The rest of the oil that cannot be recovered is assumed to stick to the walls of the oil injector during injection and the walls of the oil separator during separation.

4.2.9 Verification procedure to ensure test quality

Verification tests were conducted to ensure that the system was free of oil or nanolubricants after tests conducted with oil, and tests conducted with nanolubricants. This was done to verify that the results obtained for pure R410a could be repeated after oil or nanolubricant is separated and removed from the system. Figure 30 shows the results obtained from one of the verification series conducted at a temperature of 4°C, mass flux of $350\frac{kg}{m^2s}$ and a heat flux of $15\frac{kW}{m^2K}$ results of the R410A experiments are discussed more in detail in the results section. The verification test show that the same results could be obtained for pure R410A tests after oil is separated and removed from the system. It is to be emphasized that verification tests were critical to ensure the correct experimental methodology as a temperature differences of 0.4°C on surface thermocouple readings which could easily occur due to presence of oil or nanolubricants in the system. This deviation in temperature difference may change the results for the HTC test by up to 40%.

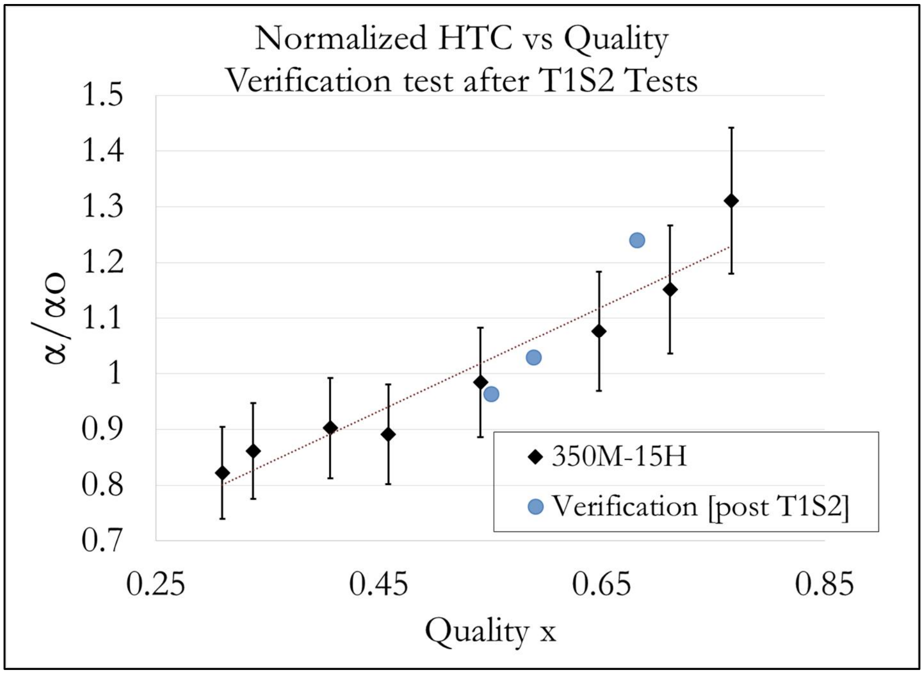

Figure 30: Verification tests to ensure repeatability and test quality

CHAPTER 5

RESULTS AND DISCUSSION

Before discussing the results, let us familiarize ourselves with some of the terminology used in this thesis, these can be found in the nomenclature section of this thesis as well, but is explained in more detail here for clarity.

Three kinds of nanolubricants were used to test for thermo-physical properties, i.e., sedimentation, specific heat, solubility, and thermal conductivity. These nanolubricants were all made of gamma Al_2O_3(alumina) nanoparticles, the difference between the three kinds of nanolubricants were the surfactants used to stabilize the suspension of the alumina particles in the POE. Information on the surfactants was not disclosed by the sponsor of the nanolubricants (Nanophase-IL) even upon request, as the details of the surfactants was considered as intellectual property. The three kinds of nanolubricants were then named Type 1, 2, and 3 nanolubricants. A terminology was developed to readily identify each kind of nanolubricant and the surfactant as well as the nanoparticle concentration of the nanolubricants. T1S20, for example, was type1 nanolubricant at a nanoparticle concentration of 20 percent by mass in RL32-MAF mixed acid polyolester oil (commonly known as POE). Similarly T2S10 would represent type 2 nanolubricant with a nanoparticle concentration of 10 percent by mass in POE. For the heat transfer coefficient and pressure drop test, the nanolubricants at a particular nanoparticle-oil(nanolubricant) concentration is injected into the refrigerant at a particular nanolubricant-refrigerant concentration ratio, which in this thesis is 1% and 3% lubricant concentration ratio.

5.1 <u>Solubility test results</u>

Figure 31 (a) and (b) shows the solubility test results obtained for type1 and type 2 nanolubricants with refrigerant R-410A respectively. The weight percent of R-410A dissolved in nanolubricant is plotted on the x-axis and pressure on the y-axis. Each line represents an isotherm, and the symbols shows the actual data points taken in the present work. The dashed lines represent the literature correlations from the ASHRAE handbook (*Refrigeration*, 2010) and the triangular symbols represent the baseline series of experiments conducted in the present work to verify the solubility of R-410A in POE. This baseline series is used to compare the behavior of the nanolubricants at same temperature and pressure conditions. Both type 1 and type 2 nanolubricants had lower solubility than that of POE oil with no nanoparticles (and with no surfactants). For example, at 400 kPa and 20°C the solubility of R-410A in nanolubricant type 1 was less than 2% while the solubility of R-410A in POE oil was close to 5%. T2S20 showed the maximum solubility at 46 weight percent refrigerant in lubricant and T1S20 was soluble up to 38.5 weight percent at approximately 0°C and 800kPa. However, T2S20 showed lower solubility at 20°C relative to T1S20. Both nanolubricants showed about the same solubility characteristics at 40°C.

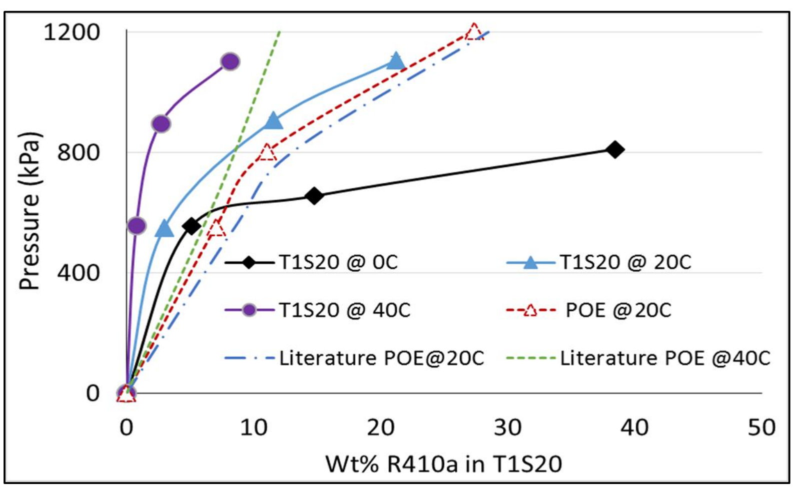

(a)

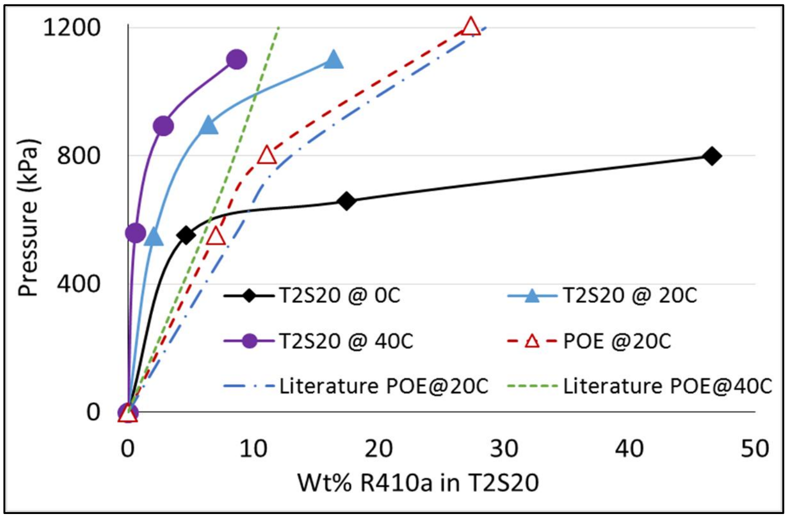

(b)

Figure 31: Pressure vs. wt. % R410a (a) T1S20 (b) T2S20

5.2 <u>Pressure Drop results of pure R410A tests</u>

Figure 32 shows the normalized pressure drop plotted with respect to quality at a temperature of 4°C at different mass fluxes and different heat fluxes. In the legend of the figure, 350M denotes a mass flux of 350 $\frac{kg}{m^2s}$ and 15H denotes a heat flux of 15 $\frac{kW}{m^2K}$.

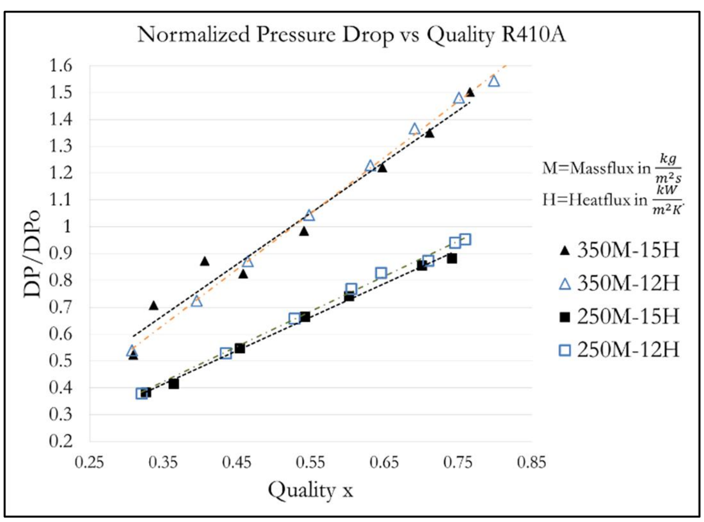

Figure 32: Normalized pressure drop vs. quality of pure R410A DP$_o$=2.98psi

From the results of the experiment, it is seen that pressure drop increases with increase in quality for all four series tested. The pressure drop of the series conducted at $250\frac{kg}{m^2s}$ at a heat flux of $12\frac{kW}{m^2K}$ and $15\frac{kW}{m^2K}$ lie very close to each other. A larger pressure drop is seen for the series conducted at $350\frac{kg}{m^2s}$ at a heat flux of $12\frac{kW}{m^2K}$ and $15\frac{kW}{m^2K}$. For the 350 series the slope of the increase in pressure drop with quality is higher for the series conducted at a heat flux of $15\frac{kW}{m^2K}$ when compared to the series conducted at $12\frac{kW}{m^2K}$. From the results, it is seen that pressure drop for the $350\frac{kg}{m^2s}$ mass flux series is much higher than that of the series tested at a lower mass flux of $250\frac{kg}{m^2s}$. DP_0 is the average value of the heat transfer coefficient at conditions of 4°C and a heatflux of $15\frac{kW}{m^2K}$ and a mass flux of $350\frac{kg}{m^2s}$, the value of DP_0 is 2.98psi. This DP_0 value is used to obtain the normalized plots for all data in the study. Because there is negligible change in pressure drop with change in heat flux, the results are compared at different mass flow rates which is the dominant factor in determination of pressure drop as shown in Figure 32.

5.2.1 Pressure drop results of R410A, R410A POE and R410A nanolubricant mixtures

The pressure drop for all three fluids, that is, R410A, R410A-POE mixture, and R410A-nanolubricant mixture, increased linearly if the refrigerant quality increased for every test conducted. The pressure drop results for tests conducted at $250\frac{kg}{m^2s}$ is shown in Figure 34. Please note that the uncertainties for the pressure drop experiments were small enough to be covered by the markers themselves so the uncertainty bars are not shown in the plots.

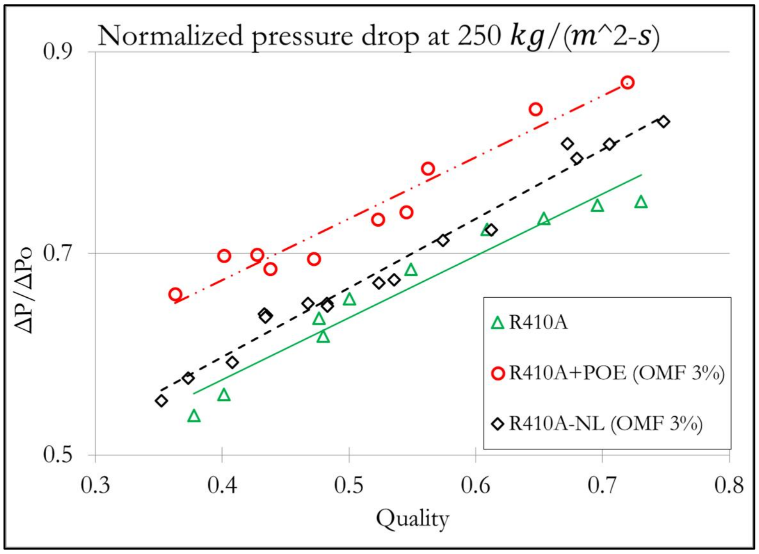

Figure 33: Pressure drop at a mass flux of 250 kg/(m2-s)

For low mass fluxes of 250$\frac{kg}{m^2s}$, R410A-POE mixture had about 20% higher pressure drop than that of refrigerant R410A. The R410A-nanolubricant mixtures showed a pressure drop slightly higher than R410A but lower than that of R410A-POE mixture. The pressure drop results for tests conducted at 350 $\frac{kg}{m^2s}$ is shown in Figure 34.

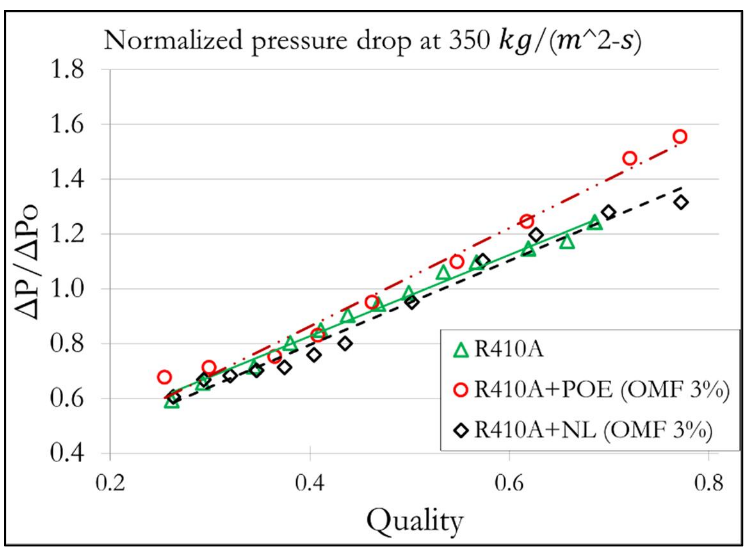

Figure 34: Pressure drop comparison at 350 kg/(m^2-s)

For experiments conducted at 350 $\frac{kg}{m^2 s}$ mass flux, the pressure drops of the three fluids were close to each other at lower quality. At at higher quality, the refrigerant R410A had the lowest pressure drop, R410A-POE mixture had the highest pressure drop and the R410-nanolubricant mixture had basically the same pressure drop measured for refrigerant R410A. At high mass flux of 425 $\frac{kg}{m^2 s}$ the experimental results showed in Figure 35 indicate that the pressure drops of the three fluids were the same.

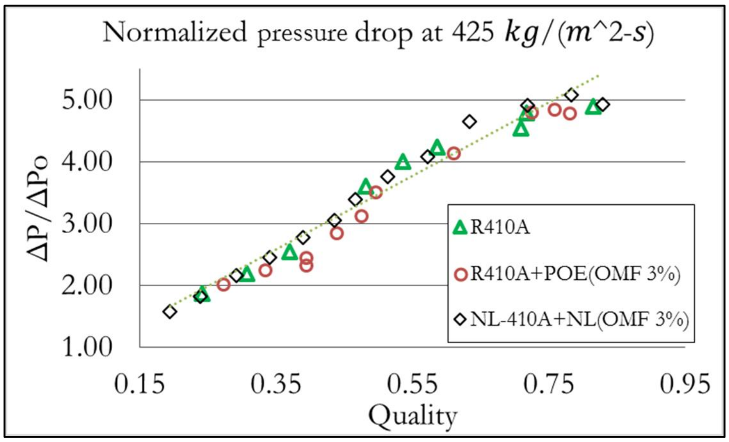

Figure 35: Pressure drop results at a mass flux of 425 kg/(m2-s)

It is worth noticing that nanolubricant did not increase the pressure drop with respect to POE lubricant at low and medium mass flux as well as high. This behavior was repeatable. In literature, similar findings were observed for in-tube flow boiling of CuO nanolubricants (Bartelt et al., 2008) where the nanoparticle volume fraction was 4% and did not seem to affect the viscosity and the pressure drop of the fluid. These results seemed to suggest a pressure drop dependency on mass flux and flow regime.

5.3 <u>Heat Transfer Coefficient test results</u>

To investigate the pattern of heat transfer coefficient of the R410A refrigerant with increase in quality, let us observe one of the series of tests conducted at a temperature of 4°C, mass flux of 350$\frac{kg}{m^2 s}$ and a heat flux of 12$\frac{kW}{m^2 K}$.

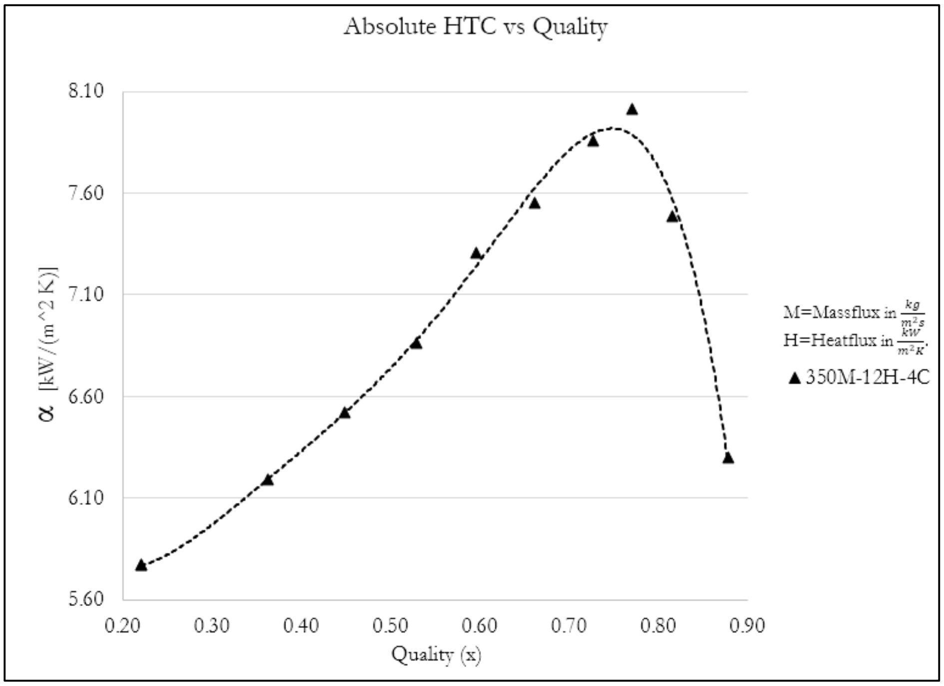

Figure 36: Absolute Heat transfer coefficient of a series performed at a temperature 4°C, mass flux of 350$\frac{kg}{m^2 s}$ and a heat flux of 12$\frac{kW}{m^2 K}$

During the heat transfer coefficient and pressure drop experiment, it is seen that the pressure drop across the test section increases with increase in quality. Due to the heat input into the test section, there is higher quality and lower pressure as the refrigerant proceeds toward the exit of the test section. Figure 37 shows the temperature pattern of 5 surface thermocouples for a point taken at an average quality of 0.65.

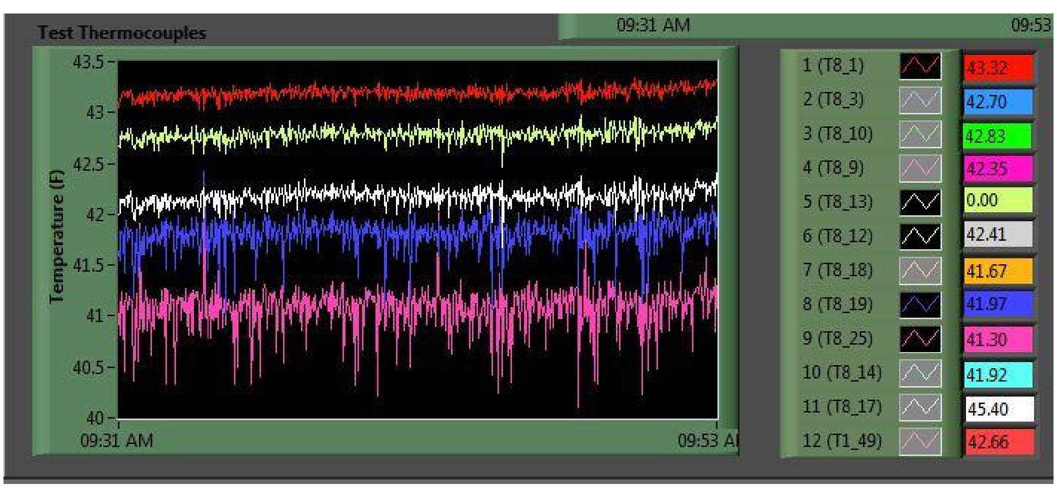

Figure 37: Temperature pattern of surface thermocouples

The surface thermocouples at the test section are labelled 1 through 12[1] in-order of its position with increase in length of the test section, i.e., thermocouple 1 is placed closest to the inlet, and 12 is placed closest to the outlet of the test section. Thermocouples 1,5,6,8 and 9 are shown in the plot to clearly show the temperature decrease with increase in test section length. T8_1 shows the highest temperature reading followed by T8_3 and so on. With lower surface temperatures, the difference between the wall temperature and the saturation temperature of the refrigerant is smaller and making the denominator in equation (15) smaller, which increases the value of the heat transfer coefficient as we increase the quality of the refrigerant during the experiment.

For the series shown in Figure 36, the heat transfer coefficient increases linearly from $5.65\frac{kW}{m^2K}$ at a quality of 0.22 to $7.5\frac{kW}{m^2K}$ at a quality of 0.77. The heat transfer coefficient then decreases linearly for qualities beyond 0.77. At a quality of 0.88 the heat transfer coefficient was found to be $6.2\frac{kW}{m^2K}$. The decrease in the heat transfer coefficient at high qualities can be explained by observing the behavior of the surface thermocouples during testing. Figure 38 shows the readings of 5 thermocouples at an average quality of 0.7.

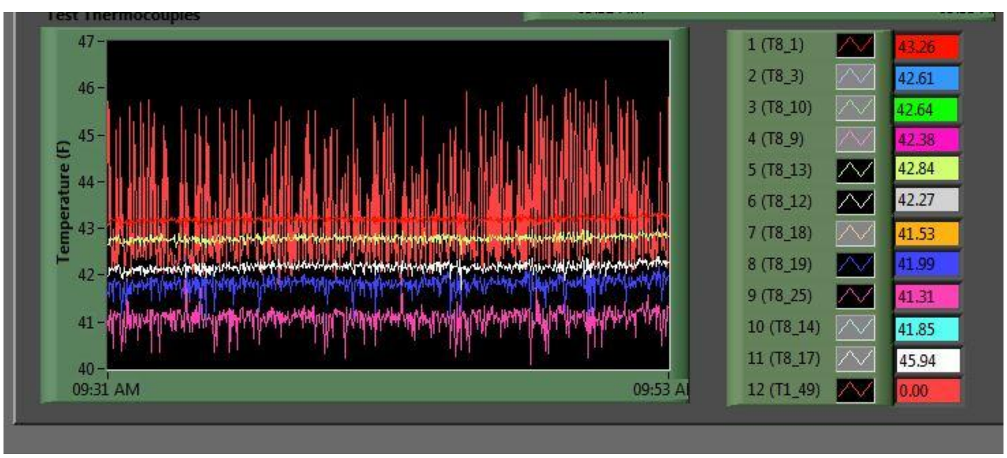

Figure 38: Surface thermocouple readings during high quality tests

[1] Thermocouple 11(T8_17) was damaged during construction and always shows a 3°F value higher than the other thermocouples it is not considered during data analysis

Thermocouple 12(T1_49) is the thermocouple placed 6 inches from the exit of the test section. When the quality of the refrigerant approaches saturated vapor at the exit of the test section, the surface thermocouples begin to fluctuate between temperatures of the liquid refrigerant and the vapor. The difference in surface thermocouple behavior is clearly seen in the above figure, where thermocouples 1,5,6,8 and 9 show a relatively stable reading, whereas thermocouple 12(pink) shows large variations in temperature. This condition represents the point taken at a quality of .7 in Figure 36. With increase in quality of refrigerant in the test section, more thermocouples begin to fluctuate as the refrigerant in the test section begin to dry out at earlier parts of the test section as shown in Figure 39 where thermocouple 10(8_14) begins to fluctuate in temperature.

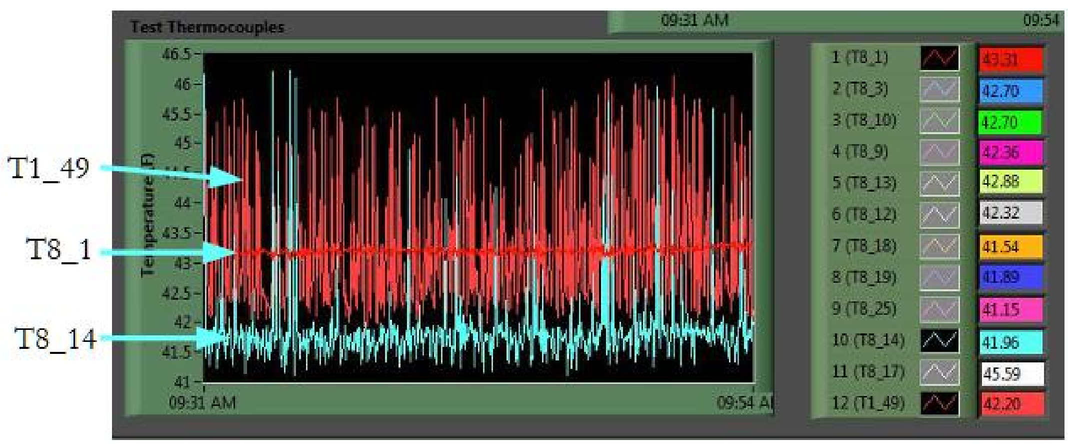

Figure 39: Surface temperature pattern approaching saturated vapor

Although the temperature fluctuations are much higher in this region, the heat transfer coefficient yet increases with increases with quality representing points taken at qualities between 0.7 and 0.78 after which super heat is seen at the exit of the test section. When the refrigerant approaches super heat the temperature at the exit of the test section departs from saturation condition as shown in Figure 40.

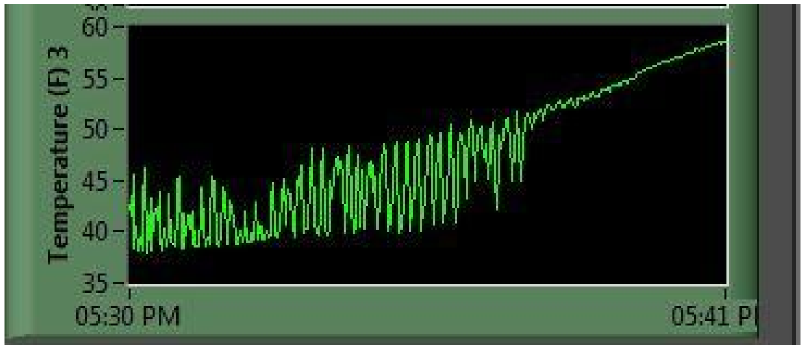

Figure 40: Departure of temperature from saturation condition

The thermocouple at the end of the test section is the first to show this pattern. With increase in quality, other thermocouples begin to show the same trend in change in temperature. When superheat is achieved, the surface temperature of the test section is higher than while in two phase. This increase in the wall temperature increases the difference represented by the denominator of equation (15), and as a result decreases the heat transfer coefficient, this represents the points taken above average qualities of .78, with more thermocouples approaching superheat, this effect is enhanced and the heat transfer coefficient is further reduced.

Figure 41 shows the results for the tests conducted for R410A.

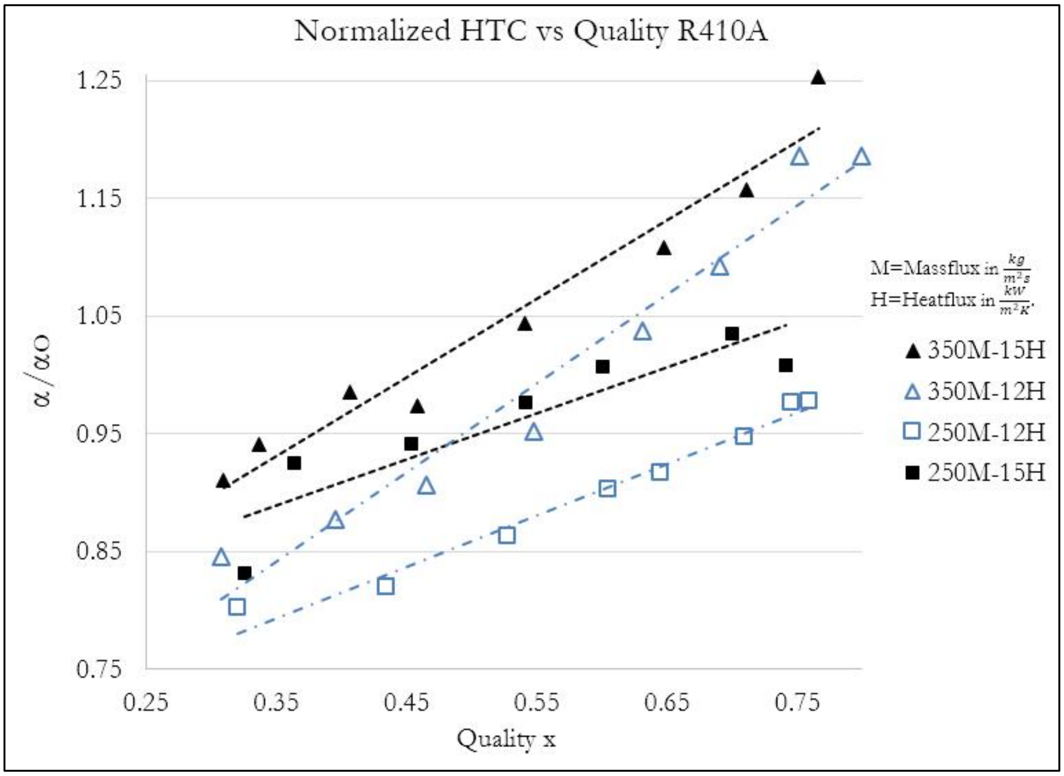

Figure 41: Heat transfer coefficient of pure R410A at different conditions ($\alpha_0 = 7.78\frac{kW}{m^2K}$)

α_0 is the average value of the heat transfer coefficient at a temperature of 4°C, a heatflux of $15\frac{kW}{m^2K}$ and a mass flux of $350\frac{kg}{m^2s}$. The value of α_0 is found to be $7.78\,\frac{\mathrm{kW}}{\mathrm{m^2K}}$, and is used to obtain the normalized plots for all HTC data in the study. For all series of pure R410A tested, the HTC of the refrigerant increases with increase in quality in the 2 phase region. The slope of the trend line plotted with increase in quality is steeper for lower heat fluxes of $12\frac{kW}{m^2K}$, whereas the $15\frac{kW}{m^2K}$ series start at a higer value of heat transfer coefficient but increases with a smaller slope compared to the $12\frac{kW}{m^2K}$ series. There is a higher HTC with increase in mass flow rate of the refrigerant which is clearly seen between the two series performed at $250\frac{kg}{m^2s}$ and $350\frac{kg}{m^2s}$.

5.3.1 Corollary 2 for the validation of the heat transfer in the preheater and test section

Before experiments are performed, an EES program is used to check if the conditions in the system meet the requirements of the test. The code is included in Appendix B. The purpose of the program is to determine the quality and the heatflux into the refrigerant in the test section to ensure that the tests are performed at the right conditions. Using this program, the quality at the inlet of the preheater, exit of the preheater (also the inlet of the test section) and the quality at the exit of the test section is calculated. The program also calculates the change in quality (delx) as the difference in quality between the exit and the inlet of the test section.

The accuracy of the instrumentation and methodology used to determine the heat flux into the test section is again confirmed by observing the refrigerant behavior with increase in quality during testing. The simulation performed in EES was in agreement with the observed temperature and pressure characteristics exhibited by the system. At lower qualities, the pressure transducers and the surface thermocouples showed behavior expected in two phase as described in Section 5.3. At high quality, surface temperature fluctuations are seen from the surface thermocouples at conditions closer to saturated vapor. At superheat, the thermocouples depart from saturation conditions which is theoretically expected. Both the pre-processing software simulation and the observed experimental behavior were in agreement with one another. Figure 42 shows an example of the results obtained from EES for the series shown in Figure 36. This was a comprehensive confirmation that all sensors such as the pressure transducers, inline thermocouples, differential pressure transducers, mass-flow sensors, surface thermocouples, watt meter were working as intended with the right calibrations.

Parametric Table: Table 1

	$\dot{m}_{ref}$ [lbm/hr]	$P_{pre,in}$ [psia]	$P_{out,TS}$ [psia]	$T_{in,preh}$ [F]	$DP_{out,ts}$ [psi]	$\dot{m}_{w,pre}$ [lbm/min]	$\dot{m}_{w,plate}$ [lbm/min]	$T_{w,pre,in}$ [F]	$T_{w,pre,out}$ [F]	$T_{w,hot,in}$ [F]
Run 1	166	132.8	131.6	34.75	2.1	0.71	0.35	77	38.5	76.1
Run 2	165	133.5	131	33.65	3	1.71	0.34	77.05	44	76.2
Run 3	165	134	130.5	30.9	4	2.68	0.36	77.2	46.8	76
Run 4	165	137.5	128	15.7	8.5	9.35	0.36	77.53	56.5	76.45
Run 5	165	138	128	11.45	9.75	10.57	0.355	77.55	57	76.45

Parametric Table: Table 1

	$T_{w,hot,out}$ [F]	$T_{jacket,in}$ [F]	Q_{pump} [kW]	Eff_{input} [-]	Eff_{linear} [-]	T_{sat} [F]	$x_{r,2}$ [-]	$x_{r,4}$ [-]	del_x [-]	x_{avg} [-]	HF [kW/m2]
Run 1	45.7	45.85	1.122	0.69	*1.02*	*39.2*	*0.09*	*0.30*	*0.22*	*0.19*	*12.03*
Run 2	45.65	45.85	1.123	0.69	*1.02*	*38.9*	*0.20*	*0.41*	*0.22*	*0.30*	*11.99*
Run 3	45.6	45.7	1.123	0.69	*1.02*	*38.7*	*0.28*	*0.50*	*0.22*	*0.39*	*12.11*
Run 4	46	46.2	1.117	0.69	*1.02*	*37.6*	*0.67*	*0.89*	*0.22*	*0.78*	*12.06*
Run 5	46.15	46.25	1.121	0.69	*1.02*	*37.6*	*0.74*	*0.96*	*0.22*	*0.85*	*12.05*

Parametric Table: Table 1

	m_{flux} [kg/m2-s]
Run 1	*352.9*
Run 2	*350.7*
Run 3	*350.7*
Run 4	*350.7*
Run 5	*350.7*

Figure 42: EES Preprocess results

5.3.2 Heat transfer coefficient results of R410A, R410A-POE and R410A-Al_2O_3 nanolubricant mixtures during two-phase flow boiling

The motivation behind the HTC experiment was to determine if the use of nanolubricants was a viable option to replace POE in systems which required the use of compressors and underwent the process of evaporative flow boiling. The goal was to determine the magnitude of degradation that was caused relative to pure refrigerant with the addition of POE, and how addition of nanolubricant instead of POE counteracted the effect of degradation. In the results, the degradation of HTC due to the addition of POE is compared to pure R410A and the enhancement with the addition of the nanoparticles is compared relative to the POE series. The mechanisms behind enhancement or degradation are discussed after the results have been described.

Figure 43 Shows the HTC results of R410A, R410A POE and R410A nanolubricant mixtures conducted at a saturation temperature of 4°C, a heatflux of $15\frac{kW}{m^2K}$ and a mass flux of $350\frac{kg}{m^2s}$.

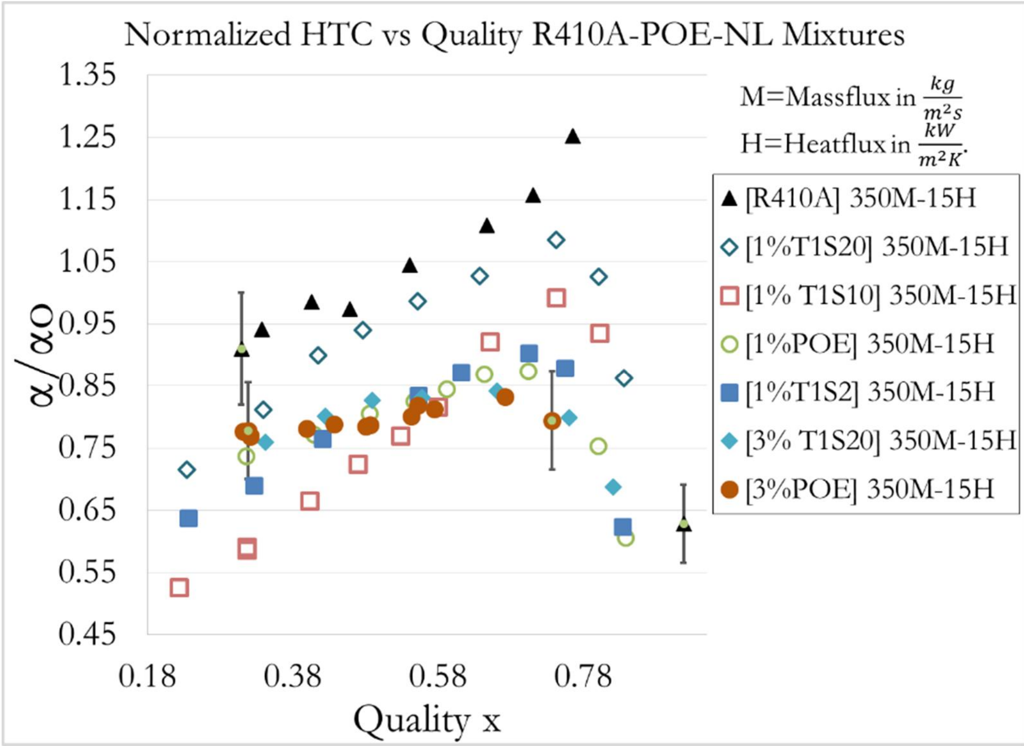

Figure 43: HTC of R410A, R410A-POE and R410A nanolubricant mixtures 4°C, a heatflux of $15\frac{kW}{m^2K}$ and a mass flux of $350\frac{kg}{m^2s}$ $\alpha_0 = 7.78\,\frac{kW}{m^2K}$

Pure R410A shows the highest heat transfer coefficient. With addition of 1% oil concentration ratio (OCR) of POE oil, the heat transfer coefficient decreases by an average of 21.2%. Tests conducted with 1% of T1S20 showed an average of 14% enhancement compared to 1% POE. Tests conducted with 1% OCR of T1S10 showed an average degradation of 3.5% for the entire series compared with 1% POE. However, for this series tested, degradation at an average of 13% was seen at qualities below 0.6 and an average enhancement of 12% was seen above that quality. For the T1S2 series at 1% OCR, a degradation of 14% is seen with respect to oil. When tests were performed with 3% POE, a degradation of 21.4% was seen compared to pure R410A. When 3% T1S20 was tested, there was negligible difference between the POE and T1S20 nanolubricant series at this OCR.

Figure 44 Shows the HTC results of R410A, R410A POE and R410A nanolubricant mixtures conducted at a saturation temperature of 4°C, a heat flux of $12\frac{kW}{m^2K}$ and a mass flux of $350\frac{kg}{m^2s}$.

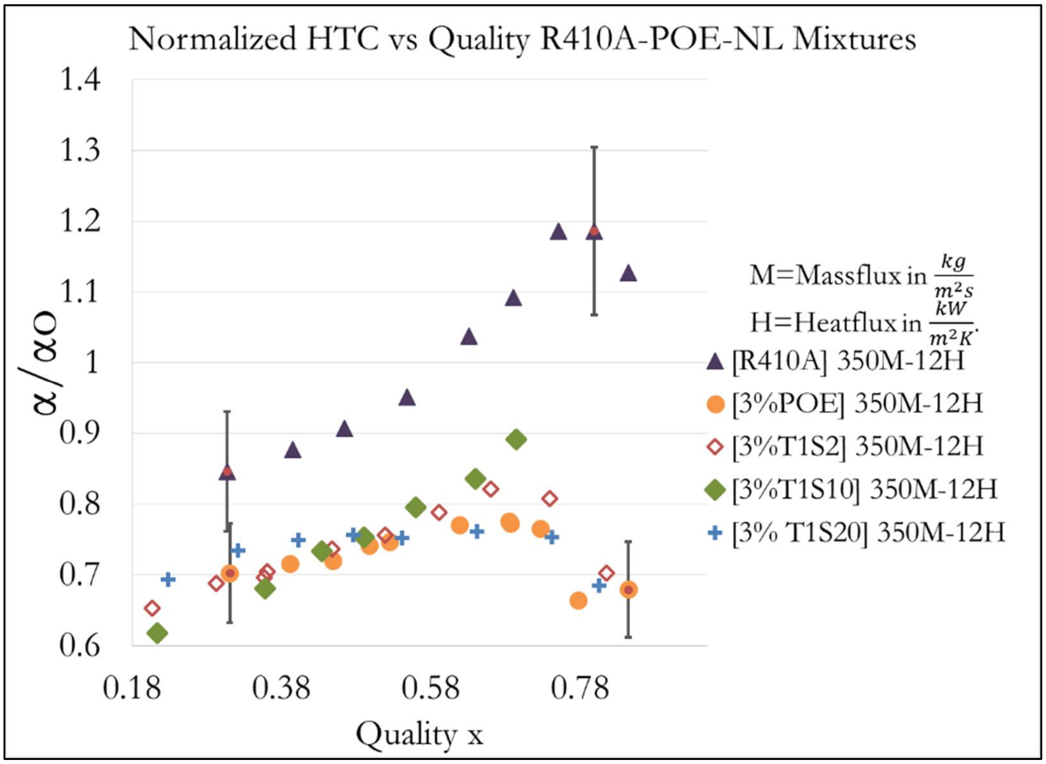

Figure 44: HTC results at a heatflux of 12$\frac{kW}{m^2K}$ and a mass flux of 350$\frac{kg}{m^2s}$

Pure R410A shows the highest heat transfer coefficient. The decrease in average HTC with addition of 3% POE into the refrigerant was 26% compared to pure R410A. At an OCR of 3%, T1S2 showed a small increase in HTC at an average of 0.36% compared to 3% oil. Further enhancement is seen when the concentration of nanoparticles were increased in the lubricant from T1S2 to T1S10, the average enhancement for the T1S10 series was 2.7%. However, T1S20 showed almost no enhancement in HTC compared to POE at 3% OCR. From the results, it is seen that increase in the number of particles in the nanolubricant increased the HTC when the nanoparticle concentration was raised from 2 to 10 %, however no enhancement was seen when the nanoparticle concentration was raised further to 20% in POE.

The results obtained from performing tests at a temperature of 4°C, a heatflux of 12$\frac{kW}{m^2K}$ and a mass flux of 250$\frac{kg}{m^2s}$ are shown in Figure 45 below.

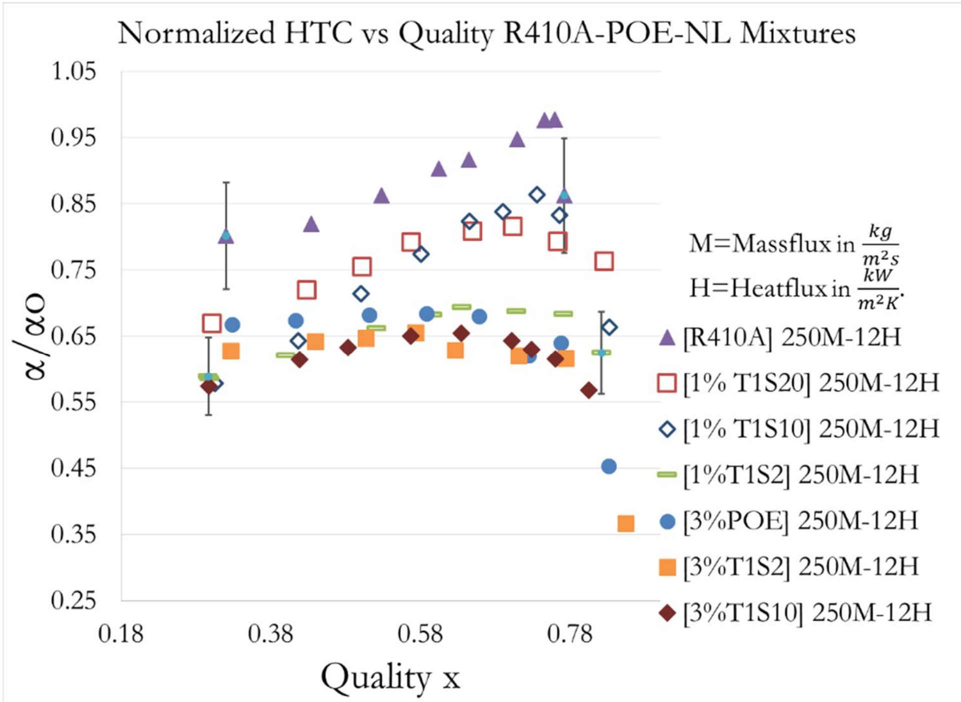

Figure 45: Heat transfer coefficient results of R410A, R410A POE and R410A nanolubricant mixtures at 4°C, a heatflux of 12kW/(m^2 K) and a mass flux of 250$\frac{kg}{m^2s}$

R410A has the highest heat transfer coefficient. T1S2 at an OCR of 1% showed an average degradation of 24% compared to R410A. An average enhancement of 10% was seen when the particle concentration was raised to T1S10, further raising the particle concentration to T1S20 showed a negligible increase in HTC enhancement when compared to T1S10 at 1%. When 3% POE is injected, the HTC decreased by an average of 36.2%. No enhancement was seen compared to 3% POE when the nanolubricant were tested at this concentration.

Figure 46 compares the HTC of R410A, R410A-POE and R410A-nanolubricant mixtures at different mass fluxes. The effect of mass flux can be compared by comparing the same markers. The filled markers represent the 350 mass flux series and the 250 mass flux series is represented by the empty markers.

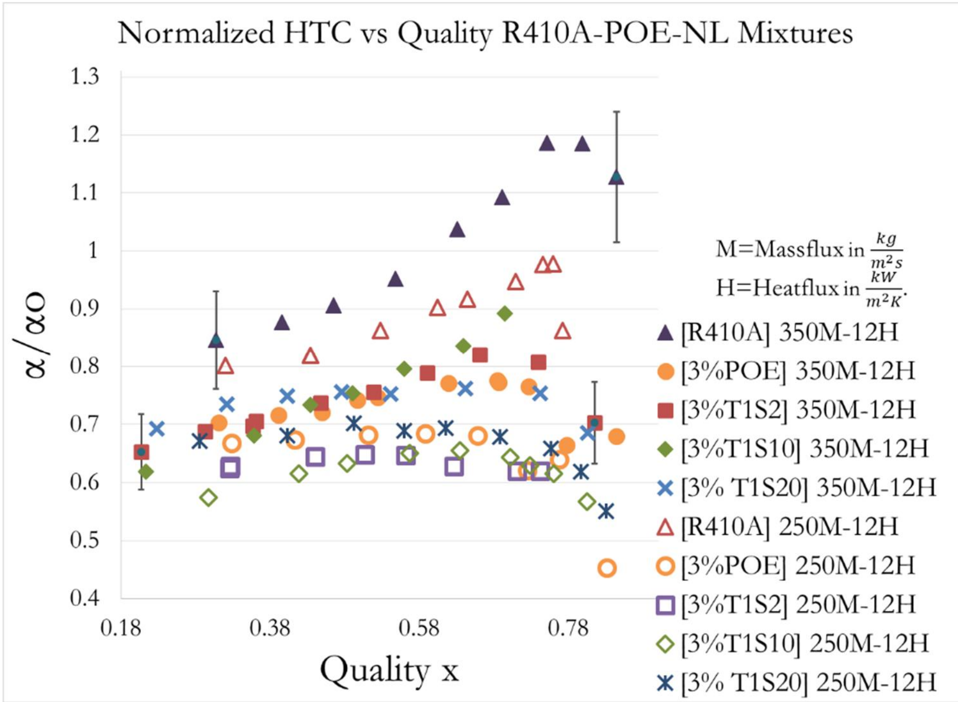

Figure 46: Effect of Mass flux on HTC

For the pure R410A tested, the average HTC was lower by 2.21 percent when mass flux is decreased from $350\frac{kg}{m^2s}$ to $250\frac{kg}{m^2s}$. Test conducted with 3% POE show that the average HTC is reduced by 13.7 when mass flux was decreased. HTC was reduced by 20.14 percent for 3% T1S2 and 20.03 for 3% T1S10 tests conducted respectively. Reduction in mass flux causes a reduction in HTC.

Comparing the results found in this experiment, the HTC enhancement is increased with increased concentration of nanoparticles in oil for 1% concentration of nanolubricant in refrigerant mixtures for the series tested. The same effect was seen in a previous experiment performed by (Baqeri *et al.*, 2014) using CuO nanolubricants in R-600a refrigerant. The increase in nanoparticle concentration in the nanolubricant from 0.5 to 2% in their experiment increased the enhancement of heat transfer coefficient. The same phenomenon is seen in the experiments conducted for this thesis work where degradation was seen with T1S2, some enhancement was seen with T1S10 above qualities of 0.6, and 14% enhancement was seen with T1S20 at an OCR of 1%. (Baqeri *et al.*, 2014) claim that adding nanoparticles with higher thermal conductivity into oil increased the thermal conductivity of the oil, and the increase in thermal conductivity of the oil is one of the reasons responsible for the enhancement. Experiments performed on thermal conductivity in this thesis work show that addition of nanoparticles increase the thermal conductivity of the lubricant. However, from the results seen in the HTC experiments, increase in nanoparticle concentration did not necessarily increase the HTC of the nanolubricant-refrigerant mixture in fact degradation was seen in some high nanolubricant concentration experiments. This suggests that the increase in thermal conductivity of the lubricant is not solely responsible for the enhancements seen during flow boiling. According to (Kedzierski, 2009b), thermal conductivity accounts for a small portion in the enhancement of heat transfer, this was estimated to be about 20%. Further, it is said that other effects like formation of secondary nucleation sites and particle mixing contributes more significantly to the enhancement of the HTC of refrigerant-lubricant mixtures. Similar observations were made after tests for T1S10 nanolubricants were concluded, and an attempt on verification was made. This is discussed next.

5.4 Discussion on the different test setups used for heat transfer coefficient and pressure drop experiments

The results obtained from the first test section (TS-1) built for the HTC and pressure drop experiments were repeatable for the pressure drop, but not the heat transfer coefficient experiments. Figure 47 shows the results of the verification tests for HTC conducted using TS-1 to ensure repeatability. It was seen that the HTC results for previous tests conducted at a mass flux of $250\frac{\mathrm{kg}}{\mathrm{m^2s}}$ and a heat flux of $12\ \frac{\mathrm{kW}}{\mathrm{m^2{-}K}}$ could not be repeated using this test section. However the pressure drop results showed consistent values and were repeatable shown in Figure 48.

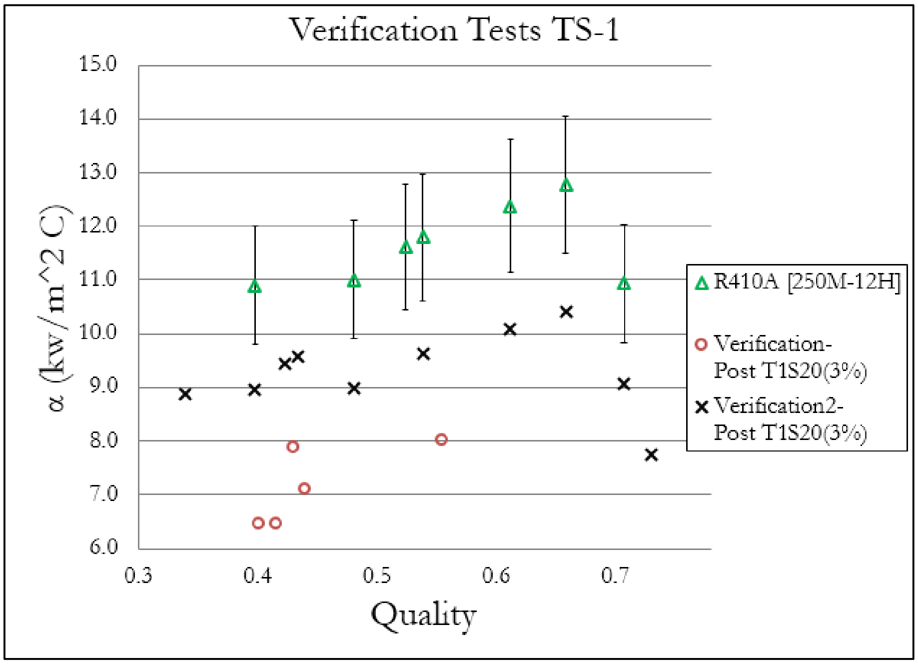

Figure 47: Attempts on verification using TS-1

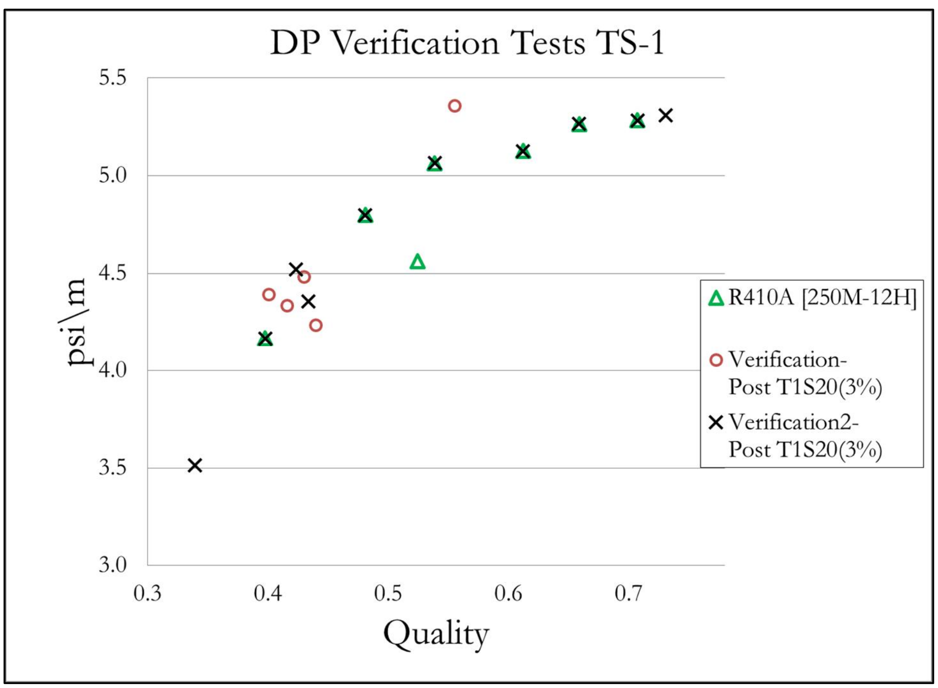

Figure 48: Pressure drop verification using TS-1

Test section 2 (TS-2) and test section 3 (TS-3) used electrical heaters to provide heat flux into the refrigerant, and due to reasons discussed in section 3.4, were not considered for the heat transfer coefficient and pressure drop tests for this thesis work.

When the fourth test section (TS-4) was built and tests were performed on this test section, it was noticed that the pressure drop per unit length of this test section was higher than those found in (TS-1). Figure 49 shows the comparison of the pressure drop results for the series conducted at $350\frac{\mathrm{kg}}{\mathrm{m^2 s}}$ and a heat flux of $12\frac{\mathrm{kW}}{\mathrm{m^2-K}}$ between TS-1 and TS-4.

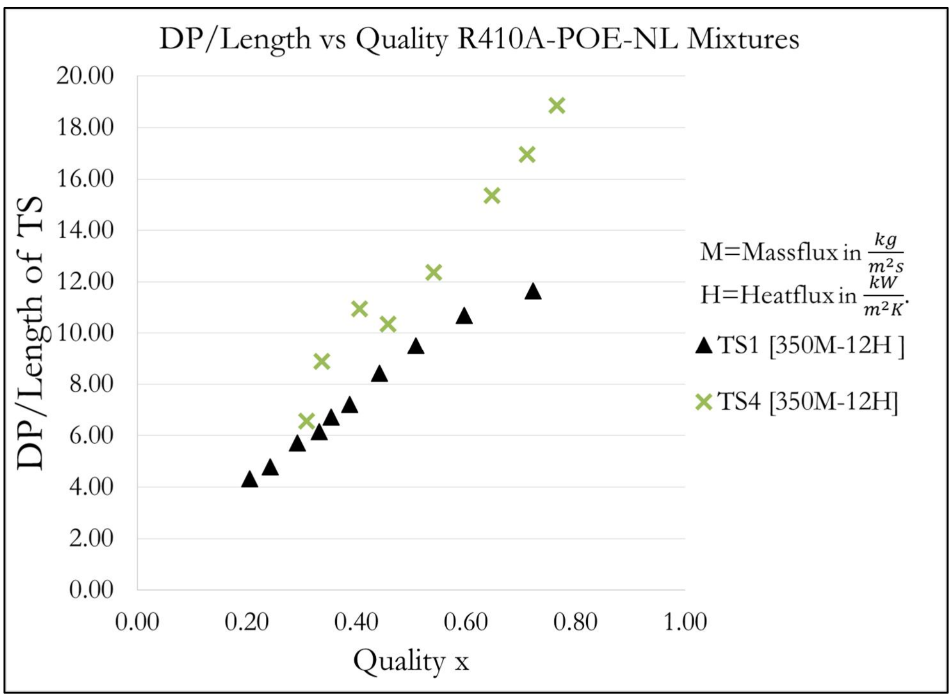

Figure 49: Pressure drop comparison of TS-1 and TS 4

To identify the cause of the difference in pressure drop, the construction of the two test sections was investigated. Figure 50 shows the construction of TS-1.

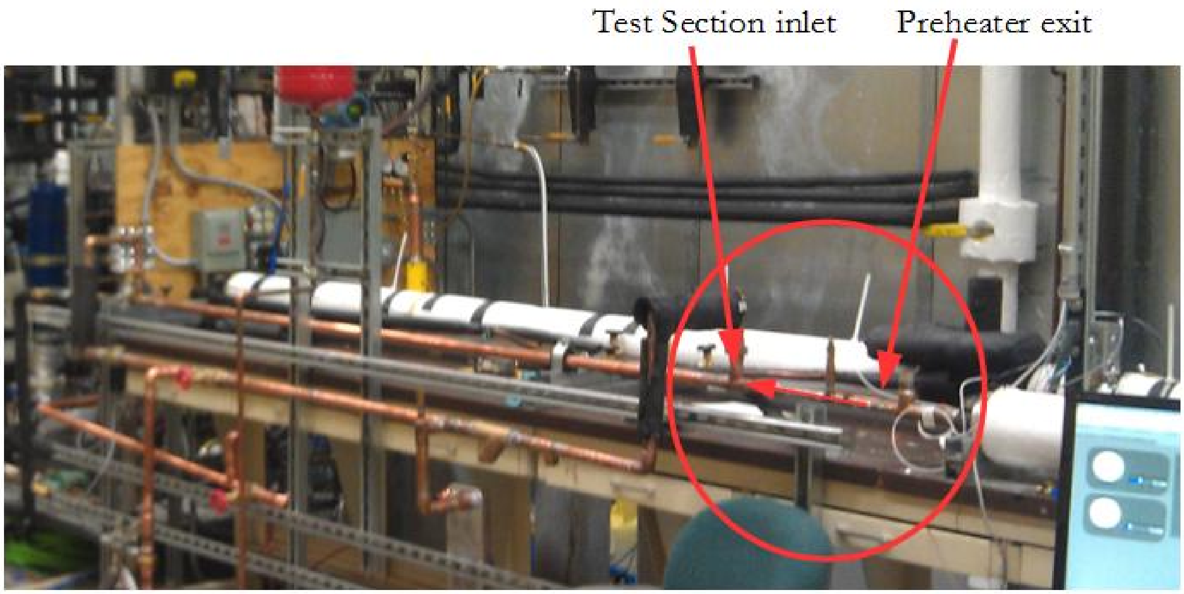

Figure 50: Construction of TS-1 test section inlet

The straight section of the preheater before entering TS-1 had an 8ft long section for flow development before entering the test section. The test section was constructed in-line with the preheater to ensure fully developed flow entering the test section, the flow of the refrigerant is indicated by the arrow inside the circle in Figure 50. Figure 27 shows the construction of TS-4 near the test section inlet.

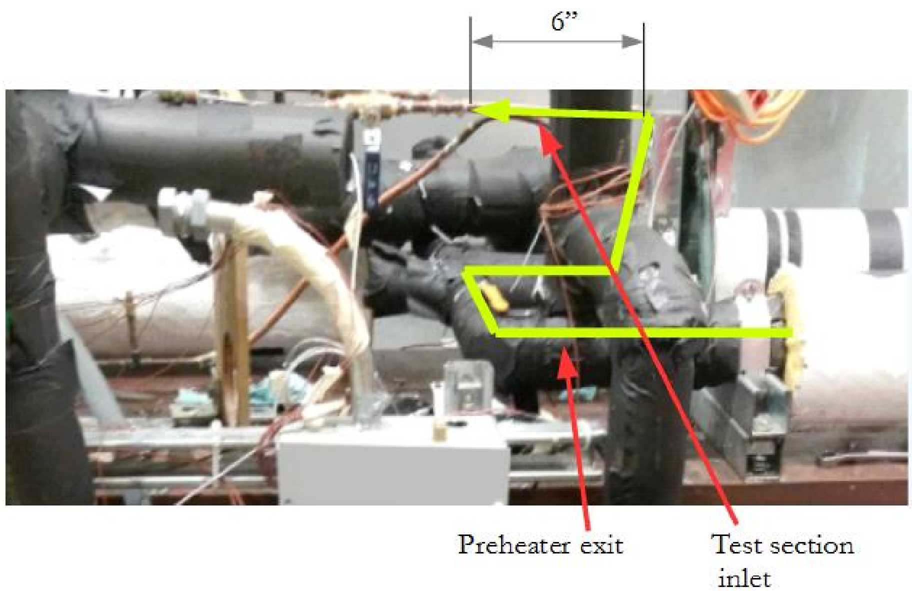

Figure 51: Construction of TS-4 test section inlet

The difference between TS-1 and TS-4 is the path taken by the refrigerant between the preheater exit and the test section inlet. For this test section, the refrigerant exits the preheater, then travels through 2 U bends indicated by the green line in Figure 51. The length of straight tube before the entrance was about 6 inches long. It was hypothesized that the refrigerant flow was not dynamically developed while entering the test section which could be a reason for higher pressure drop measurements.

When TS-5 was constructed it was made sure that the refrigerant had a longer section of tube for flow development before the entrance of the test section. The test section is shown in Figure 52 shows the entrance length of TS-5. An additional 10 inches was added to the entrance length to ensure flow development of the refrigerant.

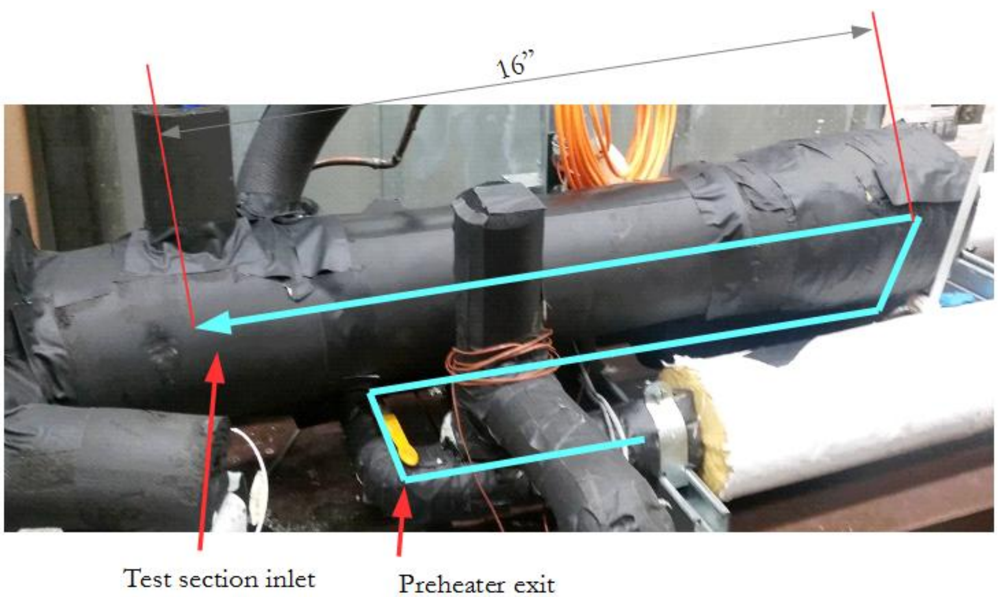

Figure 52: Construction of TS-5 test section inlet

Pressure drop measurements were conducted at a mass flux of $350\frac{\mathrm{kg}}{\mathrm{m^2 s}}$ and a heat flux of $12\frac{\mathrm{kW}}{\mathrm{m^2{-}K}}$ and the values obtained from TS-5 was compared with TS-1 and TS-4. Figure 53 shows the comparison of pressure drop measurements taken from the three test sections. It was seen that the pressure drop measurements of TS-1 which had an 8ft length of tube before the test section for flow development had the same pressure drop measurements as that of TS-5 where the entrance length of the test section was increased by 10 inches.

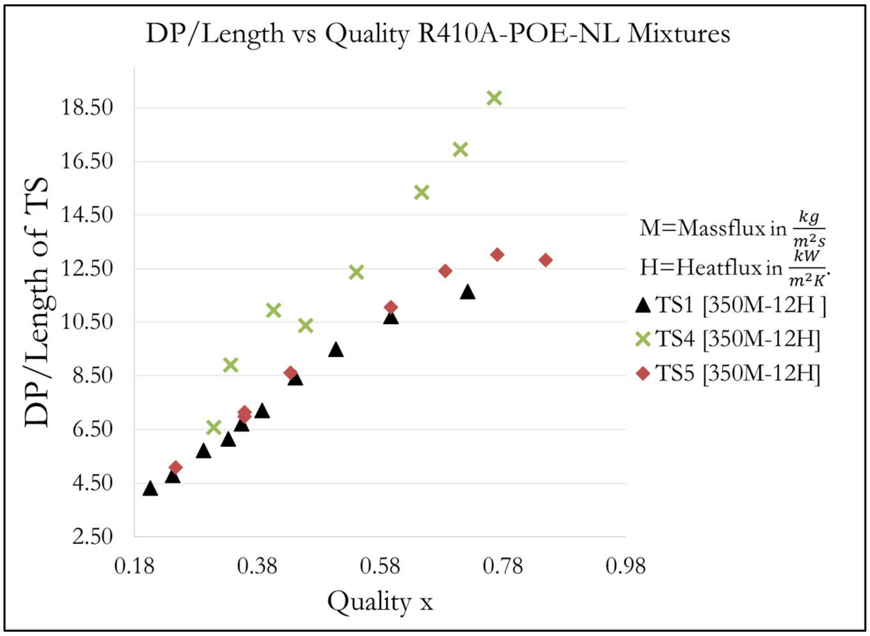

Figure 53: Comparison of pressure drop for various test sections

An attempt on verification was made comparing HTC values obtained from TS-4 and TS-5. The results of this experiment is shown in the next section in Figure 59. From the experimental results seen from the pressure drop and HTC tests of TS-1, TS-4 and TS-5 the following conclusions were made about the test sections:

1) TS-1: With the long 8 foot entrance length of tube before the inlet of the test section, the flow in the test section was both hydrodynamically and thermally fully developed. However the use of the thermal paste introduced an uncertainty in the HTC experiment, particularly from the surface thermocouple measurements. Due to this uncertainty, the HTC results could not be repeated.
2) TS-4: From the comparison of pressure drop measurements between TS-4 and TS-5 in Figure 53 it was seen that the pressure drop measurements for TS-4 were significantly higher than TS-5. According to Ghajar (2010) the local friction factor of flow that is not hydrodynamically developed is higher than that of flow which is hydrodynamically developed due to viscous effects, this results in higher pressure drop. It was concluded that the entrance length of 6inches was not sufficient to

develop the flow in TS-4 hydrodynamically, and this was the cause of higher pressure drop readings in TS-4. This conclusion is further confirmed when pressure drop measurements for TS-5 was compared.

3) TS-5: When pressure drop measurements were compared between TS-5 and TS-1, it was seen that the measurements were in agreement, i.e., both test sections had the same pressure drop measurements at the same conditions. It is to be emphasized that for TS-5 the entrance length of the test section was increased by 10 inches (compared to TS-4) for flow development. This reinforced the conclusion that both TS-5 and TS-1 had both hydrodynamically and thermally developed flow. When the HTC of TS-4 and TS-5 were compared at the same conditions (Figure 59), the results were in agreement. It was concluded that the flow in both TS-4 and TS-5 were thermally developed. TS-5 had both thermally and hydrodynamically developed flow.

5.5 Discussion on the effect of addition of nanoparticles on the heat transfer coefficient and pressure drop test setup

After addition of nanolubricants for the T1S10 tests, lubricant separation was performed on the system. The amount of nanolubricant recovered from the system was 90% by mass of what was injected into the system for the 3% T1S20 series of tests. However, during verification tests after separation of the nanolubricant with the oil separator, it was found that the heat transfer coefficient did not match that of test conducted earlier for pure R410A. The results of the verification are shown in Figure 54. The heat transfer coefficient at high quality was enhanced up to 1.8 times that of even pure refrigerant! From the results of the T1S10 tests discussed in section 5.3.2, enhancement was seen with respect to oil for low concentration of nanoparticles at qualities above 0.6.

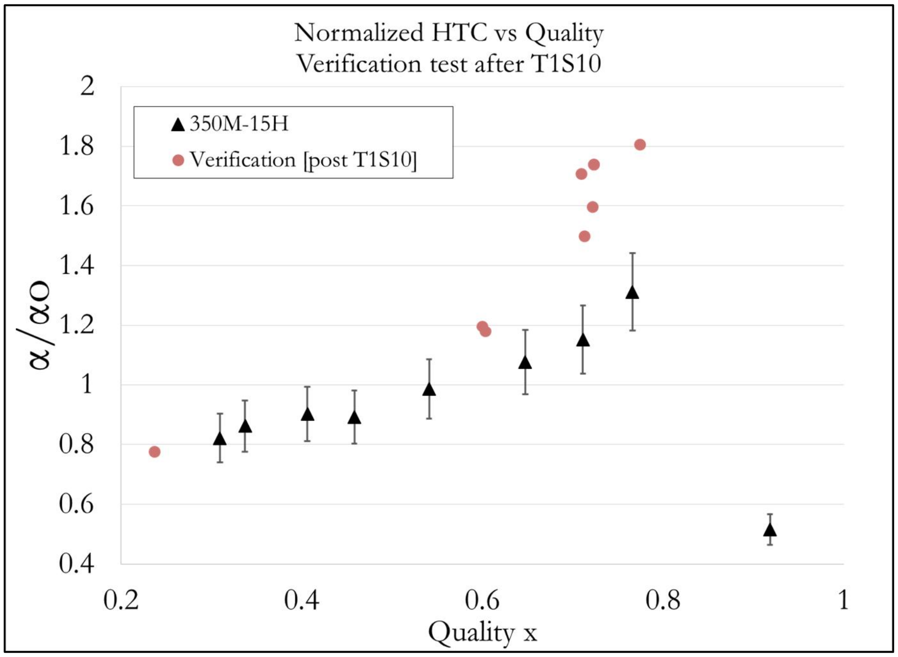

Figure 54: Verification test after T1S10 oil separation

With this observation, it was hypothesized that the increase in HTC was due to the presence of residue nanoparticles in the system. It was decided to then proceed to the next step for cleaning using solvent provided by Dupont; particularly used to flush oil from refrigeration systems.

(a)

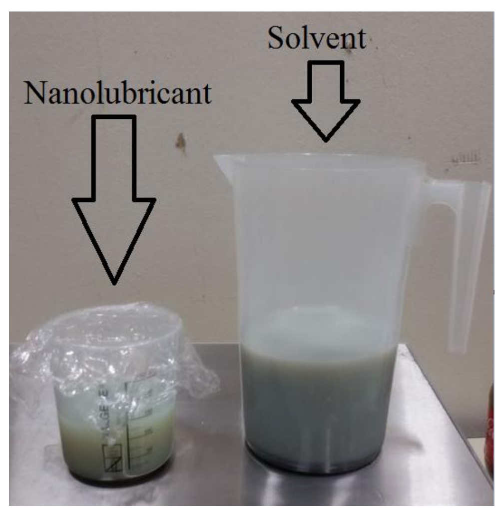

(a)

Figure 55: (a) Solvent used to flush the system after nanolubricant tests(b) Recovered nanolubricant and solvent from the system

Figure 55(a) shows the solvent used to flush the system. And Figure 55(b) shows the solvent recovered from the system. The solvent before use is transparent like water and after flushing the system with the solvent, it had an appearance like that of the nanolubricant recovered from the system. After flushing the system with solvent it was discovered that the heat transfer coefficient and pressure drop was much lower than the results discussed in section 5.3. Figure 56 shows the verification results after the solvent flush for the HTC.

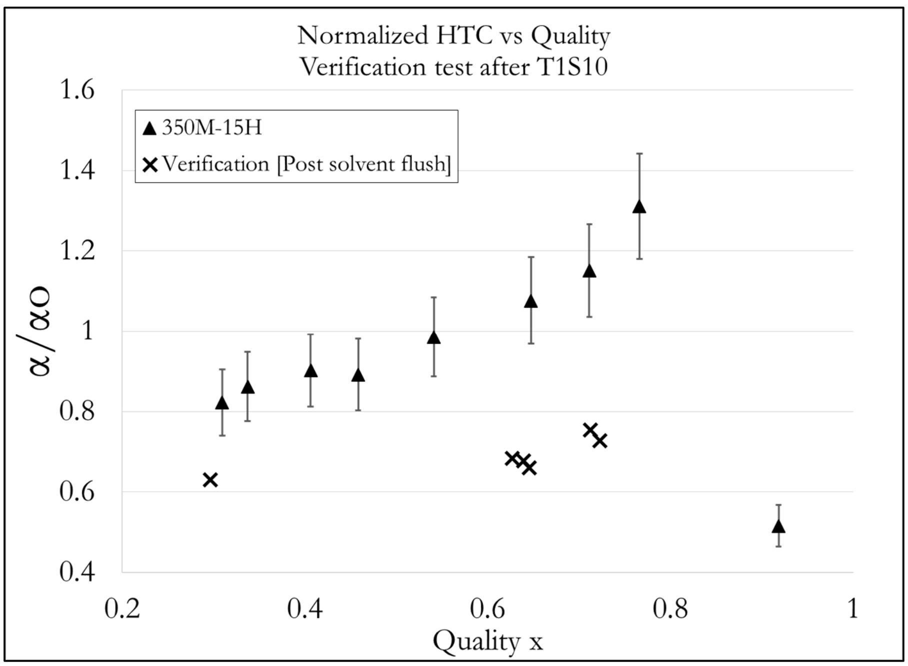

Figure 56: HTC verification after solvent flushing the system

2 inches of the refrigerant tube right before the entrance of the test section was cut out and dissected to visually confirm the change in the test section surface. Figure 57 shows the difference in surface of the microfin tube before and after the nanolubricant injection.

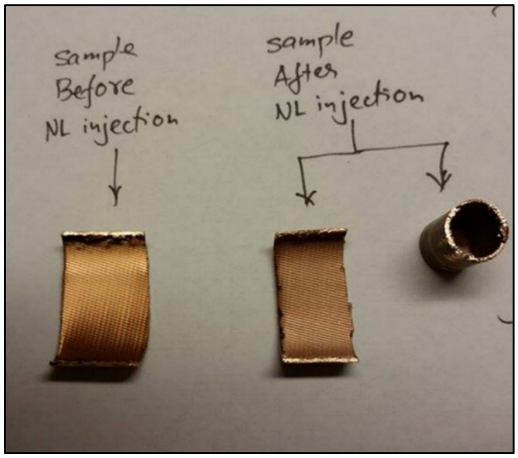

Figure 57: Inner surface of the microfin tube before and after Nanolubricant injection

It is clearly seen that the inner surface of the tube on the right in Figure 57 is less lustrous compared to the new tube on the left. The tube on the right also had a whitish coating on its surface which is the color of the Alumina nanolubricant. Pressure drop tests were then conducted to compare the pressure drop of the test section with a smooth tube, a new enhanced tube. The results of the test are shown in Figure 58.

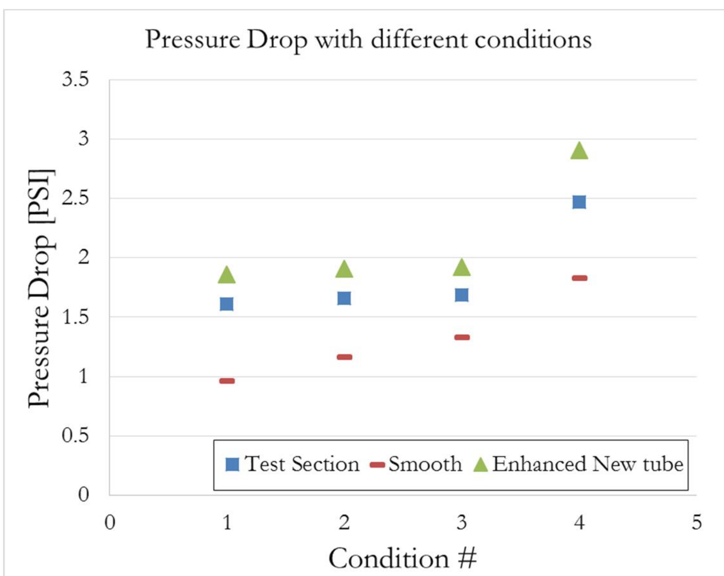

Figure 58: Pressure drop comparison of the test section with different tubes

The conditions of the pressure drop test are included in appendix B. From the figure above, it is seen that the test section had a lower pressure drop compared to the new enhanced tube. It was concluded that the use of the solvent reacted with the nanolubricant particles in the test section during cleaning and changed the heat transfer characteristics of the test section refrigerant tube. This test section was then discarded and another test section was made for the T1S20 tests.

After construction of the test section specifically for the T1S20 tests, verification tests were again performed for heat balance of the test section, the preheater and isothermal tests were conducted for the verification of the thermocouples in the test section. The details of the verification test for the second test section is included in appendix B. A comprehensive verification is represented when the HTC for pure R410A tests match tests previously conducted as shown in Figure 59.

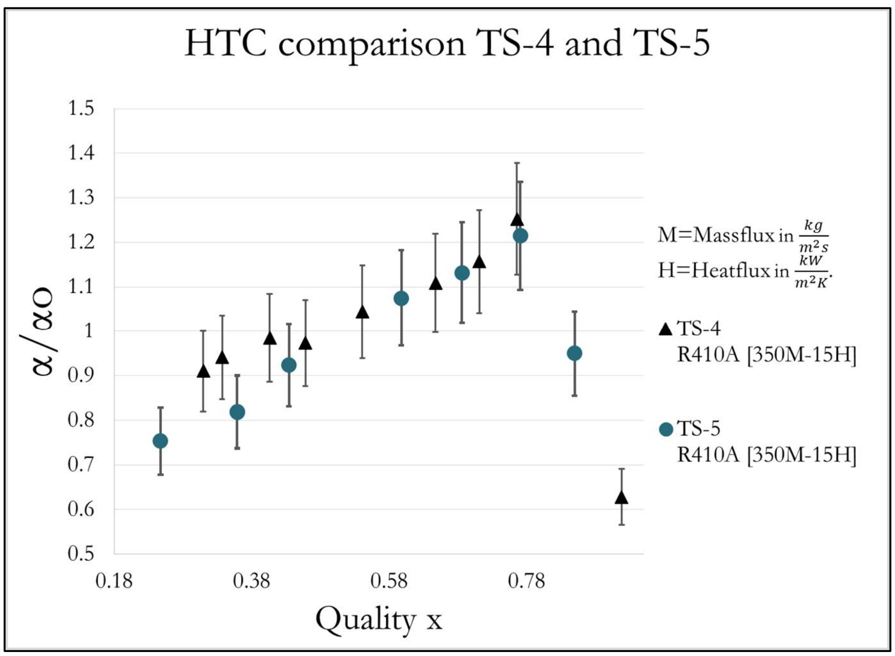

Figure 59: Verification test comparison for TS-4 and TS-5

After verification of the test section was achieved, tests for the T1S20 series were performed described in section 5.3.2. However, the cause of the significant increase in enhancement during the verification tests was not confirmed. Kedzierski (2009a) found that at smaller concentrations of 1.6% by mass Al_2O_3-polyolester nanolubricant mixed with refrigerant at a concentration of 0.5%, showed enhancement up to 400% which indicate that the HTC may be higher than the pure base fluid tested. It may be that the smaller concentration of nanolubricant left in the system before the solvent flush procedures is responsible for this enhancement in heat transfer. Further investigation is required to ascertain the cause of the enhancement.

CHAPTER 6

CONCLUSIONS AND SOME RECCOMENDATIONS FOR POTENTIAL FUTURE WORK

A literature review was performed and testing methods were reviewed to perform the experiments stated in the objectives. An experimental setup for the solubility test and experimental facility for the HTC and pressure drop tests was designed and developed to perform the experiments to achieve the goal of obtaining repeatable results for the tests conducted. Construction of several designs were made to perform the experiments with calibrated and validated instrumentation. An experimental methodology was developed to effectively test for the properties of R410A-nanolubricant mixtures. Experiments were performed, and from the verification tests described in this thesis, were repeatable. Data reduction was performed for the experiments and the uncertainty of the test setups used have been discussed. All the objectives of this thesis were achieved.

Work on nanolubricant is still in its infancy and this thesis aims to provide new experimental data of solubility characteristics for refrigerant R410A and nanolubricants mixtures. Solubility and miscibility of refrigerant R410A with two types of nanolubricants that shared the same nanoparticles but had different surfactants, were measured for temperature ranging from 0°C to 45°C. The nanolubricants had also lower solubility in refrigerant R410A with respect to POE.

This thesis presents data of pressure drop for two-phase flow boiling in a horizontal tube with internally enhanced heat transfer surfaces and it discusses the effect of the nanolubricants on the HTC and pressure drop of the mixture. Nanolubricants did not increase the two-phase pressure drop with respect to POE lubricant. Greater augmentation in pressure drop comparing R410A, R410A-POE and R410A-nanolubricant mixtures was seen with decrease in mass flux, this result was in agreement with observations made by (Peng *et al.*, 2009). Increase in mass flow rate decreased the augmentation of the 3 series tested. These results seemed to suggest a pressure drop dependency on mass flux and flow regime and will require further investigation.

Results for the effect of Al2O3 nanolubricant- R410A mixtures on flow boiling HTC were presented. Enhancement in HTC was seen up to 14% for T1S10 at an OCR of 1% compared to R410A POE mixtures, and degradation of 3.5% was seen for T1S2 at an OCR of 1%. Increase in nanoparticle concentration did not always increase the HTC comparing the 1% OCR and 3% OCR tests. Factors such as nanoparticle concentration in POE are seen to be responsible for enhancement in the case of 1% OCR tests.

After several test section designs were implemented, an effective test setup and experimental methodology was developed to achieve repeatable tests for HTC and pressure drop experiments. The facility was improved with each design, and the experimental methodology was refined with the lessons manifest from the tests performed. Testing of refrigerant nanolubricant mixtures in flow boiling is a new field of research, and despite the success of the project, there is much room for improvement with regard to the testing facility and the optimization of experimental methods implemented to execute the project. From the results of this thesis work, nanolubricants show great potential as a replacement for conventional POE oil used in vapor compression systems. However, further investigation is needed to identify the cause of enhancement to optimize the performance of using nanolubricants in vapor compression systems.

So far, for this thesis work, one type of Al_2O_3 nanoparticle was used to make the different types of nanolubricants with different surfactants. The effect of different nanoparticles like ZnO, with different thermophysical properties and particle shape will be used for future thermophysical, heat transfer coefficient and pressure drop tests. This will provide information on whether the enhancement of the nanolubricant-refrigerant mixtures compared to POE is due to enhancement in thermophysical properties, or if enhancement is due to physical phenomenon like change fluid motion, or creation of secondary nucleation sites on the heat transfer surface due to addition of nanoparticles. If the enhancement in HTC is determined to arise from physical phenomenon, the study of the effect of nanoparticles on the heat transfer surface could prove useful to identify if secondary nucleation sites are indeed created with the addition of nanoparticles. If enhancement is due to the change in characteristics of fluid motion, tests implementing particle image velocimetry could be used to study the influence of nanoparticles on the fluid motion of the refrigerant.

A recommendation for future work includes the study of the effect of surfactants on the properties of nanolubricants. For this thesis work, it is not known how the surfactants or its concentration in the POE influence the properties of the nanolubricant, or how the concentration of the surfactants influence the HTC and pressure drop characteristics. Tests could be performed with different concentrations of surfactants used to stabilize the nanolubricants and observe its effect on the thermophysical properties, and the heat transfer coefficient and pressure drop characteristics during evaporative flow boiling experiments.

NOMENCLATURE

M_d	Mass of dispersant/oil	(g)
M_n	Mass of solute/nanoparticles	(g)
m_{Nl}	Mass of nanolubricant	(g)
P	Electrical Power	(W)
Q	Heat gain	(W)
T1S2	Type 1 nanolubricant 2% by weight Al_2O_3 in POE oil	
T1S10	Type 1 nanolubricant 10% by weight Al_2O_3 in POE oil	-
T1S20	Type 1 nanolubricant 20% by weight Al_2O_3 in POE oil	-
T2S10	Type 2 nanolubricant 10% by weight Al_2O_3 in POE oil	-
T2S20	Type 2 nanolubricant 20% by weight Al_2O_3 in POE oil	-
V	Voltage through the wire heater	(V)
w_{POE}	Weight of POE	(g)
$w_{\%ref}$	Weight percent of refrigerant	(%)
$w_{\%NL}$	Weight percent of nanolubricant	(%)
w_{NL}	Weight of nanolubricant	(g)
w_{NL+Ref}	Weight of nanolubricant and refrigerant	(g)
w_{ref}	Weight of refrigerant	(g)
ϕ	Concentration of nanoparticles by mass	(g)
HTC, α	Heat transfer coefficient	W/m^2-K
α_o	Baseline value for heat transfer coefficient for normalization	W/m^2-K
DP	Pressure drop	kPa

DP_o	Pressure drop baseline for normalization	kPa
$\dot{m}_{PHwater}$	Preheater water flow rate	kg/s
T_{w_i}	Water inlet temperature of the preheater	C
T_{w_o}	Water outlet temperature of the preheater	C
$\dot{m}_{ref}$	Refrigerant flow rate in the system	kg/s
$h_{r_{pre\_in}}$	Enthalpy of the refrigerant entering the preheater	kJ/kg
Q_{TSr}	Heat transfer into the test section refrigerant	kW
Q_{plate}	Heat transfer from the plate heat exchanger at the test section	kW
Q_{pump}	Heat transfer from the pump at the test section	kW
$A_{surface}$	Heat transfer surface area of the refrigerant tube	m^2
h_{TS_in}	Enthalpy of the refrigerant entering the test section	kJ/kg
h_{TS_out}	Enthalpy of the refrigerant exiting the test section	kJ/kg
x_{TS_av}	Average quality at the test section	-
x_{TS_in}	Entering quality at the test section	-
x_{TS_out}	Exiting quality at the test section	-

REFERENCES

Bang, I., C., and Chang, S., H., 2004. Boiling heat transfer performance and phenomena of Al2O3-water nanofluids from a plain surface in a pool boiling.ICAPP,Pittsburgh

Baqeri, S., Behabadi, M. A. A., & Ghadimi, B., 2014. Experimental investigation of the forced convective boiling heat transfer of R-600/oil/nanoparticle. *International Communications in Heat and Mass Transfer*

Bartelt, K., Park, Y., Liu, L., & Jacobi, A.0., 2008,*Flow-Boiling of R-134a/POE/CuO Nanofluids in a Horizontal Tube.*12th Int. Refrigeration and Air Conditioning Conference at Purdue, West Lafayette, IN (USA).

Batchelor, G., K., 1977. The effect of Brownian motion on the bulk stress in a suspension of sperical particles. *J. Fluid Mech., 83*, 97-117

Bobbo, S., Fedele, L., Fabrizio, M., Barison, S., Battiston, S., & Pagura, C., 2010. Influence of nanoparticles dispersion in POE oils on lubricity and R134a solubility. *Int J Refrig, 33*(6), 1180-1186

Buongiorno, J., Venerus, D. C., Prabhat, N., McKrell, T., Townsend, J., Christianson, R., . . . Zhou, S. Q., 2009. A benchmark study on the thermal conductivity of nanofluids. *J. Appl. Phys., 106*(9)

Choi, J.-Y., Kedzierski, M. A., & Domanski, P. 1999. *A generalized pressure drop correlation for evaporation and condensation of alternative refrigerants in smooth and micro-fin tubes*. Gaithersburg. MD: US Department of Commerce, Technology Administration, National Institute of Standards and Technology, Building and Fire Research Laboratory.

Choi, S. U. S., 2009. Nanofluids: From Vision to Reality Through Research. *J Heat Trans-T Asme, 131*(3), 1-9

Cieslinski, J. T. T., W., 2007. 2007. Horizontal flow boiling of R22, R134a and their mixtures with oil in smooth and enhanced tubes. *Archives of Thermodynamics, 28*, 19-40

Cremaschi, L., 2012. A Fundamental View of the Flow Boiling Heat Transfer Characteristics of Nano-Refrigerants.ASME IMECE 2012 International Mechanical Engineering Congress & Exposition,Houston, Tx

Cremaschi, L., Hwang, Y., & Radermacher, R., 2005. Experimental investigation of oil retention in air conditioning systems. *Int J Refrig, 28*(7), 1018-1028

Das, S. K., Putra, N., & Roetzel, W., 2003. Pool boiling characteristics of nano-fluids. *Int. J. Heat Mass Transfer, 46*(5), 851-862

EIA,Emission of greenhouse gases in the U.S., Report Number: DOE/EIA-0573 (2009),

Ghajar, Y. A. C. A. J. 2010. *Heat and mass transfer: Fundementals and applications* (4 ed.). New York: McGrawHill.

Hu, H., Ding, G. L., & Wang, K., 2008a. Heat Transfer Characteristics of R410A-oil mixture flow boiliing inside a 7mm straight microfin tube. *Int J Refrig, 31*

Hu, H., Ding, G. L., & Wang, K., 2008b. Measurement and correlation of frictional two-phase pressure drop of R410A/POE oil mixture flow boiling in a 7mm straight micro-fin tube. *Applied Thermal Engineering, 28*

Jain, S., Patel, H. E., & Das, S. K., 2009. Brownian dynamic simulation for the prediction of effective thermal conductivity of nanofluid. *J. Nanopart. Res., 11*(4), 767-773

Kedzierski, M. A., 2009a. Effect of Al2O3 nanolubricant on R134a pool boiling heat transfer. *Int J Refrig, 34*(2), 498-508

Kedzierski, M. A., 2009b. Effect of CuO Nanoparticle Concentration on R134a/Lubricant Pool-Boiling Heat Transfer. *J Heat Trans-T Asme, 131*(4), 1-7

Mahbubul, I. M., Saidur, R., & Amalina, M. A., 2011. Pressure drop characteristics of TiO2-R123 Nanorefrigerant in circular tube.Engineering e-Transaction

Murshed, S. M. S., Leong, K. C., & Yang, C., 2008. Investigations of thermal conductivity and viscosity of nanofluids. *Int. J. Therm. Sci., 47*(5), 560-568

Ozerinc, S., Kakac, S., & YazIcIoglu, A. G., 2009. Enhanced thermal conductivity of nanofluids: A state-of-the-art review. *Microfluid. Nanofluid., 8*(2), 145-170

Peng, H., Ding, G., Jiang, W., Hu, H., & Gao, Y., 2009. Measurement and correlation of frictional pressure drop of a refrigerant-based nanofluid flow boiling inside a horizontal smooth tube. *Int J Refrig, 32*, 1756-1764

Peng, H., Ding, G. L., Hu, H. T., & Jiang, W. T., 2010. Influence of carbon nanotubes on nucleate pool boiling heat transfer characteristics of refrigerant-oil mixture. *Int. J. Therm. Sci., 49*(12), 2428-2438

Phillips, R., J.,, Armstrong, R., C.,, Brown, R., A.,, Graham, A., L.,, & Abbott, J., R.,. 1992. A constitutive euquation for concetrated suspensions that accounts for shear-induced particle migration. *Phys. Fluids, A 4*(1), 30-40

Puliti, G., Paolucci, S., & Sen, M., 2011. Nanofluids and Their Properties. *Appl. Mech. Rev., 64*(3)

Refrigeration. 2010. American Society of Heating, Refrigerating, and Air Conditioning Engineers.

Sawant, N., N., Kedzierski, M., A, & Brown, J., S,Effect of Lubricant on R410A Horizontal Flow Boiling,

Shen, & Groll, E. A., 2003. A Critical Review of the Influence of Lubricants on the Heat Transfer and Pressure Drop of Refrigeratnts, Part I: Lubricant influence on Pool and Flow Boiling. *HVAC&R Research, 11*(3), 341-359

Smith, J. (2015). *Experimental investigation of two phase flow boiling heat transfer and pressure drop of LGWP refrigerants in an internally enhanced tube evaporator.* (Masters), Oklahoma State University, Oklahoma State University.

Taylor, J. R. 1997. *An introduction to error analysis: The study of uncertainties in physical measurements*. Sausalito, CA: University Science Books.

Thome, J. R., 1995. Comprehensive Thermodynamic Approach to Modeling Refrigerant-Lubricating Oil Mixtures. *HVAC&R Research* 110-126

Vajjha, R. S., & Das, D. K., 2009. Specific Heat Measurement of Three Nanofluids and Development of New Correlations. *J Heat Trans-T Asme, 131*(7), 1-7

Venerus, D. C., Buongiorno, J., Christianson, R., Townsend, J., Bang, I. C., Chen, G., . . . Zhou, S. Q., 2010. Viscosity Measurements on Colloidal Dispersions (Nanofluids) for Heat Transfer Applications. *Appl Rheol, 20*(4)

Venerus, D. C., & Jiang, Y. R., 2011. Investigation of thermal transport in colloidal silica dispersions (nanofluids). *J. Nanopart. Res., 13*(7), 3075-3083

Wen, D. S., & Ding, Y. L., 2004. Experimental investigation into convective heat transfer of nanofluids at the entrance region under laminar flow conditions. *Int. J. Heat Mass Transfer, 47*(24), 5181-5188

Wen, D. S., & Ding, Y. L., 2005a. Effect of particle migration on heat transfer in suspensions of nanoparticles flowing through minichannels. *Microfluid. Nanofluid., 1*(2), 183-189

Wen, D. S., & Ding, Y. L., 2005b. Experimental investigation into the pool boiling heat transfer of aqueous based gamma-alumina nanofluids. *J. Nanopart. Res., 7*(2-3), 265-274

Youbi, I., 2003. Impact of Refrigerant–oil Solubility on an Evaporator Performances Working with R-407C. *Int J Refrig, 26*(3), 284-292

Appendix A

Previous work on measuring the thermophysical properties of Al_2O_3 Nanolubricants

This thesis was part of a larger research project where other additional experiments were conducted by other graduate students at Oklahoma State University. These additional experiments were conducted to measure the thermophysical properties of the same Al_2O_3 nanolubricants, which were used in this thesis to explain some the heat transfer and pressure drop experimental results. Some tests were conducted by individuals in the same research group at Oklahoma State University, where my work was performed. For these tests, I assisted with the experiments. Others measurements were performed in collaboration with an external research company, and I performed the data analysis for these results. The following is a list of the experiments and main researchers that led these experiments and their data analysis.

1) Andrea Bigi at OSU, Stillwater (U.S.): For the thermal conductivity and sedimentation and agglomeration experiments.
.
2) Amy Wong at OSU, Stillwater (U.S.): For the specific heat experiments.
3) Dr. Bianca W. Hydutsky and Dr. Thomas J. Leck at E.I. du Pont de Nemours and Company DuPont Fluoro Chemical, Wilmington (U.S.): For the viscosity and miscibility experiments.

A summary of the work conducted and of the tests results from the additional experiments carried in this research project is presented next. The additional experiments aimed to determine the thermal physical properties of Al_2O_3 nanolubricants, which are key to measure and derive the in-tube flow boiling heat transfer coefficient and two-phase pressure drop of refrigerant and Al_2O_3 nanolubricants mixtures. In other words, the sections below provide the background information for the heat transfer and pressure drop preliminary data presented in this thesis.

THERMOPHYSICAL PROPERTIES OF Al_2O_3 NANOLUBRICANTS

Objectives

To perform the HTC and pressure drop tests, preliminary experiments were performed to investigate the thermophysical properties of Al_2O_3-POE nanolubricant mixtures, and compared with pure POE. These experiments to determine the thermophysical properties constitute phase 1 of the 2 phase project. HTC and pressure drop results constitute phase 2 and was described in the main body of the thesis the significance of the experiments in phase 1 are as follows:

Thermal conductivity, viscosity and specific heat

The increase in thermal conductivity and viscosity, and decrease in specific heat due to addition of nanoparticles have attracted the attention of many reserachers. Several research have been performed to measure the thermal conductivity of nanofluids. However, literature on thermal conductivity of nanolubricants (which are high viscosity stable suspensions such as Al_2O_3-POE mixtures in particular) do not exist. It is speculated that increase in thermal conductivity could increase the heat transfer coefficient of refrigerant lubricant mixtures. An objective of the project was to investigate the effect of addition of nanoparticles to POE on its thermal conductivity, viscosity, and it's the heat transfer coefficient of refrigerant-nanolubricant mixtures and compare the values with refrigerant-POE mixtures.

Nanoparticle sedimentation and agglomeration

Studies performed on nanofluids described in chapter 2.5 have found that sedimentation and agglomeration of nanoparticles occur in low viscosity fluids and are undesired effects. The Al_2O_3-POE nanolubricants are high in viscosity compared to nanofluids. However, it is not known if the nanoparticles sediment and agglomerate with time when mixed with POE. An objective of this thesis was to determine if sedimentation and agglomeration occur with the samples of Al_2O_3-POE nanolubricants.

Literature Review

Thermal conductivity and viscosity of nanolubricants

The increase in thermal conductivity of nanofluids due to the addition of nanoparticles was investigated by numerous researchers and a comprehensive review can be found in a paper by Buongiorno *et al.* (2009) and in a paper by Ozerinc *et al.* (2009). Nanofluids have often higher thermal conductivity than that predicted by the macroscopic theory. Venerus and Jiang (2011) pointed out that for systems composed of larger diameter nanoparticles (~30nm), there was a good agreement between the measured thermal conductivity enhancement and the one predicted by the classical Maxwell-Garnett model. The thermal conductivity of nanolubricants in this work was estimated by using Eq. (2) in previous work (Cremaschi, 2012), and this equation was previously proposed by Wen and Ding (Wen & Ding, 2005a). Several existing models can be used to predict the thermal conductivity of the nanolubricant (Buongiorno *et al.*, 2009; Jain *et al.*, 2009; Phillips *et al.*, 1992), and their viscosity and specific heat (Venerus *et al.*, 2010). An example for the viscosity of the lubricant and liquid refrigerant mixture is given in eq. (3) (Batchelor, 1977) where k_1 was 2.5 and k_2 was 6.2 and they were modified by Wen and Ding to account for the addition of nanoparticles in the base fluid (Wen & Ding, 2005a). Eq. (3) applies to suspensions of non-interacting particles with a concentration smaller than about 5% by volume. $\mu_{mix,liq}$ is the dynamic viscosity of the lubricant and liquid refrigerant mixture and it accounted for the lubricant solubility of the refrigerant at given saturation temperatures. Effects of metal oxide nanoparticles dispersed in oil suggest that both thermal conductivity and viscosity increase with the presence of nanoparticles but with different trends depending on temperature range, volume fraction and particle type (Cremaschi, 2012).

$$\frac{k_{nl}}{k_{POE}} = \frac{(1-\phi)\left(k_p + 2k_f\right) + 3\phi k_p}{(1-\phi)\left(k_p + 2k_f\right) + 3\phi k_f} \tag{2}$$

$$\frac{\mu}{\mu_{mix,liq}} = 1 + k_1\phi + k_2\phi^2 \tag{3}$$

$, where\ k_{nl}\ is\ the\ thermal\ conductivity\ of\ the\ nanolubricant$
$k_{POE}\ is\ the\ thermal\ conductivity\ of\ the\ POE\ oil$
$k_p\ is\ the\ thermal\ conductivity\ of\ the\ nanoparticles$
$k_f\ is\ the\ thermal\ conductivity\ of\ the\ fluid$
$and\ \phi\ is\ the\ concentration\ of\ the\ nanoparticles\ by\ mass$

Specific heat

To author's best knowledge there are no studies that provide data for the specific heat of nanoparticles in POE lubricants in open domain literature. Models for water based nanofluids are often used to predict the specific heat of nanolubricants but their accuracy was seldom verified. Nanofluids have lower specific heats than their base fluids, according to eq. (1) valid for an ideal liquid-particle mixture:

$$c_{p(nl)} = \phi c_{p(p)} + (1-\phi)c_{p(f)} \tag{1}$$

$, where\ c_{p(nl)}\ is\ the\ specific\ heat\ of\ the\ nanolubricant$
$c_{p(p)} is\ the\ specific\ heat\ of\ the\ nanoparticles$
$c_{p(f)} is\ the\ specific\ heat\ of\ the\ fluid$
$\phi\ is\ the\ concentration\ of\ nanparticles\ by\ mass$

In several experiments, it was observed that the specific heat decreased if the volume concentration of nanoparticles (Φ) increased. Specific heat also increased with increase in temperatures (Vajjha & Das, 2009). Experiments conducted by Murshed *et al.* (2008) used a double hot-wire technique to measure the effective specific heat of different types of nanofluids. Their study concluded that fluids with nanoparticles had lower specific heat than their base fluids, and that the values for specific heat decreased with increasing volume fraction of the nanoparticles. Puliti *et al.* (2011) presented a comprehensive review of available literature on nanofluids. For specific heat, most studies have reported that nanofluids have lower specific heats than their base fluids. However conflicting studies were also presented where the specific heat was higher than the base fluids. It was recommended to conduct more experiments for measuring the specific heat of nanofluids and for verifying the correlations.

Nanoparticle sedimentation and Agglomeration

Two critical factors that must be characterized when developing nanolubricants for heat transfer enhancement are the potential for agglomeration of the nanoparticles into large clusters and for sedimentation of the nanoparticles on the heat transfer surfaces. The sedimentation due to clustering and agglomeration of nanoparticles was observed in propanol based nanofluids (Wen & Ding, 2004). Agglomeration and sedimentation of nanoparticles in the lubricant might interfere with the heat transfer process (Das *et al.*, 2003). Most heat transfer surfaces have nucleate sites that enhance heat transfer due to eddies created by the nucleate sites (Cieslinski, 2007). Sedimentation of nanoparticles that are immersed in the heat transfer fluid might deposit into the nucleate sites creating a smoother surface (Bang, 2004). According to Das *et al.* (2003) the resulting smoother surfaces can cause a considerable deterioration of the heat transfer coefficient. From previous studies, it was observed that stable suspensions of nanoparticles had minimum sedimentation. To develop such stable suspensions, the base fluid had high viscosity such as the case with polyolesters oils. The addition of dispersants and surfactants could prevent clustering and finding the correct combination often required a trial and error approach. In this approach the size of nanoparticles in suspensions is measured by using dynamic light scattering (DLS), also referred to as quasi-elastic light scattering technique.

Equipment and instrumentation

Equipment for measuring the nanoparticle sizes in dispersion in POE lubricant

A Malvern Nano-zs DLS instrument was used for measuring the size of the nanoparticles. The device was capable of measuring particles size ranging from 4 nm to 10 μm diameter. Temperature of the samples was close to room temperature for all the particle measurements in the present work. The DLS instrument implemented an electrophoretic light scattering technique with a He-Ne laser of 633 nm wavelength. An interface software of the instrument allowed to analyze the measurements on line and correlated the back scattering reflection intensity of the laser to the mean particle sizes of the sample. It should be noted that the nanolubricant was sampled and diluted with POE oil to concentration of less than 1 weight percent before measuring the particle size in order to improve the reliability and accuracy of the particle size measurements. The Malvern-Nano-zs DLS measuring device is shown in Figure 60.

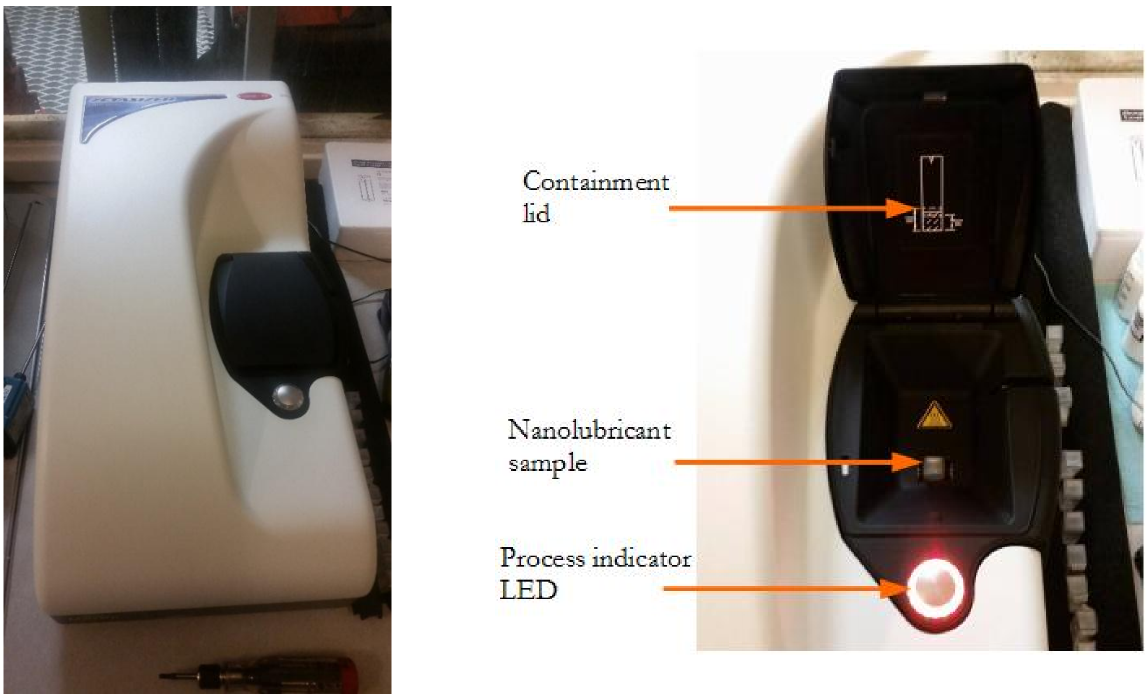

Figure 60: Malvern-nano-zs DLS measuring device

Equipment for measuring the specific heat of nanolubricants

The instrument for measuring the specific heat of the nanolubricant was custom built in the present work (see Figure 61). It consisted of three main components: a temperature bath, a small steel reservoir for the nanolubricant, and an electric heater. A precision temperature sensors and a volt meter were used to read temperature and power. The high precision temperature bath was used to maintain constant boundary temperature conditions around the insulated reservoir. A wire heater rated at 60 W at 120V AC provided heat to the small steel container with the nanolubricant inside it. A variable voltage transformer was used to regulate the power to the electric heater, which was firmly wrapped around the walls of the steel container. A custom made cylindrical stainless steel container of 150 mL of internal volume was used to store the nanolubricant during the experiments. Temperature measurements were made by using a precision thermometer with a resolution of 0.01°C and a rated accuracy of ± 0.06 °C. The probe was immersed in the center of the nanolubricant reservoir. Adiabatic condition around the small steel container was obtained by insulating the container with about 2 cm thick layer of rubber flexible foam insulation and by immersing the container in the water inside the temperature bath. A plastic water jacket was installed around the insulation to avoid water ingress into the insulation. The temperature of the bath was controlled to limit the temperature gradient between the nanolubricant inside the container and the environment surrounding the container. A schematic of the setup for the specific experiment is shown in Figure 61.

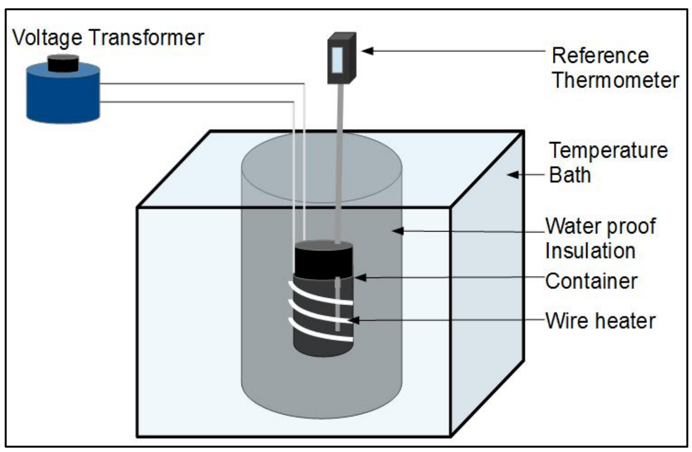

Figure 61: Schematic of the specific heat test

Instrumentation for measuring the thermal conductivity and viscosity of nanolubricants

The instrumentation for measuring the thermal conductivity of the nanolubricant included a KD2 thermal conductivity probe and a temperature bath. Figure 62 shows the equipment used for the thermal conductivity measurements.

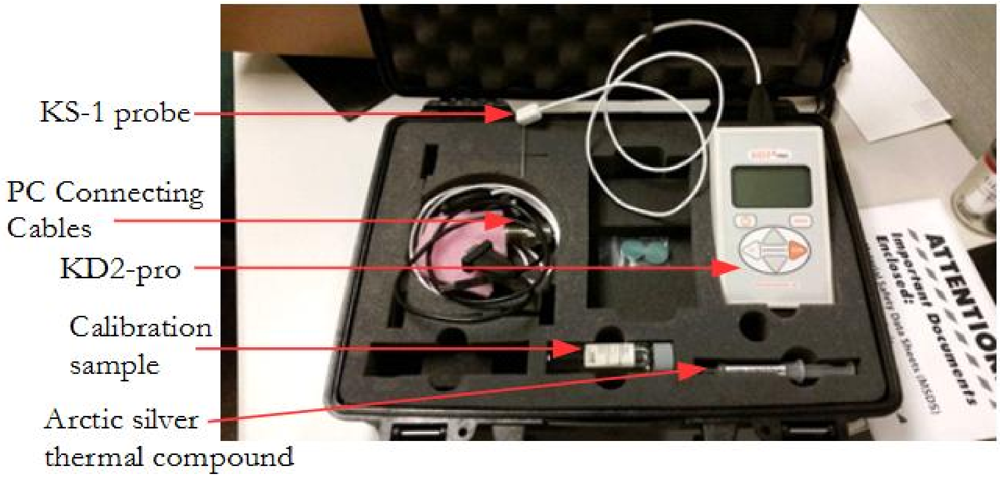

Figure 62: KD2 Pro Thermal conductivity measuring device

The thermal conductivity probe had a built in controller and it measured the thermal conductivity of the nanolubricant directly based on a double hot-wire technique. The rated accuracy of the probe was ±0.01 W/(m-K) for the range from 0.02 to 0.2 W/(m-K). The viscosity of the nanolubricants was measured by using a Cannon-Fenske type viscometer.

Uncertainty analysis

The methods of error analysis and uncertainty propagation outlined in (Taylor, 1997) was used for calculating the uncertainties of experiments, and the values of the uncertainties is shown in the table below.

Table 10. Experimental uncertainties of experiments performed on thermo-physical properties

Measurement objective	Parameter	Uncertainty
Nanoparticle size ratio	$\frac{\delta(D/D_{min})}{D/D_{min}}$	±0.03
Specific heat	δCp_{poe}	±0.18 kJ/kg-K
Specific heat ratio	$\frac{\delta(\mathrm{Cp_{nl}}/\mathrm{Cp_{poe}})}{\mathrm{Cp_{nl}}/\mathrm{Cp_{poe}}}$	±0.15
Thermal conductivity	$\delta k_{poe}, \delta k_{nl}$	±0.015 W/(m-K)
Thermal conductivity ratio	$\frac{\delta(k_{nl}/k_{poe})}{k_{nl}/k_{poe}}$	±0.17

Uncertainties are expressed with confidence level of 95.5%

Experimental Methodology

Procedure for measuring the potential of nanoparticle sedimentation and agglomeration

The procedure for conducting the sedimentation tests included the preparation of the nanolubricant samples, the storage of the samples, and the measurements of samples with few droplets of the nanolubricant from the bottom of the container and from the top of the containers used to store the nanolubricant test specimens. The measurement of particle size was performed using the Malvern DLS instrument. About 80mL of each type of nanolubricant were created with a nanoparticle concentration of 0.5 wt% and of 1 wt% (i.e. two concentration for each type of nanolubricant). A 100mL beaker was used, and the dry weight of the beaker was measured. The mass of oil required was added into the beaker using a 10 mL syringe. The concentrated solution of nanoparticle and POE oil was then added to the POE oil to achieve the required concentration according to eq. (4). The nanoparticle and oil mixture was sonicated for 24 hours with pulse on/off cyle of 30 seconds each. After the nanolubricant samples were prepared the particle size was immediately measured. Small droplets of nanolubricant were taken from the top and from the bottom of the 100mL container that stored the nanolubricant samples, a separate new cuvette was used for testing each sample.

The samples were then tested for size using the DLS measurement device. The Malvern software is used for communication between the instrument and the computer. Figure 63 shows a sample of the output obtained from the DLS instrument.

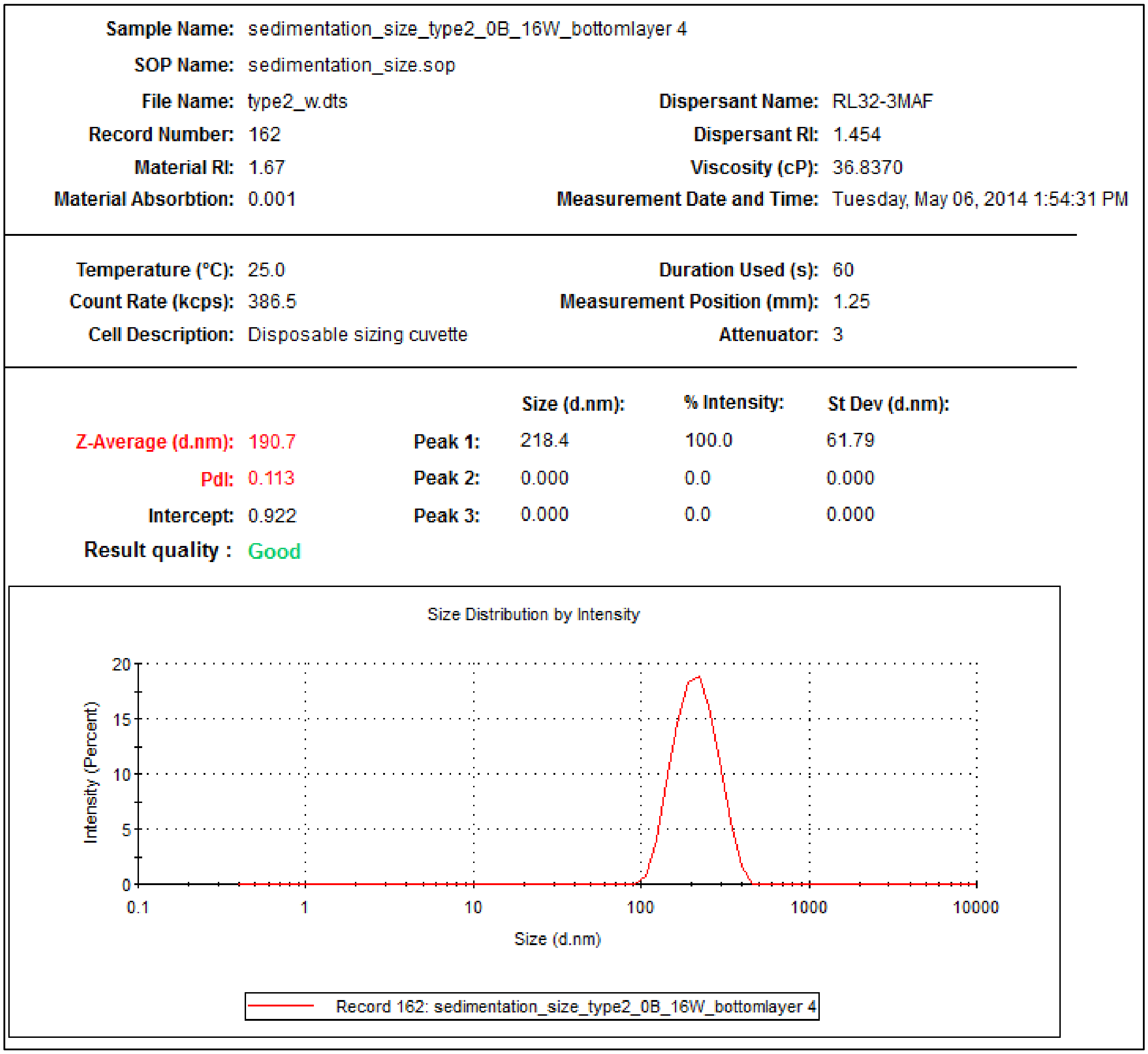

Figure 63: Zetasizer software interface

This first measurements were used as initial size of the nanoparticle and then the particles size were measured regularly every 2 weeks for a period of five months in order to check for potential agglomeration and sedimentation effects. If there was agglomeration of particles, the size measured at both the top and bottom of the 80mL sample would increase, if there was sedimentation as a result, the measured size of the bottom samples from the 80mL beaker would increase. Since only the surfactant coated nanoparticles (dispersant) and the POE (medium) are present in the samples, the size of the nanoparticles are measured by the DLS instrument.

Procedure to measure the specific heat of the nanolubricants

For the calibration and verification of the specific heat tests, experiments were conducted with water then with POE oil to calibrate instrumentation and refine testing procedures of the experiment. Three sets of calibration tests were performed to determine the heat losses in POE oil and also to confirm the repeatability of the testing methodology. A heatloss correction factor for tests conducted with POE lubricant was calculated from data and the data obtained thereafter was within 3 percent error when compared to literature values (Thome, 1995). The verification is discussed along with the results of this experiment.

Maintaining heat loss to a minimum was crucial to acquire good results for the specific heat tests. A 150mL container was used to hold the sample. The container was sealed and a thermometer was fixed onto the container using an air tight sealing putty. This set up was placed into the insulation and inside the thermal bath. The heater was then switched on and timed. The voltage transducer was dialed up to 60 V. The fluid temperature increased and it was continuously measured by the reference thermometer inserted inside the container. The bath temperature was raised to match the inside temperature as the nanolubricant was heated. Four different temperature ranges were taken, from 2 to 12°C, from 12 to 22°C, from 22 to 32°C and from 32 to 42°C. After each temperature was reached, the heater was turned off, the time was stopped and the whole system was allowed to come to thermal equilibrium. The water was stirred slightly in order to promote even temperature on the entire nanolubricant sample. The final temperature was read and was used to calculate the specific heat of the nanolubricant. The resistance of the heater was also measured. For each heating phase of the nanlubricant, the temperature of the bath was at the initial temperature of the nanolubricant. This ensured repeatability of the experiments and limit the heat losses.

Procedure to measure the thermal conductivity of the nanolubricants

The nanolubricant sample was kept at rest in a sample container provided by the manufacturer of the thermal conductivity probe. The sample container was filled with the nanolubricant and it was immersed in a thermal bath to ensure that the sample temperature was controlled. For each measurement the temperature bath was switched off before immersing the probe in order to limit forced convection effect due to the vibrations coming from the thermal bath pump. Thermal conductivity was a direct output of the probe immersed in the nanolubricant. Each measurement took few minutes for achieving thermal equilibrium and each measurement was repeated 3 times.

Results and Discussion

Sedimentation test results

The nanoparticle sedimentation tests results are plotted in Figure 64 (a). The x-axis represents the time in weeks and the y-axis shows the nanoparticle normalized diameter which is the ratio of the measured diameter and the smallest measured diameter for the entire experiment. Tests were conducted for three types of nanolubricants, namely T1S1, T2S1 and T3S1 samples. The concentration of the nanolubricant samples for the sedimentation tests was 1 weight percent. This was the minimum nanoparticle concentration and thus the least viscous solution possible. Type 1 and type 2 samples, which have the same metal Al_2O_3 nanoparticle type but different surfactants, showed that the nanoparticle size did not increase over a 20 week period. These results indicated that there was no agglomeration and no signs of clusters of the nanoparticles in these nanolubricant types, as there was no increase in particle size over time for type 1 and type 2 samples. The data also shows that both top and bottom layers of the containers had same nanoparticle size. These results indicated that there were not any signs of sedimentation and the nanoparticle suspensions type 1 and type 2 were stable.

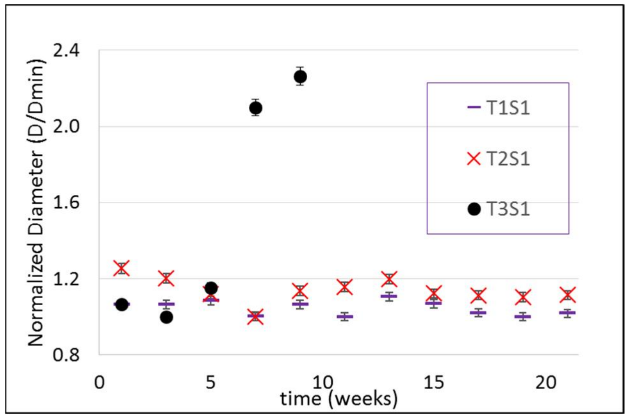

(a)

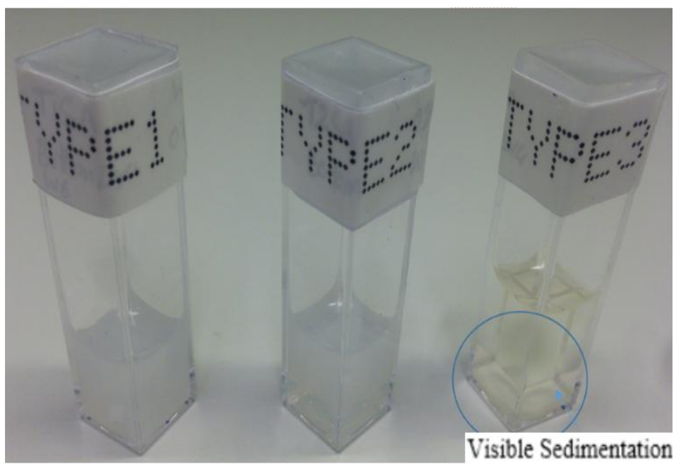

(b)

Figure 64: (a) Sedimentation test results for three types of nanolubricants and (b) visual observation of sedimentation for type 3 nanolubricant

The ratio of the measured particle size over the minimum particle size was within the range of 1 to 1.5. Visual confirmation of these results are illustrated in Figure 64(b). Type 3 nanolubricant, which had same nanoparticles but used a third different surfactant different than that of type 1 and type 2, showed agglomeration in Figure 64 (a) (solid round data points) and sedimentation (see Figure 64(b) type 3 within the blue circle). The particle sizes for type 3 increased with time, starting from a size ratio of about 1 and increasing over time to about 2.5 indicating that the particles were agglomerating and sedimentation was taking place. The samples were taken from the bottom of the sample where the largest concentration was present due to sedimentation of the type 3 nanolubricant.

It is to be noted that the given particle size in the dry state is about 40nm according to the manufacturer. However, DLS measurements recorded particle sizes of 80-100nm for the stable type1 and type 2 samples. It was confirmed with the manufacturer of the nanoparticles who used the same DLS measurement technique that a particle size within the range recorded with the DLS measurements corresponded to a particle size of about 40nm using other measurement techniques. Another research group (DuPont USA) was also consulted and confirmed that they had the same results using DLS measurements.

Sedimentation and agglomeration are undesired effects for heat transfer applications (Das *et al.*, 2003), since Type 1 and Type 2 nanolubricants did not show signs of sedimentation and agglomeration with time, these nanolubricants were chosen for further testing. Type 3 nanolubricants were no longer considered for further testing based both size test results as well as visible sedimentation and agglomeration that occurred during the size tests.

Specific heat test results

The specific heat of POE oil is showed in Figure 65 (a) and the measured data and the literature values (Thome, 1995) (dashed line) are plotted for a temperature range from 10 to 40 °C, the data points in this plot represent the validation of the experimental apparatus with literature values. The ratio of the specific heat of the nanolubricants type 1 and type 2 at concentration of 10 and 20 weight percent over the specific heat of POE oil at the same temperature are given in Figure 65 (b).

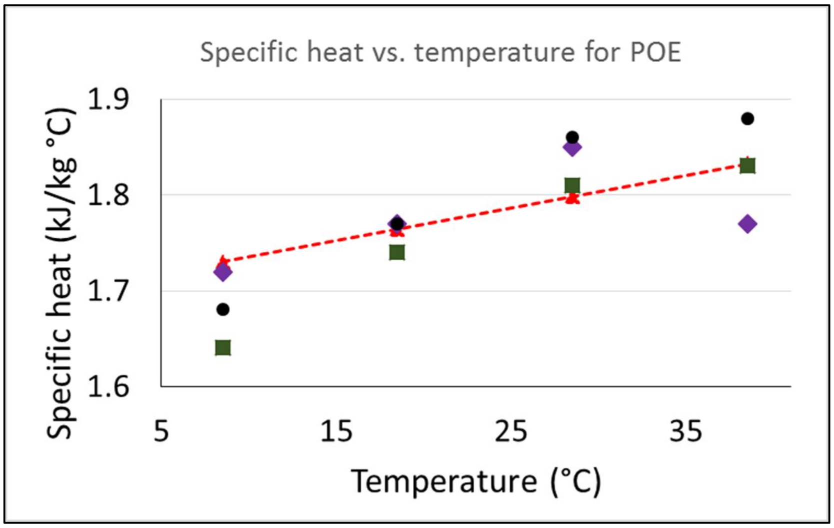

(a)

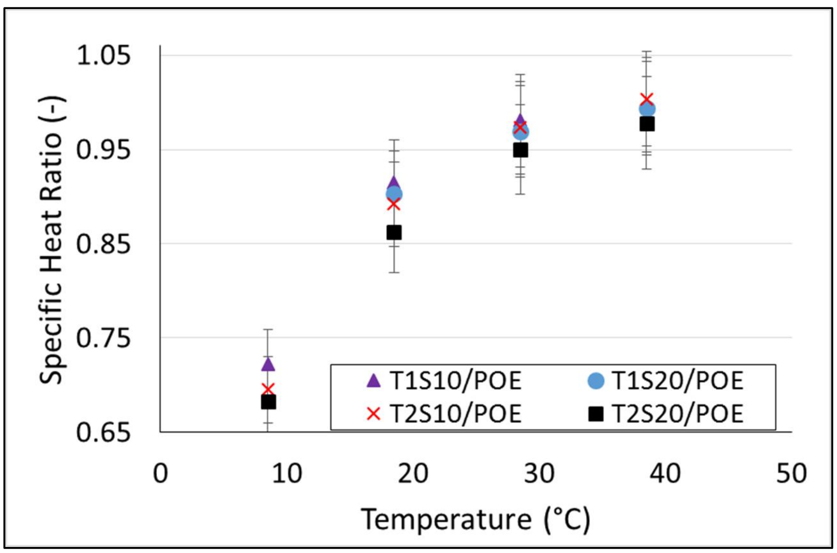

(b)

Figure 65: (a) Specific heat vs. temperature of POE (b) Specific heat ratio vs. temperature

The specific heat of the nanolubricants were lower than that of POE oil and the difference was greater at temperatures of about 10°C. When the temperatures were closer to 40°C the nanolubricants had similar specific heat as to the one of the POE lubricant.

Thermal Conductivity test results

The thermal conductivity of POE lubricant is shown in Figure 66(a) and the ratio of thermal conductivity of each nanolubricant over that of POE oil at the same temperature is shown in Figure 66(b).

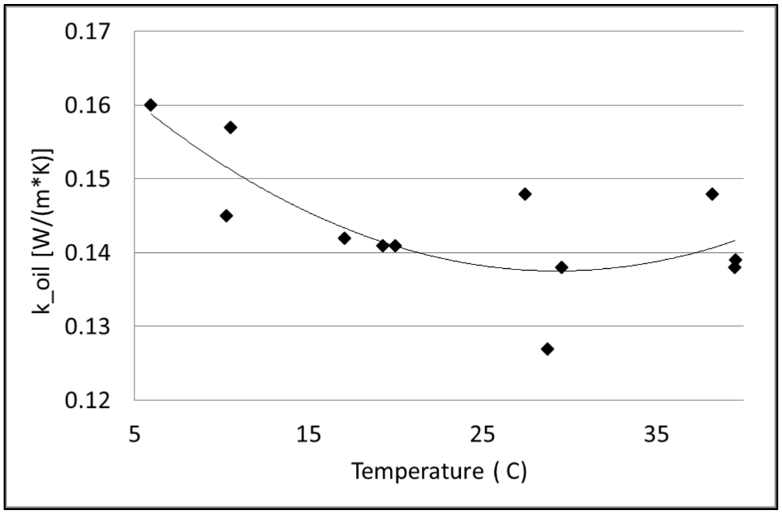

(a)

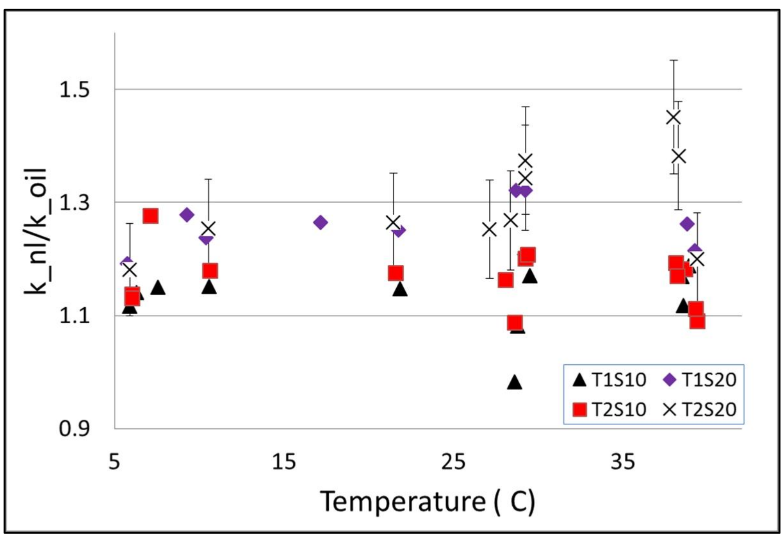

(b)

Figure 66: (a) Thermal conductivity vs. Temperature of POE and (b) Nanolubricant-POE thermal conductivity ratio

Although there are scattered data in Figure 66(a), it appears that the POE oil thermal conductivity decreased slightly if the temperature increased from 5 to 30°C. Figure 66(b) shows that the highest thermal conductivity was measured for the T2S20 nanolubricant sample followed by T1S20 sample. These samples had the highest concentration of Al_2O_3 nanoparticles of 20 weight percent and their thermal conductivity ranged from 1.5 times higher at 5 °C to 2 times higher at 40 °C than the thermal conductivity of POE oil at similar temperature. The sample T2S10 showed a higher thermal conductivity relative to T1S10 and both had the 10 weight percent Al_2O_3 nanoparticles concentration. It appears that the surfactant that was used to stabilize the nanoparticles had an effect on the thermal conductivity of the anolubricant. This is evident from the T2S20 and T2S10 data, which had higher thermal conductivity in both 10 and 20 weight percent concentrations when compared their Type 1 sample counterparts.

Viscosity test results

The viscosity of the nanoubricants was measured by using a Cannon-Fenske type viscometer. The viscosity of the nanolubricants at 45°C was the same as that of POE lubricant and the type of surfactant did not affect the viscosity at this temperature. The viscosity ratio, defined as the viscosity of a nanolubricant over the viscosity of POE lubricant at similar temperature, at 10 weight percent of nanoparticle concentration ranged from 1.8 if the temperature was 20°C to 2.9 when the temperature was 0°C. The viscosity ratio of nanolubricant with 20 weight percent nanoparticle concentration ranged from 1.9 if the temperature was 20°C to 3.3-3.8 when the temperature was 0°C.

Miscibility test results

The refrigerant/nanolubricant concentration were tested for 95/5 % to 30/70% at a temperature range of -30 to 60ºC. Miscibility results were identical for T1S5 and T1S10 samples. The refrigerant-nanolubricant samples were miscible for all concentrations tested except for 80/20% at 55-60ºC, and 70/30% at 50-60ºC. T1S20 was miscible at a concentration of 60/40% from -30 to 55ºC. At a concentration of 30/70% the samples were miscible for the entire range of temperatures. The results indicate that miscibility is dependent on the ratio of refrigerant and nanolubricant as seen in T1S10 which was not miscible for a concentration range of 95/5% to 70/30% but was miscible for 60/40% to 30/70% concentrations. Temperature also determines the miscibility of the samples as seen in T1S5 and T1S10 which were miscible at 80/20% for a temperature range of -30 to 50^{o}C but immiscible for 55-60^{o}C.

Equipment used for the Heat transfer coefficient and pressure drop experiment

Equipment/Instrument	Brand-Model	Specifications
Gear pump	MicroPump GC-M25	Flow Range: 0.4-12 L/min Max DP: 125 psi Max Speed: 3450 rpm
Variable frequency drive	Baldor	460V/ 3 phase/60 Hz 1 HP
Chiller	Cooling Technology	2 Ton Operating Fluid: HC50 480V / 3 phase / 60 Hz
Chiller fluid heater	McMaster-Carr	480V/ 3 phase / 60 Hz
Preheater circulating pump	Taco 2400-50Y	½ HP 230 V/1 phase / 60 Hz
Test section water loop pump	Flint & Walling	1 HP 480 V/ 3 phase/ 60 Hz
Subcooler	GEA FP10x20-20	Connections: 1-1/2" MPT Rated Capactiy:450,00 BTUH 20 Plates
Brazed Plate Heat Exchanger	GEA GBM500H-30	Side A: ¾" MPT Side B: 1" MPT 30 Plates
Nanoparticle size measurement device	Malvern Nanosizer: Nano-zs	0.3nm – 10.0 microns (diameter)
Sonicator	Sonics VC 750	Net power output: VC 505 - 500 Watts. VC 750 - 750 Watts. Frequency: 20 kHz
Thermal conductivity measurement probe	Decagon Devices: KD2 Pro	0 to 50°C ±5%

Appendix B:

SOFTWARE AND CODES

Microsoft Visual Basic Application code used for data analysis of the HTC experiment

```
------------------------------------//--------------------------------------

Option Explicit
Public Bottom As Integer

Sub FetchDataFromTextFile()
Dim fileToOpen As String
Dim i As Long
Dim j As Long
Dim LineText As String

Data.EnableCalculation = False
fileToOpen = Application.GetOpenFilename()

If fileToOpen <> "False" Then

'Clear Data Cells
Data.Range(Data.Cells(6, 1), Data.Cells(1806, 266)).ClearContents


Open fileToOpen For Input As #1
i = 6

While Not EOF(1)
Line Input #1, LineText
Dim arr As Variant
arr = Split(CStr(LineText), vbTab)

For j = 1 To UBound(arr)
```

```
Data.Cells(i, j).Value = arr(j - 1)
Next j
i = i + 1
Wend
Close #1
Else

Exit Sub
End If
Data.EnableCalculation = True
End Sub
Sub Row(Bottom)

Dim i As Integer

For i = 1 To 1000
If Analysis.Cells(i + 3, 6) = "" Then
Bottom = (i + 3)
Exit For
End If
Next i

End Sub
Sub Analyze()

Dim UI(1 To 6) As Variant
Dim i As Integer
Dim Flag As Boolean
Dim EESFlag As Boolean
Dim ChannelNumber As Integer
Dim deltaTTest As Double
Dim n As Long                 'edit_column counter to add columns in excel
Dim m As Integer              'number of columns


'Find bottom of the analysis sheet
Call Row(Bottom)



'Print Test Parameters
For i = 1 To 5
Analysis.Cells(Bottom, i).Value = UI(i)
Next i



DPForm.Show

'Read Data Values
```

```
Analysis.Cells(Bottom, 6) = Data.Cells(4, 137).Value     'Preheater Water
Flow Rate  IN/OUT8_7
Analysis.Cells(Bottom, 7) = Data.Cells(4, 150).Value     'Preheater Inlet
Temp       T8_24
Analysis.Cells(Bottom, 8) = Data.Cells(4, 154).Value     'Preheater Exit Temp
T8_28
Analysis.Cells(Bottom, 10) = Data.Cells(4, 142).Value    'Ref Flow Rate
IN/OUT8_12
Analysis.Cells(Bottom, 11) = Data.Cells(4, 141).Value    'Inlet Pressure
IN/OUT8_11
Analysis.Cells(Bottom, 12) = Data.Cells(4, 155).Value    'Inlet Temp
T8_29
Analysis.Cells(Bottom, 13) = Data.Cells(4, 122).Value    'Exit Temp
T1_46
Analysis.Cells(Bottom, 16) = Data.Cells(4, 140).Value    'Plate Flow Rate
IN/OUT8_10
Analysis.Cells(Bottom, 17) = Data.Cells(4, 83).Value     'Entering Hot Temp
RTD8_5
Analysis.Cells(Bottom, 18) = Data.Cells(4, 84).Value     'Leaving Hot Temp
RTD8_6
Analysis.Cells(Bottom, 20) = Data.Cells(4, 79).Value     'Test Inlet Temp
RTD8_1
Analysis.Cells(Bottom, 21) = Data.Cells(4, 80).Value     'Test Outlet Temp
RTD8_2
Analysis.Cells(Bottom, 22) = Data.Cells(4, 81).Value     'Plate Inlet Temp
RTD8_3
Analysis.Cells(Bottom, 23) = Data.Cells(4, 82).Value     'Plate Outlet Temp
RTD8_4
'Analysis.Cells(Bottom, 24) = 1.22
Analysis.Cells(Bottom, 27) = Data.Cells(4, 122).Value    'Exit Refrigerant
Temp      T1_46
Analysis.Cells(Bottom, 28) = Data.Cells(4, 139).Value    'Exit Pressure
IN/OUT8_9

Analysis.Cells(Bottom, 39) = Data.Cells(4, 56).Value     'Surface
Thermocouple 1     T8_1
Analysis.Cells(Bottom, 40) = Data.Cells(4, 58).Value    'Surface Thermocouple
2     T8_3
Analysis.Cells(Bottom, 41) = Data.Cells(4, 65).Value     'Surface
Thermocouple 3     T8_10
Analysis.Cells(Bottom, 42) = Data.Cells(4, 64).Value     'Surface
Thermocouple 4     T8_9
Analysis.Cells(Bottom, 43) = Data.Cells(4, 68).Value     'Surface
Thermocouple 5     T8_13
Analysis.Cells(Bottom, 44) = Data.Cells(4, 67).Value     'Surface
Thermocouple 6     T8_12
Analysis.Cells(Bottom, 45) = Data.Cells(4, 73).Value     'Surface
Thermocouple 7     T8_18
Analysis.Cells(Bottom, 46) = Data.Cells(4, 74).Value    'Surface Thermocouple
8     T8_19
```

```
Analysis.Cells(Bottom, 47) = Data.Cells(4, 151).Value    'Surface
Thermocouple 9     T8_25
Analysis.Cells(Bottom, 48) = Data.Cells(4, 69).Value     'Surface
Thermocouple 10     T8_14
Analysis.Cells(Bottom, 49) = Data.Cells(4, 125).Value    'Surface
Thermocouple
'Paste Formulas To Cells
Analysis.Cells(Bottom, 9).Value = "=RC[-3]*1.007*60*(RC[-2]-RC[-1])"
'Preheat Heat Input'
Analysis.Cells(Bottom, 15).Value = "=RC[-6]/RC[-5]+RC[-1]"
'Preheat Exit Enthalpy'
Analysis.Cells(Bottom, 19).Value = "=RC[-3]*60*(RC[-2]-RC[-1])"
'Plate Heat Input'
Analysis.Cells(Bottom, 24) = Data.Cells(4, 270).Value * 0.69
'Pump Work with Eff
Analysis.Cells(Bottom, 25).Value = "=RC[-6]+(RC[-1]*3412.14163)"
'Total Heat Input' Qplate+Pump
Analysis.Cells(Bottom, 26).Value = "=(RC[-1]/Constants!R6C3)*" _
& "(0.00029307107/0.092903)"                                   'Heat
Flux in SI'
Analysis.Cells(Bottom, 29).Value = "=0.9885*RC[-1] + 0.8186"
'Pressure Correction'
'Analysis.Cells(Bottom, 29).Value = "=RC[-1]"
'Pressure Correction'
Analysis.Cells(Bottom, 30).Value = "=RC[-1]"
'Test Exit Enthalpy'
Analysis.Cells(Bottom, 33).Value = "=RC[-8]/RC[-23]+RC[5]"
'Test Exit Enthalpy'
Analysis.Cells(Bottom, 35).Value = "=RC[-1]*6.89475729/" _
& "(Constants!R2C3*0.3048)"                                    'DP per
Length SI'
Analysis.Cells(Bottom, 36).Value = "=RC[-23]"
'Test Inlet Temp'
Analysis.Cells(Bottom, 37).Value = "=RC[-5]+RC[-3]"
'Test Inlet Pressure'
Analysis.Cells(Bottom, 38).Value = "=RC[-23]"
'Test Inlet Enthalpy'
Analysis.Cells(Bottom, 50).Value = "=AVERAGE(RC[-11]:RC[-1])"
'Average Surface Temp'
Analysis.Cells(Bottom, 53).Value = "=AVERAGE(RC[-14]:RC[-4])"
'Corrected Surface Temp'
'Analysis.Cells(Bottom, 52).Value = "=(((RC[-4]-RC[-3])+(RC[-2]" _
& "-RC[-1])/2)/2)+RC[-5]"
'Corrected Surface Temp'
Analysis.Cells(Bottom, 56).Value = "=AVERAGE(RC[-2]:RC[-1])"
'Average Quality'
Analysis.Cells(Bottom, 57).Value = "=(RC[-46]/Constants!R8C3)" _
& "*(0.000125997881/0.092903)"                                 'Mass
Flux in SI'
```

```
Analysis.Cells(Bottom, 58).Value = "=AVERAGE(RC[-21],RC[-30])"
'Average Pressure'
Analysis.Cells(Bottom, 60).Value = "=(-(RC[-51]/Constants!R2C3)" _
& "*LN(((3/8)/24)/(0.0288714/2))/(2*PI()*(401*0.5779)))+RC[-7]"     'Actual
Surface temp'
Analysis.Cells(Bottom, 61).Value = "=RC[-1]-RC[-2]"
'Temperature Difference'
Analysis.Cells(Bottom, 62).Value = "=('Data Analysis'!RC[-37]/" _
& "Constants!R6C3)/RC[-1]"                                          'HTC in
English'
Analysis.Cells(Bottom, 63).Value = "=RC[-1]*0.00568"                     'HTC
in SI
Analysis.Cells(Bottom, 64).Value = "=RC[-1]/Constants!R14C3"
'Normalized HTC
Analysis.Cells(Bottom, 65).Value = "=RC[-30]/Constants!R16C3"
'Normalized DP

Analysis.Cells(Bottom, 66).Value = "=RC[-42]*3412.14163 "
'Effective pump work into the system
Analysis.Cells(Bottom, 67).Value = "=RC[-1]+RC[1]"
'QTS_refrigerant
Analysis.Cells(Bottom, 68).Value = "=RC[-52]*(RC[-51]-RC[-50])*60"
'Qhot
Analysis.Cells(Bottom, 70).Value = "=RC[-1]*(RC[-50]-RC[-49])*60"
'QTS_water
Analysis.Cells(Bottom, 71).Value = "=RC[-2]*(RC[-48]-RC[-49])*60"
'Qplate
Analysis.Cells(Bottom, 72).Value = "=RC[-2]"
'Qrefwaterside
Analysis.Cells(Bottom, 73).Value = "=(RC[-6]-RC[-1])/(RC[-6]+RC[-1])/2*100"
'HEat Balance



'If Initialize Flag and try to start EES
EESFlag = False
Call InitializeEES(EESFlag, ChannelNumber)

'If EES Fails to load
If EESFlag = True Then
Exit Sub
End If

Call Excel_EESPSAT(Bottom, ChannelNumber)           'Calculate PSAT

'Dryout Condition Check'
deltaTTest = Analysis.Cells(Bottom, 27).Value - Analysis.Cells(Bottom,
36).Value
If Abs(deltaTTest) < 2 Then
```

```
Analysis.Cells(Bottom, 31).Value = "=RC[-2]-RC[-1]"
'Pressure Offset'
Analysis.Cells(Bottom, 32).Value = "=RC[-4]"
'Final Exit Pressure'

Else
UI(6) = InputBox("Dryout Condition Detected.Pressure offset to be used?")
Analysis.Cells(Bottom, 31).Value = UI(6)
'Pressure Offset'
Analysis.Cells(Bottom, 32).Value = Analysis.Cells(Bottom, 29).Value - UI(6)
'Final Exit Pressure'
End If

Call Excel_EESEnthalpy(Bottom, ChannelNumber)       'Calculate Enthalpy
Flag = False                                        'Signal correct cells
Call Excel_EESQuality(Bottom, Flag, ChannelNumber)  'calculate initial
quality
Flag = True                                         'signal change cells
Call Excel_EESQuality(Bottom, Flag, ChannelNumber)  'calculate final quailty
Call Excel_EESTSAT(Bottom, ChannelNumber)           'calculate actual TSAT

'Terminate EES Commands
Call CloseEES(ChannelNumber)

'Format Cells to read as "general"
Analysis.Range(Analysis.Cells(Bottom, 6), Analysis.Cells(Bottom,
64)).NumberFormat = "general"

End Sub

Sub DP(Bottom)

If DPForm.OptionButton1 = True Then
Analysis.Cells(Bottom, 34) = Data.Cells(4, 146).Value        '5 PSI DP
IN/OUT8_6'
ElseIf DPForm.OptionButton2 = True Then
Analysis.Cells(Bottom, 34) = Data.Cells(4, 144).Value        '8 PSI DP
IN/OUT8_14'
Else
Analysis.Cells(Bottom, 34) = Data.Cells(4, 143).Value        '15 PSI DP
IN/OUT8_13'
End If

DPForm.Hide

End Sub
Sub InitializeEES(EESFlag, ChannelNumber)

Dim myShell As String
```

```
ChannelNumber = 1
'myShell = "C:\Program Files (x86)\EES32\ees.exe"
myShell = "C:\EES32\ees.exe"

On Error Resume Next

'Open EES
Shell_R = Shell(myShell, 6)

If Shell_R = "" Then
EESFlag = True
MsgBox "The application, " & myShell & ", was not found", vbExclamation, "EES
DDE"
Else
ChannelNumber = Application.DDEInitiate(app:="ees", topic:="")
End If

End Sub
Sub CloseEES(ChannelNumber)

'Quit EES and Terminate DDE
DDEExecute ChannelNumber, "QUIT"
Application.DDETerminate ChannelNumber

End Sub
Sub Excel_EESEnthalpy(Bottom, ChannelNumber)

Analysis.Activate

Range(Analysis.Cells(Bottom, 11), Analysis.Cells(Bottom, 12)).Select
Selection.Copy

Application.DDEExecute ChannelNumber, "[Open C:\EES32\Excel_ees1.ees]"
Application.DDEExecute ChannelNumber, "[Paste Parametric 'Table 1' R1 C1]"

Application.DDEExecute ChannelNumber, "[SOLVETABLE 'TABLE 1', Rows=1]"

Application.DDEExecute ChannelNumber, "[COPY ParametricTable 'Table 1' R1
C3]"

'Paste results from EES into EXCEL'

ActiveSheet.Paste Destination:=Analysis.Cells(Bottom, 14)


End Sub
Sub Excel_EESTSAT(Bottom, ChannelNumber)

Analysis.Activate
```

```
Analysis.Cells(Bottom, 58).Select
Selection.Copy

Application.DDEExecute ChannelNumber, "[Open C:\EES32\Excel_ees3.ees]"
Application.DDEExecute ChannelNumber, "[Paste Parametric 'Table 1' R1 C1]"

Application.DDEExecute ChannelNumber, "[SOLVETABLE 'TABLE 1', Rows=1]"

Application.DDEExecute ChannelNumber, "[COPY ParametricTable 'Table 1' R1
C2]"

'Paste results from EES into EXCEL'

ActiveSheet.Paste Destination:=Analysis.Cells(Bottom, 59)


End Sub

Sub Excel_EESQuality(Bottom, Flag, ChannelNumber)

Analysis.Activate

If Flag = True Then
Range(Analysis.Cells(Bottom, 37), Analysis.Cells(Bottom, 38)).Select
Else
Range(Analysis.Cells(Bottom, 32), Analysis.Cells(Bottom, 33)).Select
End If
Selection.Copy


Application.DDEExecute ChannelNumber, "[Open C:\EES32\Excel_ees2.ees]"

Application.DDEExecute ChannelNumber, "[Paste Parametric 'Table 1' R1 C1]"

Application.DDEExecute ChannelNumber, "[SOLVETABLE 'TABLE 1', Rows=1]"

Application.DDEExecute ChannelNumber, "[COPY ParametricTable 'Table 1' R1
C3]"

'Paste results from EES into EXCEL'

If Flag = True Then
ActiveSheet.Paste Destination:=Analysis.Cells(Bottom, 54)
Else
ActiveSheet.Paste Destination:=Analysis.Cells(Bottom, 55)
End If

End Sub
Sub Excel_EESPSAT(Bottom, ChannelNumber)
Analysis.Activate
```

```
Analysis.Cells(Bottom, 36).Select
Selection.Copy
Application.DDEExecute ChannelNumber, "[Open C:\EES32\Excel_ees4.ees]"
Application.DDEExecute ChannelNumber, "[Paste Parametric 'Table 1' R1 C1]"

Application.DDEExecute ChannelNumber, "[SOLVETABLE 'TABLE 1', Rows=1]"

Application.DDEExecute ChannelNumber, "[COPY ParametricTable 'Table 1' R1
C2]"
'Paste results from EES into EXCEL'
ActiveSheet.Paste Destination:=Analysis.Cells(Bottom, 30)

End Sub
```

EES code used for data analysis

```
-----------------------------------//-------------------------------------

R$='R410a'
p_water_preheater=14.7 [psi]
ID=0.342*convert(in,ft)
Test_length=6 [ft]

"Calculation"

"Pre-Heater"
p_r[1]=P_pre_in
T_r[1]=T_in_preh
x_r[1]=0
h_r[1]=enthalpy(R$, p=p_r[1],T=T_r[1])
T_water_average_preheater=(T_w_pre_in+T_w_pre_out)/2
cp_water_preheater=Cp(Water,T=T_water_average_preheater,P=p_water_preheater)
Q_preheater=m_dot_w_pre*cp_water_preheater*(T_w_pre_in-T_w_pre_out)*Convert(Btu/min,Btu/hr)
h_r[2]=h_r[1]+Q_preheater/m_dot_ref
p_r[2]=p_r[3]
x_r[2]=quality(R$, h=h_r[2], p=p_r[2])


"Test Section"
p_r[3]=P_out_TS+DP_out_ts
h_r[3]=h_r[2]
x_r[3]=x_r[2]
p_water_ts=p_water_preheater
T_water_average_ts=(T_w_hot_in+T_w_hot_out)/2
cp_water_ts=Cp(Water,T=T_water_average_ts,P=p_water_ts)
Q_ts=(Q_pump_actual*Convert(kW,Btu/hr))+Q_plate
Q_plate=m_dot_w_plate*cp_water_ts*(T_w_hot_in-T_w_hot_out)*Convert(Btu/min,Btu/hr)
h_r[4]=h_r[3]+Q_ts/m_dot_ref
p_r[4]=P_out_TS
x_r[4]=quality(R$, h=h_r[4], p=p_r[4])
```

```
"Q_pump_old=((-0.0061 * T_rtd8_4 + 1.2473 [F]) * 2544.43358[Btu/F*hr])*Convert(Btu/hr,kW)"
"A_s=0.0088*pi#*2.54[m^2]*1.6"
A_s=ID*3.142*Test_length*1.6*convert(ft^2, m^2)

HF=Q_ts/A_s*Convert(Btu/hr,kW)
x_avg=(x_r[4]+x_r[2])/2

P_out_TS=Pressure(R$,T=T_sat,x=0)
del_x=(x_r[4]-x_r[2])

m_flux=(m_dot_ref/((ID/2)^2)/3.142)*(0.000125997881/0.092903)

Eff_linear=(-0.0118*T_jacket_in + 1.561)
Q_pump_actual = Eff_input*Q_pump
```

$ID = 0.342 \cdot \left| 0.083333333 \cdot \frac{ft}{in} \right|$

$Test_{length} = 6$ [ft]

Calculation

Pre-Heater

$p_{r,1} = P_{pre,in}$

$T_{r,1} = T_{in,preh}$

$x_{r,1} = 0$

$h_{r,1} = \mathbf{h}\left[R\$, P = p_{r,1}, T = T_{r,1}\right]$

$T_{water,average,preheater} = \frac{T_{w,pre,in} + T_{w,pre,out}}{2}$

$cp_{water,preheater} = \mathbf{Cp}\left[water, T = T_{water,average,preheater}, P = p_{water,preheater}\right]$

$Q_{preheater} = \dot{m}_{w,pre} \cdot cp_{water,preheater} \cdot \left[T_{w,pre,in} - T_{w,pre,out}\right] \cdot \left| 60 \cdot \frac{Btu/hr}{Btu/min} \right|$

$h_{r,2} = h_{r,1} + \frac{Q_{preheater}}{\dot{m}_{ref}}$

$p_{r,2} = p_{r,3}$

$x_{r,2} = \mathbf{x}\left[R\$, h = h_{r,2}, P = p_{r,2}\right]$

Test Section

$p_{r,3} = P_{out,TS} + DP_{out,ts}$

$h_{r,3} = h_{r,2}$

$x_{r,3} = x_{r,2}$

$p_{water,ts} = p_{water,preheater}$

$T_{water,average,ts} = \frac{T_{w,hot,in} + T_{w,hot,out}}{2}$

$cp_{water,ts} = \mathbf{Cp}\left[water, T = T_{water,average,ts}, P = p_{water,ts}\right]$

$Q_{ts} = Q_{pump,actual} \cdot \left| 3412 \cdot \frac{Btu/hr}{kW} \right| + Q_{plate}$

$Q_{plate} = \dot{m}_{w,plate} \cdot cp_{water,ts} \cdot \left[T_{w,hot,in} - T_{w,hot,out}\right] \cdot \left| 60 \cdot \frac{Btu/hr}{Btu/min} \right|$

$$h_{r,4} = h_{r,3} + \frac{Q_{ts}}{\dot{m}_{ref}}$$

$$p_{r,4} = P_{out,TS}$$

$$x_{r,4} = \mathbf{x}\left[R\$, h = h_{r,4} , P = p_{r,4}\right]$$

*$Q_{pump,old}$=((-0.0061 * $T_{rtd8,4}$ + 1.2473 [F]) * 2544.43358$_{Btu/F*hr}$])*Convert(Btu/hr,kW)*

*A_s=0.0088*pi#*2.54$_{m2}$*1.6*

$$A_s = ID \cdot 3.142 \cdot Test_{length} \cdot 1.6 \cdot \left| 0.09290304 \cdot \frac{m^2}{ft^2} \right|$$

$$HF = \frac{Q_{ts}}{A_s} \cdot \left| 0.000293071 \cdot \frac{kW}{Btu/hr} \right|$$

$$x_{avg} = \frac{x_{r,4} + x_{r,2}}{2}$$

$$P_{out,TS} = \mathbf{P}\left[R\$, T = T_{sat} , x = 0\right]$$

$$del_x = x_{r,4} - x_{r,2}$$

$$m_{flux} = \frac{\dot{m}_{ref}}{\left[\frac{ID}{2}\right]^2 \cdot 3.142} \cdot \frac{0.000126}{0.092903}$$

$$Eff_{linear} = -0.0118 \cdot T_{jacket,in} + 1.561$$

$$Q_{pump,actual} = Eff_{input} \cdot Q_{pump}$$

Parametric Table: Table 1

	$\dot{m}_{ref}$ [lb$_m$/hr]	$P_{pre,in}$ [psia]	$P_{out,TS}$ [psia]	$T_{in,preh}$ [F]	$DP_{out,ts}$ [psi]	$\dot{m}_{w,pre}$ [lb$_m$/min]	$\dot{m}_{w,plate}$ [lb$_m$/min]	$T_{w,pre,in}$ [F]	$T_{w,pre,out}$ [F]
Run 1	166	132.8	131.6	34.75	2.1	0.71	0.35	77	38.5
Run 2	165	133.5	131	33.65	3	1.71	0.34	77.05	44
Run 3	165	134	130.5	30.9	4	2.68	0.36	77.2	46.8
Run 4	165	137.5	128	15.7	8.5	9.35	0.36	77.53	56.5
Run 5	165	138	128	11.45	9.75	10.57	0.355	77.55	57

Parametric Table: Table 1

	$T_{w,hot,in}$ [F]	$T_{w,hot,out}$ [F]	$T_{jacket,in}$ [F]	Q_{pump} [kW]	Eff_{input} [-]	Eff_{linear} [-]	T_{sat} [F]	$x_{r,2}$ [-]	$x_{r,4}$ [-]	del_x [-]
Run 1	76.1	45.7	45.85	1.122	0.69	*1.02*	*39.2*	*0.09*	*0.30*	*0.22*
Run 2	76.2	45.65	45.85	1.123	0.69	*1.02*	*38.9*	*0.20*	*0.41*	*0.22*
Run 3	76	45.6	45.7	1.123	0.69	*1.02*	*38.7*	*0.28*	*0.50*	*0.22*
Run 4	76.45	46	46.2	1.117	0.69	*1.02*	*37.6*	*0.67*	*0.89*	*0.22*

Parametric Table: Table 1

	$T_{w,hot,in}$	$T_{w,hot,out}$	$T_{jacket,in}$	Q_{pump}	Eff_{input}	Eff_{linear}	T_{sat}	$x_{r,2}$	$x_{r,4}$	del_x
	[F]	[F]	[F]	[kW]	[-]	[-]	[F]	[-]	[-]	[-]
Run 5	76.45	46.15	46.25	1.121	0.69	1.02	37.6	0.74	0.96	0.22

Parametric Table: Table 1

	x_{avg}	HF	m_{flux}
	[-]	[kW/m2]	[kg/m2-s]
Run 1	0.19	12.03	352.9
Run 2	0.30	11.99	350.7
Run 3	0.39	12.11	350.7
Run 4	0.76	12.06	350.7
Run 5	0.85	12.05	350.7

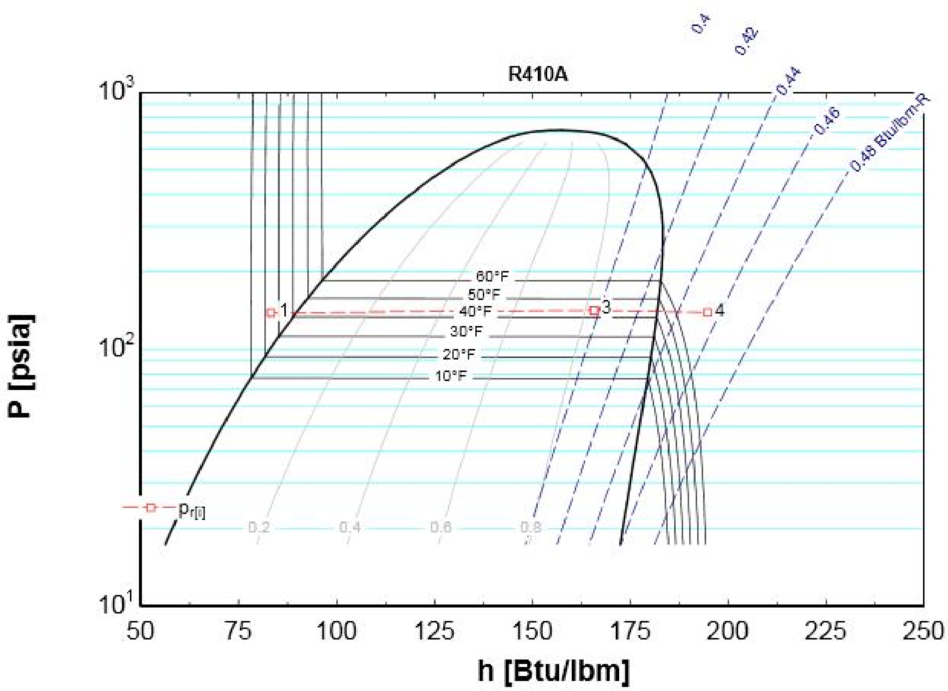

EES code used for uncertainty analysis

Data Calorimeter

$R\$ = \text{'R410a'}$

$ID = 0.342 \cdot \left| 0.083333333 \cdot \frac{ft}{in} \right|$

$Test_{length} = 6$ [ft]

$p_{water,preheater} = 14.7$ [psi]

Calculation

Pre-Heater

$h_{pre,in} = \mathbf{h}(R\$, P = P_{pre,in}, T = T_{in,preh})$

$T_{water,average,preheater} = \frac{T_{w,pre,in} + T_{w,pre,out}}{2}$

$cp_{water,preheater} = \mathbf{Cp}(water, T = T_{water,average,preheater}, P = p_{water,preheater})$

$Q_{preheater} = \dot{m}_{w,pre} \cdot cp_{water,preheater} \cdot (T_{w,pre,in} - T_{w,pre,out}) \cdot \left| 60 \cdot \frac{Btu/hr}{Btu/min} \right|$

$h_{pre,out} = h_{pre,in} + \frac{Q_{preheater}}{\dot{m}_{ref}}$

$x_{ts,in} = \mathbf{x}(R\$, h = h_{pre,out}, P = P_{pre,out})$

Test Section

$P_{pre,out} = P_{out,TS} + DP_{ts}$

$h_{ts,in} = h_{pre,out}$

$p_{water,ts} = p_{water,preheater}$

$T_{water,average,ts} = \frac{T_{w,hot,in} + T_{w,hot,out}}{2}$

$cp_{water,ts} = \mathbf{Cp}(water, T = T_{water,average,ts}, P = p_{water,ts})$

$Q_{ts} = Q_{pump,actual} \cdot \left| 3412 \cdot \frac{Btu/hr}{kW} \right| + Q_{plate}$

$Q_{plate} = \dot{m}_{w,plate} \cdot cp_{water,ts} \cdot (T_{w,hot,in} - T_{w,hot,out}) \cdot \left| 60 \cdot \frac{Btu/hr}{Btu/min} \right|$

$$h_{ts,out} = h_{ts,in} + \frac{Q_{ts}}{\dot{m}_{ref}}$$

$$x_{ts,out} = \mathbf{x}\left(R\$, h = h_{ts,out} , P = P_{out,TS} \right)$$

Q_pump,old=((-0.0061 * T_rtd8,4 + 1.2473 [F]) * 2544.43358 Btu/F*hr])*Convert(Btu/hr,kW)

A_s=0.0088*pi#*2.54 m2*1.6

$$A_s = ID \cdot 3.142 \cdot 1.6 \cdot Test_{length} \cdot \left| 0.09290304 \cdot \frac{m^2}{ft^2} \right|$$

$$HF = \frac{Q_{ts} \cdot \left| 0.000293071 \cdot \frac{kW}{Btu/hr} \right|}{A_s}$$

$$x_{avg} = \frac{x_{ts,out} + x_{ts,in}}{2}$$

$$P_{out,TS} = \mathbf{P}\left(R\$, T = T_{sat} , x = 0 \right)$$

$$del_x = x_{ts,out} - x_{ts,in}$$

$$m_{flux} = \frac{\dot{m}_{ref} \cdot \left| 0.000125998 \cdot \frac{kg/s}{lb_m/h} \right|}{\left[ID \cdot \left| 0.3048 \cdot \frac{m}{ft} \right| \right]^2 \cdot \frac{3.142}{4}}$$

$$\dot{Q}_{pump,actual} = Eff_{input} \cdot \dot{Q}_{pump}$$

$$delT_a = \mathbf{ConvertTemp}\left(F , K , T_{wall} \right) - \mathbf{ConvertTemp}\left(F , K , T_{sat,test} \right)$$

$$alfa_a = \frac{HF}{delT_a}$$

$$delT_b = \mathbf{ConvertTemp}\left(F , K , T_{wall} \right) - \mathbf{ConvertTemp}\left(F , K , T_{sat} \right)$$

$$alfa_b = \frac{HF}{delT_b}$$

$$delP_{perL} = \frac{DP_{ts}}{Test_{length} \cdot \left| 0.3048 \cdot \frac{m}{ft} \right|}$$

Verification of the test section built for the T1S20 tests

Isothermal thermocouple verification TS-5

	Thermocouple#			Difference
T1_47	0	73.23	73.23	0.00
1	1	73.06	73.19	-0.13
3	2	73.18	73.14	0.04
9	3	73.00	73.10	-0.10
10	4	72.96	73.06	-0.10
12	5	72.93	73.01	-0.08
13	6	72.84	72.97	-0.14
14	7	72.87	72.93	-0.06
30	8	72.65	72.88	-0.24
17	9	72.79	72.84	-0.06
18	10	72.77	72.80	-0.03
19	11	72.59	72.76	-0.17
25	13	72.39	72.67	-0.28
T1_46	14	72.63	72.63	0.00

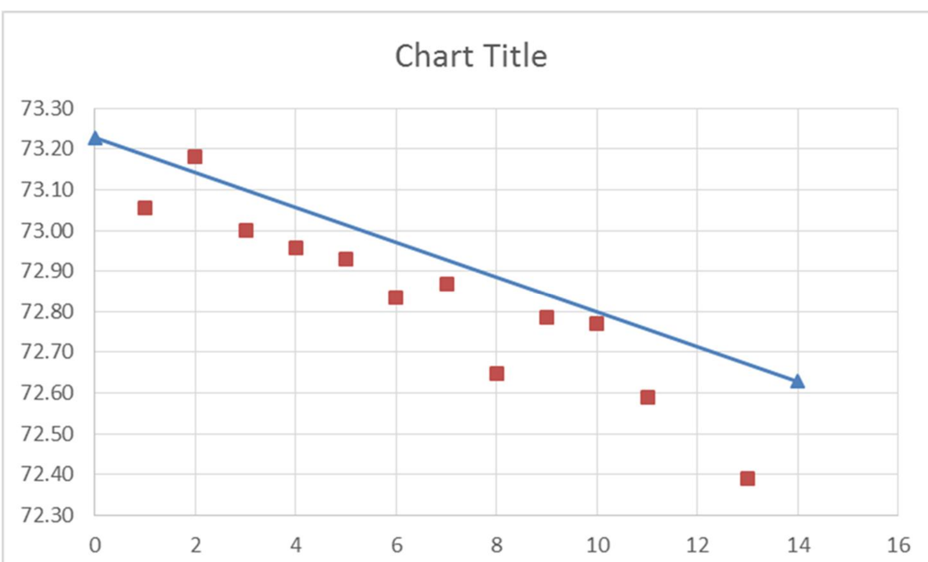

Heat balance test for TS 5

Type	Percent
heat balance with plate (TS)	6.38
Heat balance with preheater and ts	0.42
Heat Balance Pre heater	2.48

Experimental test data and data analysis

Solubility test data analysis T1S20

	Magnitude	Unit
Target P	550	Kpa
Target T	0	C
pressure [kPa]	559.37	kPa
Temperature C	33.01	C
Wo	1112.2	g
Wr+nl	1152.4	g
Wnl	1147.4	g
w%r	12.437811	%
Mass frac	0.1420455	

	Magnitude	Unit
Target P	550	Kpa
Target T	0	C
pressure [kPa]	552.95	
Temperature C	0.5	
Wo	1116.6	
Wr+nl	1152.7	
Wnl	1148.2	
w%r	12.465374	
Mass frac	0.1424051	

	Magnitude	Unit
Target P	550	Kpa
Target T	0	C
pressure [kPa]	896.87	
Temperature C	20	
Wo	1113	
Wr+nl	1192.8	
Wnl	1183.6	
w%r	11.528822	
Mass frac	0.1303116	

	Magnitude	Unit
Target P	650	Kpa
Target T	0	C
pressure [kPa]	653.96	kPa
Temperature C	0.5	C
Wo	1113.8	g
Wr+nl	1156.4	g
Wnl	1150.2	g
w%r	14.553991	%
Mass frac	0.1703297	

	Magnitude	Unit
Target P	650	Kpa
Target T	0	C
pressure [kPa]	656.8	kPa
Temperature C	0.5	C
Wo	1114.2	g
Wr+nl	1160.8	g
Wnl	1153.8	g
w%r	15.021459	%
Mass frac	0.1767677	

	Magnitude	Unit
Target P	650	Kpa
Target T	0	C
pressure [kPa]	653.96	kPa
Temperature C	0.5	C
Wo	1113.8	g
Wr+nl	1156.4	g
Wnl	1150.2	g
w%r	14.553991	%
Mass frac	0.1703297	

	Magnitude	Unit
Target P	650	Kpa
Target T	0	C
pressure [kPa]	656.8	kPa
Temperature C	0.5	C
Wo	1114.2	g
Wr+nl	1160.8	g
Wnl	1153.8	g
w%r	15.021459	%
Mass frac	0.1767677	

	Magnitude	Unit
Target P	550	Kpa
Target T	0	C
pressure [kPa]	551.3	kPa
Temperature C	0.55	C
Wo	1112	g
Wr+nl	1157.4	g
Wnl	1155.2	g
w%r	4.845815	%
Mass frac	0.0509259	

	Magnitude	Unit
Target P	550	Kpa
Target T	0	C
pressure [kPa]	550.2	
Temperature C	0.5	
Wo	1115.4	
Wr+nl	1168	
Wnl	1165.2	
w%r	5.3231939	
Mass frac	0.0562249	

	Magnitude	Unit
Target P	550	Kpa
Target T	0	C
pressure [kPa]	546.75	kPa
Temperature C	6.6	C
Wo	1114.4	g
Wr+nl	1171.8	g
Wnl	1169.8	g
w%r	3.4843206	%
Mass frac	0.0361011	

	Magnitud	Unit
Target P	812	Kpa
Target T	0	C
pressure [	794.3	kPa
Temperat	0.55	C
Wo	1114.4	g
Wr+nl	1175.8	g
Wnl	1173.2	g
w%r	4.234528	%
Mass frac	0.044218	

	Magnitude	Unit
Target P	812	Kpa
Target T	0	C
pressure [kPa]	795.65	kPa
Temperature C	0.5	C
Wo	1115.6	g
Wr+nl	1137.2	g
Wnl	1128.8	g
w%r	38.888889	%
Mass frac	0.6363636	

	Magnitude	Unit
Target P	812	Kpa
Target T	0	C
pressure [kPa]	794.3	kPa
Temperature C	0.55	C
Wo	1116.8	g
Wr+nl	1154.2	g
Wnl	1140	g
w%r	37.967914	%
Mass frac	0.612069	

	Magnitude	Unit
Target P	550	Kpa
Target T	20	C
pressure [kPa]	550.27	
Temperature C	20.08	
Wo	1104	
Wr+nl	1180.2	
Wnl	1180	
w%r	0.002624672	

	Magnitude	Unit
Target P	550	Kpa
Target T	20	C
pressure [kPa]	550.27	
Temperature C	20.11	
Wo	1114	
Wr+nl	1147.6	
Wnl	1146.6	
w%r	2.976190476	

	Magnitude	Unit
Target P	550	Kpa
Target T	20	C
pressure [kPa]		
Temperature C		
Wo	1114	
Wr+nl	1232.6	
Wnl	1230	
w%r	2.192242833	

	Magnitude	Unit
Target P	900	Kpa
Target T	20	C
pressure [kPa]	917.14	
Temperature C	20	
Wo	1113.2	
Wr+nl	1185.4	
Wnl	1177	
w%r	11.63434903	

	Magnitude	Unit
Target P	900	Kpa
Target T	20	C
pressure [kPa]	896.87	
Temperature C	20	
Wo	1113	
Wr+nl	1192.8	
Wnl	1183.6	
w%r	11.52882206	

	Magnitude	Unit
Target P	1100	Kpa
Target T	20	C
pressure [kPa]	1107.98	
Temperature C	20.11	
Wo	1112.6	
Wr+nl	1208	
Wnl	1186.2	
w%r	22.85115304	

	Magnitude	Unit
Target P	1100	Kpa
Target T	20	C
pressure [kPa]	1103.5	
Temperature C	20.11	
Wo	1112.6	
Wr+nl	1154.6	
Wnl	1146.4	
w%r	19.52380952	

	Magnitude	Unit
Target P	900	Kpa
Target T	40	C
pressure [kPa]	895.97	kPa
Temperature C	39.5	C
Wo	1113.8	g
Wr+nl	1204.2	g
Wnl	1202.8	g
w%r	1.548672566	

	Magnitude	Unit
Target P	900	Kpa
Target T	40	C
pressure [kPa]	897.69	kPa
Temperature C	39.72	C
Wo	1115.2	g
Wr+nl	1215	g
Wnl	1211.2	g
w%r	3.80761523	

	Magnitude	Unit
Target P	1100	Kpa
Target T	40	C
pressure [kPa]	1103.64	kPa
Temperature C	39.58	C
Wo	1112	g
Wr+nl	1175.8	g
Wnl	1170	g
w%r	9.090909091	

	Magnitude	Unit
Target P	1100	Kpa
Target T	40	C
pressure [kPa]	1103.2	kPa
Temperature C	39.27	C
Wo	1113.2	g
Wr+nl	1197.6	g
Wnl	1191.6	g
w%r	7.109004739	

	Magnitud	Unit
Target P	1100	Kpa
Target T	40	C
pressure [	1103.2	kPa
Temperat	39.27	C
Wo	1116.6	g
Wr+nl	1185.6	g
Wnl	1179.6	g
w%r	8.695652	

	Magnitude	Unit
Target P	813	Kpa
Target T	0	C
pressure [kPa]		kPa
Temperature C	0.55	C
Wo	1117	g
Wr+nl	1147.7	g
Wnl	1128.8	g
w%r	61.563518	%
Tare wWnl	11.8	

	Magnitude	Unit
Target P	813	Kpa
Target T	0	C
pressure [kPa]		
Temperature C	0.55	
Wo	1113.2	
Wr+nl	1185.4	
Wnl	1177	
w%r	11.634349	
Tare wWnl	63.8	

	Magnitude	Unit
Target P	813	Kpa
Target T	0	C
pressure [kPa]		
Temperature C	0.55	
Wo	1113	
Wr+nl	1192.8	
Wnl	1183.6	
w%r	11.528822	
Tare wWnl	70.6	

Solubility test analysis for T1S20

	Magnitude	Unit
Target P	550	Kpa
Target T	0	C
pressure [kPa]	547.78	kPa
Temperature C	33.01	C
Wo	1118.4	g
Wr+nl	1152	g
Wnl	1150.2	g
w%r	5.3571429	%
Mass frac	0.0566038	

	Magnitude	Unit
Target P	550	Kpa
Target T	0	C
pressure [kPa]	552.95	
Temperature C	0.5	
Wo	1120.4	
Wr+nl	1175.8	
Wnl	1173.6	
w%r	3.9711191	
Mass frac	0.0413534	

	Magnitude	Unit
Target P	650	Kpa
Target T	0	C
pressure [kPa]	659.13	kPa
Temperature C	0.5	C
Wo	1115.2	g
Wr+nl	1139.6	g
Wnl	1135.4	g
w%r	17.213115	%
Mass frac	0.2079208	

	Magnitude	Unit
Target P	650	Kpa
Target T	0	C
pressure [kPa]	656.8	kPa
Temperature C	0.5	C
Wo	1115.2	g
Wr+nl	1143.4	g
Wnl	1138.4	g
w%r	17.730496	%
Mass frac	0.2155172	

	Magnitude	Unit
Target P	812	Kpa
Target T	0	C
pressure [kPa]	800.619	kPa
Temperature C	0.5	C
Wo	1114.6	g
Wr+nl	1136.21	g
Wnl	1125.6	g
w%r	49.09764	%
Mass frac	0.9645455	

	Magnitude	Unit
Target P	812	Kpa
Target T	0	C
pressure [kPa]	800	kPa
Temperature C	0.55	C
Wo	1114.6	g
Wr+nl	1151.4	g
Wnl	1135	g
w%r	44.565217	%
Mass frac	0.8039216	

	Magnitude	Unit
Target P	550	Kpa
Target T	20	C
pressure [kPa]	549.16	
Temperature C	20.22	
Wo	1116	
Wr+nl	1165.2	
Wnl	1164.8	
w%r	0.81300813	

	Magnitude	Unit
Target P	550	Kpa
Target T	20	C
pressure [kPa]	548.2	
Temperature C	20.11	
Wo	1114.2	
Wr+nl	1155.8	
Wnl	1154.4	
w%r	3.365384615	

	Magnitude	Unit
Target P	900	Kpa
Target T	20	C
pressure [kPa]	893.5	
Temperature C	20.22	
Wo	1113.8	
Wr+nl	1171	
Wnl	1167.6	
w%r	5.944055944	

	Magnitude	Unit
Target P	900	Kpa
Target T	20	C
pressure [kPa]	897.62	
Temperature C	20.27	
Wo	1118	
Wr+nl	1170.2	
Wnl	1166.6	
w%r	6.896551724	

	Magnitude	Unit
Target P	1100	Kpa
Target T	20	C
pressure [kPa]	1099.43	
Temperature C	20.22	
Wo	1116.8	
Wr+nl	1154.2	
Wnl	1148	
w%r	16.57754011	

	Magnitude	Unit
Target P	1100	Kpa
Target T	20	C
pressure [kPa]	1103.5	
Temperature C	20.11	
Wo	1119.6	
Wr+nl	1167.4	
Wnl	1159.6	
w%r	16.31799163	

	Magnitude	Unit
Target P	550	Kpa
Target T	40	C
pressure [kPa]	553	kPa
Temperature C	40.67	C
Wo	1112.4	g
Wr+nl	1163.6	g
Wnl	1163.4	g
w%r	0.390625	

	Magnitude	Unit
Target P	550	Kpa
Target T	40	C
pressure [kPa]	566	kPa
Temperature C	39.67	C
Wo	1114.2	g
Wr+nl	1161.4	g
Wnl	1161	g
w%r	0.847457627	

	Magnitude	Unit
Target P	900	Kpa
Target T	40	C
pressure [kPa]	892.9	kPa
Temperature C	39.4	C
Wo	1114.8	g
Wr+nl	1198.8	g
Wnl	1196.8	g
w%r	2.380952381	

	Magnitude	Unit
Target P	900	Kpa
Target T	40	C
pressure [kPa]	892.87	kPa
Temperature C	39.67	C
Wo	1118	g
Wr+nl	1188.8	g
Wnl	1186.5	g
w%r	3.248587571	

	Magnitude	Unit
Target P	1100	Kpa
Target T	40	C
pressure [kPa]	1103.2	kPa
Temperature C	39.27	C
Wo	1116.6	g
Wr+nl	1185.6	g
Wnl	1179.6	g
w%r	8.695652174	

	Magnitude	Unit
Target P	1100	Kpa
Target T	40	C
pressure [kPa]	1103.2	kPa
Temperature C	39.27	C
Wo	1118.8	g
Wr+nl	1179.2	g
Wnl	1174	g
w%r	8.609271523	

Heat transfer coefficient and pressure drop data analysis

	Preheater													
	Water Side				Refrigerant Side						Hot Loop			
Test Date	Flow Rate (lb/min)	Inlet Temp (F)	Exit Temp (F)	Q (Btu/hr)	Flow Rate (lb/hr)	Pressure (psi)	Inlet Temp (F)	Exit Temp (F)	Entering Enthalpy (Btu/lb)	Leaving Enthalpy (Btu/lb)	Plate Flow Rate (lb/min)	Entering Hot Temp (F)	Leaving Hot Temp (F)	Q Plate_hot (Btu/hr)
350M-15H	1.46929	77.06049	42.9292967	3029.979684	165.35349	135.4285467	35.16707	38.8835833	87.1367051	105.4609611	0.842693	76.46115	47.6975667	1454.332795
Alfanot=	1.7452244	77.12808	44.51952	3438.457248	164.1208911	135.7051244	34.30906	38.9860067	86.8243058	107.7750649	0.859607	76.5102133	47.8839267	1476.440812
7.777966937	2.5380401	77.25845	47.1209532	4621.536014	165.758029	135.6105457	33.044265	38.5739421	86.364789	114.2460087	0.851884	76.531	47.5870267	1479.414789
	3.2875398	77.30796	49.619708	5499.805803	165.5539823	136.2433363	31.8736018	38.503354	85.9405946	119.1612138	0.85031	76.5593009	47.454885	1484.866091
	6.3425	77.47614	54.92456	8642.077795	164.557716	137.761928	26.621608	38.102608	84.0495591	136.5665605	0.836856	76.63456	47.173616	1479.274065
	7.327375	77.48081	55.7105341	9638.135087	164.4481818	138.2841705	26.2254432	38.0648864	83.9077805	142.5167294	0.831591	76.6329432	47.1761364	1469.760766
	8.3260299	77.54499	56.1587985	10758.50772	166.7004925	138.8964552	24.2612612	37.9034403	83.2059705	147.7439185	0.826082	76.6831194	46.9099403	1475.7054
	4.3377891	77.42891	51.5741564	6776.251895	163.8119673	136.9160982	29.8012655	38.3698836	85.1916535	126.5576904	0.8638	76.6270473	47.4913709	1510.043835
	10.559836	77.67193	57.3730137	12951.22247	167.0546301	141.8787123	16.2219041	43.5760411	80.358334	157.8852033	0.877466	76.7907671	50.5968767	1379.054507
350M-12H	9.3151689	77.68954	56.9198911	11689.62455	164.4322667	139.7322244	20.9633578	38.1611378	82.0331606	153.1239799	0.360282	76.3009511	46.1983267	650.7264258
	10.08634	77.65438	56.8623089	12671.03188	165.5832533	138.9018333	17.6241067	38.09604	80.8518455	157.3754771	0.363487	76.2956933	45.9792244	661.1779333
	10.768069	77.71247	57.1818622	13357.35216	165.3412644	139.7042244	14.9460533	39.0655289	139.704224	14.94605333	0.360322	76.3091156	46.4819156	644.8441792
	1.7216711	77.05285	44.2297	3414.374976	165.9907	135.4039689	34.8772711	38.8176067	87.0321157	107.6017921	0.378591	76.0988578	46.8233733	665.006291
0.4323x - 18.901	2.7434733	77.33448	48.0181244	4859.499147	165.7540867	136.1929444	33.4238067	38.72862	86.5012125	115.8187349	0.373729	76.1952044	46.7810044	659.576177
	3.7275753	77.37542	50.5423151	6043.354141	165.9710388	136.742242	31.7384886	38.5666895	85.892294	122.3043945	0.369183	76.2186119	46.6647146	654.6471637
	5.0885844	77.44603	53.3736978	7401.094262	164.9275133	137.3871378	29.6898444	38.4289511	85.1520751	130.026906	0.360033	76.20098	46.4989356	641.6235641
	6.6525556	77.45743	55.5110644	8821.285167	164.7104911	137.97968	26.7229289	38.1571089	84.0848613	137.6411655	0.356498	76.1900289	46.2461978	640.494555
	7.5962044	77.4449	55.9004733	9888.086621	165.2297333	138.6218444	24.8470156	38.05312	83.4160395	143.2605144	0.349187	76.1927911	46.12814	629.8905184
	8.5297549	77.48349	56.3955441	10868.04819	164.6900441	139.0792157	22.9063333	37.9844755	82.7245549	148.7154789	0.380623	76.2668627	46.0428284	690.2369389
250M-12H	0.9678151	76.91074	40.9834878	2100.860221	120.5626192	134.503922	36.706265	39.1042606	87.6999379	105.1254072	0.370171	76.0222739	46.9104699	646.5815958
	1.7454311	77.08806	44.7718644	3408.031744	119.3924556	134.7182444	35.0190578	38.9200156	87.0830924	115.6278754	0.365431	76.1073933	46.8196622	642.1588873
0.4295x - 18.482	1.7454311	77.08806	44.7718644	3408.031744	119.3924556	134.7182444	35.0190578	38.9200156	87.0830924	115.6278754	0.365431	76.1073933	46.8196622	642.1588873
	2.5308089	77.28396	47.5423778	4547.828469	120.1390622	135.1599978	33.0391622	38.8904578	86.3632068	124.2179094	0.37872	76.1344267	46.7794178	667.039738
	3.3270356	77.24339	49.9210467	5492.324145	119.8002467	135.3709756	30.6932533	38.7890489	85.5125598	131.358243	0.374704	76.1286133	46.6178911	663.4679265
	3.8241356	77.29403	51.1425822	6042.403426	120.7547089	135.7928933	29.83444	38.8343111	85.2023033	135.24096	0.369822	76.1331489	46.6298467	654.6586074
	4.40965	77.3734	52.044475	6748.412159	119.57395	135.824525	28.027725	38.8438	84.5544901	140.9916335	0.369725	76.15655	46.5655	656.4330577
	4.9700935	77.33508	53.1285033	7269.065494	120.1761158	135.9446258	26.4163096	38.6995011	83.9769476	144.463721	0.36741	76.1383274	46.4824967	653.7505696
	5.1512249	77.34568	53.4482094	7437.777809	120.0679465	135.9526058	25.7817416	38.7014944	83.7478385	145.6942448	0.367829	76.1463096	46.5065568	654.1407623
	5.3065434	77.35276	53.622147	7608.542531	120.0861314	136.0083029	25.2577795	39.5338797	83.5618976	146.920942	0.368853	76.1490935	46.8312962	648.8374616
	7.22645	77.39415	55.901975	9383.958775	120.38885	137.3177	19.936225	45.252175	81.6697244	159.6167998	0.373175	76.201675	49.48615	598.1739625

	Heat Sources																	
	Hot Loop				Water Loop					Total								
Test Date	Plate Flow Rate (lb/min)	Entering Hot Temp (F)	Leaving Hot Temp (F)	Q Plate_hot (Btu/hr)	Test Inlet Temp (F)	Test Outlet Temp (F)	Plate Inlet Temp (F)	Plate Outlet Temp (F)	Effective Pump W_dot (kW)	Q (Btu/hr)	q" (kW/m^2)	Exit Temp (F)	Exit Pressure (psi)	Final Exit Pressure (psi)	Leaving Enthalpy (Btu/lb)	DP @ Test Section (psi)	DP/ Length Test Section (kPa/m)
350M-15H	0.842693	76.46115	47.6975667	1454.332795	48.0230067	47.5500133	47.6335267	47.85832	0.7699204	4081.410244	14.9792	38.883583	133.34783	133.34783	130.1439	2.6167433	9.8653818
Alfanot=	0.859607	76.5102133	47.8839267	1476.440812	48.1811	47.7043622	47.7709289	48.0144111	0.78148633	4142.982863	15.2051	38.986007	133.06626	133.06626	133.01855	3.5369578	13.334681
7.777966937	0.851884	76.531	47.5870267	1479.414789	47.8854967	47.4047305	47.4863229	47.7184009	0.77920056	4138.157447	15.1874	38.573942	132.03615	132.03615	139.21106	4.3590646	16.434106
	0.85031	76.5593009	47.454885	1484.866091	47.7749469	47.2932478	47.3751416	47.6085664	0.76939885	4110.163936	15.0847	38.503354	132.25926	132.25926	143.98794	4.1239115	15.547555
	0.836856	76.63456	47.173616	1479.274065	47.506436	47.022396	47.104196	47.33818	0.776388	4128.419881	15.1517	38.102608	131.2313	131.2313	161.65454	6.107312	23.025172
	0.831591	76.6329432	47.1761364	1469.760766	47.4861477	47.0041023	47.0784545	47.3150341	0.77524636	4115.011157	15.1025	38.064886	130.88042	130.88042	167.53988	6.7490227	25.444485
	0.826082	76.6831194	46.9099403	1475.7054	47.255709	46.7609851	46.8604328	47.0858358	0.77641993	4124.96015	15.139	37.90344	130.54399	130.54399	172.48866	7.5050224	28.294678
	0.8638	76.6270473	47.4913709	1510.043835	47.78384	47.2824364	47.3703527	47.6107164	0.77570553	4156.860957	15.2561	38.369884	131.88569	131.88569	151.9335	4.9231455	18.560746
	0.877466	76.7907671	50.5968767	1379.054507	50.8601781	50.3549041	50.4581781	50.6799863	0.77360342	4018.698957	14.749	43.576041	132.83411	132.83411	181.9414	8.1549726	30.745055
350M-12H	0.360282	76.3009511	46.1983267	650.7264258	46.3526667	45.9309467	46.0206622	46.1681467	0.7777036	3304.361255	12.1273	38.161138	131.04742	131.04742	173.21956	7.7249844	29.123957
	0.363487	76.2956933	45.9792244	661.1779333	46.1332933	45.7135533	45.8043133	45.9506222	0.77738467	3313.724517	12.1617	38.09604	129.51181	129.51181	177.38791	8.2643978	31.157599
	0.360322	76.3091156	46.4819156	644.8441792	46.6509378	46.2278644	46.3234444	46.4770911	0.7782556	3300.362511	12.1126	39.065529	130.17381	130.17381	34.906966	8.4881044	32.000995
	0.378591	76.0988578	46.8233733	665.006291	46.9765044	46.5604467	46.6472	46.7983311	0.77897933	3322.994103	12.1957	38.817607	133.15813	133.15813	127.62095	2.7024378	10.188458
0.4323x - 18.901	0.373729	76.1952044	46.7810044	659.576177	46.9431089	46.5233822	46.6054889	46.7594644	0.77381353	3299.937548	12.1111	38.72862	132.84912	132.84912	135.72737	3.6207133	13.650448
	0.369183	76.2186119	46.6647146	654.6471637	46.8290228	46.4184452	46.485226	46.6480753	0.77219979	3289.502229	12.0728	38.566689	132.43608	132.43608	142.12413	4.3556667	16.421295
	0.360033	76.20098	46.4989356	641.6235641	46.6659333	46.2460533	46.3283622	46.4789311	0.76554427	3253.769026	11.9416	38.428951	132.01074	132.01074	149.75539	5.2230378	19.69137
	0.356498	76.1900289	46.2461978	640.494555	46.4394111	46.0150178	46.0829067	46.2419	0.7733842	3279.39098	12.0357	38.157109	131.41207	131.41207	157.5512	6.1413067	23.153335
	0.349187	76.1927911	46.12814	629.8905184	46.3121667	45.8828778	45.9522644	46.1082378	0.7725286	3265.867515	11.986	38.05312	131.12414	131.12414	163.02613	6.8348333	25.767999
	0.380623	76.2668627	46.0428284	690.2369389	46.2524657	45.8172059	45.8823235	46.0500049	0.76786515	3310.301573	12.1491	37.984475	130.86658	130.86658	168.81567	7.4087843	27.931851
250M-12H	0.370171	76.0222739	46.9104699	646.5815958	47.0678196	46.650735	46.7461403	46.8884165	0.77692924	3297.574209	12.1024	39.104261	133.81739	133.81739	132.47695	1.4792494	5.576917
	0.365431	76.1073933	46.8196622	642.1588873	46.9728156	46.5557711	46.6525111	46.8006244	0.77158713	3274.923466	12.0193	38.920016	133.35822	133.35822	143.05778	2.06928	7.8013907
0.4295x - 18.482	0.365431	76.1073933	46.8196622	642.1588873	46.9728156	46.5557711	46.6525111	46.8006244	0.77158713	3274.923466	12.0193	38.920016	133.35822	133.35822	143.05778	2.06928	7.8013907
	0.37872	76.1344267	46.7794178	667.039738	46.9338889	46.5241822	46.6123756	46.7656444	0.7748378	3310.896052	12.1513	38.890458	133.19214	133.19214	151.77677	2.5697622	9.6882583
	0.374704	76.1286133	46.6178911	663.4679265	46.7674822	46.3551578	46.4475067	46.5937222	0.7748332	3307.308545	12.1381	38.789049	132.88991	132.88991	158.9651	2.9967311	11.297973
	0.369822	76.1331489	46.6298467	654.6586074	46.7843222	46.3674889	46.4591444	46.6087644	0.77537293	3300.340872	12.1126	38.834311	132.9918	132.9918	162.57191	3.2299378	12.177186
	0.369725	76.15655	46.5655	656.4330577	46.7286	46.31175	46.403475	46.5457	0.7794585	3316.055854	12.1702	38.8438	132.83665	132.83665	168.72389	3.4071	12.845105
	0.36741	76.1383274	46.4824967	653.7505696	46.614833	46.1969621	46.2847283	46.4342851	0.77804492	3308.550038	12.1427	38.699501	132.58331	132.58331	171.99457	3.6721626	13.844417
	0.367829	76.1463096	46.5065568	654.1407623	46.6363786	46.2187416	46.3064143	46.4532094	0.77784976	3308.274293	12.1417	38.701494	132.52826	132.52826	173.2476	3.7182049	14.018001
	0.368853	76.1490935	46.8312962	648.8374616	46.981637	46.5645746	46.6513341	46.7986303	0.77779751	3302.79271	12.1216	39.53388	132.53897	132.53897	174.42447	3.7485768	14.132506
	0.373175	76.201675	49.48615	598.1739625	49.98385	49.60095	49.687875	49.822675	0.77719875	3250.086172	11.9281	45.252175	133.28845	133.28845	186.61337	4.170025	15.721408

	Test Section																
	Refrigerant Side																
Test Date	Entering Temp (F)	EnteringPressure (psi)	Entering Enthalpy (Btu/lb)	Surface Couple 1	Surface Couple 2	Surface Couple 3	Surface Couple 4	Surface Couple 5	Surface Couple 6	Surface Couple 7	Surface Couple 8	Surface Couple 9	Surface Couple 10	Surface Couple 11	Average T_Surface	Corrected Temp (F)	Entering Quality
350M-15H	38.883583	135.96458	105.46096	44.08228	43.424923	43.344393	43.27747	43.553157	43.146577	42.501463	42.994797	42.3119	42.81983	43.08861	43.140491	43.140491	0.1746204
Alfanot=	38.986007	136.60321	107.77506	44.071136	43.592433	43.529753	43.170282	43.603531	43.3041	42.382004	42.78378	42.152071	42.79824	43.14328	43.139146	43.139146	0.1987278
7.777966937	38.573942	136.39521	114.24601	43.726508	43.202136	43.202007	42.798833	43.27445	42.896176	42.001922	42.390922	41.724359	42.429766	42.754748	42.763802	42.763802	0.2690385
	38.503354	136.38317	119.16121	43.78292	43.107195	43.180504	42.990195	43.311549	42.831186	42.225752	42.626115	41.898168	42.500327	42.689814	42.831248	42.831248	0.322234
	38.102608	137.33862	136.56656	43.3721	42.774364	42.892756	42.552728	43.171944	42.560416	41.766576	42.038236	41.39962	42.014752	42.263904	42.437036	42.437036	0.5096048
	38.064886	137.62944	142.51673	43.272989	42.669534	42.651114	42.288489	42.886239	42.331364	41.558864	41.969557	41.318807	41.978443	42.328909	42.295846	42.295846	0.573809
	37.90344	138.04901	147.74392	43.07297	42.445485	42.497806	42.119687	42.61009	42.120739	41.399828	41.708784	41.074022	41.804746	42.246052	42.100019	42.100019	0.6301227
	38.369884	136.80883	126.55769	43.61032	43.005236	43.064105	42.701564	43.192527	42.713625	41.957982	42.330215	41.645342	42.366015	42.583044	42.651816	42.651816	0.4017965
	43.576041	140.98908	157.8852	44.622164	43.919945	44.236699	43.809137	45.112562	45.353932	45.421151	46.379521	46.580904	48.166562	48.971027	45.688509	45.688509	0.7382363
350M-12H	38.161138	138.7724	153.12398	42.729133	42.130856	42.349682	41.929187	42.350151	41.931587	41.200078	41.5566	40.964656	41.672744	42.0493	41.896725	41.896725	0.6879418
	38.09604	137.77621	157.37548	42.188987	41.602216	41.785956	41.333747	41.854293	41.45118	40.796478	41.345373	40.8806	41.812927	42.425747	41.588864	41.588864	0.7347584
	39.065529	138.66191	14.946053	42.455391	41.884429	42.058969	41.652633	42.21508	41.834967	41.294738	41.920427	41.603053	42.779527	43.688842	42.126187	42.126187	0.8
	38.817607	135.86057	107.60179	43.42952	42.942258	42.822076	42.629369	43.021044	42.697358	41.965604	42.429327	41.859018	42.426858	42.583382	42.61871	42.61871	0.1979
0.4323x - 18.901	38.72862	136.46983	115.81873	43.382524	42.848656	42.798938	42.580282	42.994647	42.618864	41.92668	42.340169	41.736524	42.361787	42.44934	42.548946	42.548946	0.2859705
	38.566689	136.79175	122.30439	43.267461	42.706384	42.720763	42.47839	42.908345	42.495922	41.835881	42.209804	41.608395	42.253664	42.308365	42.435761	42.435761	0.3557021
	38.428951	137.23377	130.02691	43.133969	42.546218	42.609133	42.341611	42.775416	42.340502	41.6981	42.010076	41.429524	42.05636	42.123058	42.278542	42.278542	0.4389054
	38.157109	137.55337	137.64117	42.940096	42.313913	42.387658	42.073182	42.526996	42.101447	41.42198	41.757182	41.200082	41.743384	41.837324	42.027568	42.027568	0.5210295
	38.05312	137.95898	143.26051	42.815244	42.212396	42.338153	41.981227	42.410944	41.999516	41.391196	41.640258	41.049571	41.548698	41.687051	41.915841	41.915841	0.5815732
	37.984475	138.27537	148.71548	42.673309	42.077799	42.215877	41.852495	42.262446	41.844132	41.120191	41.454162	40.852426	41.459961	41.657946	41.770068	41.770068	0.640524
250M-12H	39.104261	135.29664	105.12541	43.719105	43.214922	42.958726	42.815392	43.029744	42.916203	42.038722	42.616425	42.009884	42.451535	42.814967	42.780511	42.780511	0.1720223
	38.920016	135.4275	115.62788	43.609249	43.057007	42.878447	42.71388	42.973642	42.746902	41.964996	42.460973	41.749329	42.362204	42.562	42.643512	42.643512	0.28528
0.4295x - 18.482	38.920016	135.4275	115.62788	43.609249	43.057007	42.878447	42.71388	42.973642	42.746902	41.964996	42.460973	41.749329	42.362204	42.562	42.643512	42.643512	0.28528
	38.890458	135.7619	124.21791	43.527011	42.933133	42.764153	42.576596	42.969593	42.591462	41.915838	42.357667	41.687833	42.30738	42.453418	42.553099	42.553099	0.3777026
	38.789049	135.88664	131.35824	43.389956	42.770078	42.654598	42.446416	42.833707	42.398656	41.777216	42.12824	41.500347	42.104796	42.256813	42.387347	42.387347	0.4547453
	38.834311	136.22173	135.24096	43.426411	42.785267	42.729373	42.49094	42.865231	42.438622	41.830458	42.13316	41.558067	42.08012	42.264964	42.418419	42.418419	0.4963614
	38.8438	136.24375	140.99163	43.31875	42.680075	42.722125	42.40075	42.76655	42.32675	41.6368	41.90335	41.3031	42.0515	42.4386	42.322577	42.322577	0.55854
	38.699501	136.25547	144.46372	43.213323	42.538314	42.605038	42.264993	42.687301	42.245768	41.536512	41.868385	41.236906	41.810996	42.099356	42.191536	42.191536	0.5960582
	38.701494	136.24646	145.69424	43.193523	42.514399	42.578831	42.223381	42.66984	42.213171	41.498334	41.829367	41.19633	41.795203	42.25247	42.178623	42.178623	0.6093723
	39.53388	136.28755	146.92094	43.335528	42.60816	42.670909	42.279726	42.787163	42.436165	41.926608	42.438258	42.045399	42.696151	43.022209	42.567843	42.567843	0.6226443
	45.252175	137.45848	159.6168	44.501975	44.22715	44.877075	44.840875	45.934425	46.08305	46.348525	47.4977	47.58715	48.45495	48.73215	46.280457	46.280457	0.7592906

Test Date	Corrected Temp (F)	Entering Quality	Exiting Quality	Average Quality	Mass Flux (kg/m^2*s)	Average Pressure	Actual TSAT (F)	Wall Tsurf (F)	DeltaT	HTC (Btu/hr ft^2 F)	HTC (kw/m^2 C)	α/α0	ΔP/ΔP0
350M-15H	43.140491	0.1746204	0.444378	0.3094992	351.53394	134.656205	39.30341919	43.11303	3.809614	1246.416768	7.079647	0.9102	0.52335
Alfanot=	43.139146	0.1987278	0.4756426	0.3371852	348.9135	134.8347344	39.36828553	43.10799	3.739702	1288.873192	7.3208	0.9412	0.70739
7.777966937	42.763802	0.2690385	0.5433158	0.4061771	352.39398	134.2156793	39.15344648	42.72192	3.568476	1349.143924	7.663137	0.9852	0.87181
	42.831248	0.322234	0.594481	0.4583575	351.96018	134.3212124	39.19414997	42.78141	3.587259	1333.000926	7.571445	0.9734	0.82478
	42.437036	0.5096048	0.7851374	0.6473711	349.84217	134.28496	39.1931821	42.35872	3.16554	1517.295238	8.618237	1.108	1.22146
	42.295846	0.573809	0.8485326	0.7111708	349.6093	134.2549318	39.18654503	42.20851	3.021961	1584.222618	8.998384	1.1569	1.3498
	42.100019	0.6301227	0.9018093	0.765966	354.39761	134.2965037	39.2047327	42.00253	2.797793	1715.292342	9.742861	1.2526	1.501
	42.651816	0.4017965	0.6801886	0.5409925	348.25674	134.34726	39.20857934	42.59041	3.381831	1430.038351	8.122618	1.0443	0.98463
	45.688509	0.7382363	1.0982363	0.9182363	355.15049	136.9115959	40.13437267	45.57115	5.436774	859.9600261	4.884573	0.628	1.63099
350M-12H	41.896725	0.6879418	0.9094286	0.7986852	349.57547	134.9099078	39.42388935	41.79079	2.366905	1624.204646	9.225482	1.1861	1.545
	41.588864	0.7347584	0.9547695	0.8447639	352.02241	133.6440078	38.97786787	41.47404	2.496172	1544.457431	8.772518	1.1279	1.65288
	42.126187	0.8	1.6	1.2	351.50795	134.4178611	39.27504677	42.00514	2.730097	1406.428494	7.988514	1.0271	1.69762
	42.61871	0.1979	0.4174024	0.3076512	352.88862	134.5093522	39.25132815	42.58777	3.336441	1158.724299	6.581554	0.8462	0.54049
0.4323x - 18.901	42.548946	0.2859705	0.5050596	0.3955151	352.38559	134.6594722	39.30998615	42.50491	3.194924	1201.653465	6.825392	0.8775	0.72414
	42.435761	0.3557021	0.5742238	0.4649629	352.84682	134.6139178	39.29823686	42.381	3.08276	1241.436494	7.051359	0.9066	0.87113
	42.278542	0.4389054	0.6567644	0.5478349	350.62834	134.6222544	39.30640017	42.21147	2.905074	1303.057415	7.401366	0.9516	1.04461
	42.027568	0.5210295	0.7409322	0.6309808	350.16696	134.48272	39.26223313	41.94763	2.685397	1420.753679	8.069881	1.0375	1.22826
	41.915841	0.5815732	0.7999767	0.690775	351.27084	134.5415589	39.28682942	41.82624	2.539407	1496.236868	8.498625	1.0927	1.36697
	41.770068	0.640524	0.8622797	0.7514019	350.12349	134.5709755	39.30105716	41.67158	2.370525	1624.639646	9.227953	1.1864	1.48176
250M-12H	42.780511	0.1720223	0.4690431	0.3205327	256.31061	134.5570122	39.26901146	42.76147	3.492462	1098.492085	6.239435	0.8022	0.29585
	42.643512	0.28528	0.5835084	0.4343942	253.82289	134.3928622	39.21803706	42.61263	3.394591	1122.400099	6.375233	0.8197	0.41386
0.4295x - 18.482	42.643512	0.28528	0.5835084	0.4343942	253.82289	134.3928622	39.21803706	42.61263	3.394591	1122.400099	6.375233	0.8197	0.41386
	42.553099	0.3777026	0.6775782	0.5276404	255.41014	134.4770189	39.25371427	42.51189	3.258172	1182.23972	6.715122	0.8634	0.51395
	42.387347	0.4547453	0.7552131	0.6049792	254.68984	134.3882744	39.22713898	42.33758	3.110437	1237.050153	7.026445	0.9034	0.59935
	42.418419	0.4963614	0.7939094	0.6451354	256.71898	134.6067644	39.30703955	42.36366	3.056624	1256.176937	7.135085	0.9173	0.64599
	42.322577	0.55854	0.8602036	0.7093718	254.20874	134.5402	39.28751811	42.26142	2.973906	1297.265018	7.368465	0.9474	0.68142
	42.191536	0.5960582	0.8955234	0.7457908	255.48892	134.4193931	39.24702127	42.12566	2.878643	1337.161865	7.595079	0.9765	0.73443
	42.178623	0.6093723	0.9091039	0.7592381	255.25895	134.3873586	39.23651568	42.11122	2.874706	1338.88128	7.604846	0.9777	0.74364
	42.567843	0.6226443	0.9216891	0.7721667	255.29761	134.4132572	39.24650609	42.4989	3.252389	1181.443223	6.710598	0.8628	0.74972
	46.280457	0.7592906	1.5	1.1296453	255.94118	135.3734625	39.60826837	46.19542	6.587152	574.0255846	3.260465	0.4192	0.83401

	Preheater										Heat Sources					
	Water Side				Refrigerant Side						Hot Loop				Water	
Test Date	Flow Rate (lb/min)	Inlet Temp (F)	Exit Temp (F)	Q (Btu/hr)	Flow Rate (lb/hr)	Pressure (psi)	Inlet Temp (F)	Exit Temp (F)	Entering Enthalpy (Btu/lb)	Leaving Enthalpy (Btu/lb)	Plate Flow Rate (lb/min)	Entering Hot Temp (F)	Leaving Hot Temp (F)	Q Plate_hot (Btu/hr)	Test Inlet Temp (F)	Test Outlet Temp (F)
1%P-350M-15H	1.5862432	77.14211	43.4714595	3227.022467	167.8512973	135.8383243	34.6891892	39.1047838	86.962945	106.1884292	0.864243	76.5376486	48.3455946	1461.887534	48.6395676	48.1442162
	2.5574934	77.3246	46.9680396	4690.809429	164.8182335	136.0495551	32.4771762	38.8762247	86.1602083	114.6207088	0.858291	76.5909471	48.0530044	1469.631134	48.3909383	47.8925286
	3.60105	77.39571	50.278975	5899.934954	163.1715107	136.87585	30.4238143	38.9832964	85.41528	121.5731542	0.849493	76.616825	47.9470607	1461.285599	48.3019	47.8144607
	4.6141111	77.4675	52.3782133	6994.505961	163.9488756	137.0298533	28.3930111	38.70272	84.6840872	127.3468132	0.837793	76.6482911	47.7321244	1453.5463	48.0725911	47.5839467
	5.5443067	77.47181	54.2095778	7792.546707	164.6171267	137.4644733	26.9587511	38.5707956	84.1707803	131.5081799	0.842467	76.6547489	47.7273733	1462.22098	48.0292667	47.5348111
	6.5708311	77.50491	55.5239489	8726.651601	165.1878422	138.2002667	25.2974578	38.52538	83.5767104	136.4053659	0.839549	76.6758444	47.6959689	1459.801339	48.0060867	47.5154489
	7.5446911	77.54182	55.9696333	9833.68539	165.9751311	138.8329156	23.5150356	38.4784311	82.9416915	142.1896362	0.823942	76.6893	47.6714644	1434.541195	48.00128	47.5114044
	8.824014	77.64229	56.6256433	11204.9633	162.2783258	138.7304073	19.9221713	39.0288652	81.663109	150.7109208	0.861433	76.748809	48.3473146	1467.958362	48.6354466	48.1386489
	9.6937222	77.60222	56.7304844	12224.46352	165.1618889	138.2682156	16.2368044	40.1753378	80.3639593	154.3789976	0.88718	76.7378267	49.0685222	1472.859211	49.3729533	48.8526311
3%P- 350M-15H	1.6452	77.12752	43.8325733	3309.617493	167.4962089	135.6745733	33.9889756	39.2261956	86.7082741	106.4676317	0.831684	76.5247044	47.4472578	1450.995605	47.7787711	47.2828467
	1.6412911	77.1249	43.8865311	3296.142977	165.9558067	135.4334511	34.1724289	39.1523111	86.7737114	106.6352821	0.83126	76.5198511	47.3433089	1455.197549	47.6818467	47.1853933
	1.6412911	77.1249	43.8865311	3296.142977	165.9558067	135.4334511	34.1724289	39.1523111	86.7737114	106.6352821	0.83126	76.5198511	47.3433089	1455.197549	47.6818467	47.1853933
	2.5262444	77.27464	46.9679467	4625.883028	166.7616556	136.1824578	32.0065711	39.2128756	85.989967	113.7294555	0.862858	76.5507933	47.5394156	1501.961578	47.8593644	47.35176
	3.5512756	77.37087	49.88028	5898.602099	163.4923756	135.82114	29.0279	38.69532	84.9141126	120.9928721	0.852787	76.5985133	47.1271489	1507.967199	47.4423533	46.93302
	3.5519667	77.34237	49.9038756	5888.571234	161.3360044	135.7681978	28.9215933	38.6981156	84.8745123	121.3733165	0.853671	76.5843422	47.1140867	1509.474348	47.4389111	46.9458778
	4.6104978	77.44868	52.3286289	6997.600322	163.9511444	136.9496333	26.99052	38.9222444	84.1814329	126.8624422	0.857227	76.6350289	47.3468156	1506.398249	47.683	47.1993711
	5.29576	77.46692	53.87532	7548.599987	164.0162	137.8562933	25.9717333	39.13744	83.8162525	129.839755	0.853067	76.6286267	47.4313067	1494.435627	47.79396	47.3230533
	1.4968422	77.19452	42.6251267	3126.428321	166.66666	132.6719222	33.4345	37.9845689	86.5046049	105.2631756	0.829364	76.5962911	46.2000022	1512.576075	46.5479622	46.0606244
	3.0310889	77.21014	47.8866978	5370.248424	167.8471244	133.0514311	29.1020267	37.57742	84.9388692	116.9337481	0.814289	76.5457578	45.9004022	1497.250351	46.2414733	45.7355222
	5.0434956	77.32669	52.9854867	7417.446584	167.8748889	135.4545489	25.4423311	37.9786333	83.6261166	127.8104889	0.823584	76.5692489	46.3769511	1491.954408	46.7081556	46.20332
	7.1259022	77.42183	55.2081222	9564.04408	167.5136489	135.5155511	20.1599911	37.2181889	81.7470526	138.8411709	0.819578	76.6061333	45.90878	1509.532118	46.2443911	45.7312556
	8.0644378	77.43098	55.6965311	10590.18477	165.9344533	136.0963756	17.9889311	37.2821489	80.9799228	144.8014171	0.815171	76.6254422	46.0989356	1493.059581	46.4572089	45.9493222
3%P- 250M-15H	0.6588886	77.29461	38.799902	1532.476503	118.6576414	132.152882	35.7262361	38.4876704	87.3405589	100.255669	0.824904	76.960882	46.6497884	1500.22496	46.9893029	46.5073252
	2.5572511	77.18842	46.7067689	4709.692506	122.5054311	132.9511733	28.3196822	38.4059133	84.6582065	123.1029714	0.834244	76.5754067	46.7454978	1493.126146	47.0815311	46.5976067
	2.1261356	77.11712	45.6696711	4039.773628	121.1023067	133.1369067	30.0570511	38.5936933	85.2848707	118.6432248	0.836151	76.5360889	46.9219867	1485.711869	47.2585511	46.7781089
	2.12536	77.13728	45.6760422	4040.071291	121.5809044	133.0557133	30.0627333	38.5432844	85.2848595	118.5143482	0.835067	76.5400267	46.8896756	1485.601192	47.2306244	46.7492933
	2.9086842	77.21723	48.0312105	5129.229525	122.0277544	133.1940994	26.9720117	38.3724795	84.1735009	126.2068035	0.82524	76.5741813	46.7582573	1476.317168	47.0884854	46.6145088
	1.2030867	76.95657	41.2443244	2595.940938	120.7172378	132.1576289	33.5707133	38.3808422	86.5554265	108.0597368	0.817236	76.4588667	46.6056378	1463.827206	46.9641244	46.4812956
	2.2504556	77.21746	45.9746489	4248.164207	120.3843778	132.54228	29.4216356	38.4210844	85.0540496	120.3423842	0.818751	76.57622	46.8294133	1461.313861	47.1837333	46.7002444
	3.5993757	77.24888	49.9448564	5937.923728	121.2685193	133.649326	24.4803094	38.4512873	83.2827068	132.2477949	0.825641	76.5838066	46.7580663	1477.521037	47.1136961	46.6316243
	4.2648566	77.30807	51.3864303	6679.556847	121.2496932	134.2638645	22.7067211	38.9617849	82.6520314	137.7412994	0.814068	76.6017689	47.2597968	1433.181156	47.6373586	47.1548367
	5.1752581	77.30371	53.3315161	7495.84344	123.0677742	134.4027097	19.579	40.0496774	81.5413087	142.4495643	0.843742	76.6144194	48.2382258	1436.531068	48.529129	48.0413871
	1.2040271	76.95766	40.4363322	2656.828986	122.6968237	130.5549932	32.2751763	37.6328441	86.0872313	107.7408398	0.928376	76.5060339	46.366922	1678.826177	46.6980203	46.1935898

	Heat Sources																	
	Water Loop				Total													
Test Date	Test Outlet Temp (F)	Plate Inlet Temp (F)	Plate Outlet Temp (F)	Effective Pump W_dot (kW)	Q (Btu/hr)	q" (kW/m^2)	Exit Temp (F)	Exit Pressure (psi)	Final Exit Pressure (psi)	Leaving Enthalpy (Btu/lb)	DP @ Test Section (psi)	DP/ Length Test Section (kPa/m)	Entering Temp (F)	EnteringPressure (psi)	Entering Enthalpy (Btu/lb)	Surface Couple 1	Surface Couple 2
1%P-350M-15H	48.1442162	48.2264324	48.4648919	0.77270676	4098.472426	15.0418	39.104784	133.43046	133.43046	130.60571	2.8210541	10.635653	39.104784	136.25151	106.18843	44.331838	43.731216
	47.8925286	47.9735991	48.2125727	0.77265714	4106.046716	15.0696	38.876225	132.73656	132.73656	139.53328	3.7183436	14.018524	38.876225	136.4549	114.62071	44.073304	43.434207
	47.8144607	47.8873857	48.1273714	0.77434018	4103.443958	15.06	38.983296	132.76613	132.76613	146.7212	4.3095143	16.247296	38.983296	137.07564	121.57315	44.054325	43.4199
	47.5839467	47.6605289	47.9001067	0.77341027	4092.531667	15.02	38.70272	132.00967	132.00967	152.30906	5.0035067	18.863716	38.70272	137.01318	127.34681	43.78664	43.140191
	47.5348111	47.62242	47.8592533	0.77207167	4096.638855	15.0351	38.570796	131.69627	131.69627	156.39404	5.5881978	21.06806	38.570796	137.28447	131.50818	43.738322	43.074816
	47.5154489	47.5982978	47.8382622	0.77228787	4094.95692	15.0289	38.52538	131.56111	131.56111	161.19507	6.2990089	23.747888	38.52538	137.86012	136.40537	43.714831	43.0496
	47.5114044	47.5939222	47.8267	0.77217593	4069.314843	14.9348	38.478431	131.18133	131.18133	166.70725	7.0736089	26.668207	38.478431	138.25494	142.18964	43.615398	42.942
	48.1386489	48.2197781	48.463264	0.77034817	4096.495437	15.0345	39.028865	130.51154	130.51154	175.95456	7.5924185	28.624171	39.028865	138.10396	150.71092	43.792646	43.025149
	48.8526311	48.9443711	49.1872511	0.7717144	4106.058042	15.0696	40.175338	129.18923	129.18923	179.23981	8.2094489	30.950436	40.175338	137.39868	154.379	43.931667	43.002909
3%P- 350M-15H	47.2828467	47.3643444	47.5976667	0.77598167	4098.754954	15.0428	39.226196	133.19946	133.19946	130.93836	3.2956844	12.425057	39.226196	136.49514	106.46763	43.427	42.9205
	47.1853933	47.2659667	47.5106178	0.77212993	4089.814239	15.01	39.152311	133.02892	133.02892	131.27928	3.0402533	11.462056	39.152311	136.06917	106.63528	43.34846	42.829733
	47.1853933	47.2659667	47.5106178	0.77212993	4089.814239	15.01	39.152311	133.02892	133.02892	131.27928	3.0029333	11.321356	39.152311	136.03185	106.63528	43.34846	42.829733
	47.35176	47.44066	47.6854889	0.77024087	4130.132504	15.158	39.212876	132.87525	132.87525	138.49614	3.7324311	14.071635	39.212876	136.60768	113.72946	43.32992	42.736889
	46.93302	47.0156778	47.2610867	0.7663646	4122.911754	15.1315	38.69532	131.49509	131.49509	146.21063	4.5388089	17.111759	38.69532	136.0339	120.99287	42.80192	42.251384
	46.9458778	47.0035467	47.2472644	0.76639527	4124.523543	15.1374	38.698116	131.53263	131.53263	146.93812	4.4725711	16.862036	38.698116	136.0052	121.37332	42.802327	42.24198
	47.1993711	47.2549178	47.4972711	0.77209773	4140.905068	15.1975	38.922244	131.81782	131.81782	152.11939	5.15692	19.4421	38.922244	136.97474	126.86244	42.997991	42.459367
	47.3230533	47.3616	47.60772	0.7718616	4128.136725	15.1507	39.13744	132.28719	132.28719	155.00883	5.51904	20.807328	39.13744	137.80623	129.83975	43.201827	42.68428
	46.0606244	46.1192511	46.36962	0.77408647	4153.868733	15.2451	37.984569	130.29593	130.29593	130.18639	3.0318422	11.430346	37.984569	133.32778	105.26318	42.183411	41.526269
	45.7355222	45.8287022	46.0647867	0.773214	4135.56603	15.1779	37.57742	128.94652	128.94652	141.57263	4.4147911	16.6442	37.57742	133.36131	116.93375	41.664731	41.023329
	46.20332	46.3023	46.5371378	0.77436707	4134.204513	15.1729	37.978633	129.68096	129.68096	152.43719	5.8221	21.949894	37.978633	135.50306	127.81049	42.128911	41.602096
	45.7312556	45.8317667	46.0692911	0.77466147	4152.786757	15.2411	37.218189	127.65691	127.65691	163.63191	7.4964444	28.262339	37.218189	135.15335	138.84117	41.558369	41.039391
	45.9493222	46.04262	46.2796867	0.77555693	4139.36968	15.1919	37.282149	127.40102	127.40102	169.74723	8.13168	30.65724	37.282149	135.5327	144.80142	41.673336	41.122891
3%P- 250M-15H	46.5073252	46.5642071	46.8084009	0.77136468	4132.230486	15.1657	38.48767	131.40476	131.40476	135.08048	1.6525434	6.2302525	38.554771	133.0573	100.25567	42.84012	42.641339
	46.5976067	46.6590244	46.89702	0.77119613	4124.556578	15.1375	38.405913	130.56363	130.56363	156.77133	3.2119311	12.109299	38.832211	133.77556	123.10297	42.454353	41.659942
	46.7781089	46.8376156	47.0690844	0.77398373	4126.653986	15.1452	38.593693	131.14559	131.14559	152.71899	2.8577889	10.774147	38.938167	134.00338	118.64322	42.705276	41.881418
	46.7492933	46.8093133	47.0421489	0.77377827	4125.842228	15.1422	38.543284	131.05385	131.05385	152.4493	2.8953889	10.915903	38.88516	133.94924	118.51435	42.667449	41.842589
	46.6145088	46.6738187	46.9028596	0.77636298	4125.37762	15.1405	38.37248	130.52337	130.52337	160.01368	3.4687719	13.077614	38.823982	133.99215	126.2068	42.431497	41.655333
	46.4812956	46.5384044	46.7891178	0.77376907	4104.03685	15.0622	38.380842	131.09526	131.09526	142.05684	2.1905578	8.25862	38.636356	133.28581	108.05974	42.731144	42.10404
	46.7002444	46.7601289	46.9972	0.7782372	4116.769409	15.1089	38.421084	130.63844	130.63844	154.53926	2.91932	11.006126	38.753976	133.55776	120.34238	42.549862	41.743464
	46.6316243	46.7011547	46.9296906	0.77331464	4116.180116	15.1068	38.451287	130.56012	130.56012	166.19049	3.7803702	14.25237	38.921807	134.34049	132.24779	42.443928	41.686823
	47.1548367	47.2240956	47.4472789	0.77775371	4086.986952	14.9996	38.961785	130.83316	130.83316	171.44849	4.0805618	15.384122	39.090394	134.91373	137.7413	42.748709	41.982375
	48.0413871	48.0897742	48.345129	0.77397968	4077.459346	14.9647	40.049677	130.4961	130.4961	175.58138	4.4266452	16.688891	38.914677	134.92274	142.44956	43.27871	42.438548
	46.1935898	46.2451797	46.5188305	0.77723471	4330.861094	15.8947	37.632844	129.298	129.298	143.03809	2.2310068	8.4111167	37.866308	131.52901	107.74084	42.138586	41.408237

	Test Section																
	Refrigerant Side																
Test Date	Surface Couple 1	Surface Couple 2	Surface Couple 3	Surface Couple 4	Surface Couple 5	Surface Couple 6	Surface Couple 7	Surface Couple 8	Surface Couple 9	Surface Couple 10	Surface Couple 11	Average T_Surface	Corrected Temp (F)	Entering Quality	Exiting Quality	Average Quality	Mass Flux (kg/m^2*s)
1%P-350M-15H	44.331838	43.731216	43.810865	43.460568	44.065514	43.664811	42.803595	43.228216	42.593541	43.290351	43.496	43.497865	43.497865	0.1820875	0.4493096	0.3156985	356.84417
	44.073304	43.434207	43.545987	43.159626	43.805238	43.349828	42.520617	42.892811	42.256687	42.996881	43.225775	43.205542	43.205542	0.2730122	0.5460719	0.409542	350.39601
	44.054325	43.4199	43.555989	43.129754	43.776632	43.275696	42.453993	42.772654	42.237757	43.009043	43.240454	43.175109	43.175109	0.347446	0.6234351	0.4854405	346.89516
	43.78664	43.140191	43.303918	42.841638	43.518658	42.984609	42.158244	42.456451	41.928993	42.713909	42.984116	42.892488	42.892488	0.410123	0.6841823	0.5471526	348.5478
	43.738322	43.074816	43.238231	42.770998	43.432884	42.883124	42.036091	42.377656	41.820402	42.615536	42.796898	42.798633	42.798633	0.4548841	0.7282676	0.5915758	349.96847
	43.714831	43.0496	43.202016	42.728393	43.406418	42.889704	42.06312	42.485958	41.824647	42.587973	42.734196	42.789714	42.789714	0.5073932	0.7800499	0.6437215	351.18178
	43.615398	42.942	43.0954	42.6683	43.444533	43.057989	42.064458	42.490813	41.73424	42.530398	42.754198	42.76343	42.76343	0.56971	0.8394616	0.7045858	352.85552
	43.792646	43.025149	43.383421	42.771354	43.708233	43.365826	42.481239	43.064831	42.50509	43.583402	44.242475	43.265788	43.265788	0.6622507	0.9389616	0.8006062	344.99629
	43.931667	43.002909	43.484411	42.85336	44.05958	43.876344	43.262164	44.075558	43.820631	45.168487	45.969002	43.954919	43.954919	0.7025531	0.9747262	0.8386396	351.12661
3%P- 350M-15H	43.427	42.9205	42.834418	42.528613	43.367776	42.60698	41.998724	42.212151	41.673053	42.475102	42.773427	42.619795	42.619795	0.1847532	0.4531147	0.318934	356.08927
	43.34846	42.829733	42.69358	42.415696	43.248498	42.437062	41.91144	42.12144	41.611329	42.419069	42.672989	42.519027	42.519027	0.1872164	0.4569605	0.3220884	352.81444
	43.34846	42.829733	42.69358	42.415696	43.248498	42.437062	41.91144	42.12144	41.611329	42.419069	42.672989	42.519027	42.519027	0.1872744	0.4569605	0.3221174	352.81444
	43.32992	42.736889	42.76844	42.438753	43.370607	42.545542	42.015164	42.205	41.779207	42.493613	42.957693	42.603712	42.603712	0.2631676	0.5348497	0.3990086	354.52764
	42.80192	42.251384	42.399876	41.980284	42.912918	42.164451	41.58938	41.748202	41.32252	42.019733	42.505484	42.154196	42.154196	0.3424546	0.6190308	0.4807427	347.5773
	42.802327	42.24198	42.375329	41.960927	42.937918	42.144618	41.595633	41.749064	41.332247	41.969391	42.506031	42.14686	42.14686	0.3465884	0.6268488	0.4867186	342.99295
	42.997991	42.459367	42.612909	42.153409	43.17162	42.387744	41.829447	41.987042	41.604029	42.225451	42.783891	42.382991	42.382991	0.4048623	0.6822846	0.5435734	348.55262
	43.201827	42.68428	42.874067	42.382173	43.350853	42.639987	42.021787	42.212173	41.824093	42.43852	42.998693	42.602587	42.602587	0.4362152	0.7130117	0.5746134	348.69093
	42.183411	41.526269	41.501191	41.091936	41.9094	41.2075	40.683651	40.942642	40.609716	41.190776	41.600078	41.313324	41.313324	0.1763375	0.4482339	0.3122857	354.32568
	41.664731	41.023329	41.177304	40.691956	41.556004	40.936082	40.331358	40.569527	40.304022	40.912944	41.360244	40.957046	40.957046	0.3020127	0.5715545	0.4367836	356.8353
	42.128911	41.602096	41.782958	41.207724	42.05052	41.531218	40.831693	41.090882	40.819218	41.393687	41.799053	41.476178	41.476178	0.4168027	0.6873573	0.55208	356.89432
	41.558369	41.039391	41.183496	40.564016	41.431611	40.931091	40.191689	40.696693	40.243247	40.897456	41.271511	40.90987	40.90987	0.5363261	0.8084786	0.6724023	356.12634
	41.673336	41.122891	41.230402	40.716024	41.649756	41.370769	40.518644	41.006851	40.398393	41.167884	41.699827	41.141343	41.141343	0.6003674	0.8740032	0.7371853	352.76905
3%P- 250M-15H	42.84012	42.641339	41.923526	41.587808	42.272648	41.542657	40.994176	41.339575	40.826477	41.638735	41.895661	41.772975	41.772975	0.1228536	0.4995502	0.3112019	252.26071
	42.454353	41.659942	41.7638	41.50072	42.37454	41.548178	41.145987	41.404198	41.307109	41.922827	42.320036	41.76379	41.76379	0.3679751	0.7331441	0.5505596	260.44093
	42.705276	41.881418	41.917698	41.672016	42.547271	41.684869	41.352278	41.562484	41.522133	42.039598	42.519418	41.94586	41.94586	0.3196191	0.6892409	0.50443	257.45796
	42.667449	41.842589	41.871089	41.621122	42.507711	41.636851	41.29926	41.510251	41.490553	42.027949	42.521624	41.908768	41.908768	0.3182811	0.6864176	0.5023494	258.47543
	42.431497	41.655333	41.757298	41.470222	42.397187	41.523099	41.199901	41.421713	41.331193	41.931789	42.306088	41.765938	41.765938	0.401256	0.7679345	0.5845952	259.42542
	42.731144	42.10404	41.751027	41.623224	42.443891	41.54622	41.126676	41.282136	40.955689	41.632584	42.011269	41.746173	41.746173	0.2065578	0.5748106	0.3906842	256.63932
	42.549862	41.743464	41.700278	41.461453	42.582218	41.597604	41.246824	41.381753	41.386847	41.902476	42.40658	41.814487	41.814487	0.3384986	0.7091581	0.5238284	255.93167
	42.443928	41.686823	41.780564	41.488536	42.447354	41.573105	41.242972	41.494856	41.390088	41.988934	42.359956	41.808829	41.808829	0.4660108	0.8342187	0.6501148	257.81132
	42.748709	41.982375	42.056147	41.761988	42.820936	42.251442	41.765215	42.351167	41.886884	42.720068	43.434	42.343539	42.343539	0.5246798	0.8905304	0.7076051	257.77129
	43.27871	42.438548	42.32529	41.97771	43.291774	42.975387	42.048	42.759613	42.449903	43.754097	45.461548	42.978235	42.978235	0.5755234	0.9349959	0.7552597	261.63645
	42.138586	41.408237	41.14081	41.003288	41.912366	40.955556	40.546864	40.649732	40.366441	40.971346	41.490512	41.143976	41.143976	0.2056553	0.5869712	0.3963133	260.84783

tion

t Side

Test Date	Surface Couple 9	Surface Couple 10	Surface Couple 11	Average T_Surface	Corrected Temp (F)	Entering Quality	Exiting Quality	Average Quality	Mass Flux (kg/m^2*s)	Average Pressure	Actual TSAT (F)	Wall Tsurf (F)	DeltaT	HTC (Btu/hr ft^2 F)	HTC (kw/m^2 C)	α/α0	ΔP/ΔP0
1%P-350M-15H	42.593541	43.290351	43.496	43.497865	43.497865	0.1820875	0.4493096	0.3156985	356.84417	134.8409865	38.74407346	43.46862	4.724548	1009.243021	5.7325	0.737	0.56421
	42.256687	42.996881	43.225775	43.205542	43.205542	0.2730122	0.5460719	0.409542	350.39601	134.5957269	38.64221913	43.16303	4.520815	1056.674418	6.001911	0.7717	0.74367
	42.237757	43.009043	43.240454	43.175109	43.175109	0.347446	0.6234351	0.4854405	346.89516	134.9208857	38.79310742	43.12164	4.328537	1102.913505	6.264549	0.8054	0.8619
	41.928993	42.713909	42.984116	42.892488	42.892488	0.410123	0.6841823	0.5471526	348.5478	134.5114222	38.61552121	42.8291	4.213583	1129.989838	6.418342	0.8252	1.0007
	41.820402	42.615536	42.796898	42.798633	42.798633	0.4548841	0.7282676	0.5915758	349.96847	134.49037	38.60964832	42.72802	4.118369	1157.274792	6.573321	0.8451	1.11764
	41.824647	42.587973	42.734196	42.789714	42.789714	0.5073932	0.7800499	0.6437215	351.18178	134.7106178	38.71200317	42.71063	3.998631	1191.439741	6.767378	0.8701	1.2598
	41.73424	42.530398	42.754198	42.76343	42.76343	0.56971	0.8394616	0.7045858	352.85552	134.7181311	38.72017737	42.67432	3.95414	1197.300798	6.800669	0.8744	1.41472
	42.50509	43.583402	44.242475	43.265788	43.265788	0.6622507	0.9389616	0.8006062	344.99629	134.3077486	38.54467596	43.16425	4.619573	1031.679156	5.859938	0.7534	1.51848
	43.820631	45.168487	45.969002	43.954919	43.954919	0.7025531	0.9747262	0.8386396	351.12661	133.2939511	38.09349472	43.84414	5.750647	830.6964973	4.718356	0.6066	1.64189
3%P- 350M-15H	41.673053	42.475102	42.773427	42.619795	42.619795	0.1847532	0.4531147	0.318934	356.08927	134.8473022	38.11208704	42.5898	4.477716	1064.950465	6.048919	0.7777	0.65914
	41.611329	42.419069	42.672989	42.519027	42.519027	0.1872164	0.4569605	0.3220884	352.81444	134.5490444	37.97897095	42.48916	4.510186	1054.977306	5.992271	0.7704	0.60805
	41.611329	42.419069	42.672989	42.519027	42.519027	0.1872744	0.4569605	0.3221174	352.81444	134.5303844	37.97062193	42.48916	4.518536	1053.027995	5.981199	0.769	0.60059
	41.779207	42.493613	42.957693	42.603712	42.603712	0.2631676	0.5348497	0.3990086	354.52764	134.7414667	38.07115751	42.56179	4.490635	1070.016034	6.077691	0.7814	0.74649
	41.32252	42.019733	42.505484	42.154196	42.154196	0.3424546	0.6190308	0.4807427	347.5773	133.7644933	37.639681	42.10074	4.461062	1075.226136	6.107284	0.7852	0.90776
	41.332247	41.969391	42.506031	42.14686	42.14686	0.3465884	0.6268488	0.4867186	342.99295	133.7689189	37.64214498	42.0935	4.451354	1077.992472	6.122997	0.7872	0.89451
	41.604029	42.225451	42.783891	42.382991	42.382991	0.4048623	0.6822846	0.5435734	348.55262	134.3962756	37.92818056	42.31958	4.391399	1097.05008	6.231244	0.8011	1.03138
	41.824093	42.43852	42.998693	42.602587	42.602587	0.4362152	0.7130117	0.5746134	348.69093	135.0467067	38.22147654	42.53418	4.312705	1113.623361	6.325381	0.8132	1.10381
	40.609716	41.190776	41.600078	41.313324	41.313324	0.1763375	0.4482339	0.3122857	354.32568	131.8118544	36.74366154	41.28499	4.541331	1064.151853	6.044383	0.7771	0.60637
	40.304022	40.912944	41.360244	40.957046	40.957046	0.3020127	0.5715545	0.4367836	356.8353	131.1539178	36.45386257	40.90838	4.454518	1080.110657	6.135029	0.7888	0.88296
	40.819218	41.393687	41.799053	41.476178	41.476178	0.4168027	0.6873573	0.55208	356.89432	132.5920144	37.11649662	41.40896	4.292465	1120.518968	6.364548	0.8183	1.16442
	40.243247	40.897456	41.271511	40.90987	40.90987	0.5363261	0.8084786	0.6724023	356.12634	131.4051311	36.58703943	40.8232	4.236162	1140.515343	6.478127	0.8329	1.49929
	40.398393	41.167884	41.699827	41.141343	41.141343	0.6003674	0.8740032	0.7371853	352.76905	131.4668578	36.62028501	41.04538	4.425091	1088.293549	6.181507	0.7947	1.62634
3%P- 250M-15H	40.826477	41.638735	41.895661	41.772975	41.772975	0.1228536	0.4995502	0.3112019	252.26071	132.2310312	37.41898475	41.75909	4.340103	1107.690833	6.291684	0.8089	0.33051
	41.307109	41.922827	42.320036	41.76379	41.76379	0.3679751	0.7331441	0.5505596	260.44093	132.1695989	37.41008612	41.72111	4.311025	1113.09126	6.322358	0.8129	0.64239
	41.522133	42.039598	42.519418	41.94586	41.94586	0.3196191	0.6892409	0.50443	257.45796	132.5744856	37.58965816	41.90925	4.319593	1111.448166	6.313026	0.8117	0.57156
	41.490553	42.027949	42.521624	41.908768	41.908768	0.3182811	0.6864176	0.5023494	258.47543	132.5015433	37.55651705	41.87216	4.31564	1112.247463	6.317566	0.8122	0.57908
	41.331193	41.931789	42.306088	41.765938	41.765938	0.401256	0.7679345	0.5845952	259.42542	132.2577602	37.45270962	41.71946	4.266748	1124.865901	6.389238	0.8215	0.69375
	40.955689	41.632584	42.011269	41.746173	41.746173	0.2065578	0.5748106	0.3906842	256.63932	132.1905344	37.40692819	41.72265	4.31572	1106.348615	6.28406	0.8079	0.43811
	41.386847	41.902476	42.40658	41.814487	41.814487	0.3384986	0.7091581	0.5238284	255.93167	132.0981	37.37557317	41.77599	4.400418	1088.420445	6.182228	0.7948	0.58386
	41.390088	41.988934	42.359956	41.808829	41.808829	0.4660108	0.8342187	0.6501148	257.81132	132.4503066	37.54503579	41.75502	4.209984	1137.49101	6.460949	0.8307	0.75607
	41.886884	42.720068	43.434	42.343539	42.343539	0.5246798	0.8905304	0.7076051	257.77129	132.8734442	37.74075774	42.28301	4.542252	1046.805691	5.945856	0.7644	0.81611
	42.449903	43.754097	45.461548	42.978235	42.978235	0.5755234	0.9349959	0.7552597	261.63645	132.7094194	37.67047848	42.91031	5.239829	905.3292169	5.14227	0.6611	0.88533
	40.366441	40.971346	41.490512	41.143976	41.143976	0.2056553	0.5869712	0.3963133	260.84783	130.4135034	36.59827931	41.1199	4.521621	1114.330804	6.329399	0.8138	0.4462

tion

t Side

Test Date	Surface Couple 9	Surface Couple 10	Surface Couple 11	Average T_Surface	Corrected Temp (F)	Entering Quality	Exiting Quality	Average Quality	Mass Flux (kg/m²*s)	Average Pressure	Actual TSAT (F)	Wall Tsurf (F)	DeltaT	HTC (Btu/hr ft^2 F)	HTC (kw/m^2 C)	α/α0	ΔP/ΔP0
POE 3%250M12H	40.963755	41.671255	41.806298	41.710588	41.710588	0.1802298	0.4769292	0.3285795	257.67266	132.67147	37.47486607	41.69015	4.215288	915.3140013	5.198984	0.6684	0.35069
	40.852327	41.544343	41.799717	41.507185	41.507185	0.2650075	0.5614106	0.4132091	257.34031	132.2955178	37.31145406	41.47716	4.165705	923.4945742	5.245449	0.6744	0.44
	40.848238	41.550964	41.78764	41.459496	41.459496	0.3618936	0.6612519	0.5115728	255.26029	132.2508622	37.29900723	41.41881	4.119807	934.7939706	5.30963	0.6827	0.56135
	40.995616	41.671913	41.851953	41.554293	41.554293	0.4391928	0.7370606	0.5881267	255.20724	132.5135767	37.42401591	41.50464	4.080628	938.0613931	5.328189	0.685	0.65997
	40.99174	41.70924	41.937504	41.538776	41.538776	0.5103566	0.8056864	0.6580215	256.95887	132.4060689	37.38089338	41.48044	4.099546	932.0278036	5.293918	0.6806	0.7556
	41.369533	42.186613	42.567529	41.937129	41.937129	0.5780097	0.8720718	0.7250407	256.97835	132.4266967	37.39553692	41.87087	4.475329	850.2850615	4.829619	0.6209	0.84153
	41.170342	41.932769	42.373411	41.856763	41.856763	0.6217992	0.9145642	0.7681817	257.56549	132.5526211	37.45593581	41.78513	4.329194	877.0246235	4.9815	0.6405	0.912
	43.775233	45.694544	46.359191	43.230341	43.230341	0.6871436	0.9764994	0.8318215	260.27894	131.6095268	37.03319198	43.15053	6.117334	621.2899613	3.528927	0.4537	1.02077
3%POE- 350M-1	40.718699	41.44755	41.502797	41.487362	41.487362	0.2017127	0.420801	0.3112569	346.83942	132.8602751	37.70339884	41.45608	3.752685	1010.807993	5.741389	0.7382	0.61861
	40.593573	41.271183	41.486406	41.347716	41.347716	0.2820686	0.5021007	0.3920847	349.53435	132.5872614	37.58650652	41.30355	3.717042	1029.57972	5.848013	0.7519	0.79994
	40.559422	41.197949	41.409609	41.286425	41.286425	0.341015	0.5583659	0.4496905	351.08246	132.5649277	37.58097049	41.23278	3.651806	1037.649297	5.893848	0.7578	0.94029
	40.4132	41.043053	41.244243	41.140513	41.140513	0.3895337	0.6063791	0.4979564	354.57396	132.4156617	37.51728967	41.07858	3.561294	1070.226105	6.078884	0.7816	1.06269
	40.485837	41.10872	41.296867	41.208662	41.208662	0.4163752	0.633864	0.5251196	352.87574	132.614825	37.60949075	41.14281	3.533318	1077.035723	6.117563	0.7865	1.11446
	40.336579	40.960468	41.147929	41.076715	41.076715	0.509207	0.7294106	0.6193088	352.25677	132.4626548	37.54814786	40.99588	3.447728	1113.592342	6.325205	0.8132	1.38148
	40.089123	40.7335	40.89139	40.840664	40.840664	0.5778105	0.7972513	0.6875309	352.66805	131.9378062	37.31579234	40.74889	3.433098	1116.667759	6.342673	0.8155	1.56889
	40.392557	41.002972	41.152163	41.113387	41.113387	0.5760829	0.7950906	0.6855868	352.36494	132.6047236	37.61762503	41.02215	3.404525	1121.988816	6.372896	0.8194	1.54319
	40.292513	40.965747	41.157738	41.072431	41.072431	0.6176919	0.8363464	0.7270191	352.13417	132.3927989	37.52506654	40.97447	3.449404	1105.267238	6.277918	0.8071	1.65098
	41.287811	42.145009	42.5682	41.822038	41.822038	0.668598	0.8875978	0.7780979	351.16078	132.8027033	37.71437431	41.71567	4.001296	953.2948228	5.414715	0.6962	1.74624
	40.908922	42.034847	42.923338	41.634112	41.634112	0.7353965	0.9540697	0.8447331	350.21511	132.58038	37.61921708	41.51656	3.897346	976.0210937	5.5438	0.7128	1.91935
N(1% T1S2) 350M-	42.219316	42.867484	42.926262	43.249458	43.249458	0.1906625	0.4633984	0.3270305	350.32422	133.5297211	38.15873566	43.21941	5.060674	944.4583037	5.364523	0.6897	0.63376
	42.674477	43.316833	43.362312	43.692722	43.692722	0.1023905	0.3711099	0.2367502	352.98199	133.6918163	38.22428019	43.67586	5.451582	872.4615866	4.955582	0.6371	0.46755
	41.816824	42.381822	42.690584	42.884181	42.884181	0.285485	0.5583331	0.4219091	350.2925	133.7884511	38.282236	42.84058	4.558339	1046.32327	5.943116	0.7641	0.8259
	41.442695	42.085361	42.416895	42.527327	42.527327	0.4169493	0.6912554	0.5541023	350.30793	133.7587294	38.27938243	42.46495	4.185567	1142.882529	6.491573	0.8346	1.14406
	41.227293	41.884153	42.217211	42.30227	42.30227	0.4749532	0.7494943	0.6122237	349.52162	133.6421556	38.23172918	42.23158	3.999849	1193.087952	6.77674	0.8713	1.31955
	41.302769	42.0666	42.578927	42.244396	42.244396	0.5675035	0.8439845	0.705744	347.36065	133.7620133	38.29285646	42.16091	3.868054	1235.628192	7.018368	0.9023	1.52172
	41.633209	42.452331	43.022322	42.441983	42.441983	0.6189678	0.891995	0.7554814	351.82399	133.9377111	38.37548561	42.34981	3.974324	1202.172001	6.828337	0.8779	1.66732
	43.483318	44.750136	45.727273	43.676431	43.676431	0.7012781	0.9686417	0.8349599	353.52732	133.1862556	38.04465383	43.57151	5.526855	852.7131893	4.843411	0.6227	1.85549

	Test Sectior																	
	Refrigerant Si																	
Test Date	Exit Temp (F)	Exit Pressure (psi)	Final Exit Pressure (psi)	Leaving Enthalpy (Btu/lb)	DP @ Test Section (psi)	DP/ Length Test Section (kPa/m)	Entering Temp (F)	EnteringPressure (psi)	Entering Enthalpy (Btu/lb)	Surface Couple 1	Surface Couple 2	Surface Couple 3	Surface Couple 4	Surface Couple 5	Surface Couple 6	Surface Couple 7	Surface Couple 8	Su Co
POE 3%250M12H	38.548482	131.79474	131.79474	133.01325	1.753465	6.6107369	38.75588	133.5482	105.65118	42.570725	42.162525	41.806985	41.593245	42.186448	41.64519	41.090363	41.319685	4
	38.456802	131.18808	131.18808	140.81761	2.2148753	8.3502994	38.704764	133.40296	113.50049	42.247376	41.657189	41.570027	41.314813	42.092363	41.441982	40.913886	41.145016	4
	38.396864	130.8475	130.8475	150.09118	2.8067289	10.581646	38.769098	133.65423	122.52165	42.060569	41.480382	41.540502	41.229147	42.101289	41.439758	40.902904	41.113062	4
	38.462427	130.86366	130.86366	157.15456	3.2998333	12.440699	38.920622	134.16349	129.74607	42.084422	41.54904	41.65468	41.305887	42.197613	41.569358	40.999378	41.21736	4
	38.475238	130.51706	130.51706	163.52846	3.7780222	14.243518	38.890804	134.29508	136.35651	42.002533	41.503127	41.614084	41.242593	42.149402	41.537216	40.944611	41.294487	
	38.759836	130.32288	130.32288	169.70684	4.2076289	15.863178	38.873209	134.53051	142.64777	42.172302	41.615778	41.825598	41.545058	42.49	42.239653	41.403656	41.892698	4
	38.648962	130.27262	130.27262	173.66636	4.5599933	17.191627	38.896691	134.83262	146.72925	42.12236	41.661842	42.025211	41.624233	42.442158	42.107336	41.259433	41.705298	4
	41.951896	129.54317	128.57202	179.38517	5.1038667	19.242083	38.612311	133.67589	152.702	42.680407	41.979058	42.243431	41.794327	43.045878	42.712669	42.031533	43.217482	4
3%POE- 350M-1	38.33445	131.31376	131.31376	127.74025	3.0930312	11.661034	38.850448	134.40679	107.75534	42.254708	41.738777	41.714096	41.418942	42.043463	41.484552	40.888786	41.148606	4
	38.117365	130.58741	130.58741	135.23992	3.99971	15.079303	38.853792	134.58712	115.23267	41.999516	41.498566	41.637034	41.236016	41.943235	41.405886	40.748203	41.005258	4
	38.025695	130.2142	130.2142	140.45358	4.701457	17.724959	38.931703	134.91566	120.73076	41.895656	41.424605	41.607434	41.127254	41.883523	41.397469	40.692164	40.955586	4
	37.86686	129.75893	129.75893	144.88502	5.3134567	20.032258	38.907643	135.07239	125.24254	41.724213	41.293137	41.489807	40.977623	41.71422	41.277493	40.548477	40.820173	
	37.92671	129.82868	129.82868	147.46167	5.57229	21.008086	39.01509	135.40097	127.75511	41.783643	41.369167	41.56402	41.05307	41.779027	41.3491	40.61055	40.895287	4
	37.667651	129.00894	129.00894	156.3192	6.9074206	26.041661	38.967881	135.91637	136.40239	41.663151	41.285079	41.455119	40.95331	41.638849	41.212968	40.441397	40.749016	4
	37.299478	128.01559	128.01559	162.60073	7.8444361	29.574302	38.713764	135.86002	142.73686	41.424952	41.036471	41.189903	40.717348	41.375313	40.976482	40.211088	40.601733	4
	37.59489	128.74675	128.74675	162.44359	7.7159512	29.089901	39.011825	136.4627	142.63414	41.664516	41.279679	41.420138	40.961939	41.64752	41.302024	40.517289	40.906459	4
	37.479096	128.26534	128.26534	166.26582	8.2549178	31.121858	38.903478	136.52026	146.48141	41.645456	41.230327	41.375178	40.924851	41.59994	41.28322	40.463367	40.858404	4
	38.221333	128.43711	128.43711	171.07435	8.73118	32.917414	39.038671	137.16829	151.22521	42.079667	41.591562	41.926811	41.412029	42.213967	41.916811	41.196982	41.703573	4
	38.272922	127.78202	127.78202	177.25845	9.5967289	36.180619	38.820307	137.37874	157.41061	42.024533	41.450378	41.769113	41.21066	41.962522	41.58222	40.773102	41.335591	4
N(1% T1S2) 350M-	38.349744	131.94531	131.94531	131.76537	3.1688244	11.946782	38.922422	135.11413	106.8343	44.380749	43.470869	43.749211	43.191222	44.019173	43.527911	42.520189	42.871649	4
	38.539327	132.52295	132.52295	123.24669	2.337735	8.8134926	38.84382	134.86068	98.623961	44.910414	43.964508	44.105321	43.62563	44.353056	43.997033	42.95735	43.353007	4
	38.390831	131.72371	131.72371	140.58256	4.12948	15.568549	39.126564	135.85319	115.70192	43.972073	43.155287	43.472827	42.836376	43.698213	43.127042	42.11678	42.458164	4
	38.116468	130.89858	130.89858	152.89125	5.7202918	21.566067	39.134445	136.61888	127.93807	43.526203	42.742635	43.142098	42.403715	43.367007	42.799728	41.770851	42.103405	4
	37.921824	130.34327	130.34327	158.27652	6.5977689	24.874243	39.105816	136.94104	133.32702	43.270113	42.515493	42.916102	42.159778	43.129362	42.581336	41.537738	41.886391	4
	38.048816	129.9577	129.9577	167.06969	7.6086178	28.685243	39.126244	137.56632	141.92655	43.148849	42.373093	42.70226	41.884604	42.86984	42.351893	41.45374	41.955776	4
	38.311227	129.76942	129.76942	171.53552	8.3365822	31.429741	39.165851	138.106	146.71995	43.197918	42.309042	42.692713	41.996298	43.070564	42.555296	41.694978	42.23714	4
	39.884938	128.54754	128.54754	178.64917	9.2774356	34.976852	38.657722	137.82497	154.28913	43.649378	42.656469	43.29866	42.572871	43.895029	43.62554	42.988576	43.793487	4

	Preheater						Heat Sources									
	Refrigerant Side						Hot Loop				Water Loop					Total
Test Date	Flow Rate (lb/hr)	Pressure (psi)	Inlet Temp (F)	Exit Temp (F)	Entering Enthalpy (Btu/lb)	Leaving Enthalpy (Btu/lb)	Plate Flow Rate (lb/min)	Entering Hot Temp (F)	Leaving Hot Temp (F)	Q Plate_hot (Btu/hr)	Test Inlet Temp (F)	Test Outlet Temp (F)	Plate Inlet Temp (F)	Plate Outlet Temp (F)	Effective Pump W_dot (kW)	Q (Btu/hr)
POE 3%250M12H	121.2032975	132.722475	34.9204975	38.5484825	87.0467758	105.651184	0.37613	76.129305	45.975985	680.4940951	46.14192	45.74991	45.809525	45.958915	0.77249985	3316.372992
	121.046971	132.5597105	32.3911982	38.4568018	86.1272776	113.5004871	0.370933	76.039294	45.8177951	672.60941	45.9812539	45.5654944	45.6515234	45.807392	0.77196247	3306.654698
	120.0685756	132.8784756	29.6370311	38.3968644	85.1323132	122.5216529	0.366989	76.0983089	45.79816	667.1890784	45.9565844	45.5453356	45.6307067	45.7901178	0.77460013	3310.23444
	120.0436222	133.4804644	26.7801422	38.4624267	84.1054863	129.7460682	0.364104	76.1435467	45.8901444	660.9238925	46.0476822	45.6336933	45.7246667	45.8714267	0.770569	3290.214456
	120.8675467	133.7228267	23.9548667	38.4752378	83.0953548	136.356507	0.353647	76.1388067	45.893	641.7797225	46.0409667	45.6269444	45.7113844	45.8681489	0.7744192	3284.207714
	120.8767133	134.0649356	21.3106644	38.7598356	82.1546383	142.6477675	0.35112	76.1691844	46.2949244	629.3670103	46.4406022	46.0324622	46.1144378	46.2645778	0.77413093	3270.811395
	121.1528889	134.4676067	19.4124578	38.6489622	81.4820419	146.729253	0.346153	76.1673489	46.2339489	621.6927713	46.3820756	45.9724533	46.0543222	46.20794	0.7742398	3263.508624
	122.4292333	134.4039622	17.3707	41.9518956	80.7608117	152.7019985	0.370093	76.2554667	47.6723644	634.7049347	47.8508444	47.4359933	47.5256422	47.6707489	0.77139087	3266.799824
3%POE- 350M-1	163.1452918	133.696853	33.6878374	38.3344499	86.5991228	107.7553378	0.340873	76.1544722	45.7200891	622.4556612	45.8538151	45.4458374	45.5385301	45.6773987	0.77311811	3260.444139
	164.4129247	134.0888927	30.9016758	38.1173653	85.5882575	115.2326653	0.350995	76.2371142	45.6402466	644.3616485	45.7871941	45.3704338	45.4627146	45.6033813	0.77519925	3289.451269
	165.1411211	134.6830195	28.9367344	38.0256953	84.8815321	120.7307551	0.344723	76.2283086	45.6416484	632.6348841	45.7503711	45.3336523	45.422793	45.5682852	0.76913977	3257.048698
	166.7834433	134.9822067	27.2268967	37.86686	84.2671164	125.2425403	0.344417	76.24227	45.4261733	636.8146376	45.56776	45.1571867	45.2450767	45.3865933	0.7734808	3276.040675
	165.98464	135.3892133	26.40803	37.92671	83.9732482	127.7551118	0.341987	76.2458167	45.4390967	632.129249	45.6072633	45.2007233	45.28263	45.4262633	0.7733727	3270.986434
	165.6934921	136.2249206	22.4567063	37.6676508	82.5636511	136.4023902	0.355056	76.3267619	45.4576825	657.6142874	45.569254	45.1459921	45.2432619	45.3882778	0.7744319	3300.085629
	165.8869471	136.4005396	19.9888414	37.299478	81.687127	142.7368591	0.351073	76.3345749	45.2532952	654.707304	45.3555154	44.9299141	45.0213899	45.1688194	0.77383956	3295.15748
	165.7443699	137.0046423	20.5563171	37.5948902	81.8892761	142.6341446	0.348663	76.3896301	45.3816951	648.6784364	45.5465772	45.1356463	45.2184553	45.3628415	0.77213244	3283.303676
	165.63582	137.1986911	18.6583711	37.4790956	81.2169272	146.4814137	0.347229	76.4028311	45.4295956	645.28813	45.5606956	45.1451222	45.2320067	45.3766267	0.77128047	3277.006319
	165.17796	137.7512778	15.6654422	38.2213333	80.1632431	151.2252056	0.356813	76.4555733	46.1636533	648.5136569	46.3262244	45.9148089	45.9899378	46.1501733	0.77081433	3278.641333
	164.73314	138.1679911	11.3988778	38.2729222	78.6670263	157.4106128	0.348	76.4934644	46.1379422	633.823304	46.2890244	45.8766	45.9593267	46.1101867	0.7724688	3269.596254
N(1% T1S2) 350M-	164.7844644	134.5145889	33.9994933	38.3497444	86.7118453	106.8343037	0.899707	75.49628	48.1517	1476.126055	48.4440222	48.0281333	48.0406644	48.2968911	0.77140007	4108.252336
	166.0346192	134.1498419	35.9395657	38.5393274	87.4186082	98.62396102	0.906205	75.4373296	48.5257127	1463.246347	48.8271537	48.4386214	48.4345011	48.6830824	0.76930543	4088.225446
	164.7695444	135.4771978	33.4104822	38.3908311	86.4975325	115.7019177	0.889464	75.5436556	47.8012778	1480.551518	48.14084	47.6507022	47.6852622	47.9548378	0.76755907	4099.571763
	164.7768018	136.639118	32.4854766	38.1164677	86.1638853	127.9380718	0.883283	75.6102762	47.5226258	1488.560392	47.9289332	47.3366414	47.40302	47.6803541	0.76876757	4111.704229
	164.4069378	137.1465311	31.6966111	37.9218244	85.877864	133.3270197	0.87108	75.6440444	47.3261133	1480.031006	47.7680356	47.1115689	47.1919311	47.4771578	0.76838553	4101.871272
	163.3904689	138.0561356	30.77212	38.0488156	85.5417937	141.9265476	0.877753	75.6687667	47.31816	1493.09037	47.7693533	47.1044756	47.1869	47.4715622	0.76639833	4108.150029
	165.48992	138.8131978	29.98452	38.3112267	85.2568224	146.7199483	0.885627	75.6925756	47.5295244	1496.516945	47.9300956	47.3461556	47.4037978	47.6840956	0.76497693	4106.726585
	166.2911289	138.8003622	28.3283244	39.8849378	84.6628317	154.2891319	0.894209	75.6706067	48.7162711	1446.168387	49.0073844	48.6221467	48.6139089	48.8584511	0.76335927	4050.858319

	Preheater										Heat Sources					
	Water Side				Refrigerant Side						Hot Loop				Water	
Test Date	Flow Rate (lb/min)	Inlet Temp (F)	Exit Temp (F)	Q (Btu/hr)	Flow Rate (lb/hr)	Pressure (psi)	Inlet Temp (F)	Exit Temp (F)	Entering Enthalpy (Btu/lb)	Leaving Enthalpy (Btu/lb)	Plate Flow Rate (lb/min)	Entering Hot Temp (F)	Leaving Hot Temp (F)	Q Plate_hot (Btu/hr)	Test Inlet Temp (F)	Test Outlet Temp (F)
POE 3%250M12H	1.0297825	76.9966	40.75527	2254.915622	121.2032975	132.722475	34.9204975	38.5484825	87.0467758	105.651184	0.37613	76.129305	45.975985	680.4940951	46.14192	45.74991
	1.6249176	76.9638	43.2142829	3313.444106	121.046971	132.5597105	32.3911982	38.4568018	86.1272776	113.5004871	0.370933	76.039294	45.8177951	672.60941	45.9812539	45.5654944
	2.4141889	77.11439	46.3374689	4489.284767	120.0685756	132.8784756	29.6370311	38.3968644	85.1323132	122.5216529	0.366989	76.0983089	45.79816	667.1890784	45.9565844	45.5453356
	3.2149222	77.21019	49.0043467	5478.860765	120.0436222	133.4804644	26.7801422	38.4624267	84.1054863	129.7460682	0.364104	76.1435467	45.8901444	660.9238925	46.0476822	45.6336933
	4.0254622	77.24862	50.7804556	6437.544794	120.8675467	133.7228267	23.9548667	38.4752378	83.0953548	136.356507	0.353647	76.1388067	45.893	641.7797225	46.0409667	45.6269444
	4.9350444	77.28098	52.7577889	7312.210634	120.8767133	134.0649356	21.3106644	38.7598356	82.1546383	142.6477675	0.35112	76.1691844	46.2949244	629.3670103	46.4406022	46.0324622
	5.6517244	77.42662	54.27752	7904.888123	121.1528889	134.4676067	19.4124578	38.6489622	81.4820419	146.729253	0.346153	76.1673489	46.2339489	621.6927713	46.3820756	45.9724533
	6.6058778	77.45146	55.38404	8807.704355	122.4292333	134.4039622	17.3707	41.9518956	80.7608117	152.7019985	0.370093	76.2554667	47.6723644	634.7049347	47.8508444	47.4359933
3%POE- 350M-1:	1.7323385	76.99624	44.0201626	3451.536864	163.1452918	133.696853	33.6878374	38.3344499	86.5991228	107.7553378	0.340873	76.1544722	45.7200891	622.4556612	45.8538151	45.4458374
	2.6673973	77.21399	46.9720046	4873.923789	164.4129247	134.0888927	30.9016758	38.1173653	85.5882575	115.2326653	0.350995	76.2371142	45.6402466	644.3616485	45.7871941	45.3704338
	3.5725	77.24328	49.8160469	5920.180882	165.1411211	134.6830195	28.9367344	38.0256953	84.8815321	120.7307551	0.344723	76.2283086	45.6416484	632.6348841	45.7503711	45.3336523
	4.35864	77.27615	51.32571	6834.022293	166.7834433	134.9822067	27.2268967	37.86686	84.2671164	125.2425403	0.344417	76.24227	45.4261733	636.8146376	45.56776	45.1571867
	4.8393333	77.29871	52.44473	7267.11687	165.98464	135.3892133	26.40803	37.92671	83.9732482	127.7551118	0.341987	76.2458167	45.4390967	632.129249	45.6072633	45.2007233
	6.6946667	77.38841	55.334246	8920.72869	165.6934921	136.2249206	22.4567063	37.6676508	82.5636511	136.4023902	0.355056	76.3267619	45.4576825	657.6142874	45.569254	45.1459921
	7.734989	77.43238	55.7625463	10127.35367	165.8869471	136.4005396	19.9888414	37.299478	81.687127	142.7368591	0.351073	76.3345749	45.2532952	654.707304	45.3555154	44.9299141
	7.7254797	77.45113	55.8815244	10068.11995	165.7443699	137.0046423	20.5563171	37.5948902	81.8892761	142.6341446	0.348663	76.3896301	45.3816951	648.6784364	45.5465772	45.1356463
	8.4227089	77.47408	56.2319244	10810.13673	165.63582	137.1986911	18.6583711	37.4790956	81.2169272	146.4814137	0.347229	76.4028311	45.4295956	645.28813	45.5606956	45.1451222
	9.36644	77.51756	56.7763533	11737.87	165.17796	137.7512778	15.6654422	38.2213333	80.1632431	151.2252056	0.356813	76.4555733	46.1636533	648.5136569	46.3262244	45.9148089
	10.559849	77.55748	57.2265222	12971.67825	164.73314	138.1679911	11.3988778	38.2729222	78.6670263	157.4106128	0.348	76.4934644	46.1379422	633.823304	46.2890244	45.8766
N(1% T1S2) 350M-:	1.6285778	77.0556	43.3572889	3315.868535	164.7844644	134.5145889	33.9994933	38.3497444	86.7118453	106.8343037	0.899707	75.49628	48.1517	1476.126055	48.4440222	48.0281333
	0.8172183	76.8413	39.1617751	1860.476484	166.0346192	134.1498419	35.9395657	38.5393274	87.4186082	98.62396102	0.906205	75.4373296	48.5257127	1463.246347	48.8271537	48.4386214
	2.7111889	77.21986	47.8444089	4811.993242	164.7695444	135.4771978	33.4104822	38.3908311	86.4975325	115.7019177	0.889464	75.5436556	47.8012778	1480.551518	48.14084	47.6507022
	4.6195635	77.36356	52.7018909	6883.416842	164.7768018	136.639118	32.4854766	38.1164677	86.1638853	127.9380718	0.883283	75.6102762	47.5226258	1488.560392	47.9289332	47.3366414
	5.7704444	77.38219	55.0074133	7800.970391	164.4069378	137.1465311	31.6966111	37.9218244	85.877864	133.3270197	0.87108	75.6440444	47.3261133	1480.031006	47.7680356	47.1115689
	7.2726333	77.44588	56.4798622	9212.731389	163.3904689	138.0561356	30.77212	38.0488156	85.5417937	141.9265476	0.877753	75.6687667	47.31816	1493.09037	47.7693533	47.1044756
	8.2291689	77.49915	57.0417978	10171.52779	165.48992	138.8131978	29.98452	38.3112267	85.2568224	146.7199483	0.885627	75.6925756	47.5295244	1496.516945	47.9300956	47.3461556
	9.5805422	77.46549	57.4635778	11578.23605	166.2911289	138.8003622	28.3283244	39.8849378	84.6628317	154.2891319	0.894209	75.6706067	48.7162711	1446.168387	49.0073844	48.6221467

	Preheater										Heat Sources					
	Water Side				Refrigerant Side						Hot Loop				Water	
Test Date	Flow Rate (lb/min)	Inlet Temp (F)	Exit Temp (F)	Q (Btu/hr)	Flow Rate (lb/hr)	Pressure (psi)	Inlet Temp (F)	Exit Temp (F)	Entering Enthalpy (Btu/lb)	Leaving Enthalpy (Btu/lb)	Plate Flow Rate (lb/min)	Entering Hot Temp (F)	Leaving Hot Temp (F)	Q Plate_hot (Btu/hr)	Test Inlet Temp (F)	Test Outlet Temp (F)
N(1%T1S2) 250M	0.8300756	76.78995	39.4502956	1872.70202	120.89668	134.1865289	36.2726378	38.9499356	87.5391226	103.0292256	0.385107	75.0165289	47.3422289	639.4534455	47.6919844	47.0907156
	0.8317949	76.8581	39.4757219	1878.727838	120.5644691	134.1970871	36.3697949	38.9550758	87.5756588	103.1584242	0.385461	75.0491882	47.3907416	639.674609	47.7187528	47.1288399
	2.4967756	76.99602	47.3151422	4477.513797	121.4418133	134.9188467	35.0921667	38.7098467	87.1086044	123.9782268	0.376731	74.9206378	46.8753156	633.9327241	47.3165467	46.5284111
	1.5599771	76.94353	43.5246376	3149.857625	122.8127041	134.6411514	35.4551009	38.8772936	87.2434762	112.8911292	0.382727	75.0990872	47.1552982	641.6906594	47.5628142	46.8890963
	3.1507407	77.18396	49.6169259	5247.874968	120.1996049	135.1747407	34.8762346	38.7509012	87.0321076	130.6917766	0.383123	75.1212963	46.8320741	650.2958765	47.2954074	46.4873951
	3.6501463	77.23909	50.8507846	5819.72626	122.351374	135.7111748	34.6913171	38.8459837	86.9629398	134.5286195	0.38465	75.1352154	46.9134024	651.3319108	47.3453252	46.5631626
	4.3756222	77.29025	52.2414444	6622.280046	121.3089044	135.7249933	34.0892689	38.6637356	86.7446348	141.3348569	0.395129	75.1931778	46.79268	673.3114278	47.2532133	46.3928511
	5.25954	77.31509	54.2223778	7338.435636	121.0843067	135.9043133	33.4053467	38.7139667	86.4975615	147.1035627	0.403202	75.21964	46.8673022	685.9035358	47.3103067	46.4835133
	5.9530422	77.35388	55.4558756	7876.336595	120.2986444	136.0072489	32.7292156	39.7146778	86.2508314	151.7240263	0.396707	75.2167378	47.2555933	665.5423445	47.6210044	46.9409178
N(3%T1S2) 350M	0.7845578	77.7053	38.9745622	1835.952424	165.5565578	134.0747333	35.5386822	38.7083111	87.2726421	98.36222051	0.353164	75.6326556	46.5967733	615.2664728	47.0929222	46.1637133
0.4259x - 18.09	1.6024556	77.38121	43.4998889	3280.401758	165.7000867	134.8448911	33.5980222	38.7561044	86.5664962	106.3637203	0.356658	75.3260889	46.5379022	616.051841	47.0447556	46.0865467
	2.4189622	76.60581	46.8969022	4342.066882	165.1228022	135.4040711	33.1033867	38.6936667	86.3849971	112.680983	0.365647	74.7366911	46.4441644	620.704084	46.9711444	45.9770267
	2.4131067	76.36297	46.8451533	4303.695346	165.77432	135.4423233	33.0737933	38.7568767	86.3741139	112.3352842	0.36181	74.5597933	46.4483233	610.2606576	46.9792633	45.9876333
	3.5038489	77.33995	50.5201978	5677.810167	164.7825489	136.1927178	32.5794489	38.5129711	86.1964656	120.6528459	0.358767	75.1975333	46.30232	621.9983622	46.8697533	45.8244756
	4.6062978	77.34742	52.8080156	6829.62205	165.1252867	136.7618444	31.6791889	38.3447356	85.8705857	127.2308292	0.366024	75.14002	46.1853889	635.886166	46.7820378	45.6942556
	6.1176778	77.38282	55.6378978	8037.576766	165.5057911	137.6249689	30.3482022	38.1921689	85.390118	133.9538372	0.359682	75.1706844	46.0900733	627.5867297	46.7053889	45.5792844
	7.3387733	77.41805	56.5743511	9242.275633	166.4041511	138.4007444	29.1760578	38.0090667	84.968527	140.5096633	0.354809	75.1763044	45.9474822	622.2387562	46.5998222	45.4255178
	8.6817444	77.48349	57.4576267	10504.58488	165.9078467	139.2182333	27.8931222	38.0140356	84.5048285	147.8206094	0.348682	75.1953044	46.0342644	610.0761738	46.6621956	45.5225733
	10.04721	77.49879	58.0856168	11784.81371	166.0462096	140.1891796	26.2807485	38.6574551	83.9277289	154.9008257	0.351216	75.2348263	46.663012	602.0919623	47.1383593	46.234024
N(3%T1S2) 250M	1.0444535	76.94719	40.6951047	2287.71949	120.8099767	134.1660698	34.205686	39.1342326	86.7881957	105.724707	0.376	75.065407	46.9353256	634.6146363	47.3493023	46.5433953
0.4374x - 19.517	1.04226	76.91544	40.6267489	2285.220417	121.1963711	134.2511711	34.7971622	39.1643133	87.0029378	105.8584563	0.375462	75.0305511	46.9149933	633.3797881	47.3454867	46.5337089
	1.8363846	77.05542	45.05532	3550.551078	120.8086308	134.6228585	34.67368	39.1527108	86.9556147	116.345494	0.370985	75.0700338	46.7423415	630.5482821	47.2437631	46.3904246
	2.3666956	77.17911	47.17728	4290.13357	120.62132	134.7677333	34.4957533	39.0406844	86.8937387	122.460698	0.371409	75.0871333	46.7868911	630.6576911	47.23696	46.3771822
	2.8826681	77.23091	48.7631532	4958.252992	121.0572851	134.7370255	33.8276128	38.8838596	86.6500618	127.6079686	0.370136	75.100234	46.7473745	629.6651314	47.1782298	46.2822426
	3.5594024	77.24281	50.8282112	5680.699389	120.3057131	135.2455936	32.9234143	39.1017012	86.3196778	133.5385442	0.370275	75.1225339	46.9002231	627.0007983	47.3169243	46.4844622
	4.5861195	77.34771	53.1087977	6716.441326	120.8411356	135.5820483	31.7517747	39.0739839	85.8957903	141.4765434	0.375053	75.1592391	46.9769954	634.1898885	47.3805011	46.5856805
	4.9670943	77.33592	53.8914966	7035.950178	120.2898621	135.8182575	31.5120966	39.2246644	85.8089831	144.3006137	0.373577	75.1725678	47.0244506	630.9293711	47.4199609	46.6410529

	Heat Sources																	
	Water Loop					Total												
Test Date	Test Inlet Temp (F)	Test Outlet Temp (F)	Plate Inlet Temp (F)	Plate Outlet Temp (F)	Effective Pump W_dot (kW)	Q (Btu/hr)	q" (kW/m^2)	Exit Temp (F)	Exit Pressure (psi)	Final Exit Pressure (psi)	Leaving Enthalpy (Btu/lb)	DP @ Test Section (psi)	DP/ Length Test Section (kPa/m)	Entering Temp (F)	EnteringPressure (psi)	Entering Enthalpy (Btu/lb)	Surface Couple 1
N(1%T1S2) 250M	47.6919844	47.0907156	47.1702156	47.3541311	0.7721422	3274.11199	12.0163	38.949936	133.44074	133.44074	130.11113	1.5423378	5.8147663	39.07544	134.98307	103.02923	44.192144
	47.7187528	47.1288399	47.1995562	47.3919972	0.77231157	3274.911079	12.0192	38.955076	133.44731	133.44731	130.32158	1.5633736	5.8940734	39.079826	135.01069	103.15842	44.206579
	47.3165467	46.5284111	46.6533244	46.86552	0.77099067	3264.662074	11.9816	38.709847	132.48883	132.48883	150.86075	2.9862533	11.258471	39.195093	135.47508	123.97823	43.560869
	47.5628142	46.8890963	46.9886032	47.1894931	0.77179349	3275.159344	12.0201	38.877294	133.15484	133.15484	139.55905	2.2577546	8.5119586	39.244892	135.4126	112.89113	44.010048
	47.2954074	46.4873951	46.6052716	46.8308519	0.7722463	3285.309613	12.0574	38.750901	132.25801	132.25801	158.02389	3.3305309	12.556432	39.194346	135.58854	130.69178	43.433444
	47.3453252	46.5631626	46.6898659	46.9058455	0.77307768	3289.182456	12.0716	38.845984	132.3751	132.3751	161.41171	3.6822967	13.882624	39.320528	136.0574	134.52862	43.465154
	47.2532133	46.3928511	46.5786311	46.7955156	0.75669233	3255.25284	11.9471	38.663736	131.83004	131.83004	168.16927	4.1776467	15.750142	39.155487	136.00769	141.33486	43.319222
	47.3103067	46.4835133	46.6522844	46.8685844	0.75578307	3264.742401	11.9819	38.713967	131.53059	131.53059	174.06612	4.56978	17.228524	39.075871	136.10037	147.10356	43.43234
	47.6210044	46.9409178	47.0815378	47.2666556	0.76002887	3258.86848	11.9604	39.714678	131.38967	131.38967	178.81385	4.7421911	17.878531	38.966331	136.13186	151.72403	43.721473
N(3%T1S2) 350M	47.0929222	46.1637133	46.3683489	46.5797289	0.77370007	3255.240679	11.947	38.708311	132.41465	132.41465	118.02463	2.3978311	9.040061	38.929622	134.81248	98.362221	43.294929
0.4253x - 18.09	47.0447556	46.0865467	46.3058956	46.5234111	0.77274787	3252.777006	11.938	38.756104	132.28132	132.28132	125.99423	3.2429533	12.226256	39.245104	135.52428	106.36372	43.055947
	46.9711444	45.9770267	46.2044533	46.4271133	0.771995	3254.860362	11.9456	38.693667	131.92174	131.92174	132.39274	3.9783156	14.998644	39.326422	135.90005	112.68098	42.8873
	46.9792633	45.9876333	46.2120567	46.4304467	0.7721859	3245.068313	11.9097	38.756877	132.00857	132.00857	131.9105	3.8610833	14.556667	39.387853	135.86966	112.33528	42.91316
	46.8697533	45.8244756	46.0581444	46.2904556	0.77113173	3253.209052	11.9396	38.512971	131.3515	131.3515	140.39528	5.0930333	19.201241	39.365493	136.44454	120.65285	42.654482
	46.7820378	45.6942556	45.94032	46.1760689	0.77010747	3263.601913	11.9777	38.344736	130.79596	130.79596	146.99523	5.9714911	22.513113	39.393664	136.76745	127.23083	42.517809
	46.7053889	45.5792844	45.831	46.0708333	0.7746998	3270.972168	12.0048	38.192169	130.24138	130.24138	153.71733	7.1355956	26.901903	39.439842	137.37697	133.95384	42.419311
	46.5998222	45.4255178	45.6948822	45.9291622	0.77427047	3264.159248	11.9798	38.009067	129.62167	129.62167	160.12552	8.2718333	31.185632	39.390404	137.8935	140.50966	42.320084
	46.6621956	45.5225733	45.7764467	46.01748	0.77346393	3249.24466	11.925	38.014036	129.10019	129.10019	167.40524	9.3264622	35.161687	39.374811	138.42665	147.82061	42.340811
	47.1383593	46.234024	46.4291437	46.6477784	0.7752212	3247.256483	11.9177	38.657455	128.7565	128.7565	174.45717	10.393257	39.183611	39.387569	139.14975	154.90083	42.531365
N(3%T1S2) 250M	47.3493023	46.5433953	46.7199302	46.9169535	0.7722143	3269.519205	11.9994	39.134233	133.12687	133.12687	132.78803	1.9050349	7.1821704	39.26257	135.03191	105.72471	43.571465
0.4374x - 19.517	47.3454867	46.5337089	46.7149822	46.9098244	0.77219893	3268.231915	11.9947	39.164313	133.1849	133.1849	132.82487	1.9410644	7.3180054	39.28388	135.12596	105.85846	43.569331
	47.2437631	46.3904246	46.5768092	46.7836831	0.77254735	3266.589269	11.9887	39.152711	132.74557	132.74557	143.38486	2.5464246	9.6002732	39.378462	135.292	116.34549	43.251098
	47.23696	46.3771822	46.5646222	46.7783156	0.7729426	3268.047314	11.994	39.040684	132.35348	132.35348	149.55414	3.0053244	11.330371	39.344147	135.3588	122.4607	43.111187
	47.1782298	46.2822426	46.4878979	46.6997234	0.77393923	3270.455411	12.0029	38.88386	131.83214	131.83214	154.62374	3.436034	12.954189	39.234298	135.26817	127.60797	42.918932
	47.3169243	46.4844622	46.6719402	46.8732869	0.77486175	3270.938843	12.0047	39.101701	131.83792	131.83792	160.7271	3.8031713	14.338333	39.384737	135.6411	133.53854	43.032988
	47.3805011	46.5856805	46.7587678	46.9524782	0.77221786	3269.106603	11.9979	39.073984	131.42165	131.42165	168.52947	4.4916483	16.933959	39.32651	135.91329	141.47654	42.981931
	47.4199609	46.6410529	46.8106966	47.0022529	0.77138352	3262.999183	11.9755	39.224664	131.42331	131.42331	171.42675	4.689623	17.680344	39.368085	136.11293	144.30061	43.029903

Test Date	Surface Couple 2	Surface Couple 3	Surface Couple 4	Surface Couple 5	Surface Couple 6	Surface Couple 7	Surface Couple 8	Surface Couple 9	Surface Couple 10	Surface Couple 11	Average T_Surface	Corrected Temp (F)	Entering Quality	Exiting Quality	Average Quality	Mass Flux (kg/m^2*s)	Average Pressure
	Test Section																
	Refrigerant Side																
N(1%T1S2) 250M	43.854987	43.428373	43.156393	43.532811	43.498324	42.395898	42.921658	42.435631	42.761078	43.003249	43.198232	43.198232	0.1498195	0.4439116	0.2968655	257.0208	134.2119044
	43.899447	43.497087	43.216458	43.559857	43.560435	42.450008	42.962191	42.440789	42.797118	43.012011	43.236544	43.236544	0.151178	0.4461632	0.2986706	256.31454	134.2289986
	42.9138	43.067871	42.608407	43.246811	42.798529	41.943116	42.190951	41.733196	42.201158	42.43842	42.609375	42.609375	0.3754402	0.6682161	0.5218281	258.17973	133.9819556
	43.342239	43.4292	43.059743	43.59486	43.228608	42.366206	42.653381	42.17314	42.549417	42.764927	43.015615	43.015615	0.2557022	0.5460035	0.4008529	261.09418	134.2837213
	42.792543	42.962827	42.437074	43.209025	42.662173	41.789074	42.041704	41.577679	42.109864	42.427802	42.494837	42.494837	0.447826	0.7454087	0.5966174	255.53885	133.9232778
	42.843821	43.037817	42.502016	43.229549	42.740748	41.801695	42.119886	41.690528	42.248183	42.56222	42.56742	42.56742	0.4888449	0.781797	0.635321	260.11342	134.21625
	42.687962	42.886233	42.377224	43.0971	42.649096	41.765758	42.07532	41.505793	42.212418	42.306609	42.443885	42.443885	0.5624288	0.854804	0.7086164	257.89717	133.9188678
	42.645544	42.896924	42.371289	43.075538	42.559224	41.680262	42.005764	41.428984	42.150778	42.665284	42.446539	42.446539	0.624749	0.9183533	0.7715511	257.41969	133.8154833
	42.802373	43.133953	42.565498	43.289213	42.537613	41.546787	41.971213	41.613762	43.034771	44.595396	42.801096	42.801096	0.6746917	0.969333	0.8220124	255.74941	133.7607622
N(3%T1S2) 350M	42.809418	42.562807	42.323831	42.756509	42.50222	41.591249	42.019189	41.442991	42.154024	42.254562	42.33743	42.33743	0.0996626	0.3149768	0.2073197	351.96566	133.6135689
0.4259x - 18.09	42.467191	42.501409	42.186682	42.819098	42.438176	41.616509	41.980687	41.511856	42.118084	42.249556	42.267745	42.267745	0.184989	0.4008718	0.2929304	352.27079	133.9027989
	42.309142	42.50422	42.118504	42.761864	42.41606	41.579949	41.927976	41.4322	42.018316	42.161724	42.192478	42.192478	0.2527673	0.4700962	0.3614317	351.04351	133.9108956
	42.35952	42.584613	42.189737	42.795307	42.48586	41.633603	41.979717	41.447283	42.054703	42.192137	42.239604	42.239604	0.2491321	0.4648391	0.3569856	352.42861	133.939115
	42.117602	42.395407	41.945624	42.618649	42.300229	41.421589	41.775773	41.314751	41.8398	42.0062	42.035464	42.035464	0.3382716	0.5567486	0.4475101	350.32015	133.8980189
	42.025211	42.326358	41.823993	42.483138	42.19864	41.312622	41.644296	41.172524	41.687958	41.856842	41.913581	41.913581	0.4090951	0.6281107	0.5186029	351.04879	133.7817033
	41.94448	42.25792	41.767247	42.386562	42.087918	41.157404	41.487433	41.004278	41.547313	41.756011	41.801443	41.801443	0.4812143	0.7006564	0.5909354	351.85773	133.8091733
	41.842729	42.150029	41.627947	42.176	41.842204	40.940753	41.320333	40.849647	41.435236	41.635604	41.649142	41.649142	0.551818	0.7698041	0.660811	353.7676	133.7575878
	41.814213	42.04346	41.492067	42.153529	41.821673	41.018891	41.452058	40.964191	41.668364	42.046069	41.710484	41.710484	0.6306387	0.8480907	0.7393647	352.71248	133.76342
	41.969928	42.399132	41.797868	42.55809	42.29912	41.598653	42.213024	41.840802	42.824216	43.468263	42.318224	42.318224	0.7069579	0.9237233	0.8153406	353.00663	133.9531257
N(3%T1S2) 250M	43.124698	43.005523	42.637953	43.187267	42.847012	41.979349	42.363151	41.865605	42.543837	42.69636	42.711111	42.711111	0.1787922	0.4731141	0.3259531	256.83648	134.0793895
0.4374x - 19.517	43.1266	43.006167	42.639067	43.195511	42.855049	41.983031	42.378489	41.884989	42.559796	42.704189	42.718383	42.718383	0.1801574	0.4733843	0.3267708	257.65793	134.1554322
	42.700637	42.892135	42.411015	43.076326	42.717818	41.828594	42.153932	41.899034	42.509169	42.747923	42.562517	42.562517	0.2932419	0.5875018	0.4403719	256.83361	134.0187846
	42.553089	42.800951	42.287564	43.052382	42.629624	41.785053	42.071693	41.825938	42.468113	42.690389	42.479635	42.479635	0.359161	0.6542334	0.5066972	256.4354	133.8561422
	42.38926	42.681936	42.161455	42.939877	42.486443	41.67234	42.011306	41.745706	42.424387	42.559987	42.362875	42.362875	0.4149016	0.7091503	0.562026	257.36224	133.5501574
	42.516697	42.824884	42.243203	43.085291	42.778853	41.932908	42.417737	41.942175	42.651343	43.005813	42.584717	42.584717	0.4785746	0.7748225	0.6266986	255.76443	133.73951
	42.461092	42.705225	42.199094	43.150497	42.877779	42.003807	42.486329	42.016306	42.777639	43.261425	42.629193	42.629193	0.5641424	0.8588839	0.7115132	256.90272	133.6674701
	42.527352	42.84529	42.301887	43.167428	42.896789	41.996168	42.481811	41.972543	42.766071	43.375572	42.669165	42.669165	0.5944582	0.8900388	0.7422485	255.73074	133.7681172
N(3%T1S2) 250M	43.1266	43.006167	42.639067	43.195511	42.855049	41.983031	42.378489	41.884989	42.559796	42.704189	42.718383	42.718383	0.1801574	0.4733843	0.3267708	257.65793	134.1554322
	42.700093	42.89264	42.41036	43.081291	42.717271	41.829587	42.149009	41.895938	42.510873	42.751538	42.562833	42.562833	0.2923908	0.5865511	0.4394709	256.62861	134.0058333
	42.553089	42.800951	42.287564	43.052382	42.629624	41.785053	42.071693	41.825938	42.468113	42.690389	42.479635	42.479635	0.359161	0.6542334	0.5066972	256.4354	133.8561422
	42.523542	42.803609	42.279007	43.069667	42.62396	41.819667	42.187553	41.915547	42.5495	42.700784	42.502147	42.502147	0.4271145	0.7209927	0.5740536	257.39927	134.0075544
	42.514831	42.817691	42.244371	43.080633	42.76662	41.924976	42.405896	41.931489	42.643918	43.018442	42.579645	42.579645	0.4781319	0.7742914	0.6262116	255.65132	133.7420422
	42.46164	42.705918	42.198996	43.149084	42.877238	42.001631	42.483451	42.010607	42.770351	43.250204	42.626442	42.626442	0.5640251	0.8587714	0.7113983	256.89241	133.6718956
	42.576901	42.977952	42.401258	43.186313	42.906306	41.991175	42.473786	41.933397	42.783504	43.522603	42.711023	42.711023	0.625898	0.922289	0.7740935	254.3934	133.8231012

Test Date	Corrected Temp (F)	Entering Quality	Exiting Quality	Average Quality	Mass Flux (kg/m^2*s)	Average Pressure	Actual TSAT (F)	Wall Tsurf (F)	DeltaT	HTC (Btu/hr ft^2 F)	HTC (kw/m^2 C)	α/α0	ΔP/ΔP0	Effective Pump W_dot [BTU/hr]	Q_refRef	Q_hot [Btu/hr]	M_dot Jacket [lb/min]	Q_TS Water [BTU/hr]
N(1%T1S2) 250M	43.198232	0.1498195	0.4439116	0.2968655	257.0208	134.2119044	38.46212914	43.18126	4.719132	807.1707812	4.58473	0.5895	0.31	2634.66	3274.11	639.45	160.00	5772.1
	43.236544	0.151178	0.4461632	0.2986706	256.31454	134.2289986	38.46991075	43.21952	4.749608	802.1872926	4.556424	0.5858	0.31	2635.24	3274.91	639.67	160.00	5663.1
	42.609375	0.3754402	0.6682161	0.5218281	258.17973	133.9819556	38.37711387	42.5688	4.191686	906.1153546	5.146735	0.6617	0.60	2630.73	3264.66	633.93	160.00	7566.1
	43.015615	0.2557022	0.5460035	0.4008529	261.09418	134.2837213	38.50245327	42.98707	4.484618	849.6518173	4.826022	0.6205	0.45	2633.47	3275.16	641.69	160.00	6467.6
	42.494837	0.447826	0.7454087	0.5966174	255.53885	133.9232778	38.35677253	42.44728	4.090509	934.4003735	5.307394	0.6824	0.67	2635.01	3285.31	650.30	160.00	7756.9
	42.56742	0.4888449	0.781797	0.635321	260.11342	134.21625	38.49087915	42.51468	4.023803	951.0105255	5.40174	0.6945	0.74	2637.85	3289.18	651.33	160.00	7508.7
	42.443885	0.5624288	0.854804	0.7086164	257.89717	133.9188678	38.36366528	42.38387	4.020209	942.0416777	5.350797	0.6879	0.84	2581.94	3255.25	673.31	160.00	8259.4
	42.446539	0.624749	0.9183533	0.7715511	257.41969	133.8154833	38.32235036	42.38004	4.057689	936.0611858	5.316828	0.6836	0.91	2578.84	3264.74	685.90	160.00	7937.2
	42.801096	0.6746917	0.969333	0.8220124	255.74941	133.7607622	38.30182823	42.72972	4.427893	856.2563019	4.863536	0.6253	0.95	2593.33	3258.87	665.54	160.00	6528.8
N(3%T1S2) 350M	42.33743	0.0996626	0.3149768	0.2073197	351.96566	133.6135689	38.08726152	42.32079	4.233531	894.5701113	5.081158	0.6533	0.48	2639.97	3255.24	615.27	160.00	8920.4
0.4259x - 18.09	42.267745	0.184989	0.4008718	0.2929304	352.27079	133.9027989	38.22384598	42.23802	4.014172	942.7408784	5.354768	0.6885	0.65	2636.73	3252.78	616.05	160.00	9198.8
	42.192478	0.2527673	0.4700962	0.3614317	351.04351	133.9108956	38.23290817	42.15313	3.920222	965.9523979	5.48661	0.7054	0.80	2634.16	3254.86	620.70	160.00	9543.5
	42.239604	0.2491321	0.4648391	0.3569856	352.42861	133.939115	38.24520816	42.2006	3.955396	954.4824422	5.42146	0.697	0.77	2634.81	3245.07	610.26	160.00	9519.6
	42.035464	0.3382716	0.5567486	0.4475101	350.32015	133.8980189	38.23395947	41.98401	3.750053	1009.272918	5.73267	0.737	1.02	2631.21	3253.21	622.00	160.00	10034.6
	41.913581	0.4090951	0.6281107	0.5186029	351.04879	133.7817033	38.18741737	41.85169	3.664274	1036.199231	5.885612	0.7567	1.19	2627.72	3263.60	635.89	160.00	10442.7
	41.801443	0.4812143	0.7006564	0.5909354	351.85773	133.8091733	38.20547837	41.72861	3.523129	1080.145669	6.135227	0.7888	1.43	2643.39	3270.97	627.59	160.00	10810.6
	41.649142	0.551818	0.7698041	0.660811	353.7676	133.7575878	38.18786867	41.56539	3.377521	1124.365036	6.386393	0.8211	1.65	2641.92	3264.16	622.24	160.00	11273.3
	41.710484	0.6306387	0.8480907	0.7393647	352.71248	133.76342	38.19671413	41.61529	3.418578	1105.785578	6.280862	0.8075	1.87	2639.17	3249.24	610.08	160.00	10940.3
	42.318224	0.7069579	0.9237233	0.8153406	353.00663	133.9531257	38.28783926	42.21143	3.923591	962.8682514	5.469092	0.7032	2.08	2645.16	3247.26	602.09	160.00	8681.6
N(3%T1S2) 250M	42.711111	0.1787922	0.4731141	0.3259531	256.83648	134.0793895	38.24281381	42.69038	4.447566	855.2548066	4.857847	0.6246	0.38	2634.90	3269.52	634.61	160.00	7736.7
0.4374x - 19.517	42.718383	0.1801574	0.4733843	0.3267708	257.65793	134.1554322	38.27694912	42.69767	4.420726	860.1086644	4.885417	0.6281	0.39	2634.85	3268.23	633.38	160.00	7793.0
	42.562517	0.2932419	0.5875018	0.4403719	256.83361	134.0187846	38.2247277	42.53034	4.305614	882.6600369	5.013509	0.6446	0.51	2636.04	3266.59	630.55	160.00	8192.0
	42.479635	0.359161	0.6542334	0.5066972	256.4354	133.8561422	38.15704082	42.44076	4.283717	887.567876	5.041386	0.6482	0.60	2637.39	3268.05	630.66	160.00	8253.8
	42.362875	0.4149016	0.7091503	0.562026	257.36224	133.5501574	38.02400261	42.31794	4.293941	886.1069583	5.033088	0.6471	0.69	2640.79	3270.46	629.67	160.00	8601.4
	42.584717	0.4785746	0.7748225	0.6266986	255.76443	133.73951	38.11420353	42.53324	4.419036	861.1502553	4.891333	0.6289	0.76	2643.94	3270.94	627.00	160.00	7991.6
	42.629193	0.5641424	0.8588839	0.7115132	256.90272	133.6674701	38.08857325	42.56833	4.479756	849.0021027	4.822332	0.62	0.90	2634.92	3269.11	634.19	160.00	7630.2
	42.669165	0.5944582	0.8900388	0.7422485	255.73074	133.7681172	38.13621298	42.60541	4.469193	849.4189165	4.824699	0.6203	0.94	2632.07	3263.00	630.93	160.00	7477.5

Test Date	Corrected Temp (F)	Entering Quality	Exiting Quality	Average Quality	Mass Flux (kg/m²*s)	Average Pressure	Actual TSAT (F)	Wall Tsurf (F)	DeltaT	HTC (Btu/hr ft^2 F)	HTC (kw/m^2 C)	α/α0	ΔP/ΔP0	Effective Pump W_dot [BTU/hr]	Q_refRef	Q_hot [Btu/hr]
N(3%T1S2) 250M	42.718383	0.1801574	0.4733843	0.3267708	257.65793	134.1554322	38.27637288	42.69767	4.421302	859.996564	4.88478	0.628	0.39	2634.85	3268.23	633.38
	42.562833	0.2923908	0.5865511	0.4394709	256.62861	134.0058333	38.2182734	42.53078	4.312508	880.0253648	4.998544	0.6427	0.51	2636.17	3262.05	625.88
	42.479635	0.359161	0.6542334	0.5066972	256.4354	133.8561422	38.15646422	42.44076	4.284294	887.448423	5.040707	0.6481	0.60	2637.39	3268.05	630.66
	42.502147	0.4271145	0.7209927	0.5740536	257.39927	134.0075544	38.2297231	42.45595	4.226223	898.8143497	5.105266	0.6564	0.70	2639.74	3265.04	625.30
	42.579645	0.4781319	0.7742914	0.6262116	255.65132	133.7420422	38.11472529	42.52823	4.413504	861.3906361	4.892699	0.629	0.76	2644.38	3267.76	623.38
	42.626442	0.5640251	0.8587714	0.7113983	256.89241	133.6718956	38.0899754	42.56559	4.475617	849.6743081	4.82615	0.6205	0.90	2634.84	3268.67	633.84
	42.711023	0.625898	0.922289	0.7740935	254.3934	133.8231012	38.1628458	42.64432	4.481474	845.269332	4.80113	0.6173	0.98	2629.81	3255.98	626.17
Superheat	45.00498	0.7089063	1	0.8544532	254.71057	132.3150807	37.48940553	44.92981	7.440402	503.6054967	2.860479	0.3678	1.09	2633.30	3220.72	587.41
N(1%T1S10) 250I	43.942554	0.1607108	0.4507101	0.3057105	260.67021	134.1642044	39.12886891	43.92394	4.795074	792.8974362	4.503657	0.579	0.39	2648.83	3267.97	619.14
	43.448845	0.268431	0.565439	0.416935	255.27641	134.0537433	39.09665329	43.41967	4.323014	880.7868457	5.002869	0.6432	0.54	2645.17	3272.83	627.66
	43.001572	0.3525806	0.6492572	0.5009189	255.43136	134.0003233	39.08296122	42.96371	3.88075	979.4172523	5.56309	0.7152	0.69	2635.11	3267.00	631.89
	42.740198	0.4319357	0.7302495	0.5810926	254.23806	134.0594065	39.10898252	42.69431	3.585324	1060.582772	6.02411	0.7745	0.80	2635.81	3268.43	632.62
	42.515139	0.4968686	0.794607	0.6457378	256.0195	133.9518244	39.07483426	42.46207	3.387241	1128.270194	6.408575	0.8239	0.90	2638.04	3284.92	646.88
	42.533272	0.5405591	0.8399362	0.6902477	254.72554	134.14653	39.14677131	42.47587	3.329099	1148.196648	6.521757	0.8385	0.98	2638.95	3285.56	646.60
	42.293914	0.5876323	0.8847768	0.7362045	256.6256	133.7277233	39.0008406	42.23097	3.230131	1183.6911	6.723365	0.8644	1.09	2635.62	3286.43	650.82
	42.50282	0.618938	0.9137905	0.7663643	257.13084	134.02082	39.10692571	42.43637	3.329449	1141.297896	6.482572	0.8335	1.15	2626.93	3266.16	639.23
	43.335879	0.6836788	0.9805917	0.8321352	256.17735	133.9028856	39.06915809	43.26275	4.193595	910.228027	5.170095	0.6647	1.23	2619.55	3280.97	661.42
N(1%T1S10) 350I	43.523087	0.1153889	0.3324684	0.2239287	350.61536	133.7015644	38.22731155	43.50433	5.277023	719.7184894	4.088001	0.5256	0.54	2635.18	3264.51	629.33
	43.129578	0.2082362	0.427354	0.3177951	349.42799	133.9781689	38.35856675	43.09702	4.738449	802.1934077	4.556459	0.5858	0.76	2621.49	3267.24	645.75
	43.087453	0.2076956	0.426205	0.3169503	350.62224	133.9640867	38.35220027	43.05488	4.702677	808.4775592	4.592153	0.5904	0.77	2619.79	3267.98	648.18
	42.517412	0.2930344	0.5136264	0.4033304	349.91999	133.7869022	38.27972874	42.47273	4.192996	910.1803283	5.169824	0.6647	1.00	2621.81	3280.33	658.52
	42.29581	0.3601409	0.5811825	0.4706617	350.63976	134.0136211	38.38652346	42.24135	3.854823	991.3450264	5.63084	0.7239	1.18	2625.91	3284.70	658.79
	42.010823	0.4188176	0.6394248	0.5291212	351.8801	133.8639111	38.32416178	41.94757	3.62341	1054.054002	5.987027	0.7697	1.40	2631.34	3282.81	651.48
	41.776811	0.4701485	0.6913382	0.5807434	350.3609	133.8036667	38.30127347	41.70629	3.405015	1117.705829	6.348569	0.8162	1.60	2624.16	3271.24	647.08
	41.432893	0.541469	0.7626941	0.6520816	351.13172	133.8558622	38.3302889	41.35169	3.021396	1261.077918	7.162923	0.9209	1.87	2621.43	3275.03	653.61
	41.173878	0.6326425	0.8536932	0.7431679	349.51073	133.7346822	38.28322629	41.07993	2.796707	1357.864605	7.712671	0.9916	2.12	2619.26	3264.14	644.88
	41.519807	0.6928706	0.9125893	0.80273	352.41233	134.07833	38.44174843	41.41577	2.974017	1280.130121	7.271139	0.9348	2.31	2580.37	3272.38	692.01

	Preheater														Heat Sources	
	Water Side				Refrigerant Side						Hot Loop				Water	
Test Date	Flow Rate (lb/min)	Inlet Temp (F)	Exit Temp (F)	Q (Btu/hr)	Flow Rate (lb/hr)	Pressure (psi)	Inlet Temp (F)	Exit Temp (F)	Entering Enthalpy (Btu/lb)	Leaving Enthalpy (Btu/lb)	Plate Flow Rate (lb/min)	Entering Hot Temp (F)	Leaving Hot Temp (F)	Q Plate_hot (Btu/hr)	Test Inlet Temp (F)	Test Outlet Temp (F)
N(3%T1S10) 250l	0.8307667	77.11258	39.2293711	1901.544827	120.3741311	133.6177089	35.5621133	38.8231956	87.279929	103.0768847	0.370018	75.2272222	46.9600089	627.5622877	47.3844933	46.6088733
	1.6440578	76.95276	44.09162	3264.227305	119.99408	134.1009356	34.8488089	38.7604822	87.0211428	114.224379	0.367442	75.0872133	46.7083867	625.6547481	47.1844133	46.3097444
	2.2307911	76.50038	46.6876978	4018.284154	120.0949222	134.5583267	34.3167644	38.7873844	86.8282305	120.2874649	0.3657	74.7016089	46.6520711	615.4629579	47.1511778	46.2649
	3.0263018	77.21984	49.4304141	5081.272829	121.4023811	135.1781982	33.0870352	38.8003436	86.3813516	128.2361553	0.362727	75.1763392	46.6710264	620.3785767	47.1662819	46.28513
	3.7999356	77.28243	51.4402467	5933.161557	122.19156	135.5974511	32.1256	38.7357156	86.0333642	134.5895947	0.358616	75.1929133	46.6977933	613.1275974	47.1658867	46.2858667
	4.5421511	77.32972	53.2476556	6609.004594	120.3509356	135.9000467	31.1603378	38.8579644	85.6824361	140.5968791	0.367851	75.2336311	46.8212978	627.0905032	47.2587622	46.4265356
	4.9212844	77.31014	54.0279533	6922.817994	120.3599156	135.82694	30.6587933	38.8737511	85.501785	143.0194225	0.366093	75.2272889	46.8222733	623.9332097	47.2689311	46.4375867
	5.53498	77.36892	55.5560311	7294.74395	120.0841422	136.3309133	30.2629289	39.02028	85.3574671	146.1044051	0.361964	75.2387356	46.9592422	614.1702656	47.3859778	46.6235689
	6.3059244	77.38075	56.90878	7799.900265	119.9909778	136.5131178	29.6134333	39.9523222	85.1231133	150.1271695	0.369162	75.2801622	47.4760578	615.853499	47.7743778	47.1744044
N(3%T1S10) 350l	2.3164378	77.1734	46.8080156	4249.914642	164.0149356	135.75148	33.16124	38.5427867	86.4067976	112.3185514	0.376547	75.1763267	46.4029578	650.0709686	46.9644044	45.9707111
	0.8744511	76.95756	39.2528044	1992.105964	167.0423733	134.4141067	35.1590422	38.6516178	87.1340992	99.05985143	0.378487	75.1300133	46.6394867	646.9970682	47.1450222	46.2438111
	3.35424	77.25114	50.1640622	5489.55244	165.1307867	136.4005733	32.4874222	38.2349222	86.1638638	119.4075281	0.371549	75.1912689	46.0910467	648.729314	46.7201444	45.6093378
	4.27682	77.37769	52.3627178	6464.006375	166.4772222	137.0072333	31.72128	37.96038	85.8850857	124.7132586	0.368716	75.2123444	45.9137667	648.1704829	46.5813467	45.4098333
	5.6619578	77.3859	55.3524156	7537.556394	165.0872067	137.8291889	30.44318	37.8388556	85.4237731	131.0818017	0.363344	75.2405333	45.7706511	642.463079	46.4703867	45.24726
	7.1123889	77.39686	56.9521133	8785.730047	164.47074	138.6753089	29.3131689	37.5390911	85.0165197	138.4347146	0.358327	75.2339133	45.5768333	637.6153572	46.3233356	45.0220956
	8.2094978	77.43823	57.5791111	9850.479221	166.3466533	139.5326689	27.9041244	37.4449244	84.5099591	143.726535	0.351498	75.27234	45.4696222	628.5353442	46.2356511	44.8989622

	Heat Sources																		
	Water Loop					Total													
Test Date	Test Inlet Temp (F)	Test Outlet Temp (F)	Plate Inlet Temp (F)	Plate Outlet Temp (F)	Effective Pump W_dot (kW)	Q (Btu/hr)	q" (kW/m^2)	Exit Temp (F)	Exit Pressure (psi)	Final Exit Pressure (psi)	Leaving Enthalpy (Btu/lb)	DP @ Test Section (psi)	DP/ Length Test Section (kPa/m)	Entering Temp (F)	EnteringPressure (psi)	Entering Enthalpy (Btu/lb)	Surface Couple 1
N(3%T1S10) 250l	47.3844933	46.6088733	46.7806911	46.9668022	0.7682874	3249.067709	11.9244	38.823196	132.55895	132.55895	130.0683	1.8882978	7.1190698	38.906944	134.44725	103.07688	44.119587
	47.1844133	46.3097444	46.5060778	46.7126067	0.77052453	3254.793585	11.9454	38.760482	132.11028	132.11028	141.349	2.7131378	10.228798	39.022853	134.82342	114.22438	43.671064
	47.1511778	46.2649	46.4610756	46.6678133	0.77293647	3252.831653	11.9382	38.787384	131.97951	131.97951	147.37297	3.2246933	12.157414	39.116924	135.2042	120.28746	43.547738
	47.1662819	46.28513	46.4798678	46.6846696	0.77323619	3258.769968	11.96	38.800344	131.72469	131.72469	155.07887	4.0159339	15.140469	39.209385	135.74063	128.23616	43.477513
	47.1658867	46.2858667	46.4787644	46.6856244	0.7721652	3247.864622	11.92	38.735716	131.34329	131.34329	161.1697	4.7190089	17.791131	39.181036	136.0623	134.58959	43.428256
	47.2587622	46.4265356	46.6052844	46.8117556	0.77025927	3255.324213	11.9473	38.857964	131.09554	131.09554	167.64548	5.18938	19.564477	39.178913	136.28492	140.59688	43.493747
	47.2689311	46.4375867	46.6211022	46.8245778	0.77261907	3260.218891	11.9653	38.873751	130.7087	130.7087	170.10667	5.4781111	20.653022	39.041458	136.18681	143.01942	43.446627
	47.3859778	46.6235689	46.7800333	46.9723156	0.76858947	3236.706381	11.879	39.02028	130.79174	130.79174	173.05806	5.85398	22.070085	39.108051	136.64572	146.10441	43.639309
	47.7743778	47.1744044	47.29934	47.4646111	0.77207473	3250.281838	11.9288	39.952322	130.43064	130.43064	177.21489	6.31112	23.793548	38.923773	136.74176	150.12717	43.94268
N(3%T1S10) 350l	46.9644044	45.9707111	46.1946311	46.4137178	0.76630327	3264.806246	11.9821	38.542787	131.7125	131.7125	132.22409	4.44026	16.74022	39.201587	136.15276	112.31855	42.9197
	47.1450222	46.2438111	46.4464533	46.6525978	0.76409987	3254.214033	11.9433	38.651618	132.40962	132.40962	118.54122	2.6864311	10.128112	38.975504	135.09606	99.059851	43.371531
	46.7201444	45.6093378	45.8603822	46.09266	0.7647868	3258.290192	11.9582	38.234922	130.8893	130.8893	139.1391	5.8195022	21.9401	39.098591	136.7088	119.40753	42.484247
	46.5813467	45.4098333	45.6802533	45.9154444	0.7661576	3262.408725	11.9733	37.96038	130.211	130.211	144.30999	6.8810267	25.942153	39.027358	137.09203	124.71326	42.272071
	46.4703867	45.24726	45.5253533	45.76784	0.76700707	3259.599822	11.963	37.838856	129.63375	129.63375	150.82652	8.06964	30.423343	39.074458	137.70339	131.0818	42.082236
	46.3233356	45.0220956	45.32488	45.5718089	0.76834567	3259.319593	11.962	37.539091	128.83514	128.83514	158.25173	9.4214711	35.51988	38.955949	138.25661	138.43471	41.941773
	46.2356511	44.8989622	45.20304	45.4593911	0.76644127	3243.741497	11.9048	37.444924	128.37402	128.37402	163.22643	10.558744	39.807513	38.925929	138.93276	143.72653	41.830158

	Test Section																
	Refrigerant Side																
Test Date	Surface Couple 2	Surface Couple 3	Surface Couple 4	Surface Couple 5	Surface Couple 6	Surface Couple 7	Surface Couple 8	Surface Couple 9	Surface Couple 10	Surface Couple 11	Average T_Surface	Corrected Temp (F)	Entering Quality	Exiting Quality	Average Quality	Mass Flux (kg/m^2*s)	Average Pressure
N(3%T1S10) 250I	43.608831	43.533856	42.835009	43.086756	43.003504	41.883607	42.392604	41.718044	42.398493	42.49282	42.824828	42.824828	0.1511596	0.4444488	0.2978042	255.90989	133.5031
	43.020664	43.179831	42.439378	42.914682	42.723971	41.656478	42.115273	41.488313	42.132078	42.363349	42.518644	42.518644	0.270861	0.5662461	0.4185536	255.10192	133.4668467
	42.873762	43.072733	42.332391	42.904911	42.647178	41.632296	42.040727	41.455142	42.114687	42.412024	42.457599	42.457599	0.335916	0.631092	0.483504	255.3163	133.5918556
	42.777035	43.024797	42.328641	42.924407	42.618004	41.568859	41.800319	41.48759	42.193615	42.472055	42.424803	42.424803	0.4211804	0.7141742	0.5676773	258.0959	133.7326586
	42.730842	42.971478	42.298576	42.922933	42.563556	41.50386	41.702844	41.450176	42.169053	42.443938	42.380501	42.380501	0.4894938	0.7798653	0.6346796	259.77366	133.7027956
	42.80334	43.086418	42.326073	42.867918	42.235322	41.50514	42.075044	41.632404	42.396427	42.801893	42.474884	42.474884	0.5542842	0.8495988	0.7019415	255.86058	133.6902322
	42.74684	42.974527	42.086633	42.741304	42.315716	41.548482	42.110831	41.65222	42.496422	43.038533	42.468921	42.468921	0.5805434	0.8762058	0.7283746	255.87967	133.4477556
	42.925469	43.281876	42.262687	42.905029	42.615809	41.743522	42.25122	41.765571	42.675027	43.237898	42.663947	42.663947	0.6134702	0.9078299	0.76065	255.29339	133.7187256
	43.10306	43.394118	42.255793	43.037738	42.666627	41.748587	42.417576	42.129887	43.587322	44.830307	43.010336	43.010336	0.6570186	0.9525108	0.8047647	255.09532	133.5862022
N(3%T1S10) 350I	42.246756	42.534591	42.053313	42.714862	42.356824	41.49514	41.882031	41.334918	41.952387	42.07132	42.141986	42.141986	0.2485341	0.4684935	0.3585138	348.68824	133.9326322
	42.799496	42.770913	42.468153	42.928887	42.607707	41.720547	42.131896	41.505902	42.176556	42.226078	42.427969	42.427969	0.1067637	0.3205712	0.2136674	355.12443	133.75284
	41.87038	42.229338	41.676156	42.407791	42.056816	41.185047	41.554247	41.024173	41.597844	41.731738	41.801616	41.801616	0.3245162	0.5436584	0.4340873	351.06049	133.7990489
	41.717282	42.173593	41.568464	42.198738	41.984967	41.031816	41.419287	40.87392	41.42754	41.518213	41.653263	41.653263	0.3814408	0.5997621	0.4906014	353.92295	133.6515133
	41.541278	41.995973	41.401704	42.053796	41.807709	40.875169	41.242287	40.667598	41.243947	41.372111	41.480346	41.480346	0.449792	0.6701034	0.5599477	350.96784	133.6685733
	41.427067	41.830889	41.267842	41.859311	41.586229	40.63422	40.959531	40.407184	40.969467	41.137433	41.274632	41.274632	0.5289661	0.7502103	0.6395882	349.65726	133.5458756
	41.305796	41.685522	41.1216	41.692198	41.278084	40.39364	40.76794	40.222191	40.870153	41.083796	41.113734	41.113734	0.5857823	0.8037339	0.6947581	353.64536	133.6533878

Test Date	Average T_Surface	Corrected Temp (F)	Entering Quality	Exiting Quality	Average Quality	Mass Flux (kg/m^2*s)	Average Pressure	Actual TSAT (F)	Wall Tsurf (F)	DeltaT	HTC (Btu/hr ft^2 F)	HTC (kw/m^2 C)	α/α0	ΔP/ΔP0	Effective Pump W_dot [BTU/hr]	Q_refRef	Q_hot [Btu/hr]	M Ja [II
N(3%T1S10) 250I	42.824828	42.824828	0.1511596	0.4444488	0.2978042	255.90989	133.5031	38.00034098	42.8076	4.807256	786.3132232	4.466259	0.5742	0.38	2621.51	3249.07	627.56	
	42.518644	42.518644	0.270861	0.5662461	0.4185536	255.10192	133.4668467	37.99361105	42.48906	4.495453	842.3334839	4.784454	0.6151	0.54	2629.14	3254.79	625.65	
	42.457599	42.457599	0.335916	0.631092	0.483504	255.3163	133.5918556	38.05495232	42.42119	4.366233	866.7397014	4.923082	0.633	0.64	2637.37	3252.83	615.46	
	42.424803	42.424803	0.4211804	0.7141742	0.5676773	258.0959	133.7326586	38.12487245	42.37876	4.253885	891.2550832	5.062329	0.6509	0.80	2638.39	3258.77	620.38	
	42.380501	42.380501	0.4894938	0.7798653	0.6346796	259.77366	133.7027956	38.11677528	42.32674	4.20996	897.5403936	5.098029	0.6554	0.94	2634.74	3247.86	613.13	
	42.474884	42.474884	0.5542842	0.8495988	0.7019415	255.86058	133.6902322	38.1164663	42.41499	4.298528	881.0662496	5.004456	0.6434	1.04	2628.23	3255.32	627.09	
	42.468921	42.468921	0.5805434	0.8762058	0.7283746	255.87967	133.4477556	38.00958091	42.40619	4.396606	862.7067726	4.900174	0.63	1.10	2636.29	3260.22	623.93	
	42.663947	42.663947	0.6134702	0.9078299	0.76065	255.29339	133.7187256	38.13391818	42.59784	4.463924	843.5688348	4.791471	0.616	1.17	2622.54	3236.71	614.17	
	43.010336	43.010336	0.6570186	0.9525108	0.8047647	255.09532	133.5862022	38.07788049	42.93965	4.861773	777.7864451	4.417827	0.568	1.26	2634.43	3250.28	615.85	
N(3%T1S10) 350I	42.141986	42.141986	0.2485341	0.4684935	0.3585138	348.68824	133.9326322	38.03389559	42.10347	4.069578	933.3447966	5.301398	0.6816	0.89	2614.74	3264.81	650.07	
	42.427969	42.427969	0.1067637	0.3205712	0.2136674	355.12443	133.75284	37.9414252	42.40992	4.468492	847.2648057	4.812464	0.6187	0.54	2607.22	3254.21	647.00	
	41.801616	41.801616	0.3245162	0.5436584	0.4340873	351.06049	133.7990489	37.97988518	41.75187	3.771985	1004.971762	5.70824	0.7339	1.16	2609.56	3258.29	648.73	
	41.653263	41.653263	0.3814408	0.5997621	0.4906014	353.92295	133.6515133	37.9180424	41.59469	3.676644	1032.3354	5.863665	0.7539	1.38	2614.24	3262.41	648.17	
	41.480346	41.480346	0.449792	0.6701034	0.5599477	350.96784	133.6685733	37.93129236	41.41204	3.480749	1089.495975	6.188337	0.7956	1.61	2617.14	3259.60	642.46	
	41.274632	41.274632	0.5289661	0.7502103	0.6395882	349.65726	133.5458756	37.88247458	41.19502	3.312541	1144.721103	6.502016	0.836	1.88	2621.70	3259.32	637.62	
	41.113734	41.113734	0.5857823	0.8037339	0.6947581	353.64536	133.6533878	37.93506898	41.02447	3.089401	1221.535217	6.93832	0.892	2.11	2615.21	3243.74	628.54	

Pressure drop test conditions comparison of the test section

	Water Side				Refrigerant Side						Ho	
Tube type	Flow Rate (lb/min)	Inlet Temp (F)	Exit Temp (F)	Q (Btu/hr)	Flow Rate (lb/hr)	Pressure (psi)	Inlet Temp (F)	Exit Temp (F)	Entering Enthalpy (Btu/lb)	Leaving Enthalpy (Btu/lb)	Plate Flow Rate (lb/min)	Entering Hot Temp (F)
enhanced21	21.1835	83.39346	69.4695333	17821.33218	152.4668467	148.4382667	23.8728067	68.0560533	148.438267	23.87280667	3.9224467	80.79314
enhanced-16	15.827167	83.26949	65.46272	17028.20871	152.18918	147.8949333	26.5139333	67.7269267	84.011751	195.9001829	4.08384	80.70728
enhanced 11	11.297917	83.20756	60.7165931	15352.78647	154.0424552	148.215869	31.1802414	67.0945448	85.6911534	185.3570958	4.277131	80.6918
enhanced 21_mf	21.149373	83.43215	66.2769933	21921.63778	194.2737733	149.1192867	23.7369533	67.6985	83.0228316	195.8617259	3.9484667	80.82608
Enhanced 220mf	19.100509	83.54907	63.8218363	22766.26961	227.5835907	153.2856548	28.135911	66.8791032	84.595762	184.6305208	3.8016655	80.9143915
smooth21	21.18036	83.32539	69.2919867	17958.79401	153.99682	148.2312733	23.9401467	68.1554067	83.09	199.7079536	3.922	80.7503
smooth-16	15.833207	83.26955	65.4147533	17080.6514	152.7394133	147.8992467	26.5112333	67.63354	83.09	194.9187089	4.0854667	80.71718
smooth- 11	11.290947	83.18869	60.7354867	15317.55053	153.9765733	148.3690733	31.325	67.1310333	83.09	182.5697468	4.26336	80.67974
smooth-21-massflo 194	21.152767	83.43105	66.3257333	21861.44848	193.7326667	149.2419467	24.1609	67.7217	83.17	196.0133777	3.9484267	80.86766
smooth-19-massflow221	19.14563	82.76067	63.7221067	22023.40572	221.8051933	154.3499067	28.68429	67.1217767	84.79	184.0816595	3.8080733	80.24549
TS21	21.1747	83.29696	69.30408	17902.14608	153.71266	148.2777667	24.4726533	67.9704067	148.277767	24.47265333	3.9555267	80.74454
TS-16	15.852613	83.275	65.3162067	17201.1998	154.4397	148.4415533	26.9045	67.5387	84.151548	195.5296444	4.06154	80.73878
TS 21_mf	21.141133	83.4268	66.2229533	21975.28668	195.12996	148.7199	24.47638	67.6172667	83.2865067	195.9052284	3.9430667	80.8453467
TS11	11.269767	83.20047	60.6980267	15322.34574	154.19142	148.1340467	31.6529533	67.0276733	85.8609938	185.2332269	4.2241667	80.66426
	19.230083	83.57424	63.6127417	23192.90026	228.5935083	151.9056583	28.0150333	66.8578917	84.5538917	186.0130295	3.8277833	80.9429167

Tube type	Leaving Hot Temp (F)	Q Plate_hot (Btu/hr)	Test Inlet Temp (F)	Test Outlet Temp (F)	Plate Inlet Temp (F)	Plate Outlet Temp (F)	Effective Pump W_dot (kW)	Q (Btu/hr)	q" (kW/m^2)	Exit Temp (F)	Exit Pressure (psi)	Final Exit Pressure (psi)
enhanced21	80.7412	12.22391279	68.4462	68.7966733	72.1379267	76.83696	-0.5174586	-1753.418118	-6.4352	68.0560533	140.84072	3
enhanced-16	80.69134	3.905784576	68.43692	68.68508	72.11574	76.8248133	-0.5174356	-1761.657767	-6.4655	67.7269267	140.418647	2
enhanced 11	80.6787586	3.346781291	62.7035103	63.6379517	72.1820207	76.8535931	-0.51742862	-1762.192956	-6.4674	67.0945448	141.183717	1
enhanced 21_mf	80.79106	8.29651816	70.6684133	70.3604133	72.17224	76.86286	-0.5174218	-1757.219946	-6.4492	67.6985	136.03494	4
Enhanced 220mf	80.8829004	7.183118399	66.6358221	66.765847	71.9950712	76.9222384	-0.51744843	-1758.424225	-6.4536	66.8791032	134.832619	5
smooth21	80.725	5.953596	68.4762133	68.87006	72.1672267	76.8524267	-0.5174448	-1759.641347	-6.4581	68.1554067	140.83786	3
smooth-16	80.68882	6.95183008	68.5691467	68.7274933	72.1177733	76.8055733	-0.5174494	-1758.658809	-6.4544	67.63354	140.770893	2
smooth- 11	80.66254	4.39978752	63.3124333	63.1128933	72.1504467	76.8398333	-0.5174448	-1761.195156	-6.4638	67.1310333	141.605527	1
smooth-21-massflo 194	80.83462	7.827361024	69.8682533	69.7003733	72.1802	76.9078267	-0.5174586	-1757.81467	-6.4513	67.7217	136.917073	4
smooth-19-massflow221	80.2291	3.744859316	68.0965133	68.23246	72.44807	77.3236267	-0.5174494	-1761.86578	-6.4662	67.1217767	134.36193	5
TS21	80.71132	7.884155752	71.1312933	71.0203467	72.19004	76.8467933	-0.517454	-1757.742179	-6.4511	67.9704067	142.16082	2
TS-16	80.71258	6.38474088	68.5605933	68.8312667	72.1107933	76.81864	-0.5174402	-1759.194507	-6.4564	67.5387	142.4284	1
TS 21_mf	80.81554	7.051780427	68.921	69.1934133	72.15726	76.9081733	-0.5174494	-1758.558859	-6.4541	67.6172667	138.026393	4
TS11	80.6404	6.047317	55.12318	58.00178	72.1068533	76.8039733	-0.5174448	-1759.547626	-6.4577	67.0276733	142.50086	3
	80.895775	10.82688516	59.24545	62.4784417	71.9847333	76.9059417	-0.5174195	-1754.681731	-6.4398	66.8578917	136.298075	5

Tube type	Leaving Enthalpy (Btu/lb)	DP @ Test Section (psi)	DP/ Length Test Section (kPa/m)	Entering Temp (F)	EnteringPressure (psi)	Entering Enthalpy (Btu/lb)	Entering Quality	Exiting Quality	Average Quality	Mass Flux (kg/m^2*s)	Average Pressure	Actual TSAT (F)
enhanced21	12.3724828	1.92106667	7.24261177	68.2102867	4.92106667	23.8728067	68.27096	3	-7.9431869	324.13753	72.88089333	81.95622919
enhanced-16	184.324736	1.90850667	7.19525932	68.0575667	3.90850667	195.900183	100	100	100	323.54722	72.16357667	43.37697247
enhanced 11	173.917438	1.86069655	7.01501045	67.0306414	2.86069655	185.357096	100	0.91272921	50.456365	327.4872	72.0222069	43.68659854
enhanced 21_mf	186.816656	2.90784667	10.9628702	68.2061467	6.90784667	195.861726	100	100	100	413.01714	71.47139333	41.73324983
Enhanced 220mf	176.904023	4.20106406	15.8384279	67.6678399	9.20106406	184.630521	100	0.9475523	50.473776	483.83229	72.01684164	41.49448991
smooth21	188.281475	1.33478844	5.03228473	68.28414	4.33478844	199.707954	68.2633133	3	-101.09429	327.39018	72.58632422	169.8723891
smooth-16	183.404596	1.16910504	4.40764188	67.96748	3.16910504	194.918709	68.7270333	2	-98.180903	324.717	71.96999918	167.4446685
smooth- 11	171.131675	0.96448941	3.63622068	67.3932267	1.96448941	182.569747	59.2737067	1	-104.71278	327.34714	71.78500804	161.682705
smooth-21-massflo 194	186.939974	1.83	6.89928141	67.75998	5.83	196.013378	71.2371	4	-93.408192	411.86677	71.37353667	166.0872523
smooth-19-massflow221	176.138357	2.00300709	7.55153528	67.9909067	136.364937	184.081659	67.6136467	134.36193	-90.868401	471.54768	135.3634335	158.8585136
TS21	13.0374067	1.66082667	6.26148117	68.26538	3.66082667	24.4726533	75.65984	2	-1.5641191	326.78607	72.91082333	82.90861195
TS-16	184.138826	1.61014	6.07038741	67.3683533	2.61014	195.529644	100	100	100	328.33173	72.51927	44.15292115
TS 21_mf	186.892984	2.46654	9.29910031	67.32708	6.46654	195.905228	100	100	100	414.83736	72.24646667	42.4873679
TS11	173.821777	1.68402	6.34892234	67.8214867	4.68402	185.233227	100	0.91110937	50.455555	327.8039	73.59244	44.19857248
	178.337038	3.475175	13.1017542	67.677825	8.475175	186.01303	100	0.96254088	50.48127	485.97933	72.386625	41.96835935

VITA

Thiam Wong

Candidate for the Degree of

Master of Science

Thesis: DEVELOPMENT OF A TEST FACILITY AND PRELIMINARY TESTING OF FLOW BOILING HEAT TRANSFER OF R410A REFRIGERANT WITH AL_2O_3 NANOLUBRICANTS

Major Field: Mechanical and Aerospace Engineering

Biographical: Born in Shillong, India. Son of Wong How Yee and Cecilia Wong.

Education:

Completed the requirements for the Master of Science in Mechanical Engineering at Oklahoma State University, Stillwater, Oklahoma in December, 2015.

Completed the requirements for the Bachelor of Science in Mechanical Engineering at Oklahoma State University, Stillwater, Oklahoma in 2013.

Experience:

- Graduate Research Assistant at Oklahoma State University Tube Calorimeter Test Facility.

Professional Memberships:

- American Society of Heating, Refrigeration and Air-conditioning Engineers (ASHRAE)